UILU ENG 83-4005
DEPARTMENT OF MECHANICAL
AND INDUSTRIAL ENGINEERING
INIVERSITY OF ILLINOIS AT URBANA-CHAMPAIGN
IRBANA, ILLINOIS 61801

FINAL TECHNICAL REPORT

FLUID DYNAMIC MECHANISMS AND INTERACTIONS WITHIN SEPARATED FLOWS AND THEIR EFFECTS ON MISSILE AERODYNAMICS

by

A. L. Addy
W. L. Chow
H. H. Korst
R. A. White

MAY 1983

Supported by
U.S. Army Research Office
Research Grant DAAG 29-79-C-0184
and the
Department of Mechanical and Industrial Engineerin

REPORT DOCUMENTATION PAGE

READ INSTRUCTIONS BEFORE COMPLETING FORM

1. REPORT NUMBER: UILU-ENG-83-4005	2. GOVT ACCESSION NO.: ---
3. RECIPIENT'S CATALOG NUMBER: ---	
4. TITLE (and Subtitle): Fluid Dynamic Mechanisms and Interactions Within Separated Flows and Their Effects on Missile Aerodynamics	5. TYPE OF REPORT & PERIOD COVERED: Final Technical Report 1979-83
	6. PERFORMING ORG. REPORT NUMBER: UILU-ENG-83-4005
7. AUTHOR(s): A. L. Addy, W. L. Chow, H. H. Korst, R. A. White	8. CONTRACT OR GRANT NUMBER(s): DAAG 29-79-C-0184
9. PERFORMING ORGANIZATION NAME AND ADDRESS: Dept. of Mechanical and Industrial Engineering University of Illinois at Urbana-Champaign Urbana, Illinois 61801	10. PROGRAM ELEMENT, PROJECT, TASK AREA & WORK UNIT NUMBERS
11. CONTROLLING OFFICE NAME AND ADDRESS: U.S. Army Research Office Post Office Box 12211 Research Triangle Park, NC 27709	12. REPORT DATE: May 1983 13. NUMBER OF PAGES: 233
14. MONITORING AGENCY NAME & ADDRESS(if different from Controlling Office)	15. SECURITY CLASS. (of this report): Unclassified 15a. DECLASSIFICATION/DOWNGRADING SCHEDULE: NA

16. DISTRIBUTION STATEMENT (of this Report)

Approved for public release; distribution unlimited.

17. DISTRIBUTION STATEMENT (of the abstract entered in Block 20, if different from Report)

NA

JUL 13 1983

18. SUPPLEMENTARY NOTES

The findings of this report are not to be construed as an official Department of the Army position unless so designated by other authorized documents.

19. KEY WORDS (Continue on reverse side if necessary and identify by block number)

Base flows
Component method
LDV experiments
Missile aerodynamics
Projectile flight

20. ABSTRACT (Continue on reverse side if necessary and identify by block number)

The significant data and results of a joint research effort investigating the fluid dynamic mechanisms and interactions within separated flows are presented in detail. The results were obtained through analytical, experimental, and computational investigations of base flow related configurations conducted by the Gas Dynamics Group at the University of Illinois at Urbana-Champaign. The objectives of the research program focus on understanding the component mechanisms and interactions which establish and maintain separated flow regions. Flow models and theoretical analyses have been developed to describe the base flowfield and

20. Abstract (cont.)

LDV experiments are being conducted in order to provide new flowfield data. The research program approach has been to conduct extensive small-scale experiments on base flow configurations and to analyze these flows by component models and finite-difference techniques. The modeling of base flows of missiles (both powered and unpowered) for transonic and supersonic freestreams has been successful by component models. The research on plume effects and plume modeling has indicated the need to match initial plume slope and plume surface curvature for valid wind tunnel simulation of an actual rocket plume. The assembly and development of a state-of-the-art laser Doppler velocimeter system for experiments with two-dimensional small-scale models has been completed and detailed velocity and turbulence measurements are underway. The LDV experiments include the entire range of base flowfield mechanisms -- shear layer development, recompression/reattachment, shock-induced separation, and plume-induced separation. Many of the research efforts are described in detail and were presented as papers at the Huntsville Symposium on Rocket/Plume Fluid Dynamic Interactions. The future research activities of primary interest are indicated to be small-scale experiments utilizing the LDV, power-off transonic base flow analysis, and investigation of the transient nature of the near-wake mixing region.

FLUID DYNAMIC MECHANISMS AND INTERACTIONS WITHIN SEPARATED FLOWS AND THEIR EFFECTS ON MISSILE AERODYNAMICS

by

A. L. Addy[†]
W. L. Chow[††]
H. H. Korst[††]
R. A. White[††]

May 1983

Supported by

U.S. Army Research Office
Research Grant DAAG 29-79-C-0184

and the

Department of Mechanical and Industrial Engineering
University of Illinois at Urbana-Champaign
Urbana, Illinois 61801

Approved for Public Release; Distribution Unlimited

[†] Professor and Associate Head of Mechanical Engineering.
[††] Professor of Mechanical Engineering.

ABSTRACT

The significant data and results of a joint research effort investigating the fluid dynamic mechanisms and interactions within separated flows are presented in detail. The results were obtained through analytical, experimental, and computational investigations of base flow related configurations conducted by the Gas Dynamics Group at the University of Illinois at Urbana-Champaign. The objectives of the research program focus on understanding the component mechanisms and interactions which establish and maintain separated flow regions. Flow models and theoretical analyses have been developed to describe the base flowfield and LDV experiments are being conducted in order to provide new flowfield data. The research program approach has been to conduct extensive small-scale experiments on base flow configurations and to analyze these flows by component models and finite-difference techniques. The modeling of base flows of missiles (both powered and unpowered) for transonic and supersonic freestreams has been successful by component models. The research on plume effects and plume modeling has indicated the need to match initial plume slope and plume surface curvature for valid wind tunnel simulation of an actual rocket plume. The assembly and development of a state-of-the-art laser Doppler velocimeter system for experiments with two-dimensional small-scale models has been completed and detailed velocity and turbulence measurements are underway. The LDV experiments include the entire range of base flowfield mechanisms -- shear layer development, recompression/reattachment, shock-induced separation, and plume-induced separation. Many of the research efforts are described in detail and were presented as papers at the Huntsville Symposium on Rocket/Plume Fluid Dynamic Interactions. The future research activities of primary interest are indicated to be small-scale experiments

utilizing the LDV, power-off transonic base flow analysis, and investigation of the transient nature of the near-wake mixing region.

ACKNOWLEDGMENT

The members of the Research Group wish to recognize Vincent A. Amatucci, Graduate Research Assistant, for extending his endeavors beyond his own research activities to encompass major contributions to technical reports/papers and this final report.

TABLE OF CONTENTS

LIST OF APPENDICES

---

†Refers to a paper presented at the Symposium on Rocket/Plume Fluid Dynamic Interactions, Huntsville, Alabama, April 1983.

INTRODUCTION

A group research effort has been funded by the U.S. Army Research Office to investigate the fluid dynamic mechanisms and interactions within separated flows, particularly with respect to base flows. The separated flow problems which are of interest to this research program are focused into three general areas, namely

(1) missile base flows,

(2) the interaction between base and body flows, and

(3) the effects of small angle-of-attack on base and body flows.

The nature of this final technical report will be to provide the significant data, results, and extensions for the near-wake base flow problem and related problems which have been obtained under the sponsorship of the U.S. Army Research Office through Research Contract DAAG 29-79-C-0184. The results were obtained through analytical, computational, and experimental investigations of base flow related configurations.

Problem Statement

Since the early 1950's, the separated flow region at the base of a missile for flight at supersonic speeds has been studied extensively. The objectives of these studies were to develop an understanding of the mechanisms governing the separated base flow region and to formulate flow models for predicting the base region pressure, temperature, and heat transfer characteristics. The more successful models or methods, judged by their ability to predict base flow conditions in reasonable agreement with experiment, are all combinations of theoretical and empirical components which have been combined

to model this complex flow region [1-4]†. These methods leave still unanswered many questions regarding the fundamental fluid dynamic nature of the flow mechanisms and interactions within the separated base flow region.

The supersonic turbulent flow which approaches the base of the missile undergoes an expansion/compression process at the geometric corner, a shear layer mixing process between the freestream flow and the recirculating flow, and a recompression and redevelopment process. In each of the components of the base flowfield a number of flow mechanisms exist which are still in need of detailed examination. The flow mechanisms, as indicated in Figure 1, can be broadly categorized as follows:

- Geometric separation of a boundary layer to form a free shear layer. Local expansions or compressions at the separation location are important factors affecting shear layer development, turbulence intensity, and the initialization of the flow entering the base region;
- Effects on shear layer development resulting from modifications of the initial phases of the jet mixing due to adjacent wall geometry and local wake flowfields;
- Shear layer development in the presence of the recirculating base flow. The determination of the local velocity field and the turbulence characteristics of this flow are important to the characterization of the base flow;
- Recompression, reattachment, and redevelopment of the shear flow in the presence of the external and internal flows; and
- Shock wave or aerodynamically induced separation of the body turbulent boundary layer to form a shear layer at locations upstream of the geometric separation location.

These basic flow mechanisms are being investigated through analytical, computational, and experimental studies in an effort to provide a better understanding of the physical nature of the base flow problem.

---

†Numbers in brackets refer to entries in REFERENCES.

Research Objectives

The research philosophy maintained throughout the duration of this three-year contract has been to establish unified theoretical and experimental investigations of the fundamental flow mechanisms and interactions within separated flow regions. These investigations would establish a firm foundation for the development of generalized theoretical models and analysis techniques which are independent of configuration and operating condition requirements.

The general objectives of the ongoing research program can be formulated as follows:

(1) To investigate the fundamental flow mechanisms and interactions --- separation, mixing, recirculation, recompression, redevelopment, reaction, injection, etc. --- which establish and maintain separated flow regions;

(2) To develop flow models and theoretical analyses which do not require significant empirical components to describe adequately the fundamental separated flow mechanisms/interactions and their interrelationships;

(3) To develop and conduct state-of-the-art two-dimensional experiments for making LDV measurements in high-speed flows with imbedded separated flow regions; thus providing well-documented velocity and pressure data for a wide range of base flow configurations;

(4) To extend the flow models and theoretical analyses to more complex geometries and flow conditions including small angle-of-attack; and

(5) To assess the effects of separated flow regions on missile aerodynamics.

These overall objectives were the basis for all of the work which is described in each of the following sections.

Research Approach and Group Organization

The research approach has been (1) to conduct extensive small-scale experiments related to the basic flow mechanisms encountered in these flows

and (2) to analyze these flows based on component models and finite-difference techniques. The experiments utilized modern flowfield experimental techniques while the theoretical analyses emphasized the interactive nature of the various flow mechanisms.

The unified treatment of the base flow problem formally associated four senior faculty members (A. L. Addy, W. L. Chow, H. H. Korst, and R. A. White) into a group research effort. The four principal investigators have had significant research experience in the area of separated flows and related problems. Their interests span the spectrum from predominantly theoretical-numerical analyses to experimental investigations.

Final Technical Report Organization

The overall organization of this report attempts to detail the research accomplishments achieved under the sponsorship of the three-year contract. The wide range of research topics are listed and described and the appropriate literature references are cited. In each case for each research topic the work has been introduced and summarized quite briefly and the associated published literature has been included in an appendix. This particular type of organization permits quick and detailed access to special base flow topics of interest. Providing a copy of the published literature reduces the burden of obtaining conference proceedings and the like.

Since the research effort focuses on many topics, the report covers the entire range of base flow investigations. In each case when a detailed paper is available, only a brief description is given and the reader is referred to the appropriate appendix for further details. Much of the research work investigated under this contract was reported at the Symposium on Rocket/Plume Fluid Dynamic Interactions which was held at Huntsville, Alabama during early

April of 1983. All of the symposium papers which were presented by the four principal investigators have been included in the various appendices. Any computer programs which have been developed by the principal investigators or their graduate students have been listed and described in Appendices A-1 through A-5.

Once the research topics have been discussed, the continuing and future research activities of the research group are described. The strong commitment of this research group towards an understanding of the base flow problem is evidenced by the multi-year development and assembly of advanced experimental equipment which will provide well-documented data for the ongoing analytical and computational work. Lastly, some conclusions and recommendations are made concerning new information about the base flowfield and the value of a unified group research effort for this problem area.

Continuing Research Activity

Although this final technical report summarizes a three-year effort, our research group is continuing the investigations of the base flow problem and anticipates further significant contributions to the knowledge of the fundamental mechanisms and interactions of the near-wake flow. The emphasis of our ongoing research activity is focused on the following general research tasks:

(1) Well-documented small-scale experimental investigations using two-dimensional wind tunnel models focusing on the fundamental mechanisms of separation, mixing, and reattachment. The experiments will center on state-of-the-art laser Doppler velocimeter measurements of the near-wake flowfield.

(2) Power-on and power-off transonic base flow analyses based on the equivalent body concept.

(3) Steady and non-steady aspects of separation with a supersonic freestream flow, focusing on the possibility of unsteadiness of the mixing layer and the reattachment region.

A large commitment of financial resources and time has been made in order to establish a unified research group investigating the base flow phenomena with up-to-date analyses and state-of-the-art experimental techniques. A new junior faculty member, Professor N. S. Vlachos, has been the latest addition to the Gas Dynamics Group at the University of Illinois at Urbana-Champaign. While Professor Vlachos is a relative newcomer to separated flow research, his extensive experience with LDV measurements and systems and with finite-difference analyses of complex flow phenomena has enhanced and will continue to enhance our research capabilities. The interests and goals of the principal investigators and their graduate students indicate personal commitments and potential contributions for many years to come.

RESEARCH TOPICS

1. COMPONENT ANALYSIS AND MODELING OF BASE FLOW DURING POWERED FLIGHT

The base flow problem for powered missile flight has been the subject of strong analytical, computational, and experimental efforts during the three-year contract. The majority of this research work has investigated the transonic and supersonic flight regimes through somewhat varied methods. The results have demonstrated new insights into the treatment of different components of the near-wake region and have led to more accurate analyses.

1.1 Base Pressure During Powered Transonic Flight

Attempts have been made to examine the transonic base pressure under power-on, small jet pressure ratio conditions by a new computational scheme. The idea of an asymptotic equivalent centerbody, based on a one-dimensional area-ratio relationship, seems to offer a reasonable approach to the problem.

In this method, the outside transonic slipstream was described using the equivalent body concept of Professor W. L. Chow. The pressure field was produced from the transonic inviscid flowfield calculations with the equivalent body geometry. A simple recompression/reattachment analysis was employed to describe the viscous flow process near the two-stream confluence point near the end of the wake.

The preliminary results which were obtained using this analysis indicated correct trends for predicting the effects of the jet pressure ratio, Mach number, and Reynolds number. The additional model of transonic flow past a forward-facing step must be developed if the regime of high jet pressure ratio is to be explored.

1.2 Base Flow During Powered Supersonic Flight

Refinement of the component flow model for the prediction of base flow phenomena during powered supersonic flight was continued as part of this research effort. The Chapman-Korst component flow model [1] and its computer implementation [4] have served as the starting point for the flow model and the computer program enhancements. While the base pressure and temperature are the primary variables of interest, the following factors are also of interest:

(1) The prediction of the onset of plume-induced freestream separation and of the stable freestream separation location;

(2) The analysis of boundary layer effects as equivalent bleed into the base region and as an origin shift for the mixing regions;

(3) The significance and validity of potential recompression models; and

(4) The prediction of the effects of non-uniform propulsive nozzle flow on base flow.

In general, the analyses of Items (1) - (3) were based on gross empirical representations of the phenomena involved and Item (4) was by a well established approximate throat flow solution coupled with a Methods of Characteristics solution for the nozzle flowfield. While the empirical models and refinements improve the engineering usefulness of these programs, they also point to the need for better and more detailed experimental results and theoretical understanding of the flows.

Each of the above items has been investigated and has resulted in computer program enhancements. A brief description and the status of each of these programs is given in Appendix A-1.

2. COMPONENT ANALYSIS AND MODELING OF BASE FLOW DURING UNPOWERED FLIGHT

The flowfield associated with the flight of a projectile at transonic and supersonic speeds has been the subject of new and modified analyses. The research effort was to investigate new techniques and insights into the modeling of the near-wake flowfield. Once again the effort was along computational and analytical lines and a number of significant results were achieved.

2.1 Transonic Flow Past an Unpowered Missile

A computational model for determining the base pressure of a projectile within the transonic flow regime has been successfully developed by Professor W. L. Chow. The study employs the equivalent body concept to calculate the flowfield of a blunt-based projectile traveling in the transonic regime. The inviscid transonic flow is solved by finite-difference calculations of the axisymmetric potential equation where the displacement effect of the attached, turbulent viscous layer on the body is also taken into account. The viscous flow processes behind the base are treated through integral formulations.

The pressure field was produced from the transonic inviscid flow calculations with the equivalent body geometry, while the parameters needed to describe the equivalent body within the separated flow region were determined by the viscous flow mechanism. This is an illustration of its characteristic strong viscous-inviscid interaction.

The outstanding feature of this approach was that both the point of reattachment and the fully-developed wake flow state are saddle point singularities of the systems of ordinary differential equations describing the viscous recompression and redevelopment flows. Reasonable base pressure results were obtained for the transonic flow past a six-caliber secant-ogive-

cylinder projectile. Another important item of achievement was the successful development of the definition of the base pressure within this flow regime.

The details of this research effort were presented by Professor Chow at the Huntsville Symposium on Rocket/Plume Fluid Dynamic Interactions. The symposium paper has been included in this report as Appendix B and the computer programs are briefly described in Appendix A-2.

2.2 Supersonic Flow Past an Axisymmetric Unpowered Missile

The near-wake flow behind blunt-based bodies of revolution has been the subject of a research effort conducted by Professor H. H. Korst. The analysis is based on the component model and incorporates a number of new techniques to handle the influence of transition in the jet mixing region which develops within the expanded rotational shear layer.

The analysis assumes locally similar dissipative straight line entrainment profiles which are superimposed on the inviscid constant pressure slipstream contours. Then the region of pressure rise is excluded from the analysis by utilizing a semi-empirical wake closure criterion based on isentropic recompression of the stagnating streamline to a pressure level prescribed by the concept of incomplete turning of the external, inviscid flow. The treatment of the external slipstream past the boattail and near-wake is carried out by utilizing the method of sequential centered expansions.

Computer programs have been developed (see Appendix A-3) which arrive at entire flowfield solutions in a few iterative steps and produce detailed quantitative information on the transitional exchange mechanisms. This feature will provide potential support for global numerical fluid dynamic exercises. The symposium paper presented by Professor Korst is included as Appendix C and should be consulted for further details.

3. PLUME EFFECTS ON AFTERBODY AND BASE FLOWS

The advent of rocket powered flight initiated many research investigations which used a modified Chapman-Korst component model to predict the base region flowfield resulting from the interaction between the freestream flow and the rocket exhaust plume. During the launch phase of a powered vehicle, due to continually decreasing ambient pressure, the exhaust plume rapidly expands sometimes to a diameter much larger than the overall vehicle diameter. The resulting plume interaction with the freestream flow can initiate separation of the turbulent boundary layer upstream of the physical corner of the base. In any case, the nature and characteristics of the plume effects on the afterbody and near-wake flowfields are important factors in predicting the overall missile aerodynamic response. The analysis and modeling of jet plume effects have been an important research effort conducted under the sponsorship of the three-year contract.

3.1 An Overview of the Analysis and Modeling of Plume Effects on Missile Aerodynamics

The propulsive jet exiting from the rocket nozzle will interact with the external freestream flow in various degrees and modes and will affect both missile propulsive efficiency and aerodynamic performance. A thorough understanding of the physical phenomena of plume/freestream interaction is needed in order to develop predictive and interpretative capabilities through analytical and experimental methods. The central objective rests with the predictability of prototype performance from model studies.

In an effort to understand the plume effects on missile aerodynamics, a mutually supportive and cooperative program must involve analytical, experimental, and computational activities. Due to the complex nature of the flowfields arising from vehicle geometries, attitude, and the aerodynamic

interaction between the slipstream and propulsive jet, each of these activities has its own inherent limitations.

Analytical models stress the importance of strong interactions between inviscid and viscous flow mechanisms. Experimental activities receive guidance from analytical insights gained and thus focus on both component and system testing. Large-scale numerical efforts, aided by the availability of high capacity, high speed digital computers, are now being directed towards the solution of the base flow problem.

An attempt has been made by Professor H. H. Korst to categorize the tasks and the limitations imposed on the analytical, experimental, and computational efforts. The potentials and shortcomings of such supportive activities are examined individually in relation to each other and with respect to their needs for mutual support by organized interactions. Professor Korst's research on these activities was presented as a paper at the Symposium on Rocket/Plume Fluid Dynamic Interactions in Huntsville, Alabama and has been included in this report as Appendix D. The details of Professor Korst's analysis of the mutual interactions illustrate the unity-in-purpose leading to better defined and organized cooperation.

3.2 Plume-Induced Interference Flow

The interaction of rocket or jet plumes with the external flowfield and surrounding launch equipment is crucial to system performance. Such interactions determine the near-wake base pressure and temperatures, the flow over portions of the vehicle surface in the case of upstream external flow separation, the wake flowfield at angle-of-attack, and afterbody-mounted control surface effectiveness. The plume/slipstream interference flowfield affects aerodynamic performance by introducing drag penalties.

The generation of rocket or jet plumes in wind tunnel investigations must account for all or part of the factors affecting the induced flowfield. These factors include plume shape, plume deflection, mass entrainment along the shear layers, wake closure, viscous effects, temperature, and the influence of specific heat ratio and molecular weight. Professor R. A. White has conducted a research effort to determine the importance of each of the individual factors listed above. The details of his effort were presented at the Huntsville Symposium on Rocket/Plume Fluid Dynamic Interactions and the associated paper is included in this final technical report as Appendix E. Professor White discusses new research and analysis which has pointed to improvements and clarifications in the application of an analytical methodology for proper modeling between prototype and wind tunnel models.

Professor White has determined that the concept of modeling by congruent plumes of proper pliability leads to the correct simulation of plume-induced flows without the necessity for multiple empirical correlating factors. The details of this research effort are found in Appendix E and applicable computer programs are given in Appendix A-4.

3.3 Wind Tunnel Simulations of Plume-Induced Interference Effects

Under the objectives of the three-year contract, a theoretical and experimental program has been conducted in support of modeling of plume-induced aerodynamic interference effects in wind tunnels. The cooperative research project on axisymmetric flow over afterbodies involves a joint effort between the following:

(1) Professors Korst and White at the University of Illinois under the sponsorship of the U.S. Army Research Office;

(2) The U.S. Army European Office of Research under contract DAJA 37-81-C-1213; and

(3) The Aeronautical Research Institute of Sweden (FFA).

Experimental studies of aerodynamic interference effects caused by strongly underexpanded propulsive jet plumes often require the modeling of hot propellants by low temperature inert gases in wind tunnels. Mathematical modeling leads to the specification of geometrically distorted nozzle configurations and the selection of jet surface Mach numbers which assure geometrical congruence of the prototype and model plumes (with respect to initial plume slope and plume surface curvature) and plume stiffness as it interferes with the external slipstream.

Plume-induced interference effects on afterbodies with a centered jet have been simulated in wind tunnels at the Aeronautical Research Institute of Sweden, FFA (Bromma, Sweden), since 1966. An experimental facility using hot Freon 22 as the "prototype" gas (γ = 1.16) and air as the "model" gas (γ = 1.4) has been constructed by FFA for jet plume simulation. This facility has served to evaluate the merits and potential of the plume simulation methodology suggested by Korst under restricted conditions and at high angle-of-attack. The complex external flowfield is generated by aft-mounted controls in combination with angle-of-attack. Professors Korst and White have provided the overall scientific planning, guidance, coordination. and evaluation of the results.

The basis for the Korst modeling methodology is the assumption that the prototype plume is properly simulated by a model plume if the two plumes have the same contour in the flowfield adjacent to the afterbody. This means that the initial plume deflection angle and the plume radius of curvature (shape) must be duplicated by the model plume.

The validity of this modeling scheme was checked at FFA by comparing results for nozzles designed for gases with different specific heat ratios.

The results confirmed the validity of the Korst modeling methodology not only for the design jet pressure and zero angle-of-attack but also for off-design jet pressures and complex external flowfield disturbances generated by deflected aft-mounted control fins in combination with angle-of-attack.

The details of the joint research effort were presented in a paper at the Huntsville Symposium on Rocket/Plume Fluid Dynamic Interactions which has been included in this final technical report as Appendix F. The authors, S-E. Nyberg and J. Agrell, acknowledged the contributions of Professor H. H. Korst and Professor R. A. White to their program and the stimulating and fruitful cooperation they had received.

4. SMALL-SCALE BASE FLOW EXPERIMENTS UTILIZING A LASER DOPPLER VELOCIMETER

A strong research effort was begun under the sponsorship of this three-year contract to conduct small-scale base flow experiments and provide well-documented base flowfield data for comparison with analytical and computational models. The experiments utilize small-scale models of various base flowfield configurations and provide pressure and velocity information. The assembly and modification of a laser Doppler velocimeter (LDV) package during the past three years have produced a state-of-the-art measurement tool for making turbulence-type measurements in the near-wake flowfield.

The selection and assembly of an LDV system best suited for our needs has absorbed a substantial amount of time and resources but has produced a non-intrusive measurement tool quite useful in the experimental study of the base flowfield. Currently the research group under the direction of Professor A. L. Addy has four Ph.D.-level graduate students who anticipate making LDV measurements of numerous fundamental base-flow configurations.

The research effort towards making LDV measurements of the base flow region is motivated by the following research objectives:

- To develop expertise and facilities for making LDV measurements in high-speed flows with imbedded separated flow regions;
- To investigate separated flow mechanisms in plane, two-dimensional configurations; and
- To investigate axisymmetric base flows in the supersonic and transonic flow regimes.

The primary objective is to provide new, extensive, and well-documented data and thus obtain a better understanding of the basic fluid dynamic mechanisms existing in the base flowfield. The two-dimensional experiments concern the growth, development, recompression, and reattachment of a compressible turbulent free shear layer. Also examined are the effects of plume-induced and shock-induced separation of a turbulent boundary layer.

The scope, development, and status of this research effort was discussed in detail in a paper presented at the Symposium on Rocket/Plume Fluid Dynamic Interactions at Huntsville, Alabama. The paper by Professor Addy and co-workers is included in this report as Appendix G-1 and may be consulted for further details concerning development of the LDV and the two-dimensional experiments.

The two-dimensional supersonic experiments which are described in Appendix G-1 have required a significant number of small-scale models to be built. In order to illustrate the type of models which were designed and fabricated, numerous photographs of the two-dimensional models used in the investigations are included as Appendix G-2.

The physical setup of the laser Doppler velocimeter can be seen in Figure 1 of Appendix G-2. This photograph illustrates how the laser, optical elements, and photodetectors are mounted on the traversing table and situated

about the wind tunnel test section. A closer view of the wind tunnel test section and the collecting optics can be seen in the photograph which is reproduced as Figure 2 of Appendix G-2. The test section which is depicted in these photographs was the expansion/compression model (see text of Appendix G-1) used for the study of LDV particle dynamics.

A series of small-scale experiments on the initial development of a free shear layer and the effects of the recirculating flow are currently underway. Before adding the complexity of a strong expansion and recirculating flow, the problem of the development of a constant pressure free shear layer is being investigated. The small-scale model is a two-dimensional backstep with mass injected into the base region through a porous plate in quantities just sufficient to produce a free shear layer with no expansion at the corner. A photograph of the porous plate/backstep model is shown in Figure 3 of Appendix G-2.

The equipment currently being used in a blowdown mode wind tunnel operation to investigate the reattachment process include three varying modes, namely

(1) reattachment of a free shear layer on an inclined ramp (Figure 4 of Appendix G-2);

(2) reattachment of a free shear layer on a plane wall after a backstep (Figure 5 of Appendix G-2); and

(3) impingement of two free shear layers creating a compliant boundary for reattachment (Figure 6 of Appendix G-2).

A close-up view of the wind tunnel test section window (Figure 7 of Appendix G-2) and models (Figure 8 of Appendix G-2) shows the large number of static pressure ports and the anodization for LDV purposes.

A number of test models have been built for an investigation of the effects of shock-induced separation on a turbulent boundary layer. The study will utilize compression ramps of various angles to produce separation.

Several of the small-scale models are shown in the photographs of Figures 9 and 10 of Appendix G-2. The wind tunnel models illustrated in Appendix G-2 are representative of the type of models and test sections which have been built under the sponsorship of this contract in order to conduct small-scale LDV experiments.

The foundations for the research effort into small-scale two-dimensional experiments and development of the LDV have progressed quite far in the three years of the contract. A strong commitment of time and interest on behalf of Professor Addy and his graduate students has begun to produce meaningful data. The laser Doppler velocimeter measurements, extensive static pressure measurements, and flow visualization pictures should provide detailed information on some of the very basic mechanisms of the near-wake region.

The computer programs developed by Professor Addy (see Appendix A-1) demonstrate a comprehensive understanding of the base region component analysis and illustrate the need for extensive, well-documented data. The processing and statistical analysis of the LDV measurements, facilitated by the computer programs listed in Appendix A-5, will provide new insight into the velocity and turbulence characteristics of many mechanisms in the near-wake flowfield.

5. THE EFFECTS OF SUDDEN EXPANSIONS AND COMPRESSIONS ON BOUNDARY LAYER MOMENTUM THICKNESS IN A SUPERSONIC FLOWFIELD

The afterbody boundary layer and the development of the initial wake shear layer have been shown to be quite important to the evaluation of the near-wake flowfield. Prediction of the initial shear layer velocity profile is essential to the mixing layer analysis of the base region flowfield. An analytical and experimental study of the effects of expansions/compressions on the boundary layer thickness parameters was conducted during this contract.

The investigation examined the changes in momentum thickness which occurred as an afterbody boundary layer encountered a sudden expansion (boattail junction) or a sudden compression (flare). Measurements were made in a supersonic wind tunnel in order to provide data for correlation with an approximate theoretical model. The results indicated that an integral analysis provided an adequate prediction of changes in momentum thickness for the range of variables investigated. Professor R. A. White and graduate research assistant L. P. Hampton suggest further investigation of the mechanisms should be based on a laser Doppler velocimeter study.

The details of the analysis and experiments are provided in a summary paper included as Appendix H.

6. NEAR-WAKE ANALYSIS WITH THE METHOD OF SEQUENTIAL CENTERED EXPANSIONS

A new method has been investigated for treating jet and slipstream boundaries for cases of missile flight at supersonic speeds. The method of sequential centered expansions is based on a solution of the differential equation governing axisymmetric potential flow and is quite convenient for handling axisymmetric wakes in both powered and unpowered flight.

The details concerning the method of sequential centered expansions are given in a summary paper included as Appendix I. Further information concerning the method and its application can be obtained by contacting Professor H. H. Korst at the University of Illinois.

The method of sequential centered expansions has been incorporated into the analyses of powered and unpowered flight and plume modeling. The published papers which include this method appear in Appendices C, E, F, and K. The title and description of the pertinent computer programs can be found in Appendix A-3.

7. WAKE RESPONSE TO TRANSIENT PRESSURE DISTURBANCES

Non-steady phenomena during the early phases of the launch of missiles involving large amplitude pressure waves have been suspected of causing structural failures and of generating high impulse noise levels. A flow model was proposed for analyzing these phenomena based on well-established flow components. An experimental investigation was conducted under the sponsorship of this contract in order to verify both the physical and computational aspects of the components and their interactions. Excerpts from the M.S. thesis of graduate research assistant M. J. Marongiu are included as Appendix J and indicate the nature and conclusions of the experimental effort.

The flow configuration utilized in the study of the missile launch problem, as shown in Figure 1 of Appendix J, consisted of a converging-diverging nozzle discharging into a smooth channel of larger but constant cross-sectional area. The channel ends with an adjustable area reduction which produces a secondary constriction or nozzle. The dimensions of the model configuration (see Figure 2 of Appendix J) and the data acquisition system (see Figure 3 of Appendix J) indicate the nature of the two-dimensional experiments.

The non-steady operation of such a system can be expected to exhibit the following patterns:

(1) The jet emerging from the nozzle expands forming a plume which impinges on the wall (base flow problem). This will subsequently produce multiple shock wave interactions which result in subsonic flow at the entrance of the downstream (secondary) nozzle.

(2) Since irreversibilities are sustained in the flow, the local stagnation pressures will decrease, thus to maintain a steady flow would require an enlarged secondary throat area that satisfies $A^*_{II}/A^*_{I} = P_{0I}/P_{0II}$. If the area ratio of the downstream nozzle is too small, this Mach number cannot be sustained in steady flow and a left-running wave will form.

(3) The difference in the mass flowrates between the choked primary and secondary nozzles will then be stored behind the moving shock.

(4) If the traveling shock proceeds so far upstream that it reaches the end of the wake, the plume impingement is eliminated, and as the jet detaches from the wall, the flow irreversibilities decrease and the stored mass will soon discharge through the secondary nozzle.

(5) The free jet emerging from the nozzle will begin to entrain mass thus reducing the pressure near the nozzle exit and will eventually form a closed wake with resulting plume expansion and impingement.

If all these events were to occur, a cyclic system operation would result.

The analysis of the problem established criteria which made possible the quantification of the geometric and operational parameters in order to arrive at an understanding of the conditions under which non-steady operation can be expected and which time scales and pressure amplitudes can be predicted. Some of the experimental results are illustrated in Figure 4 of Appendix J. Figure 5 of Appendix J shows some of the results of the water table modeling.

Extensive computer programs have been developed in support of this study and are identified in Appendix A-3 of this technical report.

Despite the highly simplified analytical model reported here, the identification of the secondary throat area ($A_{e_{II}}$) as a critical parameter -- provided that the system configuration allows for the development of the fluidic mechanism and near-wake formation and that critical flow prevails through the exit nozzle -- has been possible.

Furthermore, the verification of the base pressure oscillations as being nearly periodical will aid in the prediction of the overall system behavior with regard to oscillation amplitude and frequency.

Detailed modeling of the fluidic entrainment mechanism as a basis for near wake development as well as accurate experimental data for the changes in base pressure levels during pump-down will be the subject of follow-up phases in this research area.

8. WAKE FLOWS OF TUBE LAUNCHED ROCKETS

The complex viscous interactions which occur during a rocket launch from a tube are quite similar in analysis to the mixing which occurs in a base region shear layer. The impingement of the underexpanded nozzle outflow on the launch tube wall creates a shock and recompression system very well suited to the Chapman-Korst component analysis. Through a joint effort between Professor H. H. Korst of the University of Illinois and Professor J. J. Bertin of the University of Texas at Austin, an analytical and experimental investigation of the flowfield for tube-launched rocket configurations was conducted.

8.1 Secondary Flows for Tube-Launched Rocket Configurations

Due to the large variety of military rockets which are launched from confined tubes, an investigation was conducted in an attempt to utilize the Chapman-Korst component analysis to predict the resulting tube flowfield during missile launch. The investigation was motivated by a need to predict the possibility of unbalanced forces acting on the rocket due to the secondary flow in the annular gap between the rocket and the launcher wall. The particular details of the analysis and experimental data were presented in an AIAA paper and are included in this report as Appendix K.

Theoretical solutions were computed for the flowfields which exist when an underexpanded nozzle is exhausted into a constant-area launch tube such that the impingement shock wave is relatively weak and the downstream flow remains supersonic. The theoretical flows were compared with experimental

data for various nozzle/launch tube configurations. For the test program, unheated air was accelerated to supersonic speed through converging-diverging nozzles over a wide range of stagnation pressure. An engineering model for the impingement flowfield was proposed, the computed flowfield solutions were compared with experimental results, and solutions were presented to illustrate the effects of variations in specific heat ratios. The theoretical wall static pressure distributions in the impingement region and the calculated value for the stagnation pressure for which there is no secondary flow in the annular gap were found to be in good agreement with the experimental data.

A limited number of computer programs were developed for this analysis and are listed in Appendix A-3.

8.2 Launch-Tube Flowfield Technology Based on Cold Gas Simulations, Flight-Test Measurements, and Theoretical Models

Modeling of the viscid/inviscid interactions which occur when a rocket is tube-launched requires knowledge of the important parameters. When a highly underexpanded nozzle exhausts into a tube, the pertinent parameters can be identified as follows:

(1) the nozzle exit angle;

(2) the nozzle exit Mach number;

(3) the ratio of specific heats for the gas;

(4) the jet expansion ratio; and

(5) the radius of curvature of the plume.

In many designs, the launch tube is not of constant area, thus the constrictions to the exhaust flow may radically alter the flowfield.

Once again Professor H. H. Korst and Professor J. J. Bertin have conducted an investigation of the launch tube flowfields which result when a highly underexpanded supersonic nozzle exhausts into a launch tube. The

details of their research were presented at the Symposium on Rocket/Plume Fluid Dynamic Interactions held in Huntsville, Alabama in the form of a paper which is included in this report as Appendix L. The analytical approach, experimental results, and comparisons of each are outlined in detail in Appendix L along with the important conclusions to be drawn.

9. COMPUTATIONAL FLUID DYNAMICS

The solution of the near-wake flowfield by computational means requires the investigation of various methods of grid generation and separated flow solution techniques. Professor W. L. Chow and his graduate students have conducted significant computational experiments under the sponsorship of this contract.

9.1 Turbulent Flow Past an Isolated Airfoil with Separation

A numerical study of the turbulent, compressible flow past an isolated airfoil with trailing edge separation was conducted for an NACA-4412 airfoil at an angle-of-attack of 13.87°. The airfoil was considered confined within a wind tunnel and computations of the flow were carried out successfully based on the Navier-Stokes equations. The computational scheme was supplemented by using a $\kappa - \varepsilon$ turbulence model. The physical region was transformed into a rectangle by adopting a body-fitted coordinate system.

The predicted pressure distribution on the surface of the airfoil agreed very well with the experimental data. The structure of the turbulence was also simulated reasonably well.

The specifics of this numerical investigation of the stalled airfoil can be found in the Ph.D. thesis of C. M. Rhie [8]. The results of this numerical study were presented at the 1981 Conference on Complex Turbulent Flows (Stanford) [9] as well as the Third AIAA/ASME Joint Conference on Thermal

Physics, Fluid, Plasma, and Heat Transfer held at St. Louis [10]. A brief description of this computer program is included in Appendix A-2.

9.2 Flow Within Ducts of Arbitrary Geometrical Configurations

A numerical investigation of the developing flow within square, rectangular, and trapezoidal ducts was conducted in an attempt to experiment with algorithms and boundary conditions for internal flows. The developing duct flow for an arbitrary cross-sectional geometry was calculated based on the Navier-Stokes equations. The $\kappa - \varepsilon$ turbulence modeling was incorporated into the Navier-Stokes solution with an additional algebraic stress model to account for the secondary flow of the second kind which occurs within the fully-developed flow region.

A detailed and thorough explanation of the objectives, techniques, and results of this numerical investigation is given in the Ph.D. thesis of A. Nakayama [11]. Professor Chow and Professor Nakayama have also presented the results of their research effort at the 1981 Conference on Complex Turbulent Flows (Stanford) [12] and have submitted a paper on this topic which will be published in an upcoming volume of the Journal of Fluid Mechanics [13].

10. COMPUTATIONAL ANALYSIS OF RELATED RESEARCH TOPICS

A number of important and interesting physical problems have been investigated computationally in an effort to develop certain numerical techniques. Although the geometry of the numerical experiment is not directly a base flow configuration, the goal is to obtain some expertise in handling the numerical solution of a separated flow.

A promising technique for numerical solution of a separated flow region exists through the hodograph transformation. As a result Professor Chow and

his graduate students have conducted some research into the applicability of the hodograph transformation method for near-wake type analysis.

10.1 Asymmetric Nozzle as a Vector Thrust Device

A numerical study was conducted into the feasibility of using an asymmetric nozzle as a vector thrust device. The investigation employed the method of hodograph transformation for calculation of the flowfield. The calculation predictions were compared and verified using the results of experiments conducted in the laboratory. Cases of choked and unchoked flow have been examined, and the results substantiate the concept of producing vector thrust from these devices.

The details of this numerical investigation are available in the Ph.D. thesis of C. W. Wu (see Appendix M). The name and brief description of the computer program developed from this research effort can be found in Appendix A-2.

10.2 Incompressible Potential Flow Influenced by Gravitation

Once again the method of hodograph transformation was examined with emphasis on its applicability to complex separated flows. In this instance the method was employed for potential flow problems with an extension for incompressible flow where gravitation exerts dominant influence on the flow solutions. Indeed, many open channel flow problems where solutions have not been well established can be treated successfully through this technique.

The types of incompressible potential flow problems suitable for this method include the following:

(1) Free overfall;

(2) Flow past a sluice gate;

(3) Flow past a sharp-crested weir; and

(4) Curved channel flow.

Each of these problems has been successfully calculated and a number of Ph.D. theses and journal articles document the results (see Appendix M).

The computer programs which were developed during this research effort are titled and briefly described in Appendix A-2.

11. AXISYMMETRIC EXPERIMENTS CONCERNING REATTACHMENT

An experimental investigation was conducted in an effort to examine the static pressure characteristics of an axisymmetric jet reattachment onto a cylindrical wall. The study examined sonic and supersonic underexpanded jets exhausting from a nozzle into a sudden enlargement. The research effort by M. J. Morris was conducted under the guidance of Professor A. L. Addy and studied the effects which each parameter had on the recompression/reattachment process.

The experiments were made for the continuous flow of a compressible fluid, namely air. The test model was axisymmetric in nature and could be fitted with either a converging or converging-diverging nozzle to produce the appropriate Mach number entrance flow. Entrance Mach numbers of 1.0, 1.5, and 2.05 were produced for various cases. The data were also collected for various values of the nozzle exit-to-enlargement area ratio, A_1/A_2, and base pressure ratio, P_B/P_0. The data were produced by means of an extensive array of static pressure taps distributed circumferentially about the tube in a manner which provided a fine grid of axial tap locations.

The primary objective of this experimental investigation was to produce data on the recompression/reattachment process. The resulting data are shown graphically in the six figures which are included in this report as Appendix O and represent new data for this type of reattachment process. The plotted data are shown for three different area ratios, A_1/A_2, three different Mach

numbers, M_1, and two base pressure ratios, P_B/P_0. The characteristic pressure rise in the vicinity of reattachment is quite evident and reaches locally high levels.

CONTINUING AND FUTURE RESEARCH ACTIVITIES

Much of the research conducted during this contract focuses on the base flow problem and related analytical, computational, and experimental interests. The complex nature of the near-wake flowfield indicates that many fundamental and interesting questions have still been unanswered. The four principal investigators, as well as many of the doctoral graduate students, have a strong commitment and interest in continuing the research effort associated with the investigation of the fundamental mechanisms associated with missile flight.

The research activities which are considered of primary interest and warrant continuing and future emphasis can be generally described as follows:

(1) Small-scale wind tunnel base flow experiments utilizing laser Doppler velocimetry as a fluid dynamic investigative tool;

(2) Power-off transonic base flow analysis; and

(3) Transient and quasi-steady aspects of the near-wake mixing phenomena.

Small-Scale Experiments Related to Near-Wake Flows

In the general description of the near-wake flowfield, the separation of a boundary layer to form a free shear layer, the development of the free shear layer in the presence of a recirculating flow, and the recompression/reattachment of a free shear layer were identified as fundamental flow mechanisms for which little detailed experimental data are available. If analytical and computational models are to be improved and refined, these data are certainly needed. As a result, three separate but related series of experiments are underway which should provide new insight and data concerning these basic flow mechanisms. The experiments, which are described in Appendix G-1, can be briefly categorized as follows:

(1) An investigation of the formation and development of a two-dimensional, turbulent free shear layer;

(2) An investigation of reattachment and redevelopment of two-dimensional compressible, turbulent free shear layers; and

(3) An investigation of the two-dimensional turbulent base flow in the presence of an inner exhaust jet.

The small-scale two-dimensional experiments will focus on extensive laser Doppler velocimeter (LDV) measurements and static pressure surveys of the fundamental mechanisms in the near-wake region.

A significant amount of time, energy, and finances have been expended to assemble and make operational a two-component, two-color LDV system. The measurement tool has already been used for studies of particle dynamics and biasing problems and is currently being used to make measurements in the free shear layer produced by supersonic flow over a backstep. The long-range commitment of Professor A. L. Addy and four of his doctoral graduate students is based on their perception (with agreement in the literature) of the suitability of an LDV measurement tool to the separated base flowfield, as well as the significant experimental data able to be obtained through the use of this state-of-the-art tool.

The research group of Professor Addy has already made plans (funded by the U.S. Army Research Office and the Department of Defense equipment grant) to add the following new instrumentation:

(1) a third velocity component measurement capability to our present two-component LDV system;

(2) a 5-watt argon ion laser (completed);

(3) a super mini-computer based laboratory data system for acquiring and processing LDV and hot-wire anemometer data; and

(4) a computer-controlled traverse system to be incorporated with our present manual LDV traverse system.

The complex nature of near-wake base flow experiments requires precision test facilities and state-of-the-art data measurement, acquisition, and analysis systems. The experiments conducted with these types of research tools will provide insightful data and information regarding the fundamental base flow mechanisms.

Power-off Transonic Base Flow Analysis

The modeling and analyses of the power-off base pressure problem currently under development will be continued in the future. The flow model is promising and has demonstrated the relative importance of base drag on system performance. The idea of using the equivalent body concept to solve the base flowfield of a projectile in a transonic flow has proven quite viable and modification and improvement of the analysis is continuing. The intention is to extend the flow regime to include low supersonic freestream Mach numbers.

Unsteady Mixing Layer Phenomena

Detailed studies of pressure-induced separation problems and free-jet recompression/reattachment problems are underway and planned for the future. The interest is motivated by the appearance of very high levels of turbulent fluctuations and high frequency oscillations in near-wake flowfields. A critical examination of transient mechanisms, which are related to separated flow processes, is needed at this time because of their importance for highly accelerating missiles and their implications for large-scale CFD calculations.

CONCLUSIONS AND RECOMMENDATIONS

The research effort directed at an understanding of the fundamental fluid dynamic mechanisms of separated flows has produced a significant amount of new information and provided new insight into the base flow problem. The support of this research contract has served to unify the efforts of the four principal investigators and their graduate research assistants and provide a balanced analytical, computational, and experimental investigation of the near-wake flowfield and related fluid dynamic mechanisms. The strong representation of this research group at the Huntsville Symposium on Rocket/Plume Fluid Dynamic Interactions is a testimony to the contributions made towards an understanding of the missile base flow and also an indication of the strong commitment of interest, time, and effort towards maintaining a strong technical expertise at the University of Illinois in the base flow area of research.

From the research conducted over the past three years, the following conclusions can be drawn. Some of those conclusions are the following:

(1) The research group has selected, assembled, and is currently using a state-of-the-art laser Doppler velocimeter system to make turbulence and velocity measurements in small-scale near-wake flowfields. The two-color, two-component LDV system has proven itself to be a useful tool for making instantaneous velocity measurements in the boundary layer, shear layer, and recirculating region of a typical base flow configuration.

(2) Much of the equipment and models necessary for small-scale experimental investigations of the mechanisms of the near wake has been built and are currently being utilized for measurements. Experimental investigations of shear layer initialization and development, shear layer recompression/reattachment, shock-induced separation, and plume-induced separation. In all cases the LDV will be the primary measurement instrument, and significant new flowfield data will be obtained.

(3) The present components of the two-color LDV system will be supplemented within a year with three very significant new items:

(i) a new super mini-computer based system for the acquisition, storage, and analysis of LDV data;

(ii) the necessary optical and electronic components for a third velocity component LDV capability; and

(iii) a new computer-controlled traversing mechanism for the LDV which will provide better measurement volume control and placement.

The finances for these items have already been approved through the ARO Department of Defense equipment grant. The research group is currently evaluating and purchasing the new equipment.

(4) The computational research effort by into the transonic power-off and power-on missile base flow problem has shown significant new results based on the use of the equivalent body concept. Reasonable base pressure results for transonic flow past a six-caliber projectile prove the applicability of this new computational scheme.

(5) Success was obtained in developing an analysis and modeling theory for jet plume effects on afterbody and base flows. The ability to predict proper generation of rocket or jet plumes for wind tunnel investigations strongly depends upon proper simulation of the initial plume deflection angle and the plume radius of curvature.

(6) An analytical and experimental investigation has successfully predicted the changes in momentum thickness which occur as an afterbody boundary layer encounters a sudden expansion or compression. The supersonic wind tunnel measurements have provided data for correlation of the analysis.

(7) The numerical application of the method of hodograph transformation for separated flows has been successfully tested. The applicability of this method for asymmetric nozzle flow as well as flows influenced by gravitation has been established and indicates possible usefulness for base flow configurations.

Numerous other conclusions may be drawn from the research work which has been completed and are indicated in each separate instance throughout this technical report.

In addition, the research which has been conducted over the past three years has identified the following items for recommendation.

(1) The further development and application of the LDV for base flow experiments is strongly recommended in light of its ability to provide turbulence measurements and its suitability to separated flowfields. Although costly to initially establish and get running, the LDV system will produce much-needed data for a variety of base flowfield mechanisms and configurations.

(2) The relative success of Navier-Stokes solutions of the transonic and supersonic base flowfields indicates an ongoing need for further research into this area. Some of the methods developed by the Gas Dynamics Group at the University of Illinois warrant further investigation.

(3) Recent experimental and observational evidences point to the possible quasi-steady nature of the near-wake mixing region. Development of further research into the transient nature of the shear layer is strongly recommended.

As indicated throughout this technical report, much new information has been obtained through the U.S. Army Research Office sponsored research effort, but many questions about fundamental mechanisms remain still unanswered. Through the unified effort of analysis, computation, and experimentation, the research group at the University of Illinois will continue to provide new information and new ideas about the base flow problem.

REFERENCES

1. Korst, H. H., Page, R. H., and Childs, M. E., "A Theory for Base Pressures in Transonic and Supersonic Flows," University of Illinois, ME-TN-392-2, March 1955.

2. Carpenter, P. W. and Tabakoff, W., "Survey and Evaluation of Supersonic Base Flow Theories," NASA CR-97129, August 1965.

3. Page, R. H., "A Review of Component Analysis of Base Pressure for Supersonic Turbulent Flow," Proceedings of the Tenth International Symposium on Space Technology and Science, Tokyo, Japan, 1973, pp. 459-469.

4. Addy, A. L., "Analysis of the Axisymmetric Base-Pressure and Base-Temperature Problem with Supersonic Interacting Freestream-Nozzle Flows Based on the Flow Model of Korst, et al., Part III: A Computer Program and Representative Results for Cylindrical, Boattailed, or Flared Afterbodies," Report No. RD-TR-69-14, U.S. Army Missile Command, Redstone Arsenal, Huntsville, Alabama, February 1970.

5. Buchhave, P., "Biasing Errors in Individual Particle Measurements with the LDA-Counter Signal Processor," Proceedings of the LDA-Symposium, Copenhagen, Denmark, 1975, pp. 258-278.

6. Walsh, M. J., "Influence of Particle Drag Coefficient on Particle Motion in High-Speed Flow with Typical Laser Velocimeter Applications," NASA TN D-8120, February 1976.

7. Zarin, N. A., "Measurement of Non-Continuous and Turbulence Effects on Subsonic Sphere Drag," NASA CR-1585, 1970.

8. Rhie, C. M., "A Numerical Study of the Flow Past an Isolated Airfoil with Separation," Ph.D. Thesis, Department of Mechanical and Industrial Engineering, University of Illinois at Urbana-Champaign, 1981.

9. Rhie, C. M., Chow, W. L., and Sharma, D., "A Numerical Study for the Two-Dimensional Stalled Airfoil," Proceedings of the 1981 Conference on Complex Turbulent Flows, Vol. III, Stanford University, California, pp. 1318-1325.

10. Rhie, C. M. and Chow, W. L., "A Numerical Study of the Turbulent Flow Past an Isolated Airfoil with Trailing Edge Separation," Paper presented at the Third AIAA/ASME Joint Conference on Thermal Physics, Fluid, Plasma, and Heat Transfer, St. Louis, Missouri, July 1982.

11. Nakayama, A., "Three Dimensional Flow Within Conduits of Arbitrary Geometrical Configurations," Ph.D. Thesis, Department of Mechanical and Industrial Engineering, University of Illinois at Urbana-Champaign, 1981.

12. Nakayama, A., Chow, W. L., and Sharma, D., "Calculation of the Secondary Flow of the Second Kind Through a Fully Elliptic Procedure," Proceedings of the 1981 Conference on Complex Turbulent Flows, Vol. III, Stanford University, California, pp. 1312-1317 (also Vol. II, pp. 919-918).

13. Nakayama, A., Chow, W. L., and Sharma, D., "Calculation of Fully Developed Turbulent Flows in Ducts of Arbitrary Cross-section," paper to be published by the Journal of Fluid Mechanics.

APPENDIX A

LIST OF AVAILABLE COMPUTER PROGRAMS

APPENDIX A

APPENDIX A-1

APPENDIX A-1

LIST OF BASE FLOW COMPUTER PROGRAMS FOR POWER-ON SUPERSONIC FLIGHT AND OTHER RELATED COMPUTER PROGRAMS

A series of computer programs were developed to investigate power-on, supersonic base flows utilizing the Chapman-Korst component model. In addition, other computer programs have been developed as standalone programs which are used to enhance the component analysis. All programs are written in FORTRAN. In the following Table, the principal computer programs are identified and described. Since these programs are at different levels of development, the status of each of the programs is also given.

Information about these programs is available from Professor A. L. Addy.

TITLE	DESCRIPTION	STATUS
TSABPP-2	This program analyzes the non-isoenergetic power-on base-pressure and -temperature problem at supersonic flight speeds of a missile with a cylindrical or boattail/conical afterbody. This program includes several empirical enhancements. This program has served as the basis for further program development here and by other investigators.	Production
TSABPP-3	Same as TSABPP-2 but has been extended to include the prediction of the onset of plume-induced separation and the stable separation location. The separation criterion is based on an empirical correlation between pressure rise and local Mach number.	Research
TSABPP-4	Same as TSABPP-3 but has been extended to include non-uniform nozzle flow. Propulsive nozzles with relatively small throat radius of curvature can be analyzed.	Research

TITLE	DESCRIPTION	STATUS
COMPBL	A computer program to calculate the two-dimensional boundary layer flow of ideal gases. This program is based on the solution technique of Walz, et al. Program is used in conjunction with TSABPP-2, -3,-4 to analyze the effects of boundary layer on base flow.	Production
TRANNOZ	A computer program for analysis of transonic throat flow in axisymmetric, planar, and annular supersonic nozzles. Program is used in conjunction with TSABPP-2, -3,-4 to analyze the effects of non-uniform nozzle flow on base flow.	Production

APPENDIX A-2

APPENDIX A-2

LIST OF AVAILABLE COMPUTER PROGRAMS (CHOW)

A number of large-scale computer programs were developed by Professor W. L. Chow and his associates in order to investigate many techniques connected to numerical computation of the near-wake base flowfield. The codes are research in nature, cover a variety of fundamental flowfield features, and are written in the FORTRAN computer language. The following list of programs provides the title and brief description of each program's capabilities. Further information concerning any of these programs can be obtained from Professor W. L. Chow or any of his associates.

TITLE	DESCRIPTION
AIRFOIL	Computation of the incompressible flow past a NACA 4412 airfoil at large angle-of-attack. The analysis is based on the Navier-Stokes equation with $\kappa - \epsilon$ turbulence modeling.
ASYJET	Computation of the compressible flow discharge from an asymmetric nozzle utilized as a vector-thrust device. The analysis includes both choked and unchoked flow.
DEVFLW	Computation of the turbulent flow within non-circular ducts; broken down into two codes. I. Calculation of the fully developed turbulent flow with secondary flow within non-circular ducts. II. Calculation of the developing turbulent flow within non-circular ducts.
JETS 1,2,3,4	Programs dealing with calculation of the incompressible potential flow with gravitational effects. The analyses are based on the method of hodograph transformations.
JET1	Calculation of the incompressible flow for a circular contractor above a horizontal bed.
JET2	Calculation of the incompressible flow for a horizontal constant-area duct.

TITLE	DESCRIPTION
JET3	Calculation of the incompressible flow for a convergent curved nozzle.
JET4	Calculation of the incompressible flow for an asymmetric nozzle.
TRAPB	Analysis of transonic flow past a projectile including the computation of the base pressure. The analysis is based on the equivalent body concept.

APPENDIX A-3

APPENDIX A-3

LIST OF AVAILABLE COMPUTER PROGRAMS (KORST)

The research which was conducted during this contract produced a number of useful computer programs which deal with base flow and related problems. These computer programs are listed in this Appendix along with a brief description of the problems of interest.* Further information concerning these programs can be obtained by contacting Professor H. H. Korst. The programs are as follows:

NAME	DESCRIPTION/TITLE
SGMOTOR	Solid grain rocket motor analysis
HCROSS	Method of characteristics (MOC) for axisymmetric flow initiated from the Kliegel third-order transonic throat solution
WSHOCK	Linearized weak shock solution for streamline deflection at the plume boundary
NOCON	Initial plume slope and curvature for free jets produced by nonideal conical flow nozzles
JETC	Free jet flowfield and plume shape by axisymmetric MOC
P-M	Two-dimensional Prandtl-Meyer expansion
PCOR	Transformation of model to prototype operating conditions for design and off-design wind tunnel experiments
AB1/AB2/AB3	Chained series of programs using method of sequential center expansions for parametric studies of afterbody flow and transitional jetmixing in unpowered flight
MIX	Transitional jet mixing using a straight line profile, two-dimensional compressible, isoenergetic

*The computer programs are all research in nature and are written in the language BASIC.

NAME	DESCRIPTION/TITLE
TBART	Turbulent boundary layer development in convergent-divergent (cooled or uncooled) nozzle
TMIX	Transitional jet mixing, two-dimensional compressible, non-isoenergetic
CYLIMP	Inviscid-viscid plume impingement on cylindrical wall
MBLEED	Bleed requirements for plume-wall interaction modeling
NON-TIP	Theoretical flow analysis for non-tip-off launchers (quasi-steady)
NON-TIP/RM	Theoretical flow analysis of non-tip-off launchers (effect of rocket motion)
FLUIDIC	Quasi-steady mass entrainment in non-steady wake response
TSHOCK	One-dimensional non-steady wave propagation in launch tubes

APPENDIX A-4

APPENDIX A-4

LIST OF AVAILABLE COMPUTER PROGRAMS (WHITE)

A computer program has been developed by Professor R. A. White in order to facilitate his studies of the base pressure problem at angle-of-attack. The program is written in FORTRAN IV language and is well-documented for production use.

TITLE	DESCRIPTION
ALPHA30	Solution of the power-on base pressure problem for an afterbody at angle-of-attack. The program utilizes various empirical models for the recompression process.

APPENDIX A-5

APPENDIX A-5

LIST OF STATISTICAL AND LDV-RELATED COMPUTER PROGRAMS (ADDY)

The assembly and development of the LDV as a measurement tool have required the writing of accompanying software for acquisition and analysis of the data. The programs were developed and modified by the graduate students conducting research under the direction of Professor A. L. Addy. The language is primarily FORTRAN and any exceptions are duly noted. Any questions or inquiries regarding these programs can be directed towards Professor Addy or any of his graduate research assistants.

TITLE	DESCRIPTION
DEADZ FREQSH TURB1 TURB2 TURB3 TURB4	Analytical analysis of the effects of fringe biasing in highly turbulent high speed flows and flows with recirculation.
DELV	Digitally simulates the technique used by an LDV counter to discretize data in order to investigate the resolution of the system in highly turbulent flows.
DEVO MEANIE	Determination of the statistical uncertainty in LDV data in turbulent flows using normal distribution statistics.
HISTCK HISTGM	Simulation of digital counter operation. These programs examine the factors which influence LDV probability density distribution functions.
HIST1	Plots the LDV velocity histograms on a graphics terminal at the test location for data evaluation.
HIST2	Plots the LDV velocity histograms (both components) and the star chart for coincident two-channel data.
LAGEST LAGSIZE	Calculation of the velocity of solid spherical particles suspended in a compressible flowfield downstream of a normal or oblique shock wave.

TITLE	DESCRIPTION
LAGEST2	Calculation of the velocity of solid spherical particles suspended in an isentropic compressible flowfield with a specified Mach number distribution.
LVD1	Performs one-channel LDV data acquisition functions, including initiating DMA data transfer from counters, decoding data into actual velocities and time between data values, calculating mean, standard deviation, maximum, and minimum values, and writing the results onto a floppy disk. These programs are written in FORTRAN but use MACRO subroutines.
LDV2	Performs two-channel LDV data acquisition functions similar in nature to those of program LDV1. These routines are also written in FORTRAN but make use of MACRO subroutines.
LVDAT2	Performs two-channel data analysis including digital filtering, bias correction, coordinate rotation, and statistical analysis. Slight differences exist between the versions on the PDP 11-03 and those on the CYBER 175 computer.
LVTOT1	Performs one-channel total burst mode data acquisition functions, including initiating DMA transfer with the counter, decoding data, calculating mean, standard deviation, minimum, and maximum velocity values, calculating mean, minimum, and maximum number of zero crossings, and writing the results onto a floppy disk. These programs are written in FORTRAN but use MACRO subroutines.
PBIASB2	Calculates and plots the weighting factors to correct for fringe biasing effects including the effects of frequency shifting. This program is based on the analysis of Buchhave [5].
PBIASB3	Calculates and plots the weighting factors for fringe biasing effects in isotropic turbulence. This program is also based on the analysis of Buchhave [5].
PDRAG	Plots and compares oil droplet drag coefficient data obtained at the University of Illinois with the drag coefficient data of Walsh [6] and Zarin [7].
PDRAG1	Determines the drag coefficient, relative Mach number, and relative Reynolds number for oil droplets as they relax downstream of a shock wave.

TITLE	DESCRIPTION
PNSIZE	Calculates and plots curves relating LDV sample size to the percent error in velocity mean and velocity standard deviation.
PROBDET	Calculates the probability of particle detection in a two-component LDV for an elliptic turbulent flowfield.
TBD	Plots the histogram for the time between data point or number of zero crossings data.

APPENDIX B

BASE PRESSURE OF A TRANSONIC FLOW PAST A PROJECTILE

Paper presented at the

Symposium on Rocket/Plume Fluid Dynamic Interactions

Huntsville, Alabama

April 1983

by

Professor W. L. Chow

APPENDIX B

Base Pressure of a Transonic Flow Past a Projectile

by Wen L. Chow
Professor of Mechanical Engineering
University of Illinois at Urbana-Champaign
Urbana, Ill.

Abstract

An equivalent body concept is employed to examine the base pressure problem of a transonic flow past a blunt-based projectile. The inviscid transonic flow is solved by finite difference calculations of the axisymmetric potential equation where the displacement-effect of the attached turbulent viscous layer on the body is also accounted for. The viscous flow processes behind the base such as the turbulent jet mixing, recompression, reattachment and redevelopment are treated through integral formulations. The viscid-inviscid interaction is manifested by the fact that the viscous flow attaches onto the inviscid flow in the sense of the boundary layer concept, while the two parameters characterizing the equivalent-body geometry upon which the inviscid flow solution is based, are to be determined by the viscous flow processes. A definition of the base pressure, compatible with that for the supersonic flow regime, has been developed which is necessary for the transonic flow regime. It is found that with this scheme of analysis, both the point of reattachment and the state of fully developed flow (far-wake condition) are saddle-point singularities of the flow. Iterative processes must be followed to determine these two parameters so that the solution follows the separatrix joining the saddle points of the flow. Preliminary results for a six-caliber Secant-Ogive-Cylinder projectile have been obtained. It is expected that this scheme of analysis is useful throughout the incompressible and subsonic flow regime. Extension to cases with small angle of incidence is also discussed.

INTRODUCTION

It is well known that the base pressure problem is governed by the strong viscous-inviscid interaction mechanisms. Since the viscous flow region is usually located at the edge of the inviscid flow field, it is joined with the inviscid flow in the sense of the boundary layer concept, and the local inviscid flow guides the growth of the viscous layer. On the other hand, in direct association with the inviscid flow field, the geometry of the wake as well as the average pressure impressed on the base are entirely governed by the viscous flow processes of jet mixing, recompression, reattachment and redevelopment behind the body. The mutual dependency between the inviscid and viscous flows was pointed out first by Crocco and Lees[1]. Since that time much work has been done on base pressures[2-16]. It is not intended to present an exhaustive review on this subject. Interested readers may consult the recent review by Page[11]. It is worthwhile to note that almost all these investigations are restricted within the supersonic flow regime. Under this situation the governing equation of the external inviscid flow is hyperbolic. Other than limited few exceptions[15,16], all these analyses did not need the consideration of the process of redevelopment after reattachment to establish the base pressure solution for the problem.

In a more detailed study of recompression-reattachment of a turbulent free shear layer[14], it was learned that this same integral analysis can be employed to study the base pressure problem in any other flow regimes. Examination of base pressure problems of incompressible wedge flow was later carried out[17-19], and the overall elliptic inviscid flow field was established through conformal mapping. The viscous flow was guided by the established inviscid flow, while the characteristic parameters describing the inviscid flow were determined from viscous flow processes. It was learned that with the established potential flow, the point of reattachment behaves as a saddle-point singularity for the viscous recompression process. This method of analysis also led to the study of the flow past a backward facing step in both two-dimensional and axisymmetric configurations within the transonic flow regime[20-23]. Indeed, since the pressure field is established from the external inviscid flow, the external inviscid flow responds to the inner viscous flow events on the basis of an "equivalent body" concept. The solution of the inviscid flow was established by a finite-difference computation of the complete potential equation. Again, the point of reattachment behaves as a saddle-point singularity for the system of equations describing the viscous recompression process. Furthermore, it was learned that the pressure at the step cannot be taken as the base pressure. It is obvious that the step-pressure coefficient approaches zero as the free stream Mach number increases toward unity, while the base pressure coefficient decreases toward more negative values. It was recognized also that the study carried out up to this point constituted only the first approximation to the problem, since the established equivalent body from the more detailed viscous flow analysis was not yet compatible to the original equivalent body configuration selected to establish the inviscid flow.

It should also be noted that all these viscous flow studies were carried out under the assumption of isoenergetic flow processes, so that the need of the consideration of the energy principle was conveniently eliminated.

Additional study has been carried out on the transonic base pressure problem. Specifically, the base pressure of a six-caliber Secant-Ogive- Cylinder immersed in a transonic flow has been examined. The flow condition of the forebody, including the attached turbulent boundary layer prior to separation and the process of redevelopment after reattachment must be included into the consideration. It will be shown that the equivalent body for such a problem can be described with the help of two characteristic parameters. It will be also demonstrated that the point of reattachment and the state of fully developed flow are the saddle-point singularities of the recompression and redevelopment processes respectively. Again this behavior can be appropriately exploited to establish these two parameters. A new definition of the base pressure for the transonic flow regime will also be given, which is compatible with what has been accepted for the supersonic flow regime. The method of calculations and the procedures of iterations will also be presented so that the solution follows the separatrix passing through the saddle-points. Extension to the case of flow with small angle of attack will also be suggested and discussed.

ANALYTICAL CONSIDERATIONS

For an external flow around a body, the pressure distribution is the utmost item of concern which supplies the basic information for the lift, drag calculations. Inasmuch as the boundary layer concept is applicable, the pressure distribution is entirely determined from the inviscid flow geometry. For the present problem of flow past a projectile, the equivalent body geometry must be established before any viscous flow processes can be examined and studied.

The Equivalent Body

For a transonic flow past a projectile, whose typical configuration is shown in Fig. 1, it is expected that after the flow separates from the base, a usually turbulent jet mixing process occurs along the wake boundary. The dividing streamline is thus energized, preparing itself for the subsequent recompression and reattachment at the end of the near wake. After reattachment, additional compression of the shear layer occurs in the early part of the redevelopment before the pressure field decays toward that of the free stream. Based on the displacement concept of the boundary layer, the equivalent inviscid body boundary would be located away from the viscous dividing streamline by a distance of the displacement thickness, δ^*, of the viscous layer above the dividing streamline. This reasoning leads to the specification of the equivalent body $R_b(z)$ by

$$\text{i.} \quad R_b(z) = 0 \qquad \text{for } z < 0 \tag{1-a}$$

$$\text{ii.} \quad R_b(z) = R_{og} + \delta^*(z) \qquad \text{for } 0 < z < z_T \tag{1-b}$$

$$\text{iii.} \quad R_b(z) = R_{cyl} + \delta^*(z) \qquad \text{for } z_T < z < z_G \tag{1-c}$$

$$\text{iv.} \quad R_b(z) = \delta^*_{asy} + (R_{cyl} + \delta^*_b - \delta^*_{asy})\, e^{\left(-\frac{\Delta 2}{1-\Delta}\right)} \qquad \text{for } z_G < z < z_R \tag{1-d}$$

$$\text{where } \Delta = (z-z_G)/(z_R-z_G) \tag{1-e}$$

$$\text{v.} \quad R_b(z) = \delta^*_{asy} \qquad \text{for } z_R < z \tag{1-f}$$

The schematic sketch of the equivalent body of a projectile is shown in Fig. 2. It will be recognized that the parameters characterizing the equivalent body geometry are z_R and δ^*_{asy} for a specific projectile. It is also worthwhile to note that Δ varies from zero to unity when z is between points G and R and the second power employed in Eq. (1-d) assures the slope continuity of the profile at the base. Furthermore, it can be shown that under the far-wake condition, the displacement thickness of the viscous layer approaches a finite value even when the viscous layer thickness approaches infinity at far downstream locations.

For a given transonic Mach number, the inviscid flow field is established from relaxative finite difference calculations of the full potential equation. In fact it follows precisely the procedures as described in the study of transonic flow past a boattailed afterbody[24,25]. The growth of the turbulent boundary layer is estimated from an integral formulation, and its displacement effect is included into the consideration in obtaining the solution of the potential flow. Thus the boundary layer thickness, momentum thickness and its displacement thickness at the base are known as soon as the inviscid flow field is established.

Turbulent Jet Mixing, Recompression and Reattachment

The integral analysis of these flow processes follows precisely the early study of a flow past a backboard facing step[23]. Only a brief description of these considerations is given here. Again, isoenergetic flow condition is assumed throughout all viscous flow regions.

Immediately behind the base, a turbulent jet mixing process occurs along the wake boundary. As one would observe later, the pressure also decreases significantly along the path of mixing in the transonic regime. Nevertheless, the mixing process can be treated on the basis of a quasi-constant pressure analysis[26]. At each location, the velocity profile is derived from a constant local pressure calculation with the same initial boundary layer profile. The eddy diffusivity required to estimate the shear stress along the dividing streamline of the new mixing region originated from the corner of the base was estimated from

$$\varepsilon = \frac{1}{4\sigma^2} x u_e \tag{2}$$

where x is the distance along the path of mixing measured from the origin of mixing, u_e is the local free stream velocity and σ, the spread rate parameter, assumes the value of twelve throughout this series of computations. This mixing process is carried out until the section of lowest pressure along the wake is reached. This also provides the initial condition for the subsequent recompression process.

Prior to the consideration of recompression, an average base pressure can be determined from the momentum principle. One observes from fig. 3 that the momentum principle, when applied between the base and the section m, the end of the mixing region, readily yields

$$p_b \pi R_o^2 = \int_{R_{dm}}^{R_o} p_d \, 2\pi r dr + \pi R_{dm}^2 p_m - \int_o^{\ell_m} \tau_d 2\pi r dz + \int_o^{\delta_b} 2\pi r \rho u^2 dr + \int_o^{h_b} 2\pi r \rho u^2 dr \tag{3}$$

and the average base pressure ratio, p_b/p_∞, may be solved from the above equation. In supersonic external flows, there is practically no pressure variation prior to recompression. Under this situation the shear stress integral in Eq. (3) balances with the forward flow momentum, and the backward flow momentum is usually negligible. Thus the base pres-

sure from Eq. (3) would be equal to the uniform pressure prevailing within the wake for supersonic flow condition. In transonic flow, the pressure variation immediately behind the base is so severe that the above expression is needed to give a more realistic estimation of the average base pressure and the base drag.

Recompression follows essentially what has been developed previously[23]. At each section the dimensionless velocity of the flow has a profile of

$$\phi = \frac{u}{ue} = \phi_d + s\zeta_a + (3(1-\phi_d) - 2s)\zeta_a^2 + [s-2(1-\phi_d)]\zeta_a^3 \qquad 0 < \zeta_a < 1 \tag{4a}$$

above the dividing streamline, a linear profile of

$$\phi = \frac{u}{u_e} = \phi_d \zeta_\ell \qquad (0 < \zeta_\ell < 1) \tag{4b}$$

below the dividing streamline for the forward wake flow, and a cosine profile of

$$\phi = \frac{u}{u_e} = -\phi_b \cos\frac{\pi}{2}\zeta_b \qquad (0 < \zeta_b < 1) \tag{4c}$$

for the back wake flow, where

$$\phi_d = \frac{u_d}{u_e},\ \phi_b = \frac{u_b}{u_e},\ \zeta_a = \frac{r-r_d}{\delta_a},\ \zeta_\ell = \frac{r-r_d+\delta_b}{\delta_b},$$

$$\zeta_b = \frac{r}{h_b},\ \delta_a = r_a - r_d,\ \delta_b = r_d - h_b \tag{4d}$$

The slope parameter, s, in Eq. (4a) is linearly coupled to ϕ_d, and the proportional constant is evaluated at the initial section of the recompression region. This manipulation assures the fact that both ϕ_d and s vanish together at the section of reattachment. A locally triangular geometry was also assumed for the wake flow so that the wake center line, which divides the forward flow from the back flow, shall also pass through the point of reattachment as it should.

A system of five ordinary differential equations was obtained to describe the process of recompression. They are given by

$$A_i \frac{dR_e}{dz} + B_i \frac{dR_d}{dz} + C_i \frac{d\phi_d}{dz} + D_i \frac{dh_b}{dz} + E_i \frac{d\phi_b}{dz} = F_i \frac{dc_e}{dz} + G_i \qquad (i = 1 \ldots 5) \tag{5}$$

The first two equations were obtained from the continuity principle for the viscous layers above and below the dividing streamline

respectively. The next two were the momentum relations for the two layers and the last was derived from the condition of local triangular wake geometry. Coefficients A_i, $B_i \ldots G_i$ (see Ref. (23) for expressions of these functions) are complicated functions of flow properties and conditions. Eq. (5) describes the variation of the locations of the edge of shear layer R_e; the dividing streamline R_d and its velocity u_d together with the back flow height h_b and velocity u_b throughout the recompression region. The turbulent shear stress along the dividing streamline, which appears in terms G_3 and G_4, is evaluated through an eddy diffusivity which is related to that at the initial section of recompression by

$$\frac{\varepsilon}{\varepsilon_m} = \frac{u_e}{u_{e_m}} \left(\frac{\delta_a}{\delta_{a_m}}\right) \left(\frac{\ell_m + x_r}{\ell_m}\right) \tag{6}$$

where δ_a refers to the shear layer thickness above the dividing streamline, and x_r refers to the distance along the recompression region. Perhaps it is worthwhile to note that with an integral analysis for the turbulent mixing and recompression process, only the emperical information of the eddy diffusivity along the dividing streamline is needed throughout these regions.

From the recompression calculation by integrating the system of equations, it was learned that the point of reattachment behaves as a saddle-point singularity for the system of equations describing the flow. For slightly different z_R values, which, of course, correspond to the different inviscid flow field, the dividing streamline velocity would either decrease to negative values during recompression, before the point of reattachment on the center line of the wake is reached, or eventually break away from the trend of continuous reduction and start to increase. In the actual calculation, since the establishment of the inviscid flow field is time consuming, the value of z_R was kept fixed, and the saddle point behavior is observed from the fact that slightly different initial boundary layer thicknesses before mixing would lead to widely different results toward the end of recompression. Fig. 4 shows a typical set of results of calculations showing the different trends of the normalized dividing streamline velocity, ϕ_d. To keep the computational effort within a reasonable level, one must attempt to reach the point of reattachment through extrapolation at the end of recompression when the initial boundary layer thicknesses of two divergent trends are within a small margin (e.g. 10^{-4}, when δ_b is normalized by R_o).

Redevelopment of Flow

At the point of reattachment, the velocity profile has the shape of

$$\phi = 3\zeta^2 - 2\zeta^3$$

according to Eq. (4a). It is now assumed that throughout the region of redevelopment, the velocity has the profile of

$$\phi = \phi_w + (1-\phi_w)(3\zeta^2 - 2\zeta^3) \tag{7}$$

where ϕ_w is the centerline wake velocity and $\zeta = r/\delta_e$; δ_e being the thickness of the viscous layer within the region of redevelopment.

The continuity equation and the equation of motion within the boundary layer formulation are

$$\frac{\partial(\rho u r)}{\partial z} + \frac{\partial(\rho v r)}{\partial r} = 0 \tag{8a}$$

$$\frac{\partial(\rho u^2 r)}{\partial z} + \frac{\partial(\rho u v r)}{\partial r} = - r\frac{dp}{dz} + \frac{\partial(\tau r)}{\partial r} \tag{8b}$$

Upon integrating across the viscous layer , Eq. (8) readily yields:

$$[1-2(1-c_e^2)I_1]\frac{d\delta_e}{dz} - (1-c_e^2)\delta_e I_4 \frac{d\phi_w}{dz} = \tan\beta_e$$

$$+ [\frac{\delta_e I_1}{c_e}\quad (1-c_e^2\frac{3\gamma-1}{\gamma-1}) + 2c_e\delta_e I_3(1-c_e^2)]\frac{dc_e}{dz} \tag{9a}$$

$$\frac{2I_2(1-c_e^2)}{\delta_e}\frac{d\delta_e}{dz} + (1-c_e^2)I_6\frac{d\phi_w}{dz} =$$

$$- \frac{dc_e}{dz}[\frac{2I_2}{c_e}(1-c_e^2\frac{2\gamma-1}{\gamma-1}) + 2c_e(1-c_e^2)I_5$$

$$+ \frac{1}{2c_e}(1-2(1-c_e^2)I_1)] \tag{9b}$$

where

$$I_1 = \int_0^1 \frac{\phi\zeta d\zeta}{1-c_e^2\phi^2} \quad , \quad I_2 = \int_0^1 \frac{\phi(1-\phi)\zeta d\zeta}{1-c_e^2\phi^2}$$

$$I_3 = \int_0^1 \frac{\phi^3\zeta d\zeta}{(1-c_e^2\phi^2)^2} \quad , \quad I_4 = \int_0^1 \frac{1+c_e^2\phi^2}{(1-c_e^2\phi^2)^2} r\zeta d\zeta$$

$$I_5 = \int_0^1 \frac{\phi^3(1-\phi)\zeta d\zeta}{(1-c_e^2\phi^2)^2} \quad , \quad I_6 = \int_0^1 \frac{1-2\phi+c_e^2\phi^2}{(1-c_e^2\phi^2)^2} r\zeta d\zeta \tag{10}$$

$$r = \frac{\partial\phi}{\partial\phi_w} = 1-3\zeta^2+2\zeta^3$$

c_e is the Crocco number of the free stream, which is related to the Mach number M_e by

$$c_e^2 = \frac{M_e^2}{\frac{2}{\gamma-1}+M_e^2} \tag{11}$$

β_e is the streamline angle at the edge of the shear layer, and all integrals, I_1 through I_6, are only functions of c_e and ϕ_w. It is to be noted that this integral analysis is equally valid for laminar or turbulent flows since the shear stress vanishes at both limits of integration. Indeed, the far-wake condition of

$$\delta_e(1-\phi_w)^{1/2} = \text{const} \tag{12}$$

is satisfied by both laminar or turbulent flows. It may be shown that the system of equations given by Eq. (9) with the assumed velocity profile is compatible with this condition.

The right side of Eq. (9) contains the pressure gradient term which is implicitly linked with the spread of the viscous layer into the already established inviscid flow region. This situation has already been encountered in the upstream recompressive flow described by Eq. (5). Iterative solution procedures must be relied upon at each step of the numerical integration if accurate results are expected.

It has been learned from this approach of the problem that the fully developed flow condition presents itself as a saddle-point singularity of the system of equations describing the flow. For a fixed z_R but with slightly different δ^*_{asy} values, the redevelopment flow after the reattachment will lead either to positive and ever increasingly large $d\delta_e/dz$ or to smaller and eventually negative $d\delta_e/dz$ value. Negative $d\delta_e/dz$ also invariably leads to negative $d\phi_w/dz$, resulting a reduction of wake centerline velocity. An example to illustrate this phenomenon is shown in fig. 5. Both these behaviors are physically unrelistic and the correct value of δ^*_{asy} lies in between. This, of course, is the typical behavior of a saddle-point. It would be interesting to examine this singular behavior in a more detailed manner, if possible. It was originally anticipated that there is no need to carry out this study in obtaining the transonic base pressure results.

Method of Calculations

For the present problem, it seems to be possible to obtain the base pressure solution through computations with a straight forward scheme described as follows:

For a given Mach number within the transonic range, the potential flow solution can be established once the initial values of z_R and δ^*_{asy} are selected. As described previously, the boundary layer on the projectile is calculated frequently during iterations to present its influence to the potential flow solution.

After the inviscid flow has been established, the mixing-recompression-reattachment computations are carried out. However, the already established boundary layer at the base may not be able to yield a recompression solution "passing" through the reattachment saddle-point. To save the computing cost, such a boundary layer thickness having the same power law profile at the base satisfying the condition of reattachment is found through interations. Redevelopment flow is calculated after-

wards. By adjusting the δ^*_{asy} value repeatedly, the correct redeveloping flow can be found to satisfy the condition of fully developed state. It is, of course, understood that for each new value of δ^*_{asy}, a new set of calculations of inviscid-flow mixing-recompression-reattachment must be repeated. The correct value of z_R is thus determined from the thickness matching of the boundary layer from the forebody calculations to that of the recompression-reattachment calculations. A typical illustration of matching is shown in Fig. 6.

It was later learned that accurate numerical integration of the systems of equations of the present problem with two saddle points is not a simple task. The systems of equations are non-linear and non-autonomous. Furthermore, as a special feature of the problem, the pressure gradient dc_p/dz implicitly depends on the growth of the viscous layer (dr_e/dz and $d\delta_e/dz$), while the growth of the viscous layer is explicity dependent upon the pressure gradient through Eqs. (5) or (9), both in the recompression and redevelopment regions. Iteration must be employed to obtain reasonably accurate results. Uniform step length of integration must be employed if smooth results are expected. This matter is further complicated by the fact that the point of reattachment must be established through extrapolation. Consistent results would be impossible to obtain when the range of δ^*_{asy}/R_c is successively narrowed beyond a certain limit. It is obvious that results of extrapolations on two different sides of the separatrix would lead to drastically different flow conditions when the second saddle point (fully-redeveloped flow) is approached. The error involved in iterations and probably the error margin for the potential function imposed for convergent inviscid flow would all affect consistency. It is thus obvious that any additional work on the numerical aspect of the problem including also the study of these saddle point sigularities would be very worthwhile.

A specific scheme based from momentum principle has been adopted to extrapolate and establish the thickness of the viscous layer at the section of reattachment. It is discussed immediately below.

Referring to Fig. 7, where the location of reattachment has been established through extrapolation, one recognized that a momentum balance would allow a check on the accuracy of calculations carried out so far, since all quantities associated with the control volume including the force on the body are known. The momentum principle readily yields

$$p_\infty \pi R_\infty^2 - \int_0^{R_\infty} 2\pi r p dr\Big|_R - F_b = \int_0^\infty 2\pi r \rho u^2 dr\Big|_R - \pi R_\infty^2 \rho_\infty u_\infty^2 + \int_{-\infty}^{Z_R} 2\pi R_\infty \rho v u dz \qquad (13)$$

with

$$F_b = \int_{fore} 2\pi r p dr - \bar{p}_b \pi R_0^2 + F_{fric.} \qquad (14)$$

Eq. (13) can also be employed to determine the correct value of δ_e at the section of reattachment so that the momentum principle is satisfied. Although all terms in Eq. (13) outside of the viscous flow region can be evaluated from the inviscid flow calculations, they can be

replaced by some of the terms from the inviscid flow considerations associated with the equivalent body. From Fig. 8, where the same boundaries enveloping the equivalent body is shown, one may also write

$$p_\infty \pi R_\infty^2 - \int_{R_{eb}}^{R_\infty} 2\pi r p dr - F_{inv} = \int_{R_{eb}}^{R_\infty} 2\pi r \rho u^2 dr - \pi R_\infty^2 \rho_\infty u_\infty^2 + \int_\infty^{Z_R} 2\pi R_\infty \rho u v dz \qquad (15)$$

with

$$F_{inv} = \int_{fore} 2\pi r p dr - \int_{eq-w} 2\pi r p dr \qquad (16)$$

where eq-w represents the wake portion of the equivalent body. Upon eliminating the common terms between Eqs. (14) and (15), one obtains

$$\left(\frac{R_e}{R_0}\right)^2 \frac{p_e}{p_\infty} - \int_{R_{eb}}^{R_e} 2 \frac{r}{R_0} \frac{p}{p_\infty} d\left(\frac{r}{R_0}\right) + C_{D_f} \frac{\gamma M_\infty^2}{2} - \frac{\bar{p}_b}{p_\infty} + \int_{eq-w} 2 \frac{r}{R_0} \frac{p}{p_\infty} d\left(\frac{r}{R_0}\right) =$$

$$\gamma M_\infty^2 \left[\int_{R_{eb}}^{R_e} 2 \frac{p}{p_\infty} \left(\frac{u}{u_\infty}\right)^2 \frac{r}{R_0} d\left(\frac{r}{R_0}\right) - 2 \frac{\rho_e}{\rho_\infty} \left(\frac{u_e}{u_\infty}\right)^2 \left(\frac{\delta_e}{R_0}\right)^2 (1-C_e^2) (I_1 - I_2)|_R\right] \qquad (17)$$

where I_1 and I_2 are evaluated from Eq. (10) with $\phi_w = 0$.

It has been found that R_e (or δ_e) so established from Eq. (17) is rarely different from the results obtained from the linear extrapolation by a few percent. For example, the solution case as presented in Fig. 6, δ_e obtained from Eq. (17) is only larger than that from extrapolation by 1.7%. It is believed however, consistency of results has been improved through this scheme.

Results of Calculations and Discussions

Computations have been carried out for the case of $M_\infty = 0.9$ at the condition of $Re_L = 4 \times 10^6$ (L = 1 foot) with the stagnation temperature of 580° R. The range of the inviscid flow calculation was from -2 to +3, where the reference length is Z_R. The reference length for recompression-redevelopment calculations was R_0, and the step lengths of numerical calculations were 0.08 R_0 and 0.05 R_0 in recompression and redevelopment. The value of Z_R/D is obtained from thickness match and is already shown in Fig. 6. The corresponding base pressure coefficient is -0.141 ($P_b/p_\infty = 0.92$). Under this condition, $C_{D\text{-fore}} = 0.0078$, $C_{D_f} = 0.0273$ and the total drag coefficient is 0.176. Obviously, the base drag is the only predominant drag. Fig. 9 shows the pressure distribution finally estalished throughout the whole region. The experimental

data on the forebody are also available[27] for comparison. The agreement between the calculated results and the experimental data on the forebody is quite good. There is practically no experimental base pressure data available for comparison. It should be noted that while the pressure distribution on the forebody is precisely the result obtained for the equivalent body, the pressure field realized in the wake region differs from that of the equivalent body since the edge of the viscous layer is already far away from the equivalent body, thereby resulting a more moderate variation.

Figure 10 shows the path of the dividing streamline, the edge of the viscous layer and the inviscid equivalent body established from iterations. The resulting equivalent body geometry, which is obtained from addition of the displacement thickness onto the path of the dividing streamline, is also shown for comparison. Other than a fairly small discrepency at far downstream positions, the agreement between the two profiles is excellent. A fast growth of the shear layer and the centerline wake velocity has been observed for all calculations in the early portion of the flow redevelopment. However, the unabated rate of growth further downstream is the behavior of the saddle point. For further illustration, Fig. 11 presents the three adjacent sets of results of redevelopment including the case of $\delta^*_{asy}/R = 0.325$. Obviously, more accurate results at downstream positions can be obtained by further narrowing the range of δ^*_{asy}/R_o.

It should be noted that the eddy diffusivity formulation both in the mixing and recompression processes are probably not accurate. The expression given by Eq. (2) is only true for fully developed flows. Although the existence of the initial boundary layer on the mixing profile development has been accounted for, the effect of the level of turbulence due to the existence of the initial boundary layer should yield eddy diffusivity somewhat higher than that given by Eq. (2). This fact may be taken into account through an origin shift concept. The correlation of the eddy diffusivity by Eq. (6) for recompression is also more or less based on geometric reasoning. Different levels of eddy diffusivity would yield different results. Hopefully future improvement on the estimation of the eddy diffusivity, e.g., based on the k-ε turbulence modeling can be incorporated into the analysis to yield more accurate results.

The original computer program for dealing with recompression process was developed[23] with a slightly different coordinate system and also did not iterate within each step of the integration. This program was modified to include intermediate iteration in order to produce consistent results. Under certain conditions, convergence of the iteration within the step of integration became a problem. It was decided that no other results for different free stream Mach numbers shall be produced, before the computer program is extensively revised for the present problem.

Extension to Flows with Small Angles of Incidence

The study carried out so far is for axisymmetric configurations; thereby the flow must be at the condition of zero angle of attack.

When the angle of attack is not zero, the flow problem becomes three-dimensional. Even under the situation of a small angle of attack the flow condition is so complicated that it seems to be hopeless to examine this problem on a simple basis. Athough the flow condition on the forebody may still be examined from the calculation of the three dimensional potential equation; even with the viscous flow effect possibly taken into account if necessary[28], the viscous flows of mixing, recompression-reattachment and redevelopment behind the body are so complicated that a clear visualization of the flow field within the wake is difficult, if not impossible. It is certain that the dividing streamlines (descriminating streamlines) are not the jet boundary streamline within different meridianal planes and open wake condition exists. A certain amount of fluid mass from the external flow is fed into the wake from the windward meridianal planes, while the same amount of fluid is pumped out from the wake along the leeward meridianal planes. Detailed study of these problems can only be relied upon the large-scaled numerical calculations of the Navier-Stokes equation.

Since the present analysis was based on an equivalent body concept, under this situation, one cannot help to assume that the effect of the small angle of attack to the viscous flow processes is small. Essentially, it is to stipulate that the angle of attack will exert its influence only on the equivalent inviscid body which is already established for the case of zero angle of attack. Hopefully, an inviscid study of the flow past this equivalent body under small angle of incidence would yield a crude estimation of the base pressure for these flow conditions.

It should be stressed that although from the limited examination of the available experimental data, this stipulation seems to lead to the correct trend of the base pressure response to angle of incidence within the supersonic flow regime[29], it is purely based on speculation. Whether this crude approximation is useful in providing a reasonably estimation of the average base pressure under these flow conditions remains to be seen. It can only be checked out after experimental data of this nature become abundantly available.

ACKNOWLEDGEMENT

This work was carried out under the partial support from the U.S. Army Research office through the contract DAAG-29-79-C-0184. This effort was actually initiated while the author served as a Senior Research Associate of the National Research Council, National Academy of Science, working in the Aerodynamic Research Branch, Launch and Flight Division of the U.S. Army Ballistic Research Laboratory. Valuable discussions and help from Dr. W. B. Sturek and his group in BRL are mostly appreciated.

REFERENCES

1. Crocco, L. and Lees, L., "A Mixing Theory for the Interactin Between Dissipative Flows and Nearly Isentropic Streams," Journal of the Aeronautical Sciences, Vol. 19, No. 10, October 1952, pp. 649-676.

2. Korst, H. H., "A Theory for Base Pressures in Transonic and Supersonic Flow," Journal of Applied Mechanics, December 1956, pp. 593-600.

3. Korst, H. H., Page, R. H., and Childs, M. E., "A Theory for Base Pressures in Transonic and Supersonic Flows," University of Illinois, ME-TN-392-2, March 1955.

4. Beheim, M. A., Klann, J. L., and Yeager, R. A., "Jet Effects on Annular Base Pressure and Temperature in a Supersonic Stream," NASA TRR-125, 1962.

5. Carriere, P. and Sirieix, M., "Resultats Recents Dans L'Etude Des Problemes De Melange Et De Recollement," ONERA T. P. 165, 1964.

6. Korst, H. H., Chow, W. L., and Zumwalt, G. W., "Research on Transonic and Supersoic Flow of a Real Fluid at Abrupt Increases in Cross Section," ME Technical Report 392-5, Engineering Experiment Station University of Illinois, December 1959.

7. Lees, L. and Reeves, B. L., "Supersonic Separated and Reattaching Laminar Flows: I. General Theory and Application to Adiabatic Boundary-Layer/Shock-Wave Interactions," AIAA Journal, Vol. 2, No. 11, November 1964, pp. 1907-1920.

8. McDonald, H., "The Turbulent Supersonic Base Pressure Problem: A Comparison Between a Theory and Some Experimental Evidence," The Aeronautical Quarterly, Vol. 17, May 1966. pp. 105-126.

9. Weinbaum, S., "Rapid Expansion of a Supersonic Boundary Layer and Its Application to the Near Wake," AIAA Journal, Vol. 4, No. 2, February 1966, pp. 217-226.

10. Chow, W. L., "On the Base Pressure Resulting From the Interaction of a Supersonic External Stream With a Sonic or Subsonic Jet," Journal of the Aerospace Sciences, March 1959, pp. 176-180.

11. Page, R. H., "A Review of Component Analysis of Base Pressure for Supersonic Turbulent Flow," Proceedings of the Tenth International Symposium on Space Technology and Science, Tokyo, Japan, 1973, pp. 459-469.

12. Alber, I. E. and Lees, L., "Integral Theory for Supersonic Turbulent Base Flows," AIAA Journal, Vol. 6, No. 7, July 1968, pp. 1343-1351.

13. Addy, A. L., Korst, H. H., White, R. A., and Walker, B. J., "A Study of Flow Separation in the Base Region and Its Effects During Powered Flight," AGARD Conference on Aerodynamic Drag, AGARD-CP-124, April 1973.

14. Chow, W. L., "Recompression of a Two-Dimensional Supersoic Turbulent Free Shear Layer," Developments in Mechanics, Vol. 6, Proceedings of the 12th Midwestern Mechanics Conference, August 1971, pp. 319-332.

15. Chow, W. L., and Spring, D. J., "Viscous Interaction of Flow Redevelopment after Flow Reattachment with Supersonic External Streams," AIAA Journal, Vol. 13, No. 12, December 1975, pp. 1576-1584.

16. Weng, C. H. and Chow, W. L., "Axisymmetric Supersonic Turbulent Base Pressures," AIAA Journal, Vol. 16, No. 6, June 1978, pp. 553-554.

17. Chow, W. L. and Spring, D. J., "Viscid-Inviscid Interaction of Two-Dimensional Incompressible Separated Flows," J. of Applied Mechanics, Vol. 43, Series E, No. 3, September 1976, pp. 387-395.

18. Warpinski, N. R. and Chow, W. L., "Base Pressure Associated With Incompressible Flow Past Wedges at High Reynolds Numbers," J. of Applied Mechanics, Vol. 46, No. 3, September 1979.

19. Warpinski, N. R. and Chow, W. L., "Viscid-Inviscid Interaction associated with Incompressible Flow past Wedges at High Reynolds Numbers," ME-TR-395-4, UILU ENG 77-4001, Engineering Experiment Station, Department of Mechanical and Industrial Engineering, University of Illinois at Urbana-Champaign, February 1977, also NASA CR-135246.

20. Chow, W. L. and Shih, T. S., "Transonic Flow past a Backward Facing Step," AIAA Journal, Vol. 15, No. 9, pp. 1342-1343, 1977.

21. Liu, J. S. K. and Chow, W. L., "Base Pressures of an Axisymmetric Transonic flow past a backward facing step," AIAA Journal, Vol. 17, No. 4, 1979, pp. 330-331.

22. Chow, W. L. and Shih, T. S., "The Viscid-Inviscid Interaction associated with a Two-Dimensional Transonic Flow past a Backstep," ME-TR-395-3, UILU ENG 75-4005, Engineering Experiment Station, Department of Mechanical and Industrial Engineering, University of Illinois at Urbana-Champaign, Final Report prepared for the Research Grant, U. S. Army DAHC04-75-G-0041, October 1975.

23. Liu, J. S. K. and Chow, W. L., "Base Pressure problems associated with an Axisymetric Transonic flow past a backward Facing step," ME-TR-395,5, Department of Mechanical and Industrial Engineering, University of Illinois at Urbana-Champaign, Final Report prepared for the Research Grant, U. S. Army DAAG29-76-G-0199, November 1977, AD A050658.

24. Chow, W. L., Bober, L. J. and Anderson, B. H., "Strong Interaction associated with Transonic Flow past Boattails," AIAA Journal, Vol. 13, No. 1, 1975, pp. 112-113.

25. Chow, W. L., Bober, L. J. and Anderson, B. H., "Numerical Calculation of Transonic Boattail Flow," NASA TN D-7984, June 1975.

26. Brink, D. F. and Chow, W. L.," Two-Dimension Jet Mixing with a Pressure Gradient," J. of Applied Mechanics, Vol. 42, Series E, No. 1, pp. 55-60, March 1975.

27. Kayser, L. D. and Whiton, F., "Surface Pressure Measurements on a Boattailed Projectile Shape at Transonic Speeds," Memorandum Report ARBRL-MR-03161, Ballistic Research Laboratory, Aberdeen Proving Ground, MD., March 1982.

28. Nakayama, A. and Chow, W. L., "Calculations of Transonic Boattail Flow at a Small Angle of Attack," ME-TN-395-6, Department of Mechanical and Industrial Engineering, University of Illinois at Urbana-Champaign, report prepared for the Research Grant NGL 14-005-140, April 1979. Also NASA CR-158471.

29. Kayser, L. D., "Experimental Study of Separation from the Base of a Cone at Supersonic Speeds," BRL Report No. 1737, Ballistic Research Laboratory, Aberdeen Proving Ground, MD, August 1974.

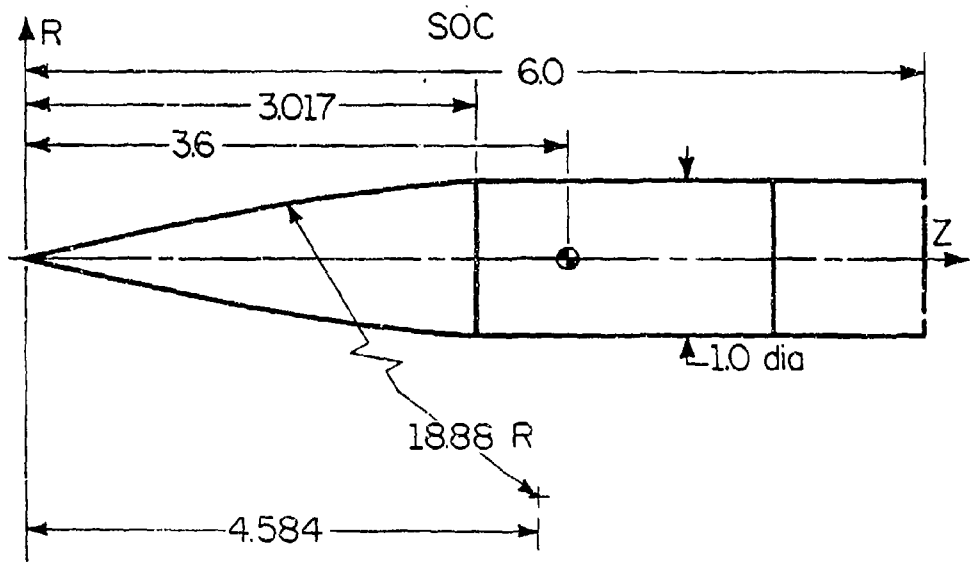

Figure 1 The Geometry of a Six-Caliber Projectile

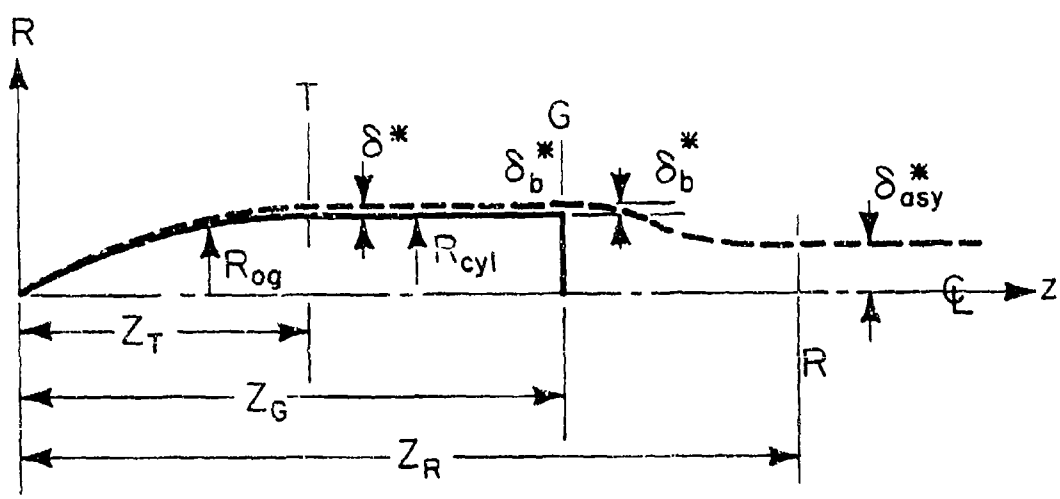

Figure 2 The Equivalent Body

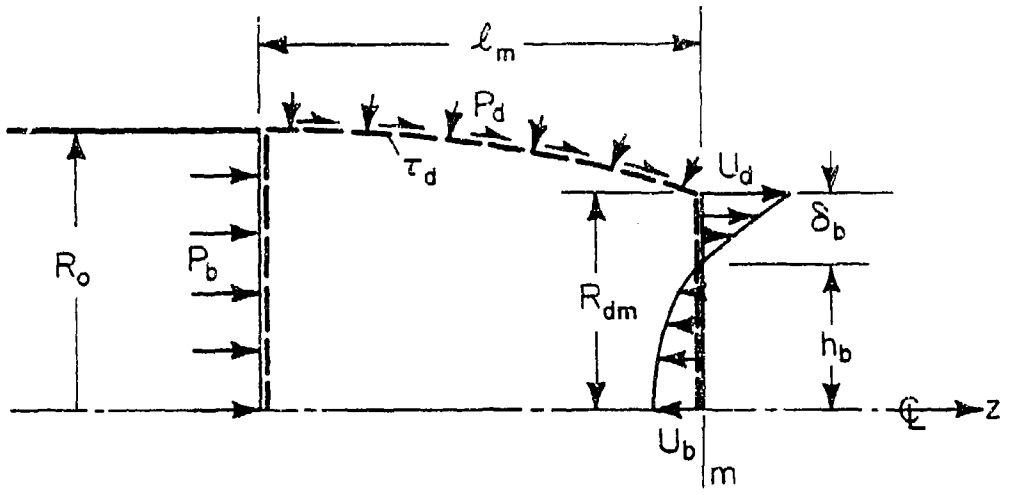

Figure 3 The Control Volume Related to the Definition of Base Pressures

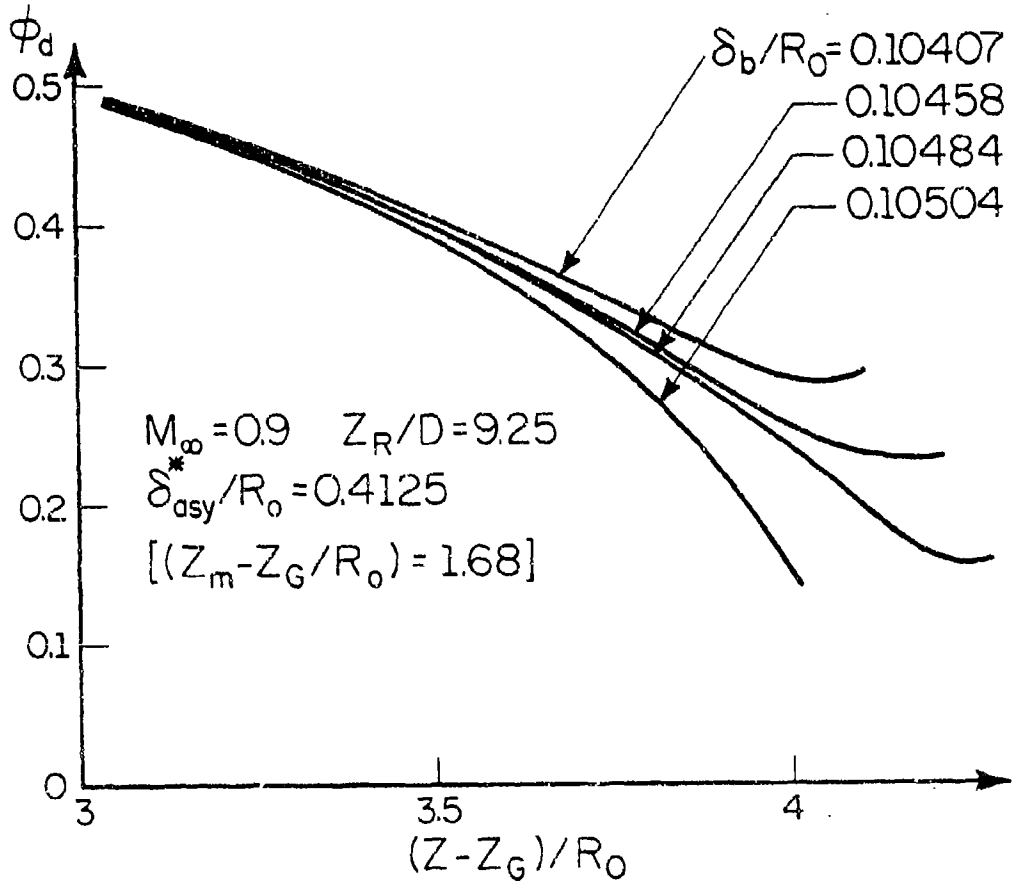

Figure 4 The Saddle Point Behavior of Reattachment

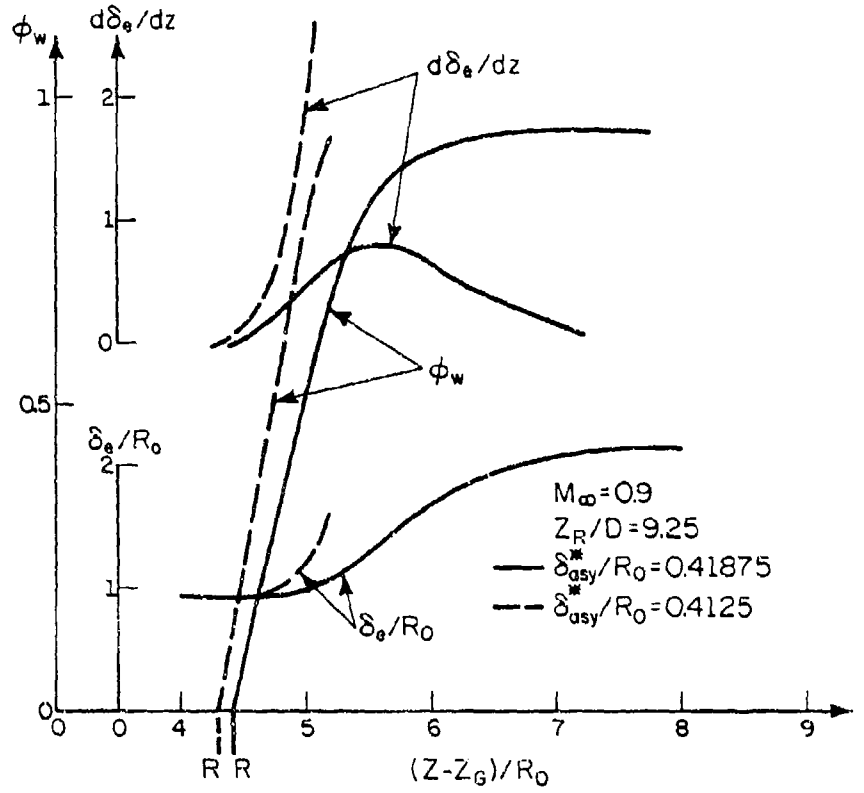

Figure 5 The Saddle Point Behavior of the Fully Redeveloped State

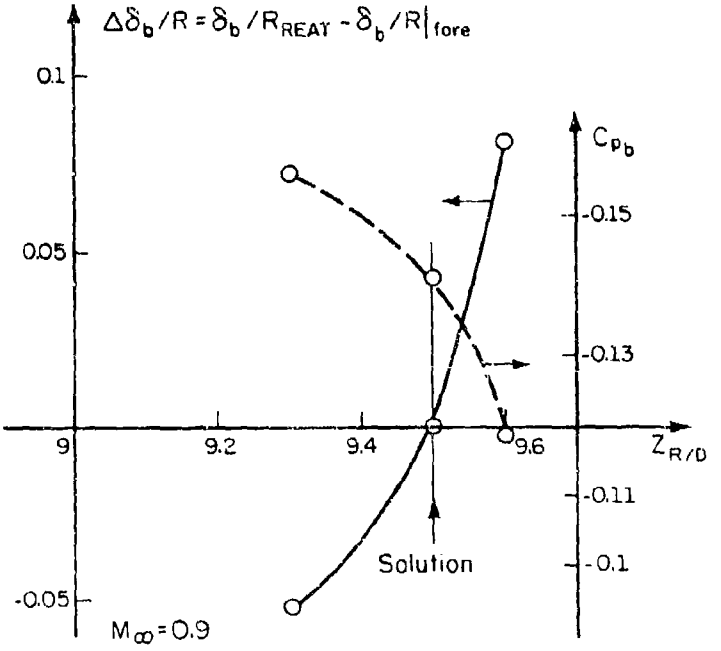

Figure 6 The Matching of the Boundary Layer Thickness

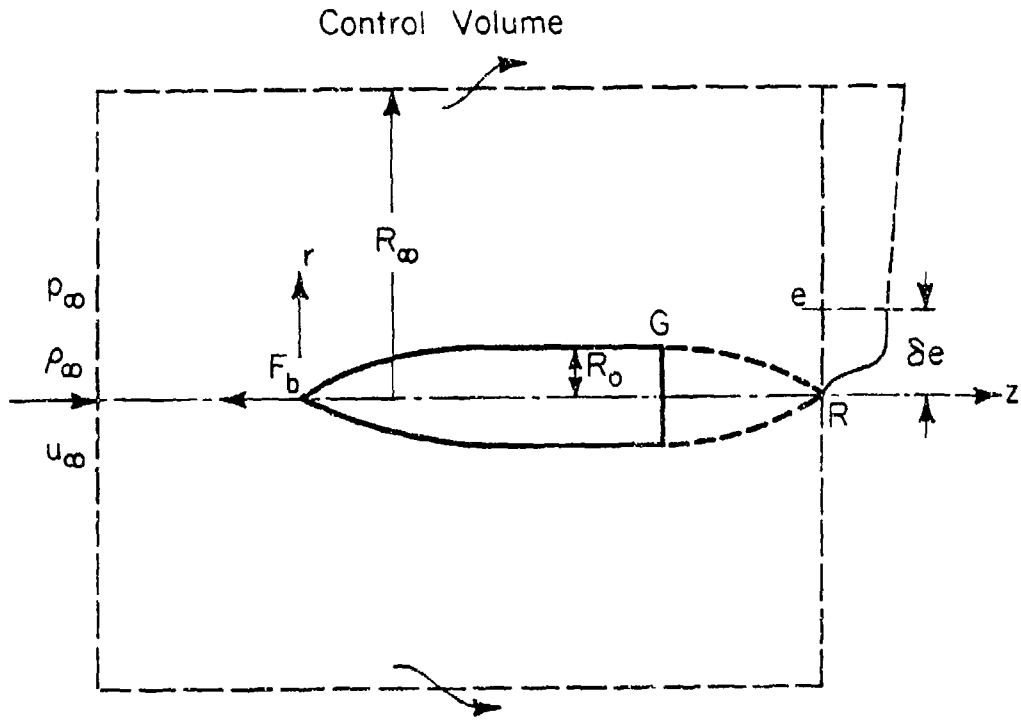

Figure 7 The Control Volume Related to Momentum Balance

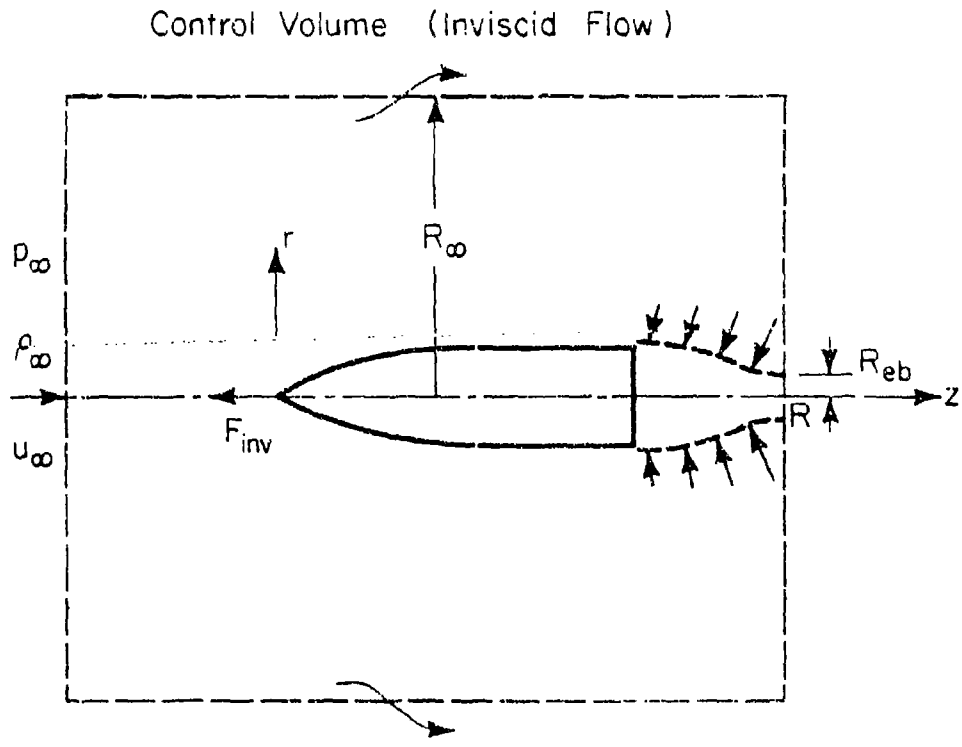

Figure 8 The Control Volume Related to the Equivalent Body

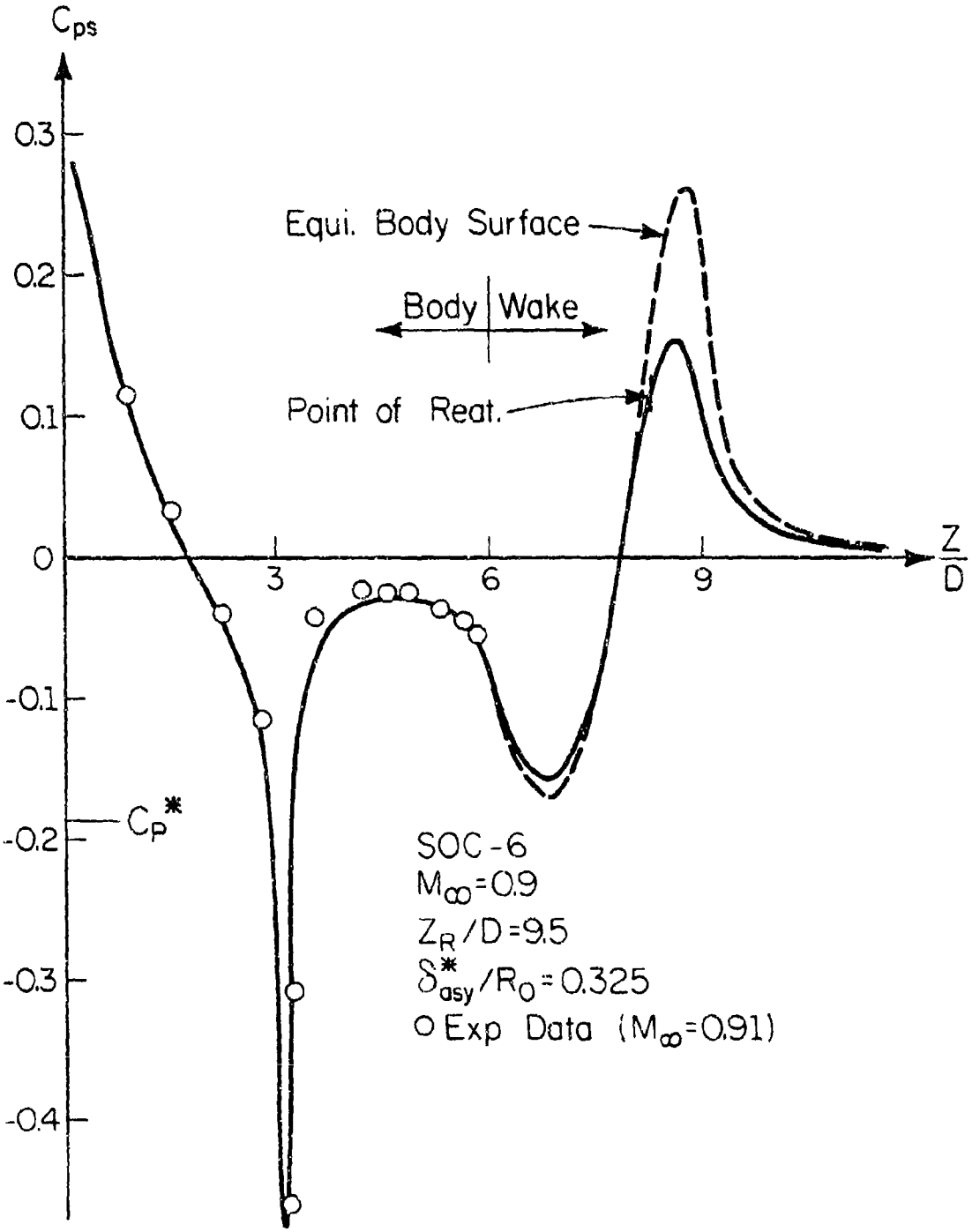

Figure 9 The Resulting Pressure Distribution for M_∞ = 0.9

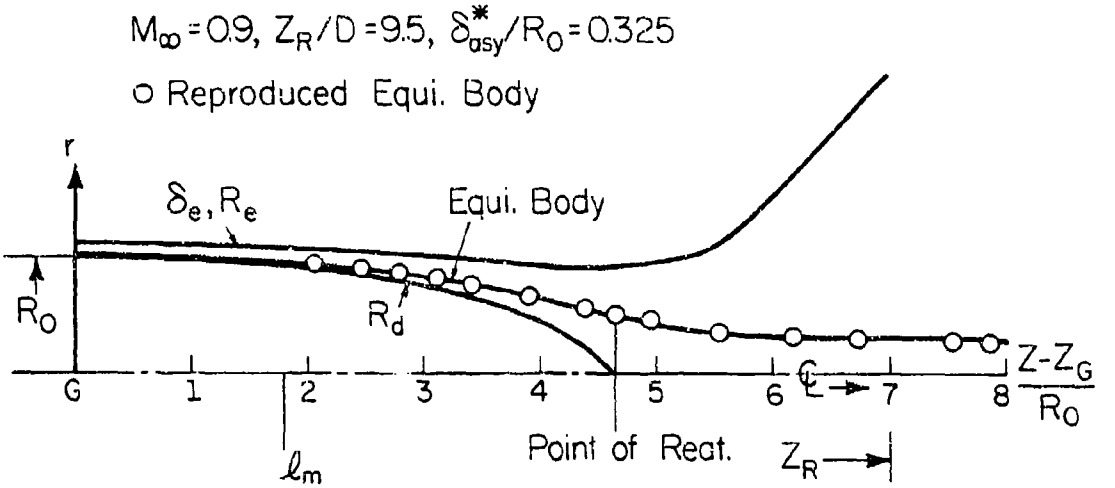

Figure 10 Resulting Wake Flow Geometry and Reproduced Equivalent Body

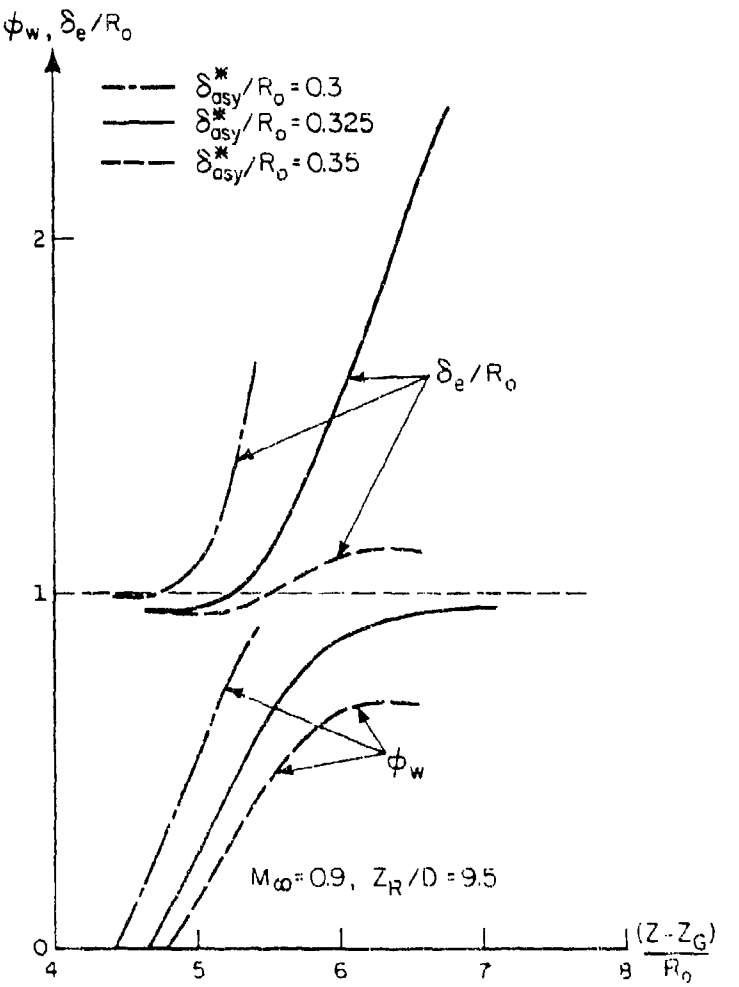

Figure 11 Additional Results Related to Redevelopment of Wake Flow

APPENDIX C

AXISYMMETRIC WAKES IN SUPERSONIC UNPOWERED MISSILE FLIGHT

Paper presented at the

Symposium on Rocket/Plume Fluid Dynamic Interactions

Huntsville, Alabama

April 1983

by

Professor H. H. Korst

APPENDIX C

AXISYMMETRIC WAKES IN SUPERSONIC UNPOWERED MISSILE FLIGHT

H. H. Korst
Department of Mechanical and Industrial Engineering
1206 West Green Street
University of Illinois at Urbana-Champaign
Urbana, IL 61801

NOMENCLATURE

δ	boundary layer thickness, m
δ^{**}	boundary layer momentum thickness, m
Δ	thickness of mixing region, m
p	absolute pressure, N m^{-2}
ρ	density, kg m^{-3}
μ	absolute viscosity, N sec m^{-2}
U	velocity, m sec^{-1}
R	radius, m
x	streamwise coordinate, m
y	local coordinate across velocity profile, m
τ	shear stress, N m^{-2}

Dimensionless Quantities

C	Crocco number, $M/(2/(\gamma - 1) + M^2)^{1/2}$
C_D	drag coefficient
C_p	pressure coefficient $= \dfrac{p - p_\infty}{\frac{1}{2}\rho_\infty U_\infty^2}$
γ	specific heat ratio
M	Mach number
N	exponent of boundary layer profile
RE	Reynolds No. (further specififed in text)
T	shear stress function
E	eddy viscosity function
ϕ	velocity ratio
$J\phi$	velocity ratio for zero streamline
σ	spread rate parameter for dissipative mixing region

Subscripts

1	approaching (attached) boundary layer
2	expanded (rotational) profile
5	at wake closure
M	at match point of dissipative and rotational profile
a	adjacent, freestream condition
b	base

1. INTRODUCTION

The near-wake flow behind blunt-based bodies of revolution has been the subject, in this order, of experimental, analytical and computational studies. It has been well established experimentally that the problem is characterized by the strong interaction of inviscid and viscous flow mechanisms. In particular, both the external inviscid flow and the details of the viscous layers approaching the base are known to determine the near-wake flow structure and with it the afterbody or (base) drag[1].

Analytical efforts can be classified with respect to the fashion in which the viscous flow mechanisms are treated--similar to the distinction made in the classical boundary layer theory: Integral methods (Crocco-Lees model) as contrasted by mechanical energy considerations applied to individual streamlines (Chapman-Korst flow component model). In this sense, the earlier studies of Zumwalt[2], Mueller[3], Minyatov[4], Mueller, Hall and Roache[5], Mueller and Kayser[6], among others, belong to the flow component approach, while the work of Peters and Phares[7] is, formally, an integral method and Weng[8] and Chow and Weng[9] combine certain aspects of both concepts.

Finally, entirely numerical efforts, such as represented by Wray's code, have demonstrated the capabilities of large computers to deal with the base flow problems by establishing global solutions by means of solving the Navier-Stokes equation[10]. The above listed publications have been selected not for the sake of presenting complete documentation but rather to establish a frame of reference for the present analysis.

2. NEAR WAKE FLOW MODEL

It has already been observed by Chapman[7] that the method of characteristics for axisymmetric flow does not allow its extension toward the axis of symmetry. While the actual wake flow does not encounter this "mathematical difficulty" as the recirculating flow will occupy a finite diameter stream tube near the centerline, flow component analyses which depend upon the method of characteristics had to circumvent this calamity by ways of excluding the near axis region (trailing wake radius ratio). Minyatov[4] selected an averaged, experimentally extracted value of 0.5 for the trailing wake radius ratio, while Mueller[3] based his model treatment on the more detailed experimental values reported by Chapman[1], observing that base pressures were quite insensitive to this empirical parameter.

2.1 Flow Model for Base Flows in Unpowered Flight

The present analysis will not encounter this problem inasmuch as the portion of the control surface near wake closure is placed just upstream of the region of terminal pressure rise and by treating the recirculating flow as returning at the pressure level of the base, fully mixed. Thus the need for introducing a ficticous sting is replaced by the option of discussing the effects an actual sting may impose on the wake flow solution, see Fig. 1.

2.2 Viscous Component Analysis

A second distinctive aspect of the present model is concerned with the mechanism of viscous jet mixing. The importance of shear layer transition on base flow problems has long been established[11] and must attract due consideration in view of the direct observation of mixing layer relaminarization[12] and the detailed information on the behavior of turbulence in supersonic shear flows strongly out of equilibrium[13]. The proposed model treats the expansion of the approaching boundary layer, (having a velocity profile exponent 1/N, a Reynolds number RE_{1,δ_1} and a thickness ratio δ/r, base) by the streamline expansion method. This is followed by a two-layer concept where the dissipative jet mixing region is developing in the rotational, but non-dissipative expanded

boundary layer as a straight line profile having an initially laminar, then turbulent exchange mechanism, see Fig. 2. Utilization of a locally similar[14] straight line profile is consistent with the description of the laminar and turbulent exchange mechanisms as related to the rate of rotation of the profile slope[15], which in turn can be linked to the spread rate parameter σ which is reasonably well established. Selection of a transition criterion is of importance and meager information given by Chapman, Kuehn and Larsen[11] is here interpreted by using the lower boundary (disturbed environment) of the experimentally determined transition Reynolds number versus Mach number field[16] ("natural transition").

2.3 Recompression at the End of the Wake

Restriction of the model control volume to the constant pressure region of the near wake places extra emphasis on the energetic formulation for the wake closure. Isentropic recompression of the discriminating (stagnating) streamline has been assumed, together with the concept of incomplete turning of the external flow[17]. In the present case, it has been found advantageous to utilize the Page criterion[18] which, together with the use of a straight line mixing profile, can be brought into a very convenient and simple to use quantitative form[19]. It is of interest to note that the present method, while conceptually different from the concept of equivalent base bleed in dealing with the effects of approaching boundary layers[18], generally does not produce different trends in results[19]. One notable exception is in some preliminary evidence that transitional shear layers may, under certain conditions, cause limit cycle behavior of near wakes[13].

2.4 Inviscid Flow Field Representation

Observation of near wakes in unpowered flight, but even more so the restriction of the present model to the constant pressure region, suggests that the inviscid flow field can be analyzed with sufficient accuracy by an approximate treatment based on a second-order solution to the potential equation for axisymmetric supersonic flows near centered expansions. Originally developed to describe jet plume boundaries near

the exit of convergent-divergent nozzles[20], the analysis is easily modified to deal with external flows past boattails and wakes[19]. Even though accuracy may be limited beyond downstream distances exceeding the initial body radius, the convenience of the method makes it attractive to deal with short boattails and near wakes, see Fig. 3. The method of sequential centered expansions also allows to treat non-uniform flows approaching the afterbody[21].

2.5 Component Synthesis

By utilizing computer programs dealing with the flow model as shown in Fig. 1, one expects to obtain information on afterbody drag (boattail and/or base drag), near wake geometry (location of the point of initial pressure rise, x5, and the value of y5, which should be somewhat larger than the trailing wake radius ratio), peak pressure ratio (somewhat exceeding free stream pressure--a special feature of axisymmetric wakes), and "reattachment" conditions if a sting is present.

3. COMPUTER PROGRAM ARCHITECTURE

Three separate computer programs have been written and subsequently chained together to provide the following (iterative) solution procedure:

3.1 Input Program AB1

Program AB1 is receiving all the input needed for obtaining a solution. A printout of the input is shown in Table 1. As can be seen, the program is prompting to receive very detailed information (even differentiating between free stream Mach number and the flow conditions approaching the boattail: approach Mach number, approach angularity, acceleration and forebody curvature prompted by the program, but not shown in the printout Table 1--these parameters are needed for dealing with non-conical boattails.) An initial seed for the energy level of the stagnating streamline is also req sted. This is expressed in form of a fraction of the similarity value for fully developed mixing profiles, $J\phi$ (a value of unity would refer to a fully developed mixing profile and would also correspond to the case of vanishing boundary layer thickness).

3.2 System Synthesis Program AB2

Program AB2 is iterative, starting with two internally selected values of base pressures and determining such a value for which the model component synthesis is satisfied for the given sting radius ratio (normally zero for free flight). One notices that this solution, which is still based on the seed value of $J\phi$ entered in program AB1, yields information on the wake geometry, and especially on the length of the constant pressure mixing region.

3.3 Jet Mixing Program AB3

Program AB3 calculates the transitional jet mixing process using the results of AB2, thus arriving at a new value $J\phi < 1$ by interpolation for the length of the mixing zone as determined by program AB2.

3.4 Iterative Chaining of Programs AB2 and AB3

Iterative procedure for determining the final solution consists of the alternative use of programs AB2 and AB3, which will be terminated if $ABS(J\phi_{i+1} - J\phi_i) < 0.01$. Table 2 shows the final result corresponding to the input conditions listed in Table 1 while details of the jet mixing profile development are given in Fig. 4.

3.5 Non-steady Aspects of the Near-Wake Problem

Under certain conditions, when the transition criterion as used indicates a close proximity between the transition location and the region of recompression, alternating solutions for the wake problem appear instead of convergence to a single configuration. While the narrrowness of conditions leading to such oscillations between two repeating solutions may not find quantitative support, non-steadiness of near wakes has been observed under similar conditions[13].

4. RESULTS

One must emphasize that the present treatment of individual flow components and their subsequent integration into the overall model has

not required the introduction of special coefficients or factors to promote agreement between calculated results and experimental data. The large number of parameters entering the calculations are merely indicative of the flexibility of the method in dealing with a variety of configurations and operational conditions. On the other hand, results will have to be judged strictly on their merits and any agreement, or disagreement, with experimental evidence will reflect on the correctness of component treatment and synthesis. In this respect, the present analysis must be considered a versatile tool, convenient in use, which still has to be applied to a wide variety of specific tasks to fully explore its potential and/or limitations.

4.1 Afterbody Drag Evaluation

Experimental data on base pressures behind axisymmetric blunt bodies often lack the detailed information on the approaching flow conditions, especially on the boundary layer profile, as are required for the proper analytical treatment. Indeed, speculative assumptions concerning the initial boundary layer profile may have to be made[7]. The ratio of momentum thickness to body radius together with the approaching Mach number and a characteristic Reynolds number can determine the solution, provided that the boundary layer velocity profile exponent can be extracted from this information. It is within these limitations that comparisons between different analyses and experimental data are possible.

4.1.1 Cylindrical Afterbodies in Supersonic Uniform Flow

Shown in Fig. 5 is the relationship between the base pressure coefficient $C_{p,b} = (p_b - p_\infty)/\rho_\infty U_\infty^2/2$, base pressure ratio p_b/p_∞ and the radius Y5 (which should be somewhat larger than the trailing wake radius ratio) plotted as a function of the free stream Mach number. For this diagram, a representative vlue of $J\phi = 0.85$ has been chosen instead of going through the full iterative sequence of computer program AB1, AB2, AB3.

4.1.2 Cylindrical Afterbodies in Supersonic Flow--Influence of Approaching Boundary Layer

It is attractive to view the results of the present analysis in light of those reported by Peters and Phares[7]. Not only does this allow comparison of the analytical solutions with each other and with experimental data but it is also possible to critically examine the different approaches taken in dealing with the jet mixing mechanisms as shall be discussed later in more detail. Shown in Fig. 6 are the results for the base pressure ratio p_b/p_∞ as functions of the ratio of boundary layer momentum thickness to base radius for the free shear Mach number of 2.

One must recall that both analyses require a more precise definition of the approaching boundary layer configuration than that usually offered with experimental data. Also indicated in Fig. 6 is the choice of transition criterion in program AB3 (which does not appear to have much influence in case of the free stream Mach number of 2.) However an interesting result of using the "natural transition" criterion is obtained for a freestream Mach number 3.9: solutions alternate between the laminar and turbulent near wake closure conditions.

4.1.3 Afterbody with Conical Boattail or Flare

Shown in Fig. 7a are the results of an afterbody drag optimization study carried out for the approach conditions identified in Table 1 for boattail angles of -4 (flare) to +10 degrees and a boattail length of one caliber. It can be seen that a broad minimum exists for boattail angles between 4 and 8 degrees. Base pressures are also plotted together with peak pressures, see Fig. 7b, the latter indicating overshoot over free stream pressure as will be expected for axisymmetric wake problems. Finally, Fig. 7c represents theoretical wake radius ratios for the range of boattail angles. In this series of calculations, the full iterative procedure was followed in determining the solutions. Transition of the dissipative jet mixing layer was assumed to occur according to the lower limit for $RE_{T,X}$ as function of slip stream Mach number as given by Chapman, et al.[11]. This assumption will now be scrutinized in light of never indirect and direct evidence.

4.2 Transitional Aspects of Jet Mixing

The afterbody performance evaluations carried out with the help of the iterative computer programs described in section 3 included, as an essential feature, criteria for the transition of the dissipative jet mixing region in the initially relaminarized expanded rotational shear layer. This, together with the assumption of locally similar mechanisms in both the laminar and turbulent dissipative regions of the two-layer viscous mixing component, generated results which could be compared directly with other quantitative base pressure evaluations. These criteria shall then be reexamined and confronted with detailed measurements of exchange mechanisms. Subsequently an interpretation of their meaning for global computational exercises can be sought.

4.2.1 Comparison with Other Quantitative Jet Mixing Models

The near-wake base pressure ratio solutions obtained for a free stream Mach number of 2 and a boundary layer parameter of $\delta^{**}/R_B = 0.01$ showed only very slight dependence upon the choice of the transition location, see Fig. 6. Yet the development of the two-layer mixing region as presented in Figs. 8a,b exhibits on first sight startling differences. This is, of course, a visual effect caused by the logarithmic presentation of the downstream coordinate x/δ_1. A closer examination reveals that there is but little influence on $RE_{T,x}$ and $J\phi$ remaining as the mixing layer approaches wake closure even though the widths of the dissipative regions are different. The reasonably close agreement with theoretical results for finite initial boundary layer thicknesses given by Peters and Phares[7] shall now be traced to a common root.

4.2.1.1 Turbulent Reynolds Number

Peters and Phares[7] utilized an empirical expression for an apparent turbulent Reynolds number, based on earlier work of Mueller[3] and Tani[22] in the form $R_{T,P}$, $B = 390 - 333e^{-(0.495 \times M)}$.

This can be compared directly with the results of the transitional calculations of Program AB3, in equating

$$R_{T,P} = RE_{T,x} \cdot \phi_2 \cdot (\Delta/b)(\Delta/\delta_1)/(x/\delta_1)$$

where the ratio $\Delta/b = \pi/2$ for the mixing profiles as specified in the two different approaches. Shown in Fig. 9 is the relationship for $RE_{T,P}$ as function of the slipstream Mach number only while Table 3 lists the streamwise changing values obtained from the results of Table 4. As can be seen, agreement develops with increasing distance from the point of transition. For a jet Mach number 4.35, Peters' equation yields 351, compared with downstream values between 347 and 389 obtained with program AB3.

4.2.1.2 Turbulent Cell Reynolds Number

Yoshikawa and Wray[10] define and use for their global numerical calculations an effective turbulent Reynolds number [R] based on a characteristic cell width ΔL. Again, there is a direct relationship between the results obtained form program AB3 in the form

$$RE_{T,\Delta L} = \frac{C_1}{C_2}\left[\frac{(1-C_1^2)}{(1-C_2^2)}\right]^{1/(\gamma-1)} \frac{1-C_2^2}{1-J\phi^2 C_2^2}\,\Delta L\, RE_{T,x}/\left(\frac{x}{\delta_1}\right)$$

While Yoshida and Wray selected a value of [R] = 75 in order to make their wake calculations agree with experimental data, program AB3 exhibits a strong dependency of [R] upon the downstream location but also shows that the region $7 < x/\delta_1 < 10$, where the mixing region approaches wake closure at the sting, the value of [R] as selected by "cut and try" appears to be well explained, see Table 5.

4.2.2 Comparison with Detailed Measurements of Exchange Mechanisms

It has been pointed out before that reasonable agreement is found between the results obtained with program AB3 and some simpler expression dealing with the turbulent mixing process. This should not be entirely surprising since the more detailed treatment represented by the

transitional two-layer mixing model uses experimentally established spread rates for its locally similar turbulent velocity profiles. On the other hand, it is attractive to seek a direct comparison with the results obtained by Gaviglio, et. al.[13] as their measurement should provide needed insights. Surprisingly, the analysis carried out by the present method led to a dramatic confrontation:

4.2.2.1 Indication of Near Wake Limit Cycles

Calculations carried out for the higher Reynolds number experiments $RE_1\delta^{xx} = 33600$ and assuming "natural transition" produced iterative solutions which converged to yield a base pressure closely in agreement with the measured value if the boundary layer profile approaching the base had a velocity profile exponent of the order 1/8; however, for values of N = 6, oscillating solutions have been obtained which could be traced to the alternating appearance of transitional flow conditions approaching wake closure location.

4.2.2.2 Theoretical and Experimental Shear Stress Levels and Mixing Profile Spread Rates

All hot wire anemometer measurements reported by Gaviglio, et. al., have been conducted at the lower Reynolds number level of $RE_1\delta^{xx} = 16,800$ and it was attractive to compare their direct measurements of local turbulent stress levels with results obtained form program AB3. Programming "natural transition", in particular, the relationsip between the reported shear stres ratios $\tau_j/\tau(0)$ where $\tau(0)$ represents the wall shear stress of the ttached boundary layer before separation, can be expressed in the form

$$\frac{\tau_j}{\tau(0)} = \frac{2}{\sigma C_{fo}} \frac{T}{} \frac{p_2}{p_1} \frac{1-C_1^2}{C_1^2} \frac{C_2^2\phi_2^2}{1-C_2^2\phi_2^2}$$

For the present conditions, where $C_1^2 = 0.5141$, $C_2^2 = 0.5854$, $p_2/p_1 = 0.5705$, and $C_{fo} = 0.0029$, the program AB3 yielded the values shown in Table 6 which, suprisingly fell about one order of magnitude below those reported by Gaviglio[13]. In addition, the measured velocity profiles appeared to have a spread rate exceeding those expected from

results of earlier observations. While the discrepancies concerning the profile spread ratios could be reduced significantly by repeating the theoretical calculations with the assumption of instantaneous transition, the shear stress levels still could not be reconciled and remain therefore unexplained. This is most startling since there was reasonable agreement on the global near-wake data (base pressure ratio and pressure recovery at wake closure), see Fig. 10. In any case, the lack of support for apparently useful empirical and semi-empirical shear stress models by direct hot-wire measurements certainly deserves further scrutiny, particularly in view of the remarks made[13] that the dividing streamline was determined by the average location within a "randomly fluctuating interface". The sensitivity shown in our own calculations as to the exact boundary layer approach conditions together with the not fully documented corresponding details of the experimental conditions[13] clearly indicate where future efforts must be concentrated. Indeed, the occurence of "flapping"[23] instabilities of plane jets and jet boundaries has been related to abnormally high measured mass entrainment rates and broadening of mixing profiles[24,25].

5. CONCLUSIONS

A flow component model for axisymmetric base flows in unpowered flight has been developed which directs attention to the influence of transition in the jet mixing region developing within an expanded rotational shear layer. Assuming locally similar dissipative straight line entrainment profiles superimposed on the inviscid constant pressure slipstream contour, the region of pressure rise is excluded from the analysis by utilizing a semi-empirical wake closure criterion based on isentropic recompression of the stagnating streamline to a pressure level prescribed by the concept of incomplete turning of the external, inviscid flow. Since the recirculating flow is re-entering the control cross section at constant pressure, there arises no need for introducing a ficticious sting; instead, the effects of actual sting supports can be evaluated. Since the flow fields as represented in the present model extend over distances not much exceeding the afterbody radius, the

treatment of the external slipstream past boattail and near wake is carried out on the basis of a second-order solution of the potential equation replacing the conventional method of characteristics for axially symmetric supersonic flows. By utilizing this approach in the form of a method of sequential centered expansions, it is possible to handle a large variety of afterbody geometries with uniform or non-uniform approaching flows. Computer programs have been developed which arrive at entire flow field solutions in a few iterative steps and produce detailed quantitative information on the transitional exchange mechanisms, thus providing potential support for global numerical fluid dynamics exercises. In this respect, the proposed model is elevated from serving as a convenient tool capable of dealing with a large variety of practical performance parameters to the level of an instrument to be used for exploring the controlling mechanisms.

REFERENCES

1. Chapman, D. R., "An Analysis of Base Pressure at Supersonic Velocities and Comparison with Experiments," Report 1051, 1951, NACA, Washington, D.C.; supersedes TN-2137, 1950, NACA, Washington, D.C.
2. Zumwalt, G. W., "Analytical and Experimental Study of the Axially-Symmetric Supersonic Base Pressure Problem," Ph.D. Dissertation, University of Illinois, 1959.
3. Mueller, T. J., "Determination of the Turbulent Base Pressure in Supersonic Axisymmetric Flow," J. Spacecraft, Vol. 5, No. 1, Jan. 1968, pp. 101-107.
4. Minyatov, A. V., "Raschet Donnogo Davleniya v Sverkhzvukovom Potoke Obekayushchem Telo Vrashcheniya," "(Calculation of the Base Pressure in the Supersonic Flow about a Body of Revolution),: Mekhanika i Mashinostroenie, Izvestia Akademii Nauk USSR., Otdelenie Tekhnicheskikh Nauk, No. 3, May-June 1961, pp. 32-39.
5. Mueller, T. J., C. R. Hall, Jr., and P. J. Roache, "Influence of Initial Flow Direction on the Turbulent Base Pressure in Supersonic Axisymmetric Flow," AIAA J. of Spacecraft and Rockets, Vol. 7, No. 12, Dec. 1970, pp. 1484-1488.
6. Mueller, T. J. and L. D. Kayser, "A Method of Determining the Turbulent Base Pressure in Uniform and Non-Uniform Supersonic Axisymmetric Flows," Technical Report ARBRL-TR-02374, Oct. 1981.
7. Peters, C. E., and W. J. Phares, "Analytical Model of Supersonic, Turbulent, Near Wake Flows," AEDC-TR-76-127, Arnold Engineering Development Center, Ardnold Air Force Station, Tenn., 1976.
8. Weng, C. H., "Base Pressure Problem associated with Supersonic Axisymmetric External Flow Configurations," Ph.D. Dissertation, University of Illinois, 1975.

9. Chow, W. L., and C. H. Weng, "Axisymmetric Supersonic Base Pressures," AIAA J., Vol. 16, No. 6, 1978, pp. 553-554.
10. Yoshikawa, K. K., and A. A. Wray, "Steady and Nonsteady Supersonic Turbulent Afterbody Flow," NASA Technical Paper 1769, 1981.
11. Chapman, D. R., D. M. Kuehn, and H. K. Larson, "Investigation of Separated Flows in Supersonic and Subsonic Streams with Emphasis on the Effect of Transition," NACA TN 3869, 1957.
12. Page, R. H., and V. Sernas, "Apparent Reverse Transition in an Expansion Fan," AIAA J., 8, 189-190, 1970.
13. Gaviglio, J., J.-P. Dussauge, J. F. Debieve, and A. Favre, "Behavior of a Turbulent Flow Strongly out of Equilibrium at Supersonic Speeds," The Physics of Fluids, 20, 179-193, 1977.
14. Korst, H. H., "Dynamics and Thermodynamics of Separated Flows," Heat and Mass Transfer in Flows with Separated Regions, Pergamon Press, Oxford, 1972.
15. Korst, H. H., and W. L. Chow, "On the Correlation of Analytical and Experimental Free Shear Layer Similarity Profiles by Spread Rate Parameters," J. Basic Eng., Trans. ASME, Series D, Vol. 93, 1971, pp. 377-382.
16. Gerhart, P. M., and H. H. Korst, "On the Free Shear Layer Downstream of a Backstep in Supersonic Flow," J. of Fluids Eng., ASME, 95, 1973, Series 1, 361-366.
17. Carriere, P., M. Sirieix, and J. Delery, "Methodes de Calcul des Ecoulements Turbulents Decolles en Supersonique," Progress in Aerospace Sc., 16, 385-429, 1975.
18. Page, R. H., T. J. Kessler, and W. G. Hill, Jr., "Reattachment of Two-Dimensional Supersonic Turbulent Flows," ASME Paper 67-FE-20, 1967.
19. Korst, H. H., and R. A. White, "Internal and External Ballistics of Missiles with Special Consideration of Jet-Plume Interference Effects during Launch and Free Flight Phases," University of Illinois Report UILU ENG 80-4007 (1980).
20. Johannesen, N. H., and R. E. Meyer, "Axially-Symmetrical Supersonic Flow near the Centre of an Expansion," The Aero. Quarterly, Vol. 2, 1950, pp. 127-142.
21. Korst, H. H., "Slipstream Boundaries for Supersonic Flow Separating from Bodies of Revolution," Technical Report UILU ENG 74-4007, Gas Dynamics Lab., Dept. of Mech. and Ind. Eng., University of Ill. at U-C., Sept. 1974.
22. Tani, I., "Experimental Investigation on Flow Separation over a Step," paper presented at Symposium on Boundary Layer Research, Freiburg, Germany, August 26-29, 1957.
23. Cervantes de Gotari, J., and V. W. Goldschmidt, "The Apparent Flapping Motion of a Turbulent Plane Jet--Further Experimental Results," ASME Paper 80-WA/EE-13, ASME Winter Annual Meeting, Chicago, Ill., Nov. 16-21, 1980.
24. Korst, H. H., "Evaluation of Plane Slot Jet Flow Entrainment Enhancement by an Oscillating (Pitching) Vane in the Core Region," University of Illinois, Dept. of Mech. and Ind. Eng. Report, prepared under U.S. Navy Contract No. N62271-80-M-2142, Feb. 1982.
25. Simmons, J. M., J. C. S. Lai, and M. F. Platzer, "Jet Excitation by an Oscillating Vane," AIAA J., Vol. 19, 1981, pp. 763-767.

Table 1 Printout of Input, Program AB1

Table 2 Near Wake Solution for Input Conditions in Table 1

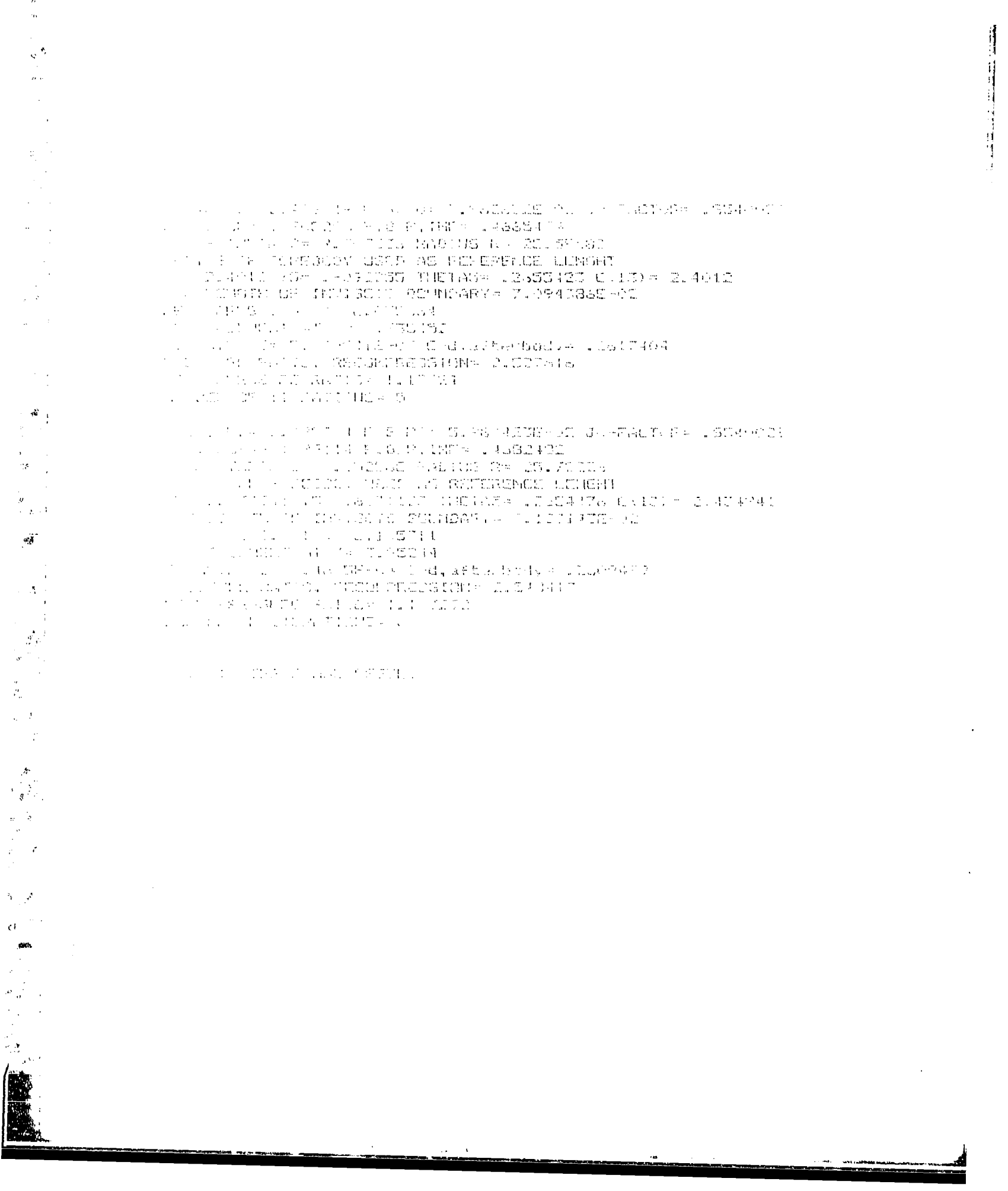

Table 3 Streamwise Development of Turbulent Reynolds Number as Calculated by Program AB3--Comparison with Assumption of Peters[7] (see Table 4)

Point No.	21	22	23	24	25	26	27	28
RE-T	2650	2660	2620	2560	2490	2420	2340	2270
ϕ_2	.6948	.7248	.7561	.7885	.8219	.8562	.8912	.9269
x/δ_1	.4568	.903	1.678	2.966	5.033	8.250	13.126	20.35
Δ/δ_1	.04275	.08257	.15095	.2635	.4421	.7172	1.1298	1.7354
$RE_{T,P}$	270.67	276.92	279.92	281.69	282.38	282.94	281.96	281.85

Table 4 Printout of Program AB3 (Input for Table 3)

```
TH[illegible] [illegible]SION WITH PLOT,AAH [illegible]
L[illegible]EAR RI[illegible]ING PROFILE IN E[illegible]PANDED [illegible] PROFILE B.L.
[illegible] REGION OF [illegible] CAN HANDLE THIN APPR. B.L.
GAMMA= 1.4[illegible]00E+00     UPSTREAM B.L. PROFILE EXP.= [illegible].0000E+00
M[illegible] [illegible]E+00     [illegible]E+00     [illegible]1= [illegible].0410E-01
REYNOLDS #-1-A-DELTA1 = 4.[illegible]701E+04     SIGMA (CONST.)= 1.5410E+01
# OF INTEGRATION STEPS= 2.0000E+01     REYNOLDS #, TRANS.= 1.0000E+01
SIMILARITY VALUE FOR J0= [illegible].0[illegible]74E-01
```

J	X DELTA,1	DELTA.DELTA,1	PHI-J	PE-T
1	1.46E-19	1.76E-11	2.97E-01	0.00E+00
2	4.73E-16	3.80E-08	2.99E-01	0.00E+00
3	2.57E-11	1.37E-06	3.03E-01	0.00E+00
4	1.27E-08	1.50E-05	3.07E-01	0.00E+00
5	7.63E-07	9.16E-05	3.16E-01	0.00E+00
6	1.32E-05	3.91E-04	3.25E-01	0.00E+00
7	2.44E-04	1.32E-03	3.35E-01	0.00E+00
8	2.73E-05	4.49E-04	3.26E-01	0.00E+00
9	4.01E-05	5.14E-04	3.27E-01	0.00E+00
10	5.59E-05	5.85E-04	3.28E-01	0.00E+00
11	7.59E-05	6.65E-04	3.29E-01	0.00E+00
12	1.01E-04	7.54E-04	3.30E-01	0.00E+00
13	1.33E-04	8.52E-04	3.31E-01	0.00E+00
14	1.73E-04	9.61E-04	3.32E-01	0.00E+00
15	2.23E-04	1.08E-03	3.34E-01	0.00E+00
16	2.35E-04	1.21E-03	3.35E-01	0.00E+00
17	2.85E-04	1.21E-03	3.35E-01	6.58E+01
18	1.88E-03	1.36E-03	3.36E-01	3.37E+02
19	2.76E-02	3.76E-03	3.46E-01	2.03E+03
20	8.72E-02	9.27E-03	3.58E-01	2.52E+03
21	2.13E-01	2.07E-02	3.71E-01	2.65E+03
22	4.57E-01	4.27E-02	3.86E-01	2.66E+03
23	9.03E-01	8.26E-02	4.01E-01	2.62E+03
24	1.68E+00	1.51E-01	4.16E-01	2.56E+03
25	2.97E+00	2.63E-01	4.33E-01	2.49E+03
26	5.03E+00	4.42E-01	4.50E-01	2.42E+03
27	8.25E+00	7.17E-01	4.68E-01	2.34E+03
28	1.31E+01	1.13E+00	4.86E-01	2.27E+03
29	2.04E+01	1.74E+00	5.06E-01	2.20E+03
30	3.09E+01	2.61E+00	5.25E-01	2.12E+03
31	4.59E+01	3.84E+00	5.46E-01	2.05E+03
32	4.59E+01	3.84E+00	5.46E-01	2.05E+03
33	6.73E+01	5.91E+00	5.67E-01	1.96E+03

```
J= 2.1000E+01

PHI-1(I)= 5.0000E-01     PHI-1(I+1)= 5.5000E-01
PHI-2(I)= 5.6620E-01     PHI-2(I+1)= 6.2431E-01
YL  YI= 1.4490E-02     DELTH DELTHI= 4.2745E-02      2.8716E-02
JN= 5.3559E-01     YL DELTHI=-2.8255E-03
JN-RATIO= 4.1367E-01
(DELTHI) TURB.= 4.5664E-01
SHEAR STRESS FUNCTION= 2.8247E-02     EDDY-VISCOSITY FUNCTION= 7.4000E-02

J= 2.2000E+01

PHI-1(I)= 5.5000E-01     PHI-1(I+1)= 6.0000E-01
PHI-2(I)= 6.2431E-01     PHI-2(I+1)= 7.2484E-01
YL  YI= 2.9285E-02     DELTH DELTHI= 4.2766E-02      4.2745E-02
JN= 4.9060E-01     YL DELTHI=-5.4480E-03
JN-RATIO= 4.6353E-01
(DELTHI) TURB.= 4.8300E-01
SHEAR STRESS FUNCTION= 2.3637E-02     EDDY-VISCOSITY FUNCTION= 7.6899E-02

J= 2.3000E+01

PHI-1(I)= 6.0000E-01     PHI-1(I+1)= 6.5000E-01
PHI-2(I)= 7.2484E-01     PHI-2(I+1)= 8.5614E-01
YL  YI= 5.1446E-02     DELTH DELTHI= 1.5045E-01      8.2566E-02
JN= 4.6381E-01     YL DELTHI=-4.4911E-02
JN-RATIO= 4.3367E-01
(DELTHI) TURB.= 1.6776E+00
SHEAR STRESS FUNCTION= 5.1501E-02     EDDY-VISCOSITY FUNCTION= 7.9982E-02

J= 2.4000E+01

PHI-1(I)= 6.5000E-01     PHI-1(I+1)= 7.0000E-01
PHI-2(I)= 7.5614E-01     PHI-2(I+1)= 7.8854E-01
YL  YI= 8.9831E-02     DELTH DELTHI= 3.6347E-01      1.5095E-01
JN= 4.4290E-01     YL DELTHI=-1.7264E-01
JN-RATIO= 7.1703E-01
(DELTHI) TURB.= 2.9661E+00
SHEAR STRESS FUNCTION= 3.4258E-02     EDDY-VISCOSITY FUNCTION= 8.3253E-02

J= 2.5000E+01

PHI-1(I)= 7.0000E-01     PHI-1(I+1)= 7.5000E-01
PHI-2(I)= 7.8854E-01     PHI-2(I+1)= 9.2192E-01
YL  YI= 1.5054E-01     DELTH DELTHI= 4.4210E-01      2.6347E-01
JN= 4.2810E-01     YL DELTHI=-2.3156E-01
JN-RATIO= 7.4552E-01
(DELTHI) TURB.= 5.0334E+00
SHEAR STRESS FUNCTION= 3.7590E-02     EDDY-VISCOSITY FUNCTION= 8.6713E-02

J= 2.6000E+01

PHI-1(I)= 7.5000E-01     PHI-1(I+1)= 8.0000E-01
PHI-2(I)= 9.2192E-01     PHI-2(I+1)= 9.5618E-01
YL  YI= 2.4147E-01     DELTH DELTHI= 7.1716E-01      4.4210E-01
JN= 4.1798E-01     YL DELTHI=-4.7369E-01
JN-RATIO= 7.7511E-01
(DELTHI) TURB.= 8.2501E+00
SHEAR STRESS FUNCTION= 4.1144E-02     EDDY-VISCOSITY FUNCTION= 9.0364E-02

J= 2.7000E+01

PHI-1(I)= 8.0000E-01     PHI-1(I+1)= 8.5000E-01
PHI-2(I)= 9.5618E-01     PHI-2(I+1)= 9.7114E-01
YL  YI= 3.3171E-01     DELTH DELTHI= 1.1238E+00      7.1716E-01
JN= 4.0647E-01     YL DELTHI=-7.4014E-01
JN-RATIO= 8.0578E-01
(DELTHI) TURB.= 1.1136E+01
SHEAR STRESS FUNCTION= 4.5134E-02     EDDY-VISCOSITY FUNCTION= 9.4212E-02

    2.8000E+01

PHI-1(I)= 8.5000E-01     PHI-1(I+1)= 9.0000E-01
PHI-2(I)= 9.7114E-01     PHI-2(I+1)= 9.8678E-01
YL  YI= 4.2133E-01     DELTH DELTHI= 1.7734E+00      1.1238E+00
JN= 3.9451E-01     YL DELTHI=-1.1581E+00
JN-RATIO= 8.3746E-01
(DELTHI) TURB.= 1.4015E+01
SHEAR STRESS FUNCTION= 4.8538E-02     EDDY-VISCOSITY FUNCTION= 9.7267E-02
```

Table 5 Theoretical Values for Streamwise Development of the Cell Reynolds Number as Calculated by Program AB3--Freestream Mach No. 2.5*--Comparison with Assumption of Yoshikawa[10]

Point No.	x/δ_1	Jφ	Re - T	[R]
17	3.1277	0.43349	6,690	545.4
18	6.0819	0.4583	4,050	172.66
19	13.927	0.4886	3,120	59.5
20	32.44	0.522	2,720	22.82

*$M_1 = 2.5$, $C_1 = 0.74536$, $M_2 = 3.1$, $C_2 = 0.81103$, $\gamma = 1.67$.

Table 6 Theoretical and Experimental[13] Shear Stress Ratios along Transitional Mixing Layer

Point No.	20	21	22	23	24	25	26	27	28
x/δ_1	.2083	.4832	.9867	1.863	3.323	5.673	9.3415	14.92	23.24
ϕ_2	.663	.692	.7224	.754	.787	.8204	.854	.890	.9263
T_j	.02075	.02266	.0248	.0272	.02987	.03284	.03614	.03982	.043907
$\tau(j)/\tau(o)$	.1912	.2347	.2901	.3609	.4520	.568	.7193	.9161	1.1792
x/d	.0208	.048	.0987	.1863	.3323	.5673	.93415	1.492	2.324

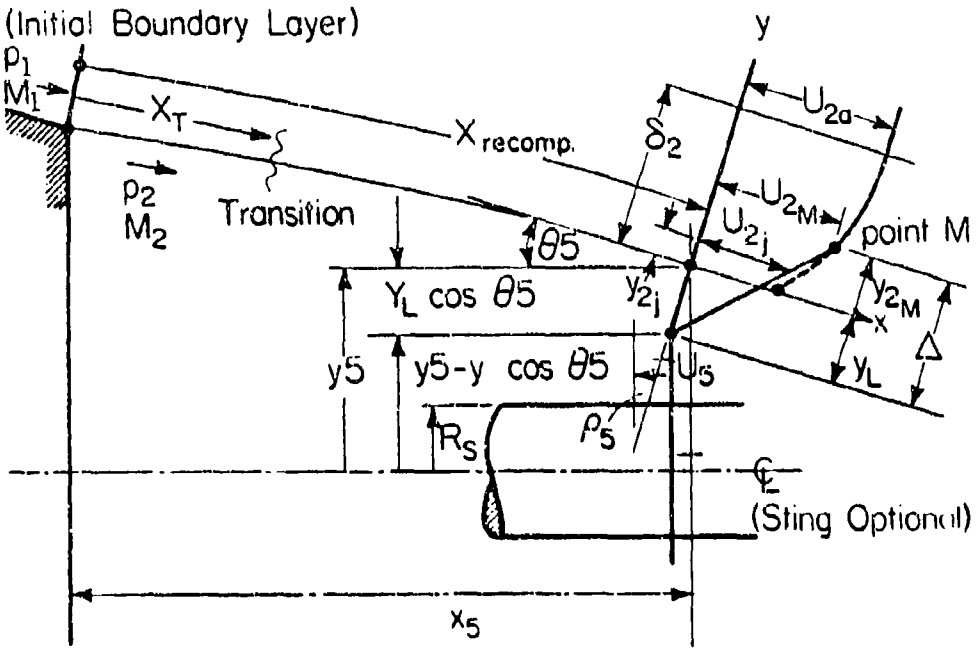

Figure 1 Near Wake Flow Model--Power Off with Closure at Location of Initial Pressure Rise

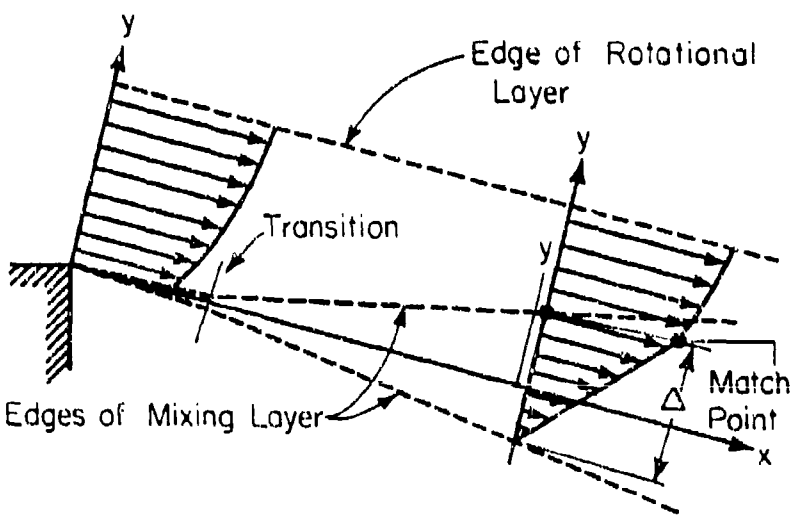

.Figure 2 Boundary Layer Expansion followed by Development of Two-Layer Transitional Mixing Profile

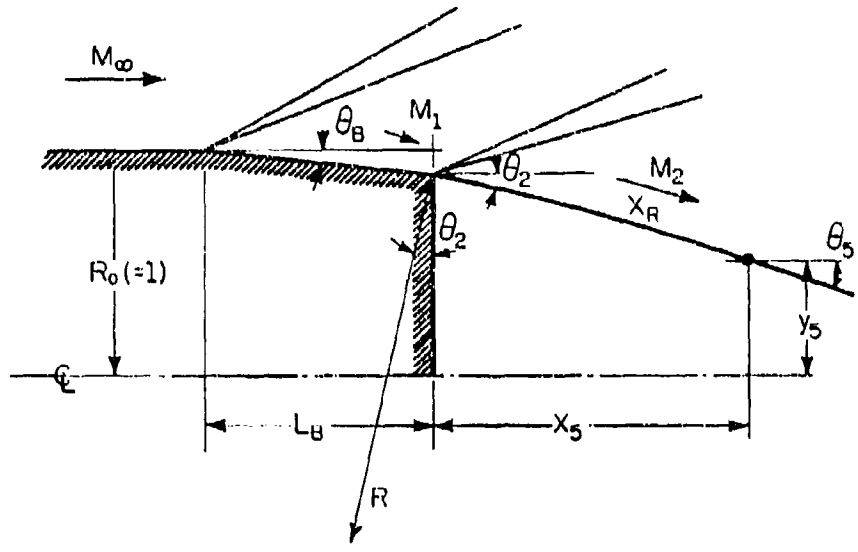

Figure 3 Inviscid External Flow past Boattail and Near Wake (by Method of Sequential Centered Expansions)

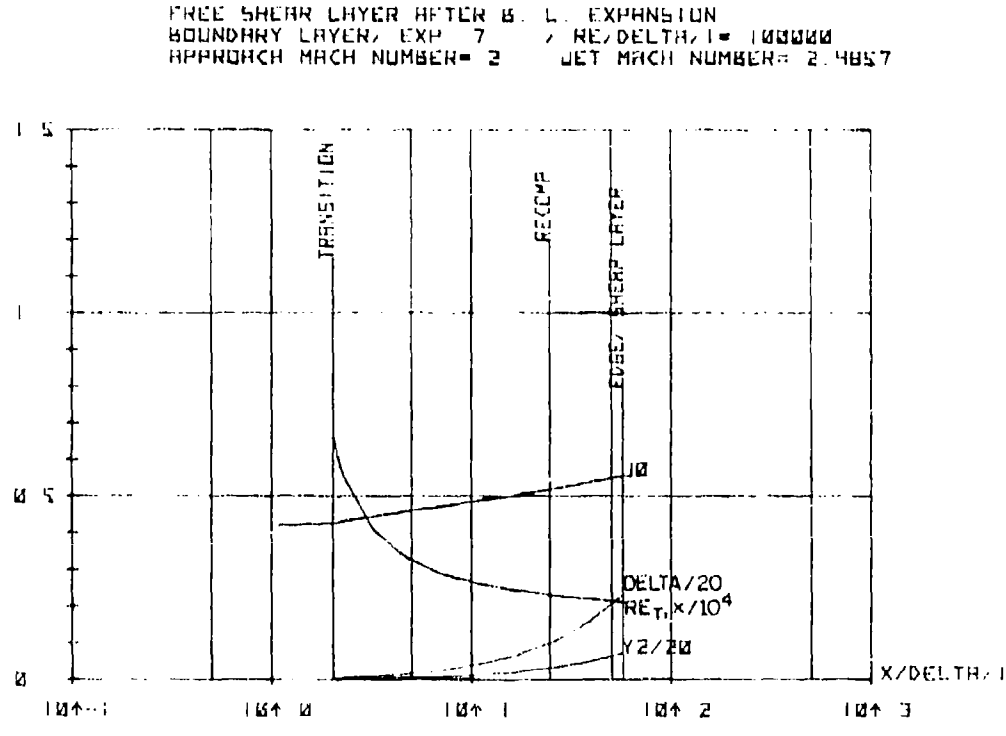

Figure 4 Development of Two-Layer Mixing Profile for Input of Table 1, Solution of Table 2 ("Natural Transition")

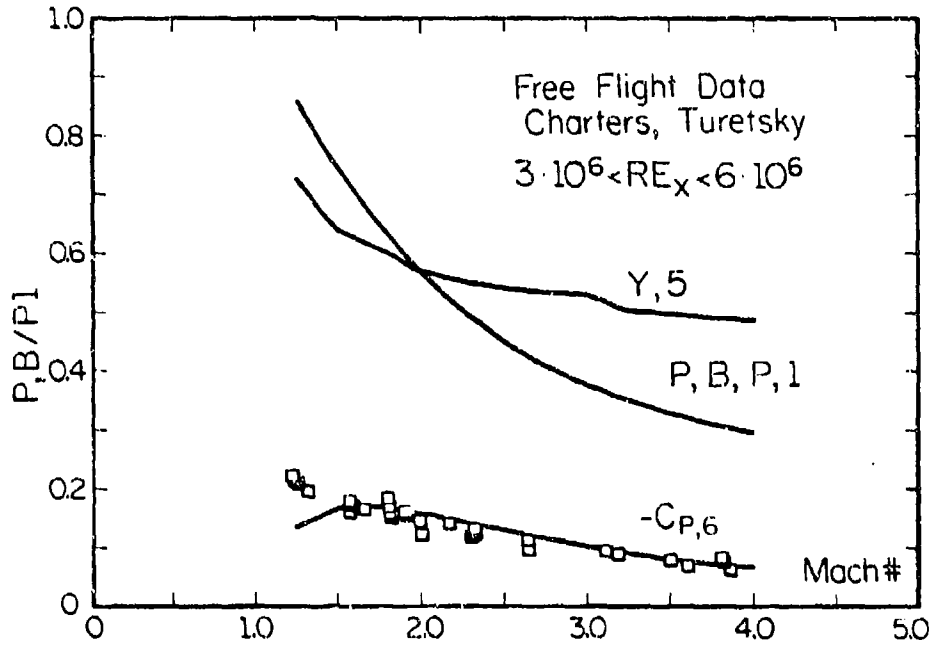

Figure 5 Cylindrical Afterbodies in Supersonic Unpowered Flight--Theory and Selected Free Flight Data

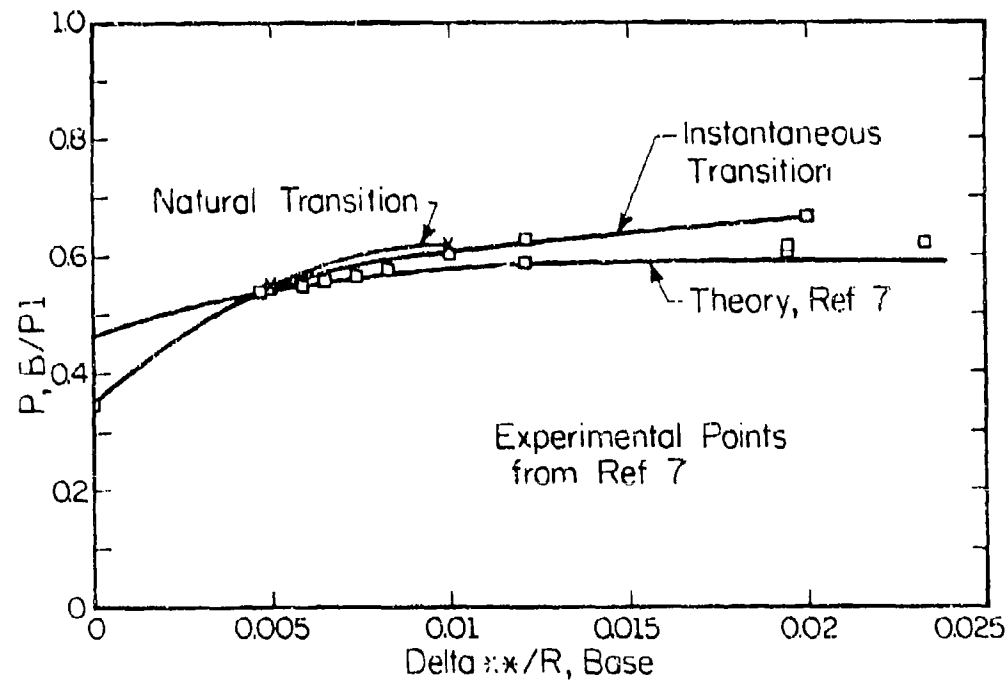

Figure 6 Effect of Approaching Boundary Layer Thickness on Near Wake Solution for Cylindrical Afterbody at Freestream Mach No. 2--Comparison of Theoretical and Experimental Results

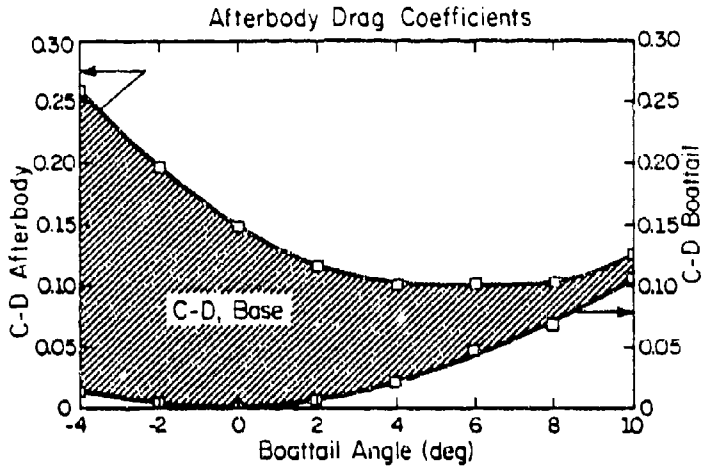

Figure 7a Afterbody Drag for Boattailed Bodies of Revolution in Supersonic Unpowered Flight --Apportionment of Base and Boattail Drag and Drag Optimization--Freestream Mach No. 2

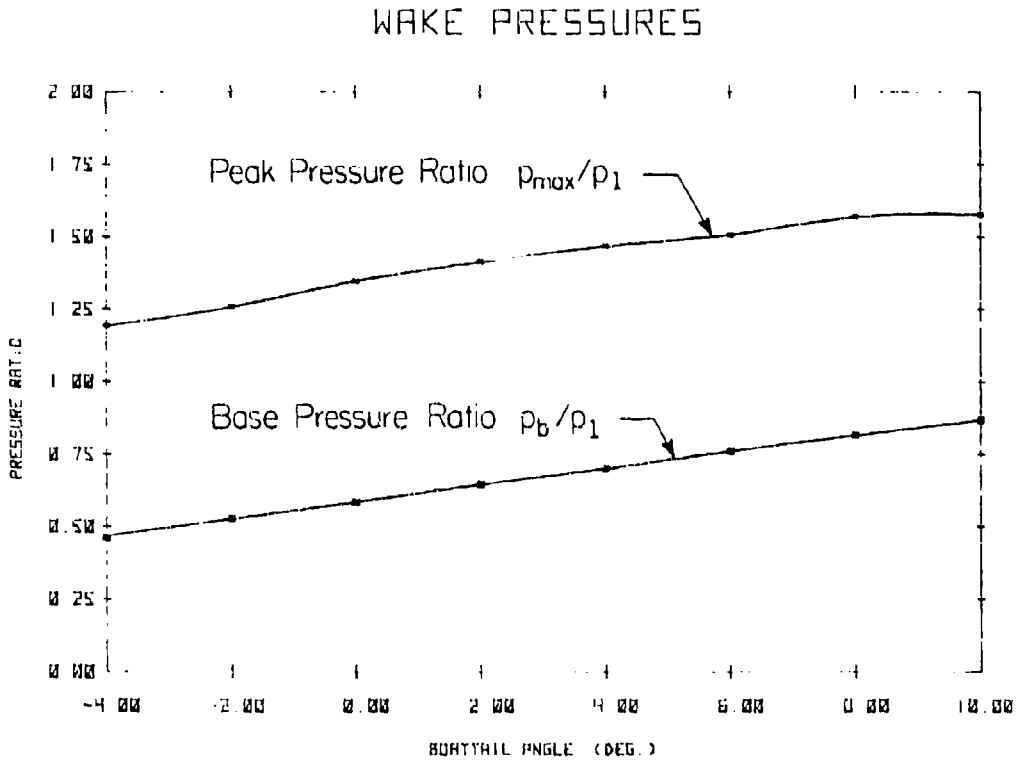

Figure 7b Boattailed Bodies of Revolution: Base Pressure and Peak Pressure Ratio (M = 2)

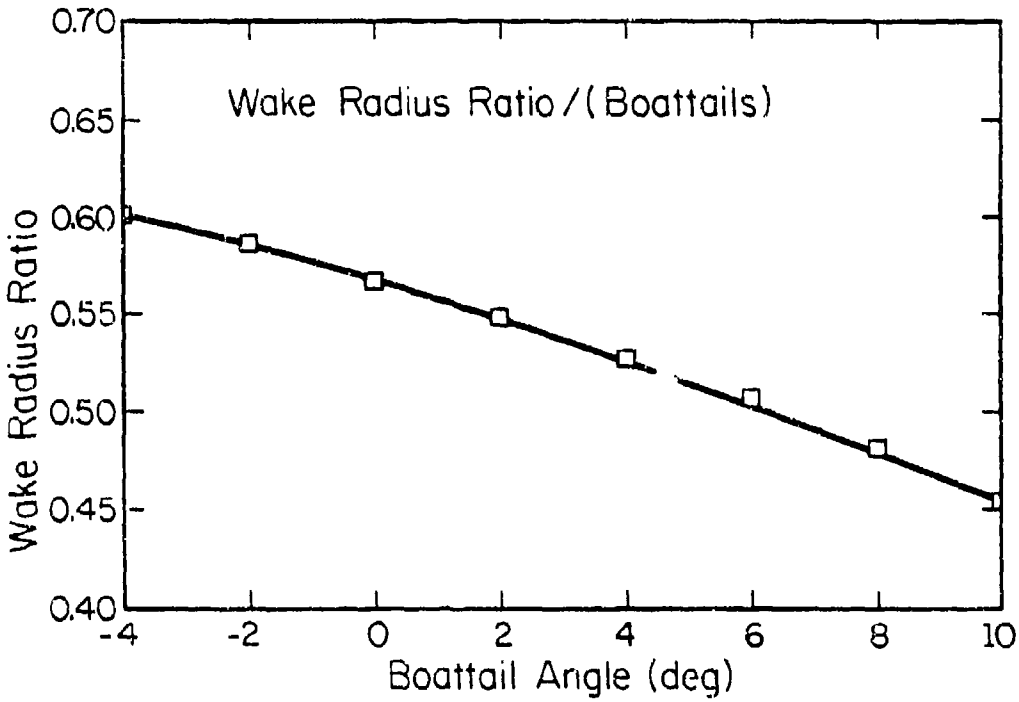

Figure 7c Boattailed Bodies in Unpowered Supersonic Flight at Freestream Mach No. 2 Theoretical Values for Wake Radius Ratio

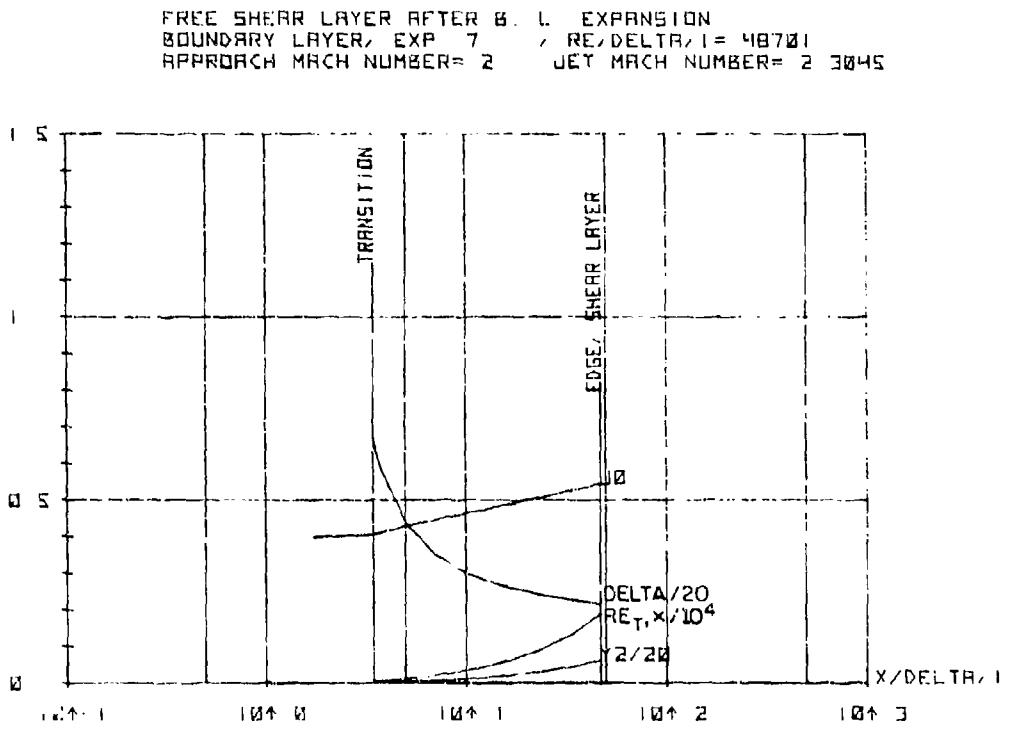

Figure 8a Mixing Layer Development, Case Table 1, for "Natural Transition" Criterion

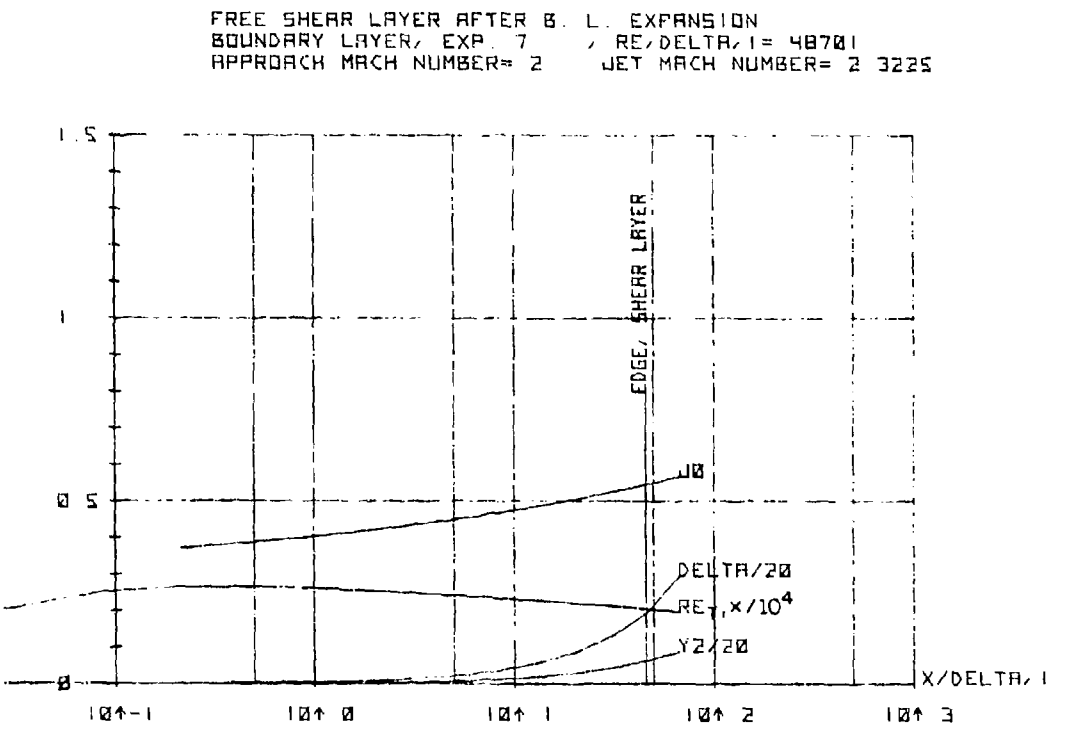

Figure 8b Mixing Layer Development, Case Table 1, for "Instantaneous Transition" Criterion

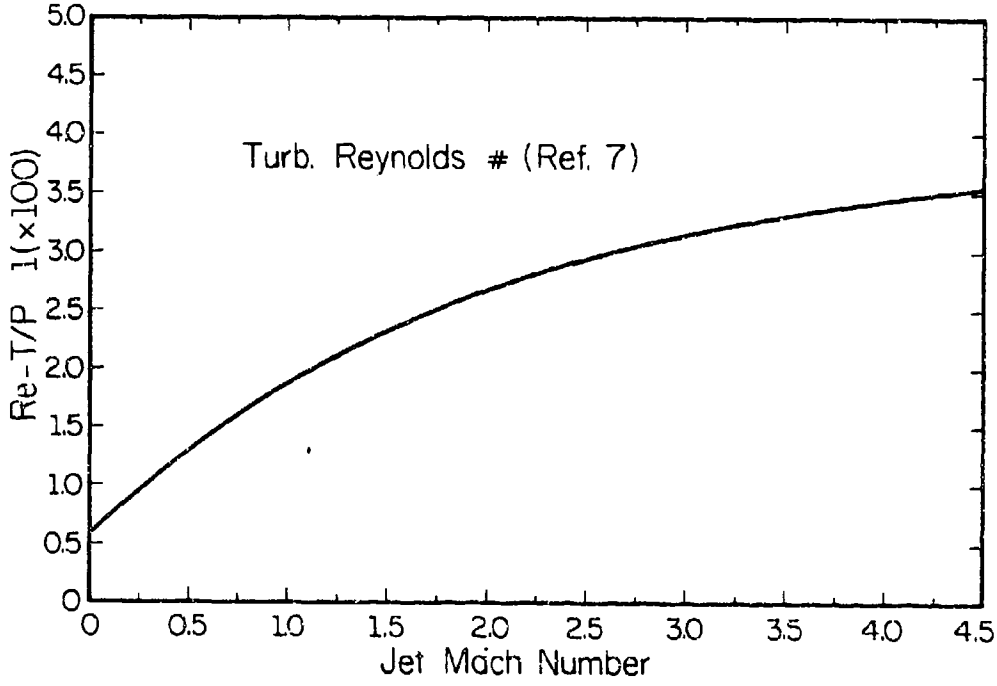

Figure 9 Turbulent Reynolds Number as Unique Function of Slipstream Mach Number[7]

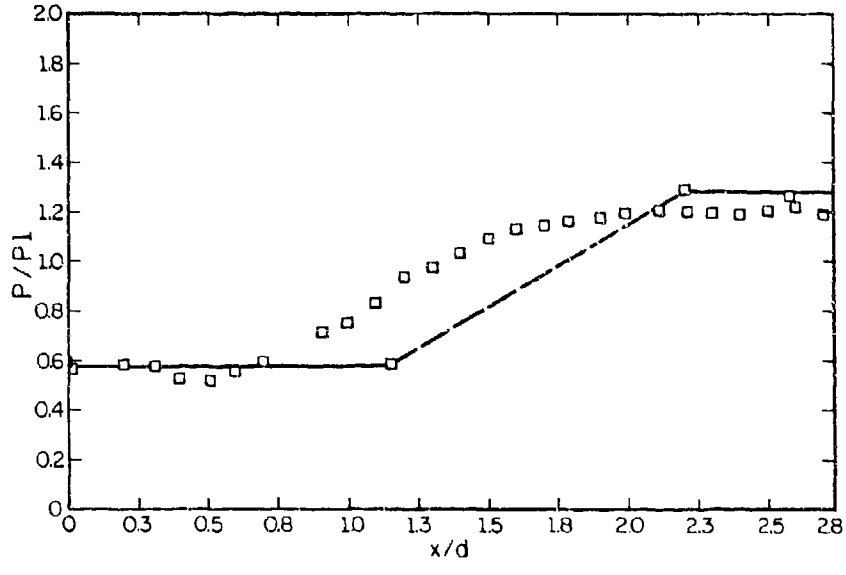

Figure 10 Comparison between Theoretical and Experimental[13] Near Wake Pressure Levels

APPENDIX D

ANALYSIS AND MODELING OF PLUME EFFECTS ON MISSILE AERODYNAMICS -- AN OVERVIEW

Paper presented at the

Symposium on Rocket/Plume Fluid Dynamic Interactions

Huntsville, Alabama

April 1983

by

Professor H. H. Korst

APPENDIX D

Analysis and Modeling of Plume Effects on Missile Aerodynamics--An Overview

H. H. Korst
Department of Mechanical and Industrial Engineering
University of Illinois at Urbana-Champaign
Urbana, IL 61801

1. OBJECTIVES

The objective of evaluating missile performance falls into two main categories:

1. Internal flow analysis which includes the burning conditions in the rocket chamber and the expansion of the propellant gases in the nozzle, and

2. External aerodynamics concerned with lift, drag, and moments acting on the entire missile body.

It must be generally expected that the propulsive jet exiting from the nozzle will interact with the external flow in various degrees and modes affecting both propulsive efficiency (e.g. as a consequence of base drag) and aerodynamic performance. In serious cases of plume induced flow separation from the afterbody and/or control surfaces, catastrophic trajectory degradation may be encountered.

A thorough understanding of the physical phenomena is needed to develop predictive and interpretative capabilities through analytical and experimental methods.

Figure 1 gives an account of different types of activities in support of these general objectives. It is the purpose of this symposium not only to examine the state-of-the-art and individual achievements of these different approaches but, what appears to be more important, to define the needs for and specific benefits expected from closer coordination of all these efforts. Without going into such details as will be brought forth in subsequent sessions, it can be stressed that the central issue rests with the predictability of prototype performance. Consequently, the peripheral and therefore supportive activities must be examined with respect to their ability, or potential, to deal with all pertinent parameters and variables of the flight performance. Since it will be seen that this is generally impossible, a critical evaluation of realistic objectives and limitations inherent in the different methodologies is in order. At the same time it will serve the purpose of the symposium to emphasize the mutually supportive potential of cooperative programs.

As suggested by Fig. 1 the merits of peripheral activities (A), Analytical; (E), Experimental; and (C), Computational, are to be examined individually, in relation to each other and, most of all, with

respect to their potential of predicting or explaining prototype performance. The nature of the supporting activities shall now be discussed in chronological order of their development.

1.1 Experimental Programs

In absence of any viable theoretical concepts, the near wake problem originally had to be studied with strong reliance on experimental evidence[1]. Going beyond the gathering of empirical information, the fundamental observations of Chapman concerning the importance of transition in approaching, free and reattaching shear layers[2] ushered in an era of analytical approaches. This work drew special attention to essential details of the overall flow problem and logically led to the delineation of component mechanisms, their interactions and their subsequent synthesis into overall systems evaluations. In turn, experimental activities received guidance from analytical insights gained and could then focus on both component and system testing.

Indeed it was up to analytical methods to furnish a rational basis for the proper modeling of plume interference effects in wind tunnel experiments[3].

1.2 Analytical Models

Developed in early 1950, such models stress the importance of strong interactions between inviscid and viscous flow mechanisms.

Two major generic concepts have been pursued, namely integral methods (following the approach of Crocco and Lees[4]), and the component models (Chapman-Korst[5,6]) and its derivatives. A comprehensive review of the ensuing developments has been made by Carriere, Sirieix and Delery[7].

One observes that the physically perceptive features of the component models draw immediate attention to both their merits and shortcomings: While delineating all individual flow processes in detail, they do not equally well in dealing with their interactive modes, especially in the region of wake recompression. Even though the Chapman-Korst model gives proper attention to the energetic aspects of individual streamlines, the wake closure condition exhibits some well understood, yet uncomfortable, complexities. This can be illustrated by the formal adapcation of the second law of thermodynamics to the recompression process of the stagnating streamline.

The analysis[6] which assumes the preponderance of transversal exchange mechanisms, a Prandtl number of unity, the validity of Crocco's integral and isoenergetic conditions throughout the reattachment zone, shows that the process of recompression is nearly isentropic. In this respect, the "escape criterion" as originally stated[5] emerges directly. However, while the essential validity of the isentropic compression process has been verified[7], it is the elusiveness of pinpointing the pressure level at the reattachment point--the environment

against which the flow above the stagnation streamline has to exit and where the local value of the availability function cannot be negative--which obscures the issue. This was recognized at the outset[8], but entirely analytical solutions to resolve the problem have not been found despite much efforts.

Reverting to the physical aspects of the recompression component, the concept of incomplete turning of the adjacent inviscid flowfield (and the possible modification of the impressed pressure field by streamline curvature in the viscous region) has been explored with some success[7,9]. While addressing itself to an essential and actual feature of the reattachment process, empirical formulations had to be retained.

1.3 Computational Fluid Mechanics

The availability of high capacity, high speed digital computers, together with the development of efficient algebraic algorithms has encouraged large scale numerical efforts directed to the solution of flow problems heretofore untractable. No longer depending, in principle, upon the simplifications introduced by boundary layer approximations, the numerical simulation of entire flowfields dealing with inviscid-viscid interactions as well as with elliptic, parabolic, and hyperbolic regions of flow interdependency in a global sense appears to be in reach. Yet from a physical point of view, certain stringent impediments become immediately apparent, namely:

1. The need for adaptive grid geometries with localized very high resolution requirements,

2. The need for accurate quantitative information on viscous mechanisms, and

3. The availability of substantial computer time on the most powerful machines.

An additional concern emerges from the observation that near wakes (especially those having transitional free shear layers) may exhibit essential non-steady features in the sense of short duration limit cycles.

2. INDIVIDUAL CAPABILITIES AND RELATIONSHIPS BETWEEN DIFFERENT PREDICTIVE METHODS

In the following, an attempt is made to categorize the tasks and the limitations imposed on analytical, (A); experimental, (E); and computational, (C) efforts. This is presented in the form of Tables 1, 2, and 3.

Table 1 evaluates and compares analytical versus experimental programs; Table 2 is concerned with computational versus analytical; Table 3 is concerned with computational versus experimental

activities. Even though these tables may lack some additional and possibly important criteria, they can serve to identify areas of mutual interest and interdependency. A few specific problems shall now be discussed.

Figure 2 shows a Schlieren photograph of a complete missile configuration including a finned boattail tested in a supersonic wind tunnel at Mach 2.0 at an angle of attack. The complexity of the flow is well borne out and points directly to the principal difficulties to be encountered in efforts of both categories (A) and (C). Yet there are two serious limitations in experimental programs which may effect the direct applicability of aerodynamic performance parameters to the prototype:

1. The problem of scaling a Reynolds number influence which is of special importance when transitional wake flow components become an issue.

2. The problem of plume simulation--(correct plume effect simulation is needed when wind tunnel operations do not permit the use of actual propellant gases).

2.1 Analytical versus Experimental Efforts

As suggested in Table 1, these questions can, in principle, be studied (at least in an approximate manner) by utilizing analytical modeling schemes. On the other hand, improvements in analytical modeling can only be expected by extracting detailed information from component and full configuration testing in wind tunnels.

2.2 Computational versus Analytical Efforts

Table 2 addresses the comparison between efforts of categories (C) and (A). In some way the limitations appear to be of similar nature, yet they present evidence indicating that computational efforts have so far not yet coped with the very serious problems related to turbulent mixing in shear layers strongly out of equilibrium[10]. In particular, the initial shear layer development after strong expansions and compression leads to grid size assignment problems which have not been resolved in needed detail[11,12]. Figure 3 strikingly demonstrates the disappearance of coherent structures generated in the attached boundary layer and the development of a new transitional free shear layer for a flow near an expansion corner[13] while Fig. 4 gives an account of the corresponding jet mixing calculations based on a transitional two-layer model[14,15]. It is of interest to note that the analytical turbulent cell Reynolds numbers can be determined[15] which before could only be utilized in a crude parametric trial and error fashion[12].

2.3 Computational versus Experimental Efforts

Table 3 gives a direct comparison between activities (C) and (F). Tasks and limitations of both methods have already been identified in

the preceeding sections but the correspondence of efforts dealing with global flowfield presentations becomes more clearly defined.

3. SPECIFIC EXAMPLES FOR INFORMATION INTERDEPENDENCY

The exchange of information is indicated by reference to the identifying symbols (A), (E), and (C).

3.1 Needs of Computational Fluid Mechanics

Chosing as a focal point a most recent and representative effort at NASA, Ames Field Research Center, by Deiwert[11], one notices the direct reference to an experimental program carried out at FFA, Bromma, Sweden, by Agrell and White[16] which leads to the following comments:

1. The adoption of an initial grid point system conforming with a Schlieren picture (as a computer-time saving feature) is immediately recognized, (E) → (C).

2. Assumption of conical source flow emerging from the propulsive nozzle cannot be accepted since it is well known that the throat geometry can strongly effect the flow field near the nozzle exist, see Fig. 5, (A) ↔(E) → (C).

3. Initiation of viscous jet mixing, resulting from the expansion of the nozzle flow near the nozzle lip deserves close scrutiny in view of the well documented, but seldom considered, behavior of turbulent flow strongly out of equilibrium[10].

4. Strongly expanded shear layers may produce an initially laminar jet entrainment region[13], subject to subsequent transition, (E) → (A) ↔ (E).

5. It is well known that the transition location significantly effects the recompression mechanism at the end of the near wake[2], (E) → (A) → (C).

6. The recompression mechanism itself is controlled by turbulent momentum exchange not represented by equilibrium conditions[10], (E) → (C).

7. As shown in Fig. 2, the complexity of flowfields representative of prototype missiles in flight will generally impose insurmountable difficulties to both computational and analytical efforts.

3.2 Needs of Experimental Programs

To allow prediction of overall prototype performance, the problems of proper plume simulation and Reynolds number scaling must be carefully examined. Here, experimental programs need direction and support from analytical and computational methods, (A) → (C) → (E).

1. An example of closely coordinated activities for determining the feasibility and merits of a mathematical modeling scheme for plume interference effects[3] is illustrated by an organizational chart, Table 4. Preliminary results obtained in a hot Freon 22 facility at the FFA have been encouraging[17]. The importance of accurately defining the flowfields near the nozzle lip has been fully confirmed, (A) → (E) → (A). On the other hand, jet temperature effects are still subject to analytical interpretation, (A) ↔ (E).

2. Reynolds number effects fall into two distinctively different categories, namely the scaling of attached, nearly equilibrium viscous layers, (A) → (E) and (C) → (E), and the more sensitive problem of how to deal with transition and turbulence under "strongly out of equilibrium" conditions. The present state-of-the-art in this matter is unsatisfactory inasmuch as the strong evidence for the importance of the problem[2,10,18] is not yet complemented by adequate quantitative formulations permitting fully predictive modeling.

3.3 Needs of Analytical Modeling

The capabilities and limitations of component models are well enough understood to restrict the analysis to cases where distinction of individual model mechanisms is retained. But, as indicated in the preceeding sections, this is also the strength of analytical modeling: to identify areas of flow component testing and allowing the rational interpretation of such results for subsequent component integration. In this respect, the exchange of information can be identified by the sequences (A) → (E) → (C) and (A) → (E) → (A).

4. CONCLUDING REMARKS

Interaction between analytical, experimental, and computational efforts is needed to improve predictive and/or interpretative capabilities for prototype applications.

Specific areas and topics requiring coordinated planning and subsequent exchange of information have been identified and examples for already existing cooperative efforts have been presented.

The present symposium covers a plurality of approaches but should also serve to underline the unity in purpose leading to better defined and organized cooperation.

REFERENCES

1. Chapman, D. R., "An Analysis of Base Pressure at Supersonic Velocities and Comparison with Experiments," Report 1051, 1951, NACA, Washington, D.C.; supersedes TN-2137, 1950, NACA, Washington, D.C.

2. Chapman, D. R., D. M. Kuehn, and H. K. Larson, "Investigation of Separated Flows in Supersonic and Subsonic Streams with Emphasis on the Effect of Transition," NACA TN 3869, 1957.

3. Korst, H. H., and R. A. Deep, "Modeling of Plume Induced Interference Problems in Missile Aerodynamics," AIAA Paper 79-0362, 17th Aerospace Sciences Meeting, New Orleans, La., 15-17 Jan. 1979.

4. Crocco, L., and L. Lees, "A Mixing Theory for the Interaction between Dissipative Flows and Nearly Isentropic Streams," J. Aero. Sc., 19, 649-676, 1952.

5. Korst, H. H., "A Theory for Base Pressures in Transonic and Supersonic Flow," J. of Applied Mech., 23, 593-600, 1956.

6. Korst, H. H., W. L. Chow, and G. W. Zumwalt, "Research on Transonic and Supersonic Flow of a Real Fluid at Abrupt Increases in Cross Section," University of Illinois ME Tech. Report 392-5, 2nd ed., Oct. 1964.

7. Carriere, P., M. Sirieix, and J. Delery, "Methodes de Calcul des Ecoulements Turbulents Decolles en Supersonique," Progress in Aerospace Sc., 16, 385-429, 1975.

8. Chapman, D. R., and H. H. Korst, "Theory for Base Pressures in Transonic and Supersonic Flow," Discussion; J. Applied Mech., 24, 484, 1957.

9. Page, R. H., T. J. Kessler, and W. G. Hill, Jr., "Reattachment of Two-Dimensional Supersonic Turbulent Flows," ASME Paper 67-FE-20, 1967.

10. Gaviglio, J., J.-P. Dussauge, J. F. Debieve, and A. Favre, "Behavior of a Turbulent Flow Strongly out of Equilibrium at Supersonic Speeds," The Physics of Fluids, 20, 179-193, 1977.

11. Deiwert, G. S., "A Computational Investigation of Supersonic Axisymmetric Flow over Boattails containing a Centered Propulsive Jet," AIAA Paper 83-0462.

12. Yoshikawa, K. K., and A. A. Wray, "Steady and Nonsteady Supersonic Turbulent Afterbody Flow," NASA Technical Paper 1769, 1981.

13. Page, R. H., and V. Sernas, "Apparent Reverse Transition in an Expansion Fan," AIAA J., 8, 189-190, 1970.

14. Gerhart, P. M., and H. H. Korst, "On the Free Shear Layer Downstream of a Backstep in Supersonic Flow," J. of Fluids Eng., ASME, 95, 1973, Serie 1, 361-366.

15. Korst, H. H., and R. A. White, "Internal and External Ballistics of Missiles with Special Consideration of Jet-Plume Interference

Effects during Launch and Free Flight Phases," University of Illinois Report UILU ENG 80-4007 (1980).

16. Agrell, J., and R. A. White, "An Experimental Investigation of Supersonic Axisymmetric Flow over Boattails containing a Centered Propulsive Jet," FFA Tech. Note AU-913, 1974.

17. Korst, H. H., R. A. White, S.-E. Nyberg, and J. Agrell, "The Simulation and Modeling of Jet Plumes in Wind Tunnel Facilities," J. of Spacecraft and Rockets, 18, 427-434, 1981.

18. Baca, B. K., D. R. Williams, and S. M. Bogdonoff, "A Study of Reattachment of a Free Shear Layer in Compressible Turbulent Flow," AIAA Paper 80-1408, 1980.

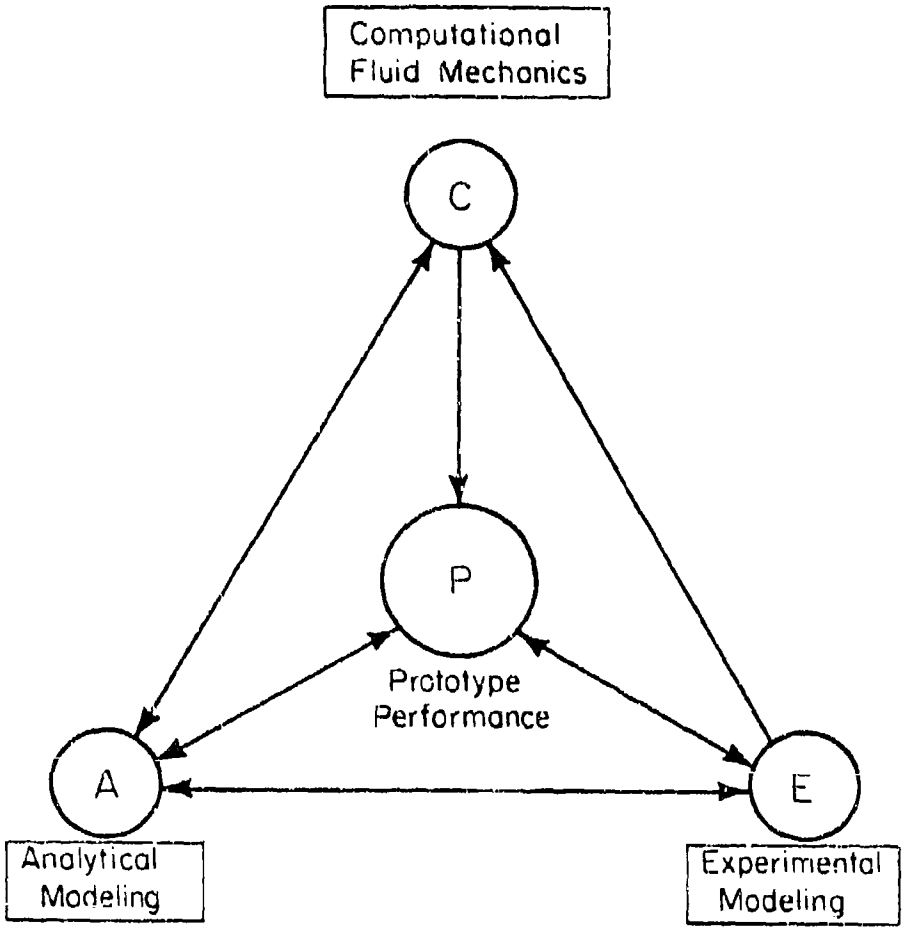

Figure 1 Prediction and Interpretation of the Aerodynamic Performance of Missiles: Central Purpose and Supporting Activities

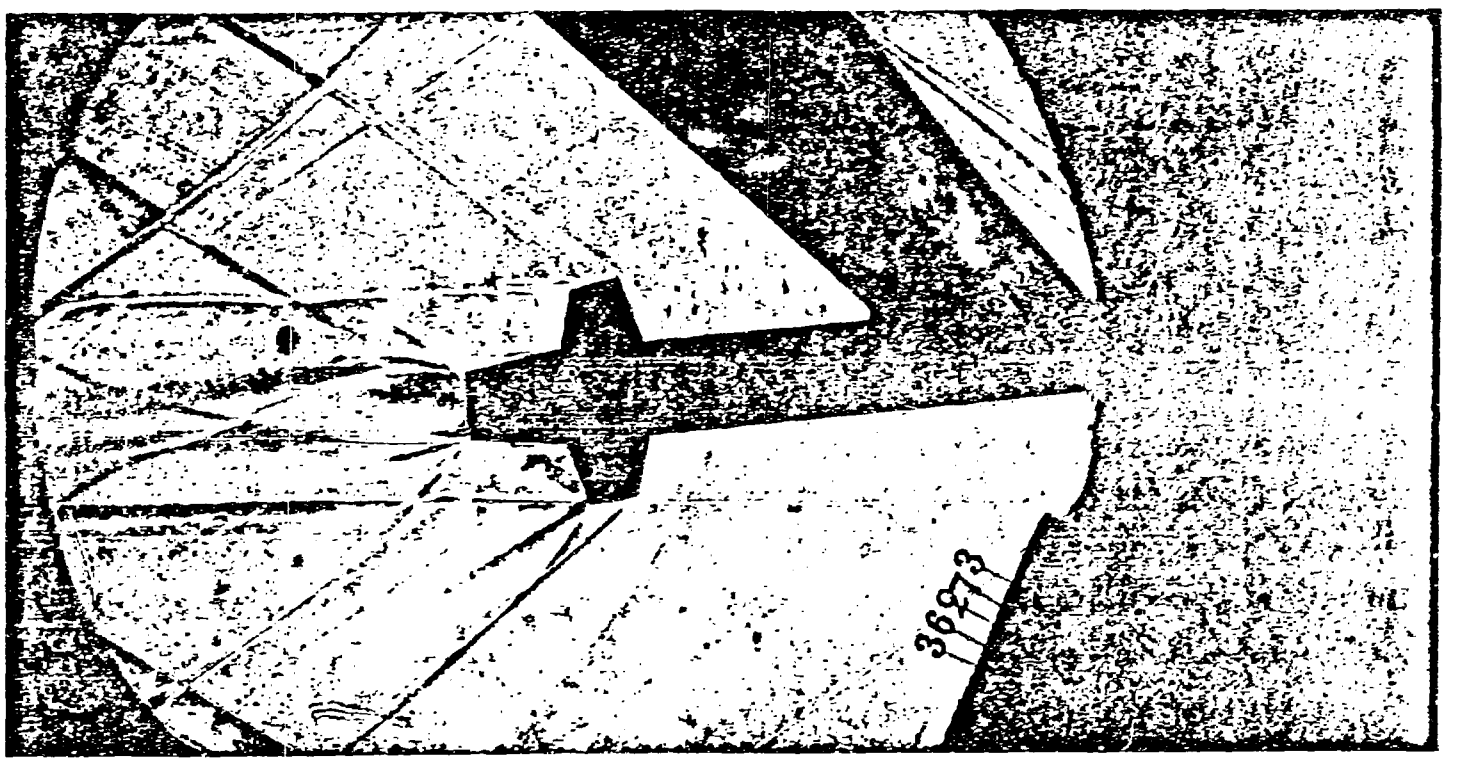

Figure 2 Finned Missile Afterbody in Supersonic Flow, $M_\infty = 2$; Angle of Attack, $\alpha = -6°$; Control Surface Angle, $+10°$ (FFA, Bromma, Sweden)

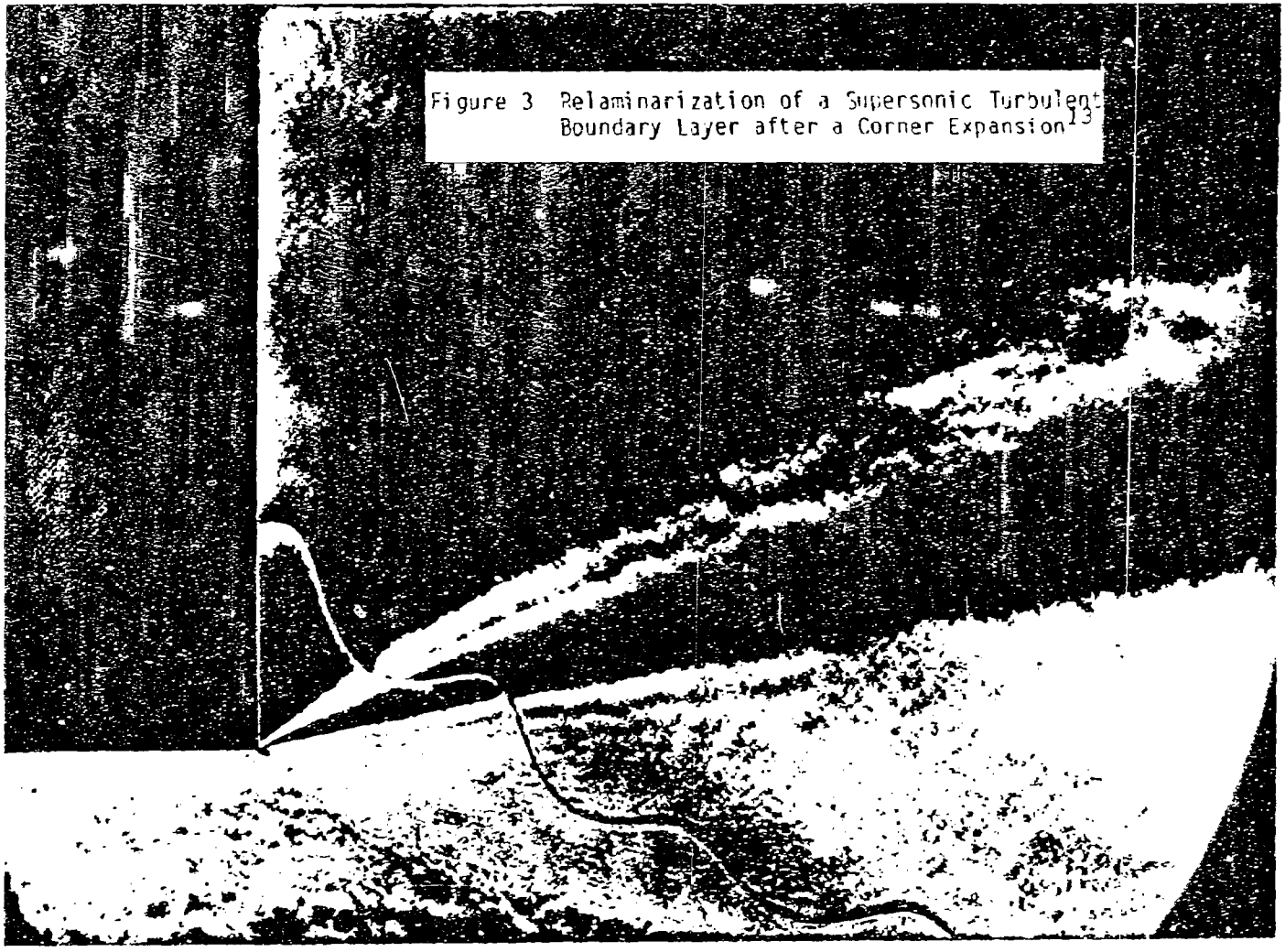

Figure 3 Relaminarization of a Supersonic Turbulent Boundary Layer after a Corner Expansion[13]

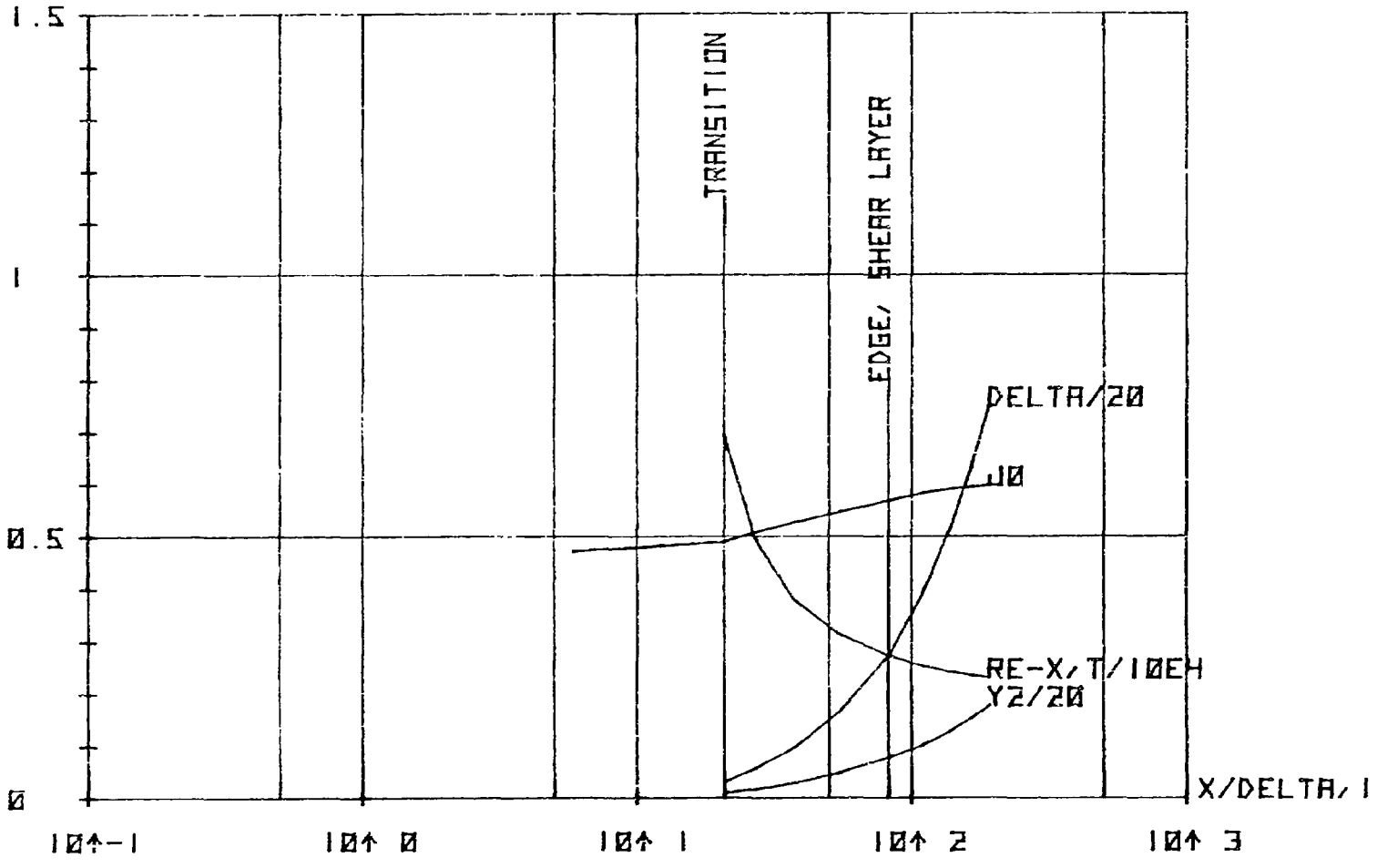

Figure 4 Development of a Free Shear Layer after the Corner Expansion of a Turbulent Boundary Layer

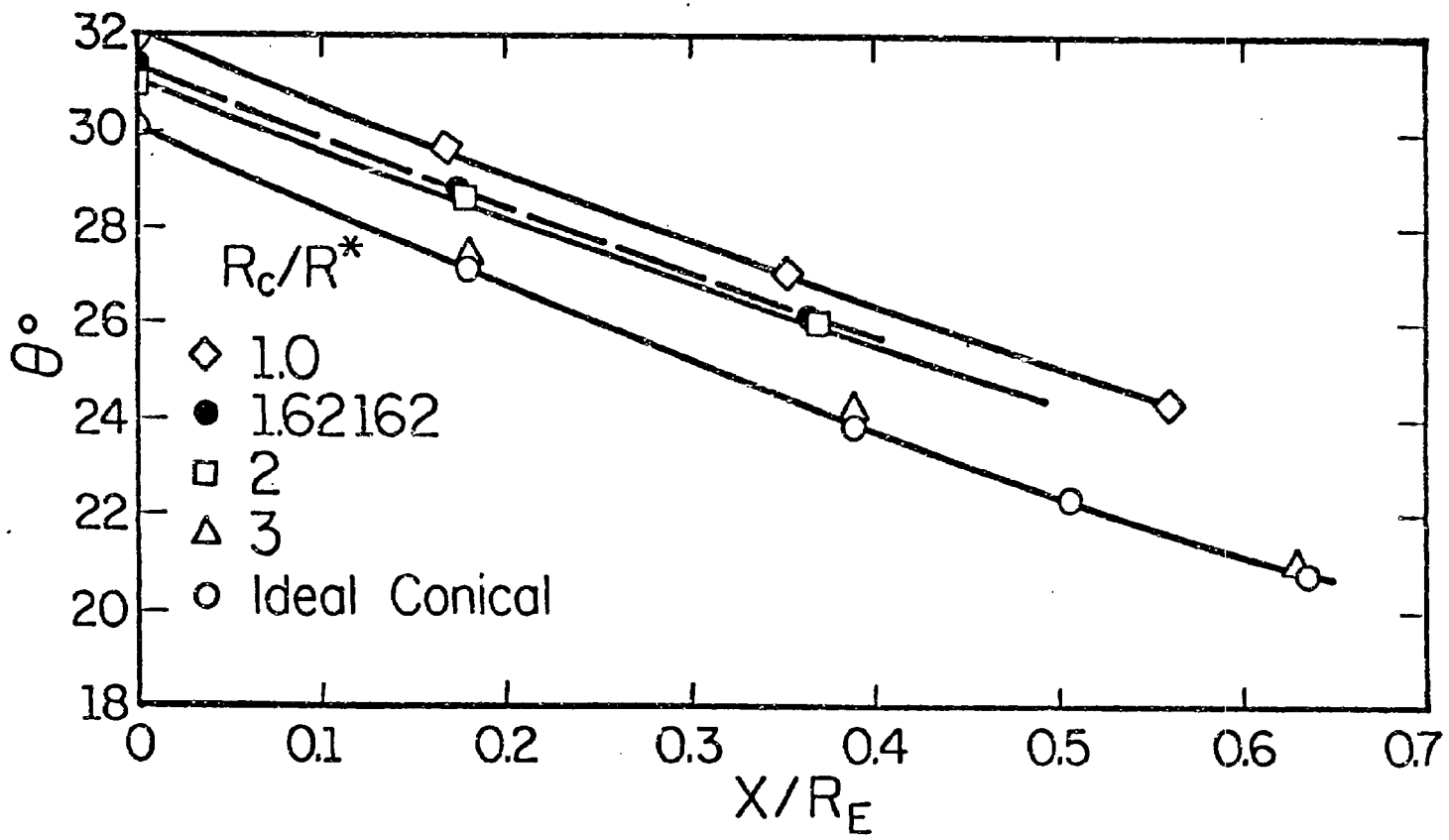

Figure 5 Effect of Nozzle Throat Curvature on the Jet Plume Development near the Lip of Conical Nozzle

Table 1 Comparison of Analytical, A, and Experimental, E, Modeling of Missile Prototype Aerodynamics

		A	E
Tasks		Component Analysis, Component Synthesis	Component Experiments, Full Configuration Modeling
Limitations			
(i)	Geometry	yes	no
(ii)	Inadequate component treatment	yes	no
(iii)	Component merging	yes	no
(iv)	Scale effects	no	yes
(v)	Plume analysis	no	Correct Plume Modeling Required
(vi)	Cost	no	yes

Table 2 Comparison of Computation, C, and Analytical, A, Modeling of Missile Prototype Aerodynamics

Tasks		C	A
		Global strategy	Overall component synthesis
		(Regional) Modeling of inviscid-viscid interactions	Component analysis
Limitations			
(i)	Geometry	yes	<u>yes</u>*
(ii)	Inadequate accuracy of component treatment	<u>yes</u>	yes
(iii)	Component merging	no	yes
(iv)	Scale effects	no	no
(v)	Plume analysis	no	no
(vi)	Cost	<u>yes</u>	no

*Underlining stresses the comparatively stronger limitations.

Table 3 Comparison of Computational, C, and Experimental Modeling of Missile Prototype Aerodynamics

	C	E
Tasks	Global Flowfield Calculations	Corresponding Experiments (full configurations)
	Critical appraisal of assumptions	Interpretation with the help of component definition and testing
Limitations	As stated in Tables 1 and 2	

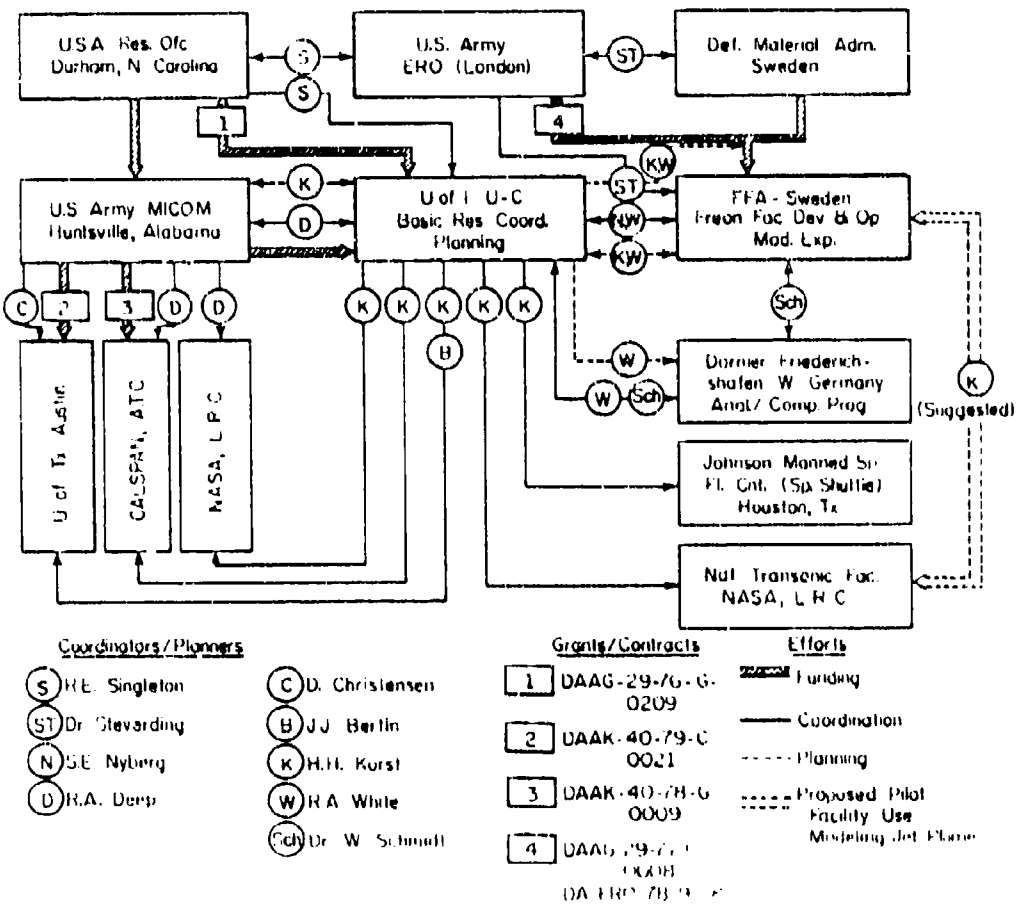

Table 4 Organizational Chart, Research Coordination under U.S. Army Grant DAAG-29-76-G-0209

APPENDIX E

ADVANCED RESEARCH/ANALYSIS OF PLUME INDUCED INTERFERENCE FLOW

Paper presented at the

Symposium on Rocket/Plume Fluid Dynamic Interactions

Huntsville, Alabama

April 1983

by

Professor R. A. White

APPENDIX E

ADVANCED RESEARCH/ANALYSIS OF PLUME INDUCED INTERFERENCE FLOW

Robert A. White
Department of Mechanical and Industrial Engineering
University of Illinois at Urbana-Champaign
Urbana, Illinois

ABSTRACT

An analysis of the relation between rocket plumes and the induced separated flow is presented which emphasizes the necessity for a complete understanding of the plume shape and surface Mach number in the vicinity of the nozzle exit plane. The internal nozzle flow is shown to be an important factor in determining the initial plume contour and that the common assumption of conical flow can lead to improper modeling procedures and anomalies in test results which are difficult to explain. Proper modeling procedures to account for the plume and its interaction with the freestream flow including effects of the nozzle, separation and design point considerations, and recompression are also included. The range of applicability of the methodology is discussed and related to ongoing experimental investigations.

NOMENCLATURE

Geometry

Afterbody

D	forebody diameter, m
L	boattail length, m
α	angle of attack, deg.
β	boattail angle, deg.

Nozzle

R_L	exit of lip radius, m
R^*	throat radius, m
R_c^*	radius of throat wall curvature, m
θ_L	conical divergence angle, deg .

Tunnel flow

p_{oE}	stagnation pressure, MPa
p_E	freestream static presure, MPa
M_E	freestream Mach No., dimensionless
γ_E	specific heat ratio

Nozzle flow

M_L	lip Mach No., dimensionless†
p_{0l}	nozzle stagnation pressure, MPa
p_L	lip pressure, MPa
T_{0l}	nozzle stagnation temperature, °C
γ	specific heat ratio, dimensionless
ω_L	Prandtl-Meyer angle corresponding to M_L, deg.

Plume

M^*	critical Mach No., dimensionless
M_F	surface Mach No., dimensionless
R_c	initial surface curvature, m
r_c	R_c/R_L, dimensionless
θ_F	initial surface slope, deg.
θ	local plume surface slope, deg.
ω_F	Prandtl-Meyer angle corresponding to M_F, deg.

Wake conditions

p_b	wake (base) pressure, MPa
s	separation distance measured from end of boattail, m

Subscripts

A	air
F	Freon
M	model
P	prototype

INTRODUCTION

The papers in this segment of the symposium represent a coordinated presentation on the role of design and modeling on the prediction of missile drag and stability. The inter-relationsips of theory, design, and modeling to prototype development and eventually operational vehicles is shown schematically in Table 1. Note that modeling, particularly with respect to wind tunnel testing, spans the entire development

†Conical source flow assumed; otherwise nozzle geometry and lip conditions have to be specified in greater detail[9].

lifetime of a missile design. The broad overview of the first paper pointed to the importance of advanced research and analysis methods. Their role in the overall structure is also established in the matrix of contributions of Table 1. The next presentation will discuss the latest experimental results on the methodology presented in this paper and how they fit into the past[1] and present programs of wind tunnel testing, verification, and range of applicability.

The interaction of rocket or jet plumes with the external flowfield and surrounding launch equipment or adjacent surfaces is crucial to system performance[2]. Such interactions determine the near wake base pressure and temperatures, the flow over portions of the vehicle surface in the case of upstream external flow separation, the wake flowfield at angle of attack, afterbody mounted control surface effectiveness, and launch equipment performance. Thus, the plume-slipstream interference flowfield affects aerodynamic performance by introducing drag penalties through lower than ambient base pressures or leads, as the ratio of jet stagnation to ambient pressure increases as for highly accelerated vehicles, to plume-induced separation[3]. In extreme conditions, such separation can lead to loss of stability and/or degradation of control effectiveness[4].

The understanding of plume induced separation is consequently a vital factor in missile design. Once again referring to Table 1, it can be seen that the design and wind tunnel testing phases dominate early portions of model and prototype work. Both the analytical and wind tunnel test programs also must be viewed as crucial future contributors to improved theoretical models and the rapidly expanding field of computation fluid dynamics (CFD) which is still strongly dependent on experimental results for guidance[5].

The generation of rocket or jet plumes in wind tunnel investigations must, consequently, account for all or part of the factors affecting the induced flowfield, see Fig. 1, including plume shape, plume deflection, mass entrainment along the shear layers, wake closure (impingement), viscous effects, temperature, influence of specific heat ratio and molecular weight, and temperature. The difficulty in attempting to simulate all of these parameters simultaneously is well known[6] and indeed a research program to determine and validate simulation techniques for special conditions such as those of the cryogenic National Transonic Facility (NTF) has been suggested[7]. Since all parameters cannot, in general, be simulated simultaneously in a wind tunnel, it becomes essential to determine the importance of the individual factors discussed above. This information has, in general, been lacking although recent simulation studies[1] have contributed strongly to this area of knowledge and strictly empirical correlations have been suggested[8] for specific applications such as the space shuttle.

This presentation discusses the analytical methodology for proper plume modeling as suggested by Korst and Deep[3] and its initial and ongoing experimental verification[1]. It then examines new research and analysis which has pointed to improvements and clarifications in the application of this methodology which are essential for proper modeling

between prototype and wind tunnel models. The following presentation will examine additional experimental work underway to further support the appropriate basis for modeling of plume induced interference flows.

Analysis

While rocket testing has long recognized the need for some method of producing a plume, or its equivalent, the success of, and understanding of, the approaches utilized has had a rather non-uniform history. This is despite the fact that a basic understanding of the problem and even the establishment of relations accounting, in principle, for the influence of all pertinent variables was given 25 years ago by Korst, et al.[10]. The importance of generating the correct jet plume geometry has been stressed in prior efforts to establish modeling laws between propellant gases having dissimilar specific heat ratios[8,11,12]. This was brought about by at least the partial recognition of the fact that modeling of plume interactions requires geometrically congruent jet boundaries, correct pressure-rise jet boundary deflection characteristics, and similar mass entrainment characteristic along the wake boundaries.

The geometrical requirements, however, were only given[8] in terms of the initial expansion angle of the jet, θ_e in Fig. 1. This may be sufficient to deal with cases in which plume-induced separation is not present and where there is little initial plume curvature, see Fig. 2, but not for high engine to freestream pressure ratios typical of highly accelerating missiles. For cases with plume induced separation, however, as in Fig. 1, additional constraints, both geometric and dynamic, are obviously necessary.

Recently Korst and Deep[9] proposed a modeling technique which allows the matching of both the initial deflection angle and the plume shape through its local radius of curvature, see Fig. 3. Initially a second order approximation for dealing with axisymmetric centered expansions was used for calculating the plume curvature[1,13]. This approach in conjunction with conditions at the nozzle outlet allows for sweeping simplifications in interpretation of the results if the nozzle flow can be assumed to be locally concical. The latter was assumed to be reasonable for typical prototype nozzles of relatively high Mach number, although it was recognized[9] that this may not always be truly representative particularly for wind tunnel models. While such a generalization is not correct in many cases, the overall conclusions relative to the modeling procedures remain correct. An improved analysis will be discussed later which removes the conical flow restriction albeit with additional computational complications.

The methodology of Korst and Deep leads to a corresponding family of nozzles based on prototype specifications, which have the same plume boundary geometry (congruent plumes). While these plumes are all of similar shape to the prototype plume, the selection of the one which will satisfy the near wake dynamic conditions remains to be determined. This selection is based on the one remaining free parameter

in the solutions after having satisfied the geometric constraints[9]. This remaining specification can be tied to the impingement process (recompression) or other wake characteristics such as entrainment[11].

The documented importance of the effects of plume stiffness[1] i.e. plume surface pressure deflection characteristics, underscores the importance of selecting plume flexibility as the remaining parameter for the simulation process. Thus having selected the recompression process, as represented by the linearized (weak shock) approximation for the pressure rise streamline deflection relation, i.e.

$$[\gamma_M M_{F,M}^2/(M_{F,M}^2)^{1/2}] = [\gamma_p M_{F,p}^2/(M_{F,p}^2 - 1)^{1/2}] \qquad (1)$$

it is possible to determine model nozzle exit conditions in terms of local Mach number and nozzle divergence angle which will geometrically duplicate the jet contour produced by the prototype (including a different specific heat ratio) as it expands from a given nozzle to specified adjacent conditions that is (refer to Fig. 3):

$$\theta_{F,m} = \theta_{F,p} \text{ and locally } r_{C,m} = r_{C,p} \qquad (2)$$

with subscripts p and m for prototype and model, respectively.

The mass entrainment characteristics of the separated region bounding shear layers will generally not be simultaneously satisfied. While this effect is generally of second order compared to the recompression process[9], see Table 2, corrections can be made if necessary by wake mass bleed[16].

With the simulation concept established, it is necessary to select the type of wake, see Figs. 1 and 2, to be investigated in order to establish the design operating pressure ratio. For plume induced separation, a given prototype afterbody pressure distribution due to non-separated external flow can be determined and from which it is possible to estimate the pressure rise due to separation by using information on free interactions[16] in the presence of disturbances such as local surface slope discontinuities[17]. The resulting plateau pressure determines the wake region pressure and consequently the prototype jet surface Mach number, $M_{F,p}$. Thus the prototype conditions, i.e. nozzle flow and jet surface Mach number are all known and the model nozzle exit conditions $M_{L,m}$ and $\theta_{L,m}$ as well as model jet surface Mach number may be determined[9]. At this design point, Eq. (2) and the plume streamline deflection characteristics will be satisfied, Eq. (1). The model condition of using air or nitrogen to simulate hot, low specific heat ratio propellant gases, leads to nozzles which are of lower Mach number with substantially reduced stagnation pressures which simplifies testing for plume induced separation.

An example of the modeling procedure is seen in Fig. 4 for a Mach 2.6 prototype conical nozzle with exit half angle of 15 degrees and specific heat ratio of 1.16 and the resulting model nozzles for air as the gas. Both model nozzles are of lower Mach number and smaller exit angle. The Mach number 1.41 nozzle is sufficiently short that it would

be anticipated that detailed throat and complete nozzle calculations would be necessary to define the plume and that the conical flow assumption would be invalid. This will be discussed in more detail in the next section.

For off design operating conditions, it would be expected[1,9] that only the more stringent condition of plume slope matching needs to be retained. This would appear to be particularly correct for plume induced separation where the pressure level in the wake is primarily determined by the slip stream separation pressure rise. Thus in the vicinity of the design point, it should be sufficient to retain

$$\theta_{F,m} = \theta_{F,p} \tag{3}$$

and the angular relation

$$\omega_{F,p} = \theta_{L,m} - \theta_{L,p} + \omega_{L,p} - \omega_{L,M} + \omega_{F,M} \tag{4}$$

Since the nozzle flows and therefore $\theta_{L,m}$, $\theta_{L,p}$, $\omega_{L,m}$ and $\omega_{L,p}$ remain identical for design and off design operation, one expects that the wake pressure ratios shall still be closely modeled; hence,

$$p_b/p_E|_p = (p_b/p_E)_m = f(p_{oI,m}/p_{oE}) \tag{5}$$

Thus one finds the pressure ratio for the prototype flow from the Prandtl-Meyer relation

$$M_{F,p} = f(\gamma_p, \omega_{F,p}) \tag{6}$$

and the identify

$$p_{oI,p}/p_{oE} = (p_{oI,p}/p_b)_{m_{F,p}} (p_b/p_E)_m \tag{7}$$

Consequently, for each modeled flow experiment series for which the relation

$$(p_b/p_E)_m = f[M_E(p_{oI,m}/p_{oE}), \gamma_m] \tag{8}$$

has been established, the corresponding operating condition of the prototype flow can be determined.

The transformation of model and prototype results into the appropriate plane is shown in Fig. 5 for results reported in[1]. Figure 6 shows the data of Korst, et al.[1] in the prototype plane as correlated by Eq. (8) and the agreement in base pressure between the prototype and model nozzles is seen to be excellent and extend on either side of the selected design point.

3. ANALYSIS MODIFICATIONS

The discussion of the previous section and nozzle designs presented emphasized ideal conical flow for the internal nozzle flow although the possible limits to its applicability were stressed. For the prototype

nozzle, Fig. 4, ideal conical flow had been assumed due to its relatively long length and high Mach number although detailed calculations were carried out for the two model designs. The plume shapes for the three nozzles are shown in Fig. 7 and are seen to be essentially congruent, both in terms of plume surface, shape, and local slope. In actual wind tunnel tests (details of the experimental results are presented in the next paper) the two air (model) nozzles were found to agree closely but the agreement with the prototype data was less satisfactory.

Initial efforts to explain the difference focused on the model nozzles, the Mach number 1.41 nozzle in particular, due to its short length and to difficulties in providing good stagnation inlet flow in the wind tunnel model. Improved internal wind tunnel model flow to the nozzles and careful calibration resulted in no improvement in agreement. The strong effect of throat curvature pointed to in the previous paper, Fig. 8, suggested that it may be appropriate to examine the internal flow of the prototype nozzle and its effect on the plume shape.

Figure 9 shows the plume for the prototype nozzle for the ideal conical flow assumption and for full calculations using the method of characteristics plus centered expansions. The latter is required to obtain the initial radius of curvature at the actual nozzle lip where the characteristic net is not sufficiently fine to accurately predict the local curvature. The conical flow assumption is seen to produce a plume with greater initial curvature, leading to significant differences in plume surface slope and radius in the vicinity of the impingement point for cases with plume induced separation. Figure 10 graphically demonstrates the problem by comparing the solutions for the model nozzles with the same initial deflection angle as a function of initial curvature and Mach number. In the range of acceptable solutions indicated in Fig. 10 the $M_L = 1.55$ and $\theta_L = 7.095$ degrees nozzle has been selected for comparison to the ideal conically based nozzle of $M_L = 1.41$ and $\theta_L = 3.070$ degrees.

Thus, the original model nozzles were both correctly modeled, and hence the agreement of the resulting test data for these two nozzles, but for the wrong protoype plume. The plume shape for the $M_{L,m} = 1.55$ and $\theta_L = 7.095$ model nozzle and the actual plume shape of the prototype nozzle are shown in Fig. 11. The agreement in shape and surface slope obtained using non-ideal flow calculations is seen to be excellent.

Based on these results it is obvious that the interval flow in both prototype and model nozzles must be examined in detail including local accelerations in the vicinity of the nozzle exit due to disturbances along characteristics emanating from the throat and over expansion at the intersection of throat wall curvature and conical wall section. Indeed the local wall curvature to throat radius ratio alone can cause significant differences in plume shape as seen in Fig. 8. Thus proper plume modeling requires a careful examination of the internal flow of the proposed designs if the correct plume shape is to be obtained.

4. CONCLUSIONS

The results of ongoing analytical and experimental studios on plume modeling have lead to a strong interchange of information, Table 1, providing explanations for observed test conditions and pointing to improvements in the modeling procedures. This type of relationship demonstrates the value of such programs and the need for closer cooperation between the triad of contributions, analytical, experimental, and CFD. The cooperation between those working on the analytical modeling methodology discussed in this paper and experimental program sponsored by ERO has proven to be mutually beneficial. Simultaneously, it has shown that the concept of modeling by congruent plumes of proper pliability leads to the correct simulation of plume induced flows without the necessity for multiple empirical correlating factors.

The latter factor is particularly significant since the hope of accurately computing, CFD, the complex flow fields of the type shown in Fig. 12 or determining practical empirical correlating parameters for such flows is at this time at best remote. The design of such vehicles will consequently rely on wind tunnel testing and proper plume simulation for the foreseeable future. The limits of the applicability of modeling by congruent plumes for different gases are still being investigated and the next paper will report on some of those results. Regardless it is essential to recognize that correct simulation of plume induced separation requires, in addition to the methodology, an accurate and detailed computation of the entire propulsive flow from the throat through to the plume.

REFERENCES

1. Korst, H. H., R. A. White, S.-E. Nyberg, and J. Agrell, "Simulation and Modeling of Jet Plumes in Wind Tunnel Facilities," J. Spacecraft. Vol. 18, No. 5, Sept.-Oct., 1981, p. 427.

2. Addy, A. L., Korst, H. H., Walker, B. J., and White, R. A., "A Study of Flow Separation in the Base Region and Its Effects during Powered Flight," AGARD-CP-124, AGARD Conference Proceedings No. 124 on Aerodynamic Drag, Specialists' Meeting, April 10-13, 1973. (Available from NASA Langley Field, Va. 23365, ATTN: Report Distribution and Storage Unit.)

3. Alpinieri, L. J. and Adams, R. M., "Flow Separation due to Jet Pluming," AIAA Journal, Vol. 4, 1966, pp. 1865-1866.

4. Deep, R. A., Henderson, J. H., and Brazzel, C. E., "Thrust Effects on Missile Aerodynamics," U.S. Army Missile Command, RD-TR-71-9, May 1971.

5. Deiwert, G. S., "A Computational Investigation of Supersonic Axisymmetric Flow over Boattails containing a Centered Propulsive Jet," AIAA Paper 83-0462.

6. Blackwell, K. L. and Hair, L. M., "Space Shuttle Afterbody Aerodynamics/Plume Simulation Data Summary," NASA Technical Paper 1384, 1978.

7. "Hight Reynolds Number Research," NASA CP-2009, Oct. 27-28, 1976.

8. Sims, J. L. and Blackwell, K. L., "Base Pressure Correlation Parameters," Missile and Plume Interaction Flow Fields Workshop, Redstone Arsenal, Ala., June 7-8, 1977.

9. Korst, H. H. and Deep, R. A., "Modeling of Plume Induced Interference Problems in Missile Aerodynamics," AIAA Paper No. 79036, Jan. 1979.

10. Korst, H. H., Chow, W. L., and Zumwalt, G. W., "Research on Transonic Flwo of a Real Fluid at Abrupt Increases in Cross Section (with Special Consideration of Base Drag Problems)--Final Report," University of Illinois, ME-TN-392-5, Dec. 1959.

11. Goethert, B. H. and Barnes, L. T., "Some Studies of the Flow Pattern at the Base of Missiles with Rocket Exhaust Jets," Arnold Engineering Development Center, Tullahome, Tenn., AEDC-TR-58-12, June 1960.

12. Herron, R. D., "Investigation of Jet Boundary Simulation Parameters for Underexpanded Jets in a Quiescent Atmosphere," Arnold Engineering Development Center, Tullahoma, Tenn., AEDC-TR-65-6, Sept. 1968.

13. Johannesen, N. H. and Meyer, R. C., "Axially-Symmetrical Supersonic Flow near the Centre of an Expansion," The Aerospace Quarterly, Vol. 2, 1950, pp. 127-42.

14. Dods, J. B., Jr., Brownson, J. J., Kassner, D. L., Blackwell, K. L., Decker, J. P., and Roberts, B. B., "Effect of Gaseous and Solid Simulated Jet Plumes on an 040A Space Shuttle Launch Configuration at M = 1.6 to 2.2," NASA TMX-3032, April 1974.

15. Reid, C. F., "Effects of Jet-Plume and Pressure Distributions over a Cylindrical Afterbody at Transonic Speeds," Calspan, AA-4017-W-15, W. A. T17-160, T17-170, Feb. 1979.

16. Carriere, P., Siriex, M., and Delery, J., "Methods de Calcul des Ecoulements Turbulents Decolles en Supersonique," Progress in Aerospace Science, Vol. 16, No. 4, 1975, pp. 385-429.

17. White, R., and Agrell, J., "Boattail and Base Pressure Prediction including Flow Separation for Afterbodies with a Centered Propulsive Jet and Supersonic External Flow at Small Angles of Attack," AIAA/SAE Preprint No. 77-958, July 1977.

Table 1 Aerodynamic Interference Problems and Missile Performance Relationships between Contributing Methodologies and Procedures for the Determination of Aerodynamic Forces, Stability, and Control Problems and Aerothermal Environment of the Afterbody and Near Wake

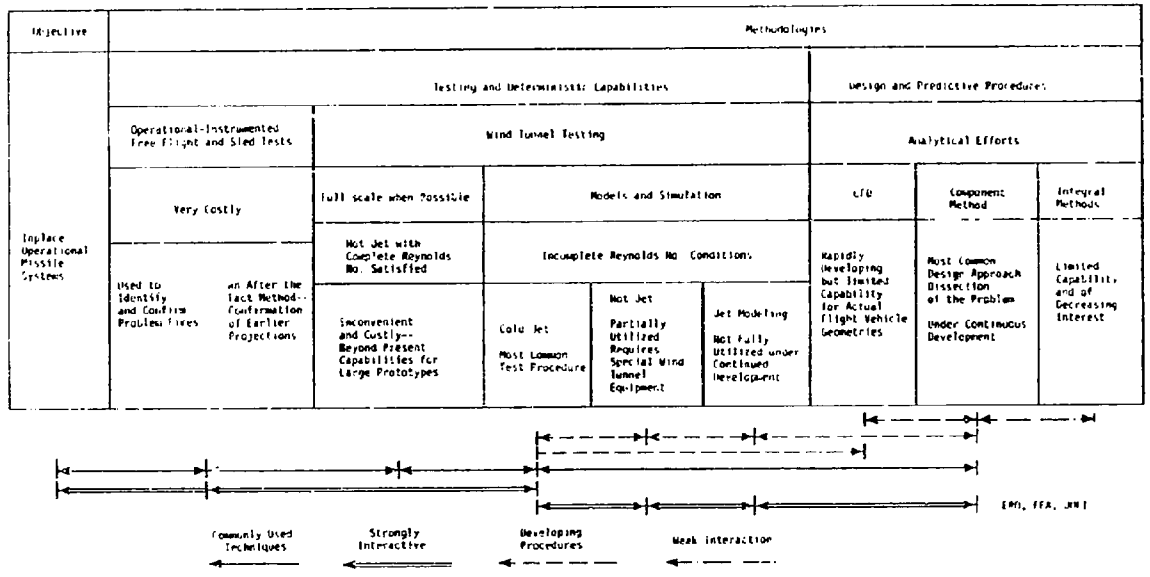

Table 2 Simulation Concepts

Freestream Mach No.	(a) Geometry of Plume	(b) Jet Surface Mach No. (Pliability)	(c) Ratio of Specific Heats
M < 1	Dominates	Apparently Not Significant	Important
M = 1 (transonic)	Important	Attains Increasing Significance	Important
M > 1	Important	Important	Important

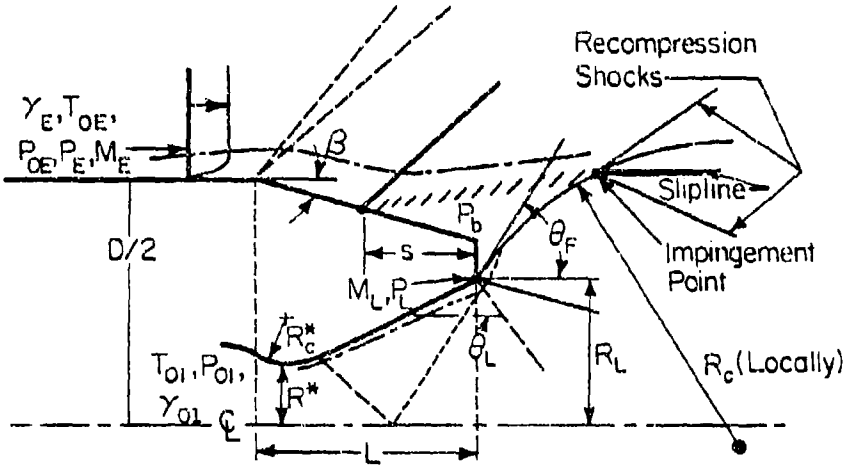

Figure 1 Flow Configuration for Plume Induced Separation from a Conical Afterbody and Identification of Geometric and Operational Parameters

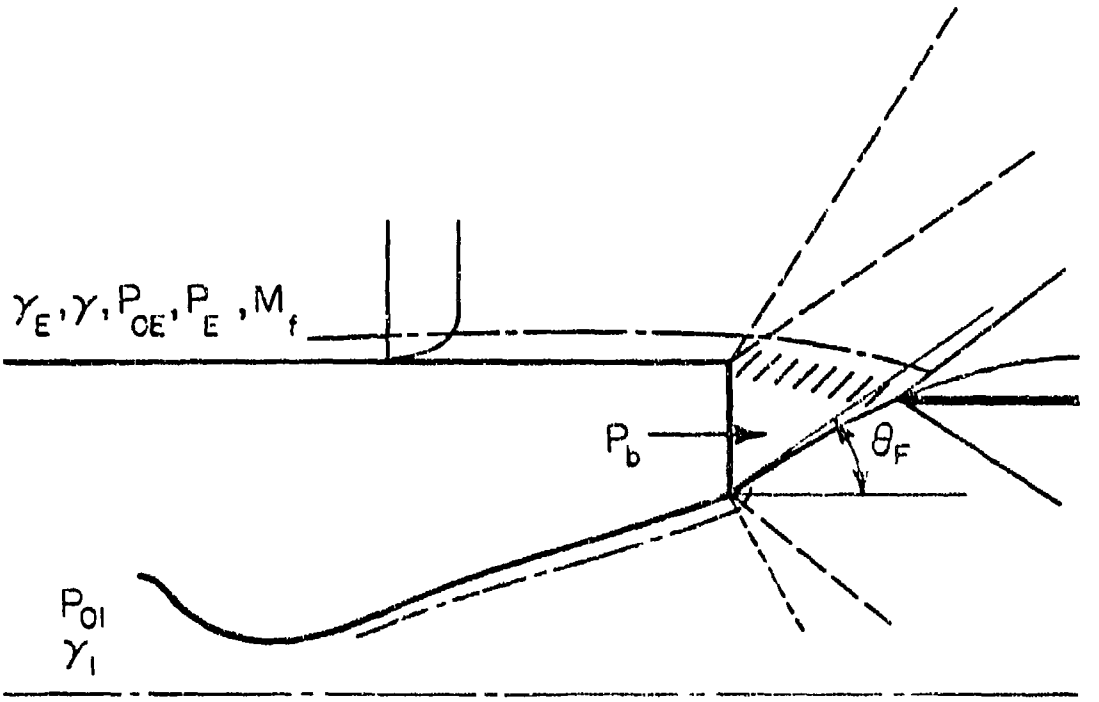

Figure 2 Flow Configuration for the Base Pressure Solution without Plume Induced Separation of the Slipstream

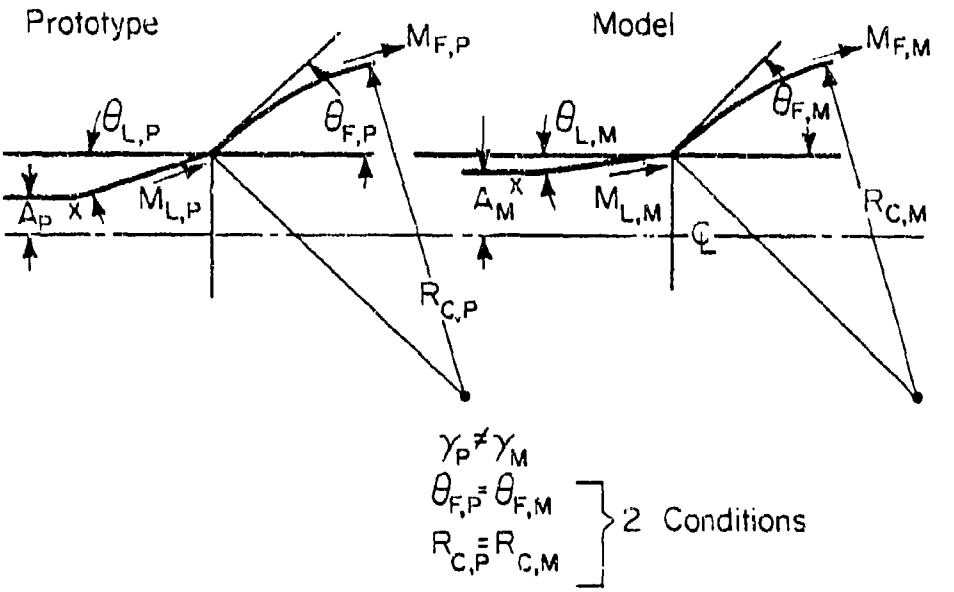

Figure 3 Schematic of Geometrical Plume Modeling

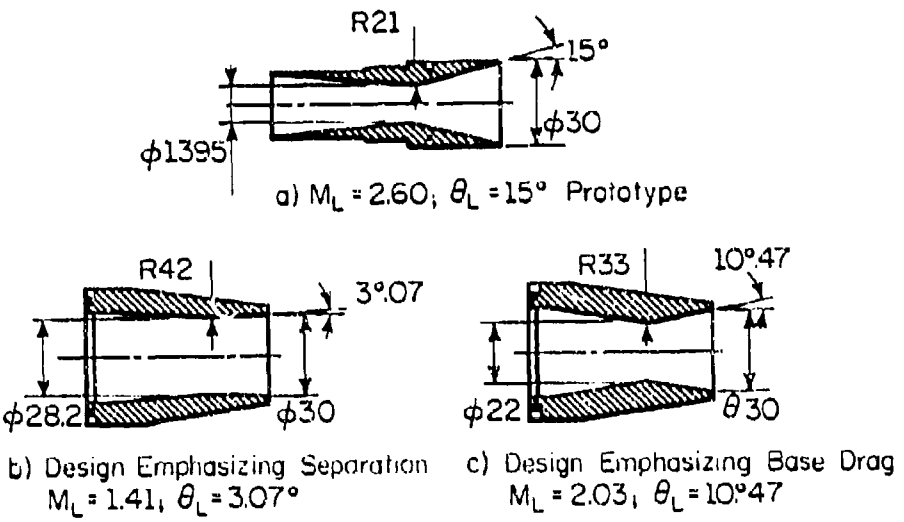

Figure 4 Prototype Nozzle with $\gamma = 1.16$ and Two Model Nozzles (Air, $\gamma = 1.40$) Emphasizing Different Operating Conditions

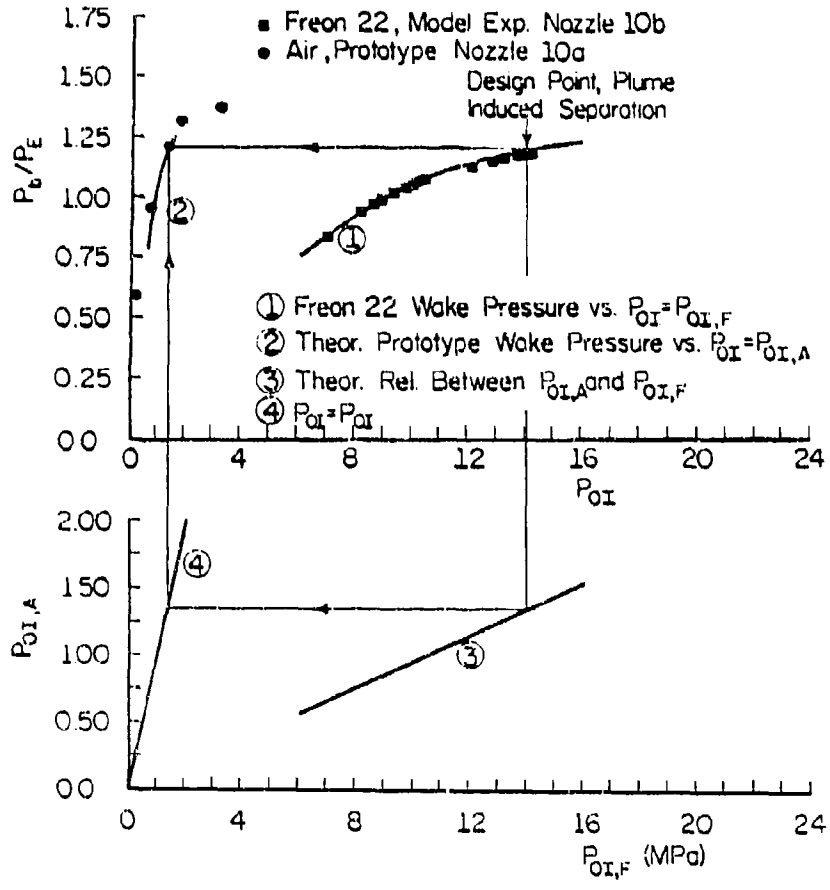

Figure 5 Correlation, Eq. (8), between Prototype and Model Test Data in the Vicinity of the Design Point

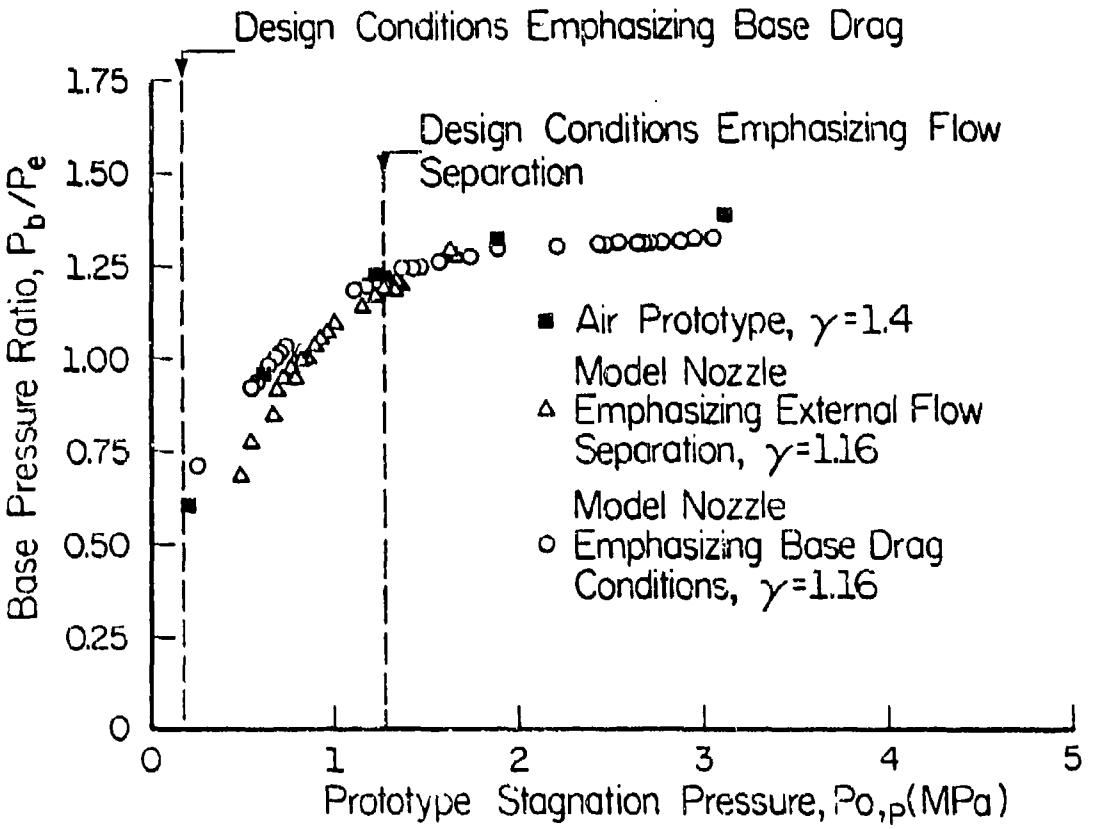

Figure 6 Wake Base Pressure Ratio for Air (Prototype) and Freon (Model) Tests versus Prototype (Air) Nozzle Stagnation Pressure

Prototype and Models

□ Ideal Conical Source Flow, Prototype Plume Boundary

△ Plume Surface Slope

Model, Non-Ideal Flow Emphasizing Base Pressure

M = 2.03; θ_L = 10.47°

✕ Plume Boundary

○ Plume Surface Slope

Model, Non-Ideal Flow, Emphasizing Plume Induced Separation

M = 1.411; θ = 3.0659°

▽ Plume Surface

◐ Plume Surface Slope

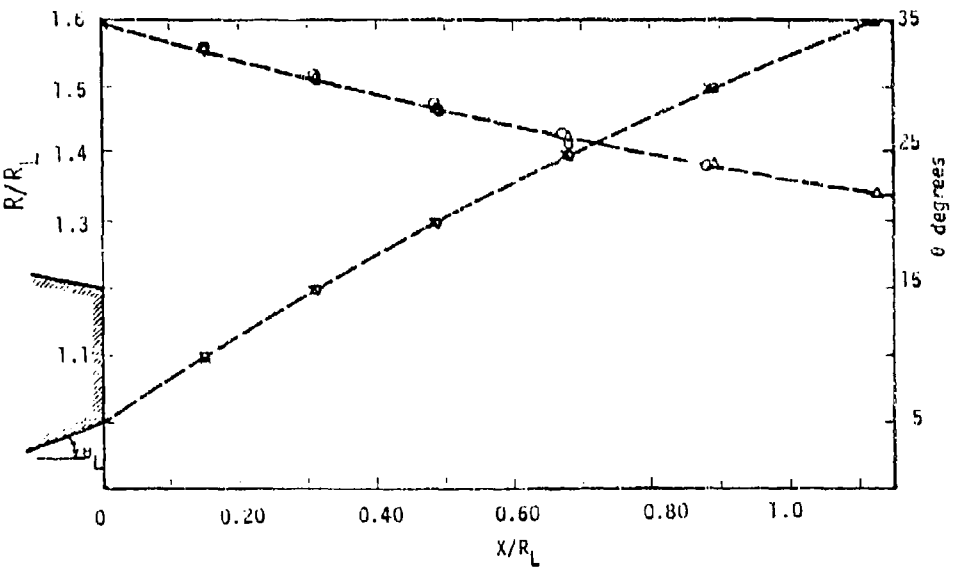

Figure 7 Comparison of Plume Shape and Surface Slope for the Prototype and Model Nozzle of Fig. 4

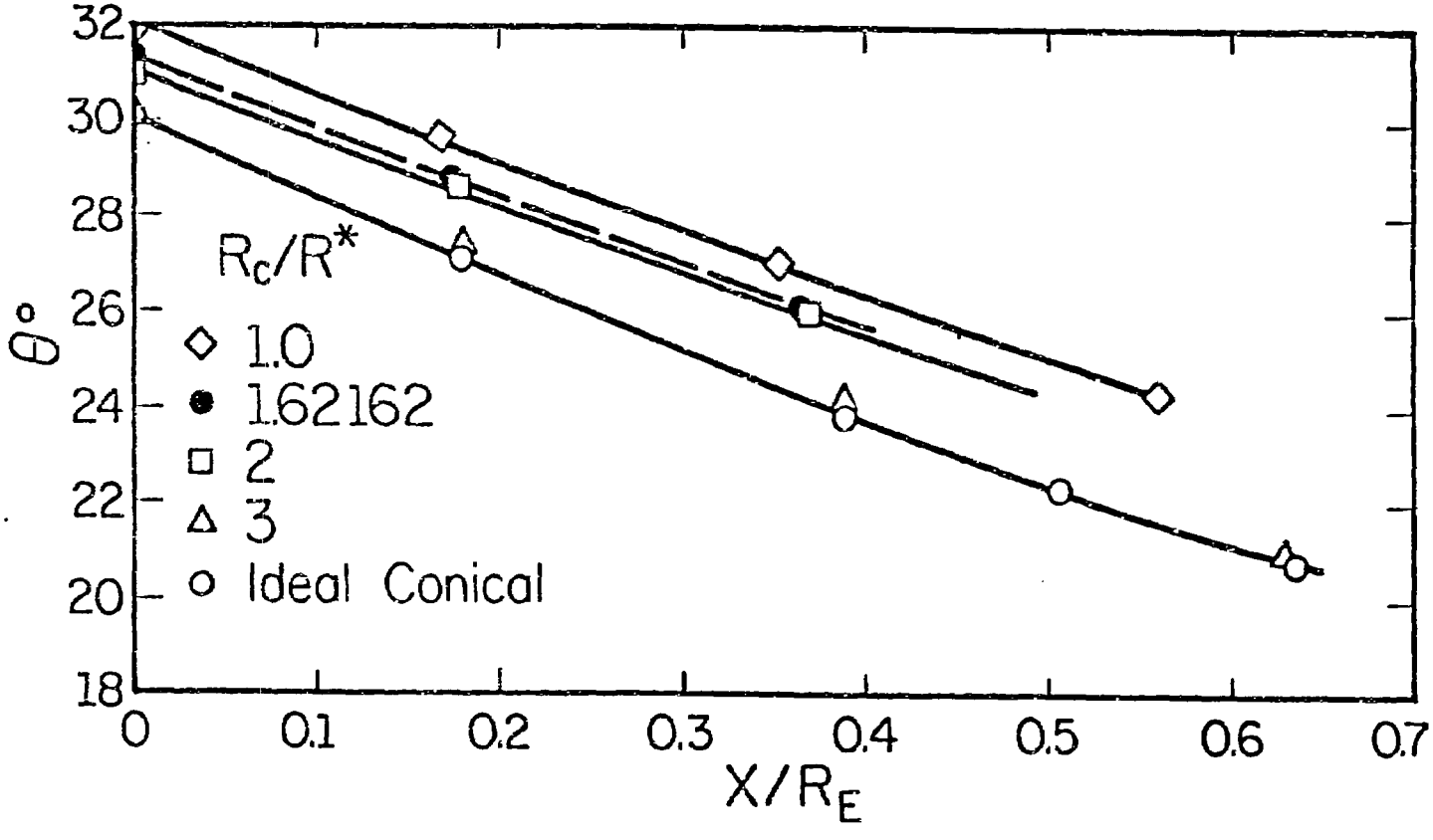

Figure 8 Effect of Nozzle Throat Curvature on the Jet Plume Development near the Lip of Conical Nozzle

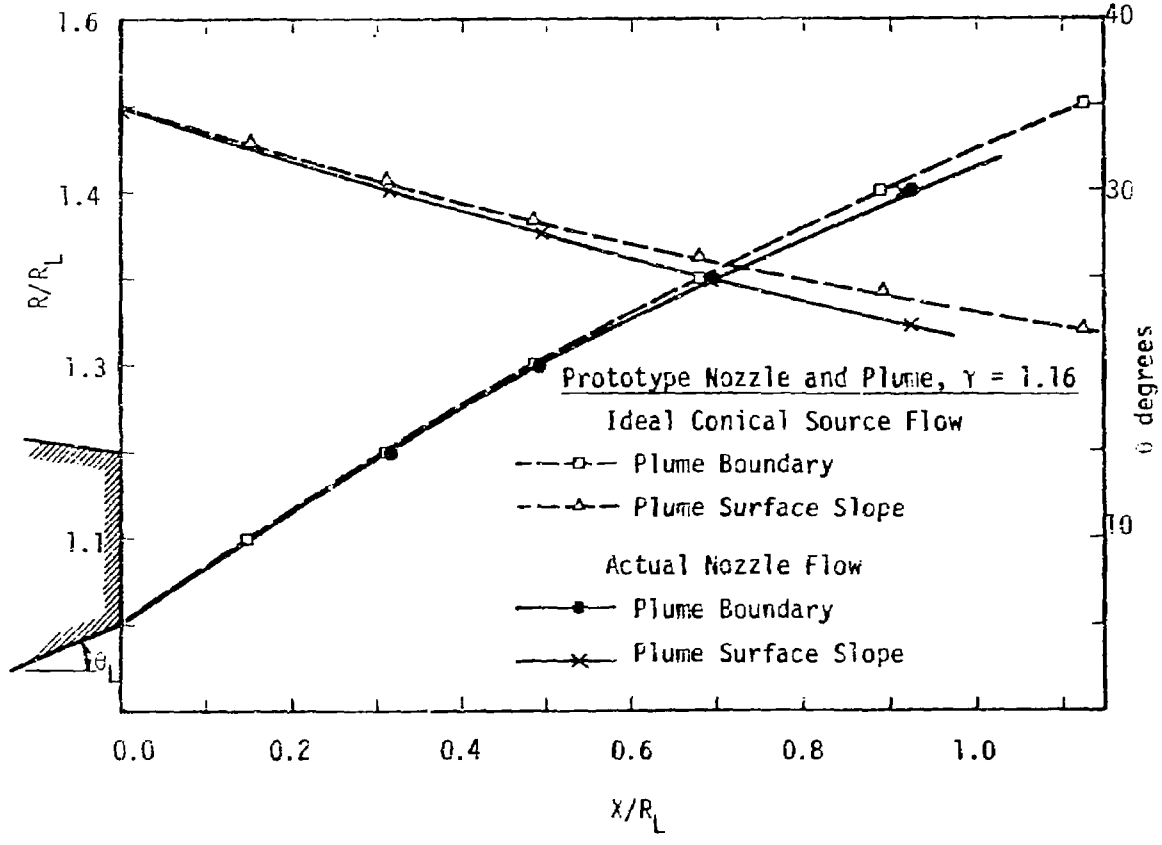

Figure 9 Comparison of Plume Shape and Surface Slope for the Prototype Nozzle based on Ideal Conical Flow and Non-Ideal Complete Nozzle Calculations

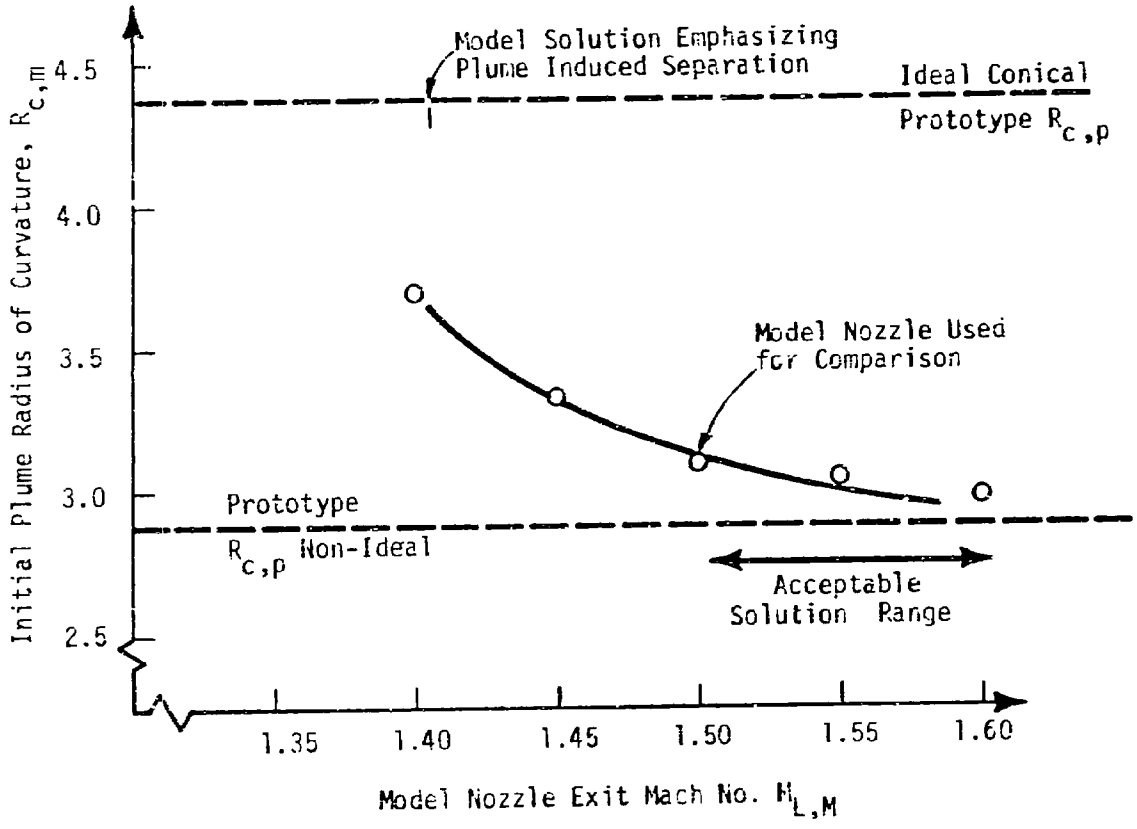

Figure 10 Initial Plume Radius of Curvature for Ideal Conical and Non-Ideal Nozzle Flows

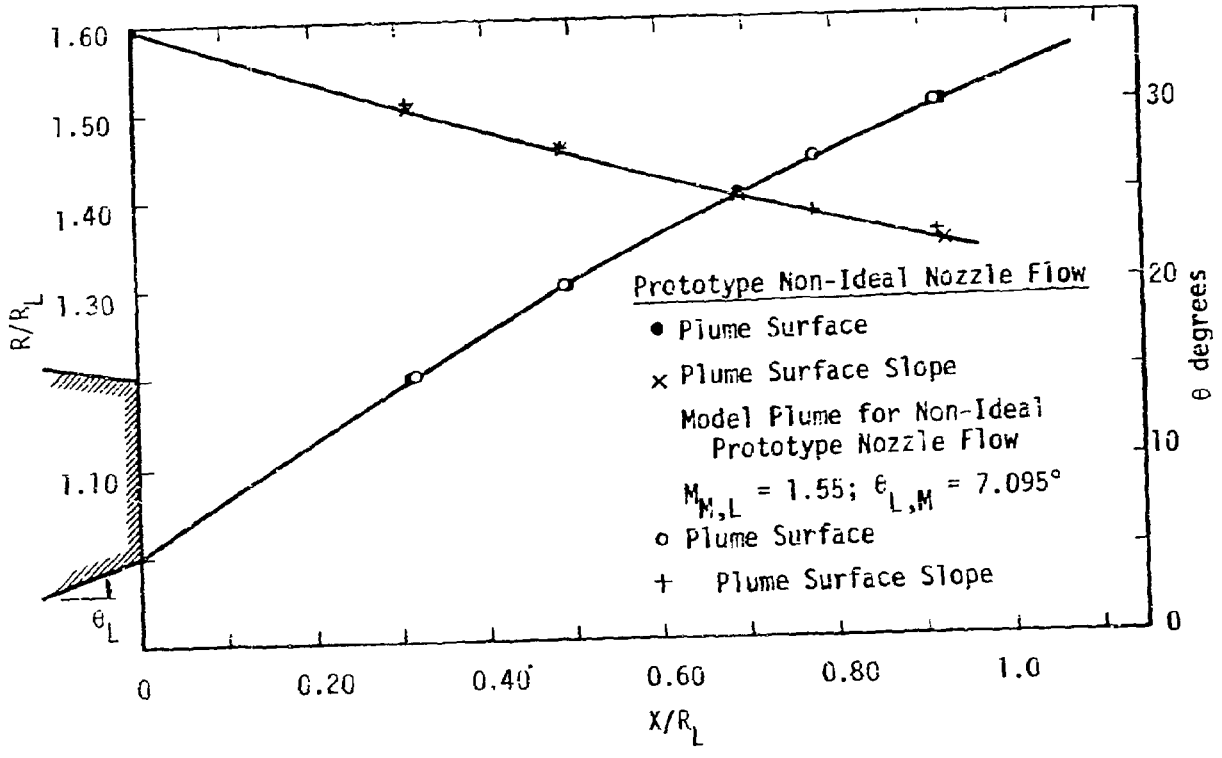

Figure 11 Comparison of Prototype and Model Plumes for Non-Ideal Flow Calculations

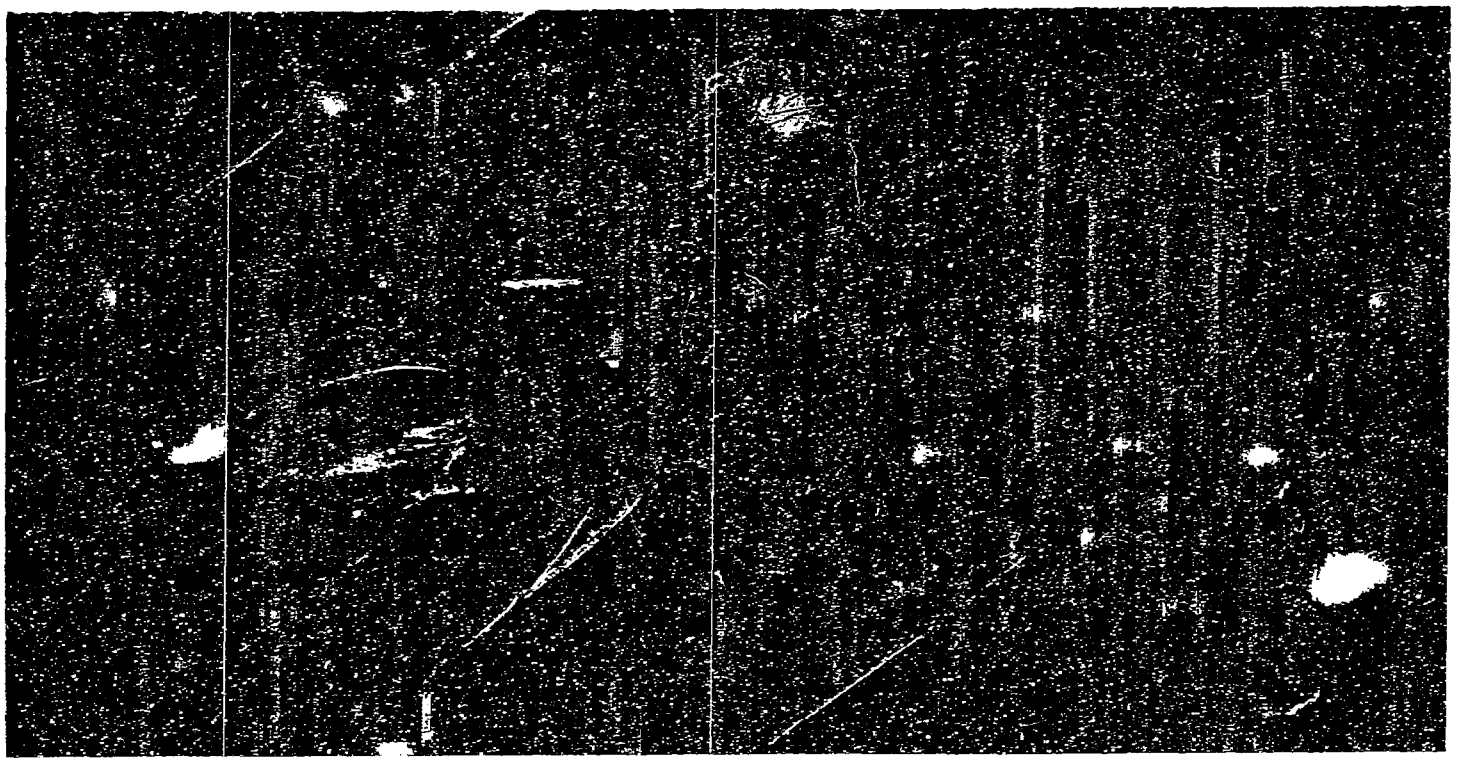

Figure 12 Finned Missile Afterbody in Supersonic Flow, $M_\infty = 2$; Angle of Attack, $\alpha = -6°$; Control Surface Angle, +10° (FFA, Bromma, Sweden)

APPENDIX F

WIND TUNNEL SIMULATIONS OF PLUME-INDUCED INTERFERENCE EFFECTS

Paper presented at the

Symposium on Rocket/Plume Fluid Dynamic Interactions

Huntsville, Alabama

April 1983

by

S.-E. Nyberg and J. Agrell

APPENDIX F

WIND TUNNEL SIMULATIONS OF PLUME-INDUCED INTERFERENCE EFFECTS

by

S-E. Nyberg and J. Agrell

FFA, The Aeronautical Research Institute of Sweden
P.O. Box 11021, S-161 11 BROMMA, Sweden

ABSTRACT

A brief review is made of the technique used at FFA in wind tunnel simulations of plume induced interference effects and some illustrative results are presented. With cold air as propellant a comprehensive test program has been carried out to determine the effects of the following parameters on the plume-afterbody interference in supersonic external flow: afterbody length and cone angle, nozzle exit angle and Mach number, jet to free stream pressure ratio, free stream Mach number, angle of attack and influence of aft-mounted controls. Measurements of the flow in the body boundary layer and in the separated region have been made by probes and by LDV.

The validity of the plume modeling methodology suggested by Korst has been confirmed by comparison of results for two propellants with different specific heat ratios, Freon-22 (γ=1.16) and air (γ=1.4). The modeling scheme is satisfactory even at high angles of attack $\alpha \leq 20^{\circ}$ and effects of controls are acceptably simulated.

SYMBOLS (Reference to Figs. 1, 4, 5, 6, and 12)

C_D	Total afterbody drag coefficient
$C_{N_{Bt}}$	Boattail normal force coefficient
D	Forebody diameter
L	Boattail length
M	Mach number
P	Pressure
R	Radius
S	Separation distance
X	Axial coordinate
α	Angle of attack
β	Boattail angle
γ	Specific heat ratio
δ	Boundary layer thickness or Control deflection angle
δ^*	Boundary layer displacement thickness
θ	Boundary layer momentum thickness or Conical angle
φ	Circumferential angle

Subscripts

B,b	Base condition
E,e	External flow (free stream)
i	Condition upstream shock
I	Internal flow
L	Nozzle lip condition
M	Model
0	Stagnation condition
P	Prototype
φ	Condition at circumferential angle φ

INTRODUCTION

Plume induced interference effects on afterbodies of schematic models with a centered jet have been simulated in wind tunnels at FFA since 1966. The major part of the tests have been carried out at supersonic speeds with cold or heated compressed air as the propellant gas. In recent years also heated Freon-22 has been used for this purpose.

The activities started in 1966 when Harris[1] made some tests with a cylindrical afterbody. The model was supported by a long sting mounted upstream of the sonic section of the wind tunnel. The parametric variations were the base-to-jet diameter ratio, the jet Mach number and the boundary layer thickness for free stream Mach numbers of 0.9, 1.1, 1.5 and 2.0. One drawback observed with this type of model support system is the difficulty to get a realistic ratio of boundary layer thickness to model diameter even with boundary layer suction.

In 1971 a new research project on axisymmetric flow over afterbodies was started in collaboration with prof. R.A. White from the University of Illinois. A new model set up was constructed for the purpose of giving experimental data to support further development of an existing computer program reported by Addy[2]. The experiment was also supposed to verify a separation criterion by Zukoski[3] and to give values for an empirical recompression factor for conical afterbodies. The results of this program[4] indicated that a more detailed knowledge of the flow was needed as a basis for further development of the computer program. Measurements of the body boundary layer and of the flow in the separated region of the afterbody were initially made by probes[4, 5, 6, 20] and recently by Laser Doppler Velocitymeter[7].

The effects of angle of attack and of aft mounted controls on base pressures and afterbody flow separation have been studied experimentally[5, 6, 18, 19] and a calculation methodology for small angles of attack using the Addy-program for axisymmetric flow has been suggested and tested[6].

In wind tunnel tests simulating plume-afterbody interference effects it is mostly important to minimize the influence of the model support. At FFA we have in most cases preferred to use a strut supporting the model. The interference of the support on the afterbody flow has been studied by comparison with a sting supported model[5, 8].

Plume modeling studies have been a major part of the activities in recent years. The method to use solid surfaces with simulated plume shape to imitate a gas plume has been investigated[8, 11]. A hot gas facility has been constructed for jet plume simulation with a variety of gases[9, 10, 11]. The facility has served to evaluate the merits and potential of the

plume simulation methodology suggested by Korst[12,13] in an earlier investigation[14] under restricted conditions and in a current study[15] at high angles of attack and with the complex external flow field generated by aft-mounted controls in combination with angle of attack.

It is the purpose of this paper to review briefly the technique used in the above mentioned investigations and to present some illustrative results.

EXPERIMENTAL EQUIPMENT

Simulation test facility

The two wind tunnels available for plume simulation by compressed air and Freon-22 are S4 and S5[16]. They are of an intermittent suck down type and have two-dimensional solid nozzle blocks for supersonic speeds and test sections of 0.92×1.15 m^2 and 0.45×0.57 m^2, respectively. Tunnel stagnation pressure and temperature are approximately equal to atmospheric conditions.

Compressed dry air for plume simulation is available from the high pressure storage of the FFA's hypersonic facilities, which allows the storage of 50 m^3 of air at a pressure of 25 MPa. The temperature can be selected in the range $-20° - +300°$C and the maximum flow rate is 2.7 kg/s.

A hot gas facility, primarily intended for various types of heated Freon, is also available for plume simulation. Freon-22 has been chosen for all tests up to now. Cost and chemical stability - which allows it to be heated to sufficiently high temperatures without chemical break down - were major factors in its selection. The ratio of specific heats at nozzle exit and plume expansion conditions, γ, is in the range of 1.16 to 1.18, which is appropriate for simulation of combustion type jet products.

The basic system makes use of the above mentioned high pressure storage which is used in the simulation system as an essentially constant pressure driver for the Freon. Fig. 2 is an annotated schematic of the Freon system, the test model and the high pressure driver. Details of component design, construction and operating procedures are given in Ref.[9] along with a discussion of the temperature control requirements and the system developed for this purpose. The systems performance tests are presented in Ref.[10] and a condensed review of the facility can be found in Ref.[11].

Wind tunnel model

The basic model Figs 3 and 4 is built up of a 14 degree half-angle nose cone, a cylindrical centerbody of 50 mm diameter and a set of interchangeable afterbodies and propulsive nozzles. The over-all length is 9 diameters (9.5 diameters in the plume-modeling tests). The model is supported just behind the conical nose by a strut with 40° sweep back which also provides the air for the jet. The model can also be mounted on a sting with or without the capability of simulating a gas jet. In this case the jet plume effect can also be simulated by solid bodies. Fig. 3 shows the model in the wind tunnel. The rear part of the center body, the boattail and the base region are all instrumented with pressure taps (Fig. 5). A set of four stabilizing or control fins can be attached to the afterbody (Fig. 6). The control deflection angle δ can be varied.

Instrumentation

The afterbody pressures are recorded by pressure transducers and the output signals are fed into the wind tunnel data recording and reduction system, based on a General Automation SP16/65 real time computer.

During several years experiments have been conducted in order to develop a technique for applying Laser-Doppler-Velocimetry (LDV) to the measurement of the velocities in the separated regions on the afterbody. The main difficulty has been to find a suitable technique to seed the flow in the separated region[17]. The method currently used[18] is to seed the external wind tunnel flow by silicon particles and to seed the separated region by condensed acetone vapor. One-component LDV results obtained by this technique are presented below. Two-component measurements will begin in the near future.

COLD AIR JET EXPERIMENTS

Zero angle of attack

These experiments[4,6] were carried out to provide values for an empirical recompression factor for conical afterbodies to support further development of the computer program by Addy[2]. The test geometries and parameters investigated are shown in Table 1. A typical pressure distribution is shown in Fig. 7 together with a photo-montage where the flow field is visualized by a spark schlieren picture and an oil flow picture. The separation line is discernible from the oil-flow and from the shock impingement in the schlieren photograph. The determination of the location of separation from the pressure distribution is in this single case quite

inaccurate because the pressure tap density is low, but with a family of pressure-distributions for different jet pressures the accuracy is increased. A summary of the data on pressure rise for the zero angle of attack results [4,6] at $M_E = 2.01$, using the form suggested by Zukoski[3], that is

$$P_B/P_i = 1 + CM_i$$

is shown in Fig. 8 as an illustrative example. This kind of results have allowed the determination of experimental-theoretical correlation for the recompression coefficient for both conical afterbodies and non-parallel outflow nozzles[21].

It might be of interest to mention that experimental data for this FFA-model[4] has been selected as test cases No. 9-12 by AGARD Fluid Dynamics Panel Working Group 08 "Aerodynamics of Aircraft Afterbody" for comparative calculations of afterbody flows with exhaust jet.

Effects of angle of attack

Supported by experimental data as those presented above the modified Addy-program[2] turned out to be a very useful resource for computation of the plume-afterbody interaction for a wide range of practical configurations. The program is, however, basically only valid for the axisymmetric case, and an experimental investigation was therefore carried out in order to establish the limitations of the applicability. Off-design effects of angle of attack and of external flow disturbances from aft-mounted controls (treated in the next paragraph) were studied. The test geometries and parameters investigated[18] are shown in Table 2 and a few illustrative examples of the results are presented in Figs. 9-12, which all show results at $M_E = 2.0$ for boattails at $\alpha = 6°$.

The pressure distribution on the afterbody and the oil flow pictures in Fig. 9 show the separated region for a fairly high jet pressure $P_L/P_E = 9$ on the $L/D = 1$, $\beta = 8°$ boattail. The pressure differences in the separated region generate marked secondary flow, which is seen in the oil flow pictures.

Fig. 10 shows the circumferential pressure distribution on the base for the same boattail also at $\alpha = 6°$ and with the jet pressure ratio P_L/P_E as parameter. The base pressure can be seen to be fairly constant over the base region at jet-off but increasing jet pressure ratio is followed by growing unevenness in the base pressure distribution. That this variation is dependent on boattail configuration is demonstrated in Fig. 11, which shows the base pressure distribution of various boattails at constant test conditions.

Fig. 12 shows an example of the circumferential variation of the separation location and of the base pressure ratio for the L/D = 1 and ß = 8° afterbody at $\alpha = 6°$ and $P_L/P_E = 9$. The separation distance is presented dimensionless in two ways, S/D in relation to the body diameter D and S/δ_φ in relation to the boundary layer thickness δ_φ at X/D = 7,6 and at the corresponding circumferential angle φ upstream of the separation. It can be seen that the S/δ_φ-curve has a pronounced maximum at the side of the afterbody ($\varphi = 90°$) due to quite large separation distance S in combination with a rather thin boundary layer (see Fig. 16, presented below).

The boattail normal force coefficient is presented in Fig. 13 versus jet pressure ratio. The results can give an idea about the order of magnitude of the stability disturbances that can be expected.

Effects of controls

The effects of controls on the pressure distribution for one cylindrical and two conical (L/D = 1; ß = 4° and 8°) afterbodies were studied[19]. The tests were made with the model described above at $M_E = 2.0$ with a propulsive jet Mach number $M_L = 2.5$ with controls as in Figs 4 and 6 at control angles $\delta = 0$ and $\pm 10°$ and at zero angle of attack. Fig. 14 shows the pressure distribution on the ß = 8° boattail with all controls deflected. The corresponding results for the model without controls are also presented for comparison. It can be seen that the influence of the controls is considerable. The effect increases with boattail angle and jet pressure ratio. The total afterbody drag (Fig. 15) is, however, little influenced by the presence of controls and control deflections except for the jet off case.

Body boundary layer

The conical nose of the model was equipped with a carborundum transition strip 85 mm from the apex. The body boundary layer has been measured by a probe at the body station X/D = 7.6 for $M_E = 2.0$ and 3.0[18]. Fig. 16 shows the variation of the boundary layer around the body. The displacement and the momentum thickness curves for $\alpha = 6°$ are seen to have a maximum at $\varphi = 30°$, indicating that the angle of attack is close to vortex separation. Measurements with LDV in the boundary layer have given results, which agree well with the probe results.

Flow in the separated region

When the results from the experimental plume-afterbody interference program mentioned above were analyzed in terms of

recompression factor to be used in the computations, it was found that this factor in some cases reached impossible values. It was suggested that the assumption used of zero velocity in the separated region was not accurate enough, and therefore an experimental program was initiated to investigate the flow in the separated region. Measurements have been made with probes[20] and with one-component LDV[7]. Fig. 17 shows the measured Mach number distribution over the afterbody at a jet pressure ratio of 15. The separated region and the surrounding free stream have been surveyed at five axial locations. At the same distance from the surface the locally generated acetone particles tended to have lower velocities than the silicon particles coming from the free stream. This is believed to be due to a too large size of the acetone particles, which results in to slow acceleration. In Fig. 18 an attempt has been made to draw the most probable lines through the measured values of Fig. 17. The profiles are superimposed on a schlieren picture. The highest Mach number in the reversed flow was found to be close to 0.1.

PLUME MODELING EXPERIMENTS

Plume simulated by annular jet and solid body

In a test comparing strut and sting supports[8] a study was also made of the possibility to use a solide body to simulate the gas plume. Fig. 19 shows some typical afterbody pressure distributions from this study. The annular nozzle had the same axial flow distribution as the circular nozzle. The shape of the solid body was identical with the plume shape of the circular nozzle as recorded on a schlieren photograph. On the pressure distributions it can be seen that the plume interference on the afterbody in this case is underrated by the annular nozzle and considerably exaggerated by the solid body.

Plume modeling methodology suggested by Korst

Zero angle of attack

The merits and potential of the plume simulation methodology by Korst[12,13] have been evaluated in an earlier investigation[14] which is extended in a current study[15] to more severe off-design conditions. Results from these investigations will probably be analyzed in detail by other authors at this meeting, but we will also present a few samples from the test results.

Basis for the Korst modeling methodology is the assumption that the prototype plume is properly simulated by a model plume if the two plumes have the same contour in the flow-field adjacent to the afterbody. This means that the initial plume deflection angle and the plume radius of curvature (shape) must be duplicated by the model plume.

The validity of this modeling scheme has been checked by comparing results for nozzles designed for gases with different specific heat ratios. The earlier tests[14] started with modeling from air (γ=1.4) as prototype to Freon-22 (γ=1.16) as model. The air (prototype) and the two Freon (model) nozzles investigated are depicted in Fig. 20. A typical base pressure result is shown in Fig. 21. The agreement between prototype and model base pressures is satisfactory not only for the design point but also for a rather wide range of off-design conditions. Also shown are a few results for the Freon nozzle run with air to illustrate the shortcomings of retaining nozzle similarity. Slope modeling of these results gives reasonable correspondence to tne prototype data but at effectively much lower pressure ratios. At these conditions, with essentially no separation, the radius of curvature is less important. In contrast to the proposed technique based on distorted nozzle geometries, very high stagnation pressures would be required for modeling with gases of higher than prototype specific heat ratios. For the separation location, as shown in Fig. 22, the nozzle designed according to "weak shock modeling" provides the best correlation, particularly near the design pressure ratio.

In the later part of the earlier tests[14] and in the current tests[15] nozzles modeling from Freon (prototype) to air (model) have been used. As the specific heat ratio for Freon-22 is γ=1.16, which is appropriate for simulation of combustion type products, this modeling is relevant for typical plume simulation in wind tunnels. The geometry of the prototype was chosen to be as realistic as possible, i.e. to have a shape similar to a typical rocket nozzle, see Fig. 23.

Base pressure results are shown in Fig. 24. The correlation between the two air (model) nozzle results is very good and the correlation Freon-air is as good as in the earlier tests, although it seems possible that a minor systematic discrepancy exists.

Schlieren pictures of the flow for the three nozzles at the design stagnation pressure are presented in Fig. 25 together with a plot overlay of some of the significant features in the pictures. In this scale no differences in plume shape have been observed, but minor differences in the location of the separation shock are detected and appreciable differences in the shape of the inner (barrel) shock are noticed.

Effects of angle of attack

Although the modeled nozzles have been calculated for axisymmetric flow tests have been made earlier at low angles of attack ($-6° < \alpha < +6°$)[14] and currently at high angles of attack ($-20° < \alpha < +20°$)[15] to examine the applicability of the modeling procedure. To facilitate the evaluation of the simulation of the angle of attack effects on the base pressure the pressure difference $\Delta(P_B/P_E)_\alpha = (P_B/P_E)_\alpha - (P_B/P_E)_{\alpha=0}$ at the circumferential angle $\varphi=0$ has been calculated and is shown as a function of angle of attack in Fig. 26 for the three nozzles. It can be seen that the angle of attack effect of the Freon (prototype) nozzle is quite well simulated.

The separation location S/D at the circumferential angle $\varphi=0$ is in Fig. 27 shown versus the angle of attack for the design jet stagnation pressure. It can be seen that the simulation is quite good, except at low positive angles of attack, which means when the vortex flow starts to build up. Oil flow and schlieren pictures for the angle of attack $\alpha=10°$ and the design jet stagnation pressure is presented in Fig. 28.

The results confirm that the basic validity of the Korst modeling methodology is satisfactory also within the angle of attack range investigated ($-20° < \alpha < +20°$).

Effects of control fins

A wind tunnel test has been carried out[15] to investigate the limitations of the Korst modeling methodology when the afterbody is exposed to the complex external flowfield generated by aft-mounted controls in combination with angle of attack. The angle of attack range was $-6° < \alpha < +6°$ and the controls were set at $\delta=0°$ and $\pm 10°$.

To isolate the effects of controls on base pressure ratio more clearly the difference between the results with and without controls have been calculated and the results for all three nozzles have for comparison been plotted together versus angle of attack. The results at the design jet stagnation pressure and for the circumferential angle $\varphi=0$ is shown as a sample in Fig. 29.

After analyzis of all test results it is concluded that the effects of the fins on base pressure obtained with the Freon (prototype) nozzle is in general satisfactorily simulated by the air (model) nozzles. A few local exceptions seem to occur in areas, where interaction between control wakes and the separated base region might be very sensitive to one parameter, e.g. the jet stagnation pressure. Apart from this few points the modeling seems to be valid even for severe combinations of control angles, angle of attack and off-design jet stagnation pressure. It is noted, however, that

the effect of controls on base pressure ratio obtained with the air (model) nozzles is often somewhat larger than the effect with the Freon (prototype) nozzle.

CONCLUDING REMARKS

A brief review has been presented of wind tunnel simulations of plume induced interference effects carried out at FFA. We have in this survey emphasized the general information about the existing data base on plume-afterbody interference tests. The presentation of test results has due to space limitations been restricted to one or a few samples from each investigation.

Two main problem areas have been treated. The first concerns cold air jet experiments. The results obtained have been used for modification and updating of existing computer programs and have improved the knowledge about the details of the flowfield. The second problem area concerns plume modeling experiments using hot Freon and cold air as prototype and model propellant respectively (or vice versa). The results have confirmed the validity of the Korst modeling methodology not only for the design jet pressure and zero angle of attack but also for off-design jet pressures and complex external flowfield disturbances generated by deflected aft-mounted control fins in combination with angle of attack.

ACKNOWLEDGEMENT

The cold air jet research program is partially sponsored by the Defence Material Administration of Sweden, The Air Material Department and by the Aeronautical Research Institute of Sweden (FFA).

The plume-modeling research program is jointly supported by the European Research Office, U.S. Army, Grant No. DA-ERO-78-G-028 and Contract No. DAJA37-81-C-1213 and by FFA.

The authors wish to thank Professor H.H. Korst and Professor R.A. White at the University of Illinois for their contributions to this program and for stimulating and fruitful cooperation.

REFERENCES

1 Harris, M.H. Pressure on axisymmetric base in a transonic or supersonic free stream in the presence of a jet. FFA Report 111, 1967.

2 Addy, A.L. Analysis of the axisymmetric base pressure and base temperature problem with supersonic interacting freestream - nozzle flows based on the flow model of Korst, et al. Part III. A computer program and representative results for cylindrical, boattailed, or flared afterbodies. U.S. Army Missile Command, Report No. RD-TR.69-14, Febr. 1970.

3 Zukoski, E.E. Turbulent boundary layer separation in front of a forward facing step. AIAA Journal (5), 10, pp. 1746-53, Oct. 1967.

4 Agrell, J. White, R.A. An experimental investigation of supersonic axisymmetric flow over boattails containing a centered propulsive jet. FFA TN AU-913, 1974.

5 Agrell, J. Experimental investigation of flow separation on afterbodies with a centered propulsive jet and supersonic external flow at small angles of attack. FFAP-A-445, presented at DGLR-Symposium "Strömung mit Ablösung", Munich, 19-20 Sept. 1979.

6 White, R. Agrell, J. Boattail and base pressure prediction including flow separation for afterbodies with a centered propulsive jet and supersonic external flow at small angles of attack. Paper 77-958 presented at the AIAA/SAE 13th Propulsion Conference, Orlando, Florida, 11-13 July, 1977.

7 Agrell, J. Wind tunnel investigation of separated flow over an afterbody in supersonic axisymmetric stream utilizing one-component Laser Doppler velocimetry. FFA TN 1983-10, 1983.

8 Agrell, J. Wind tunnel investigation of a conical afterbody with three propulsive jet simulators at angles of attack in subsonic and supersonic flow. FFA TN (Job No. AU-1034, to be published).

9 Nyberg, S-E.
Agrell, J.
Hevreng, T.
Investigation of modeling concepts for plume-afterbody flow interactions.
Grant DA-ERO-78-G-028, 1st Annual Technical Report, Febr. 1979.

10 Nyberg, S-E.
Agrell, J.
Hevreng, T.
Investigation of modeling concepts for plume-afterbody flow interactions.
Grant DA-ERO-78-G-028, 2nd Annual Technical Report, Febr. 1980.

11 Korst, H.H.
White, R.A.
Nyberg, S-E.
Agrell, J.
The simulation and modeling of jet plumes in wind tunnel facilitics.
Paper 80-0430, presented at the AIAA 11th Aerodynamic Testing Conference, Colorado Springs, Colorado, U.S.A., 18-20 March 1980. Also published in J. of Spacecraft and Rockets, Vol. 18, No. 5, Sept-Oct. 1981, pp. 427-434.

12 Korst, H.H.
Approximate determination of jet contours near the exit of axially symmetrical nozzles as a basis for plume modeling.
TR-RD-72-14, Aug. 1972, US Army Missile Command, Redstone Arsenal, Ala., U.S.A.

13 Korst, H.H.
Deep, R.A.
Modeling of plume induced interference problems in missile aerodynamics.
AIAA Paper No. 79-0362, 17th Aerospace Sciences Meeting, New Orleans, LA., 15-17 Jan. 1979.

14 Nyberg, S-E.
Agrell, J.
Investigation of modeling concepts for plume-afterbody flow interactions.
Grant DA-ERO-78-028, Final Technical Report, Nov. 1981.

15 Nyberg, S-E.
Agrell, J.
Effects of control fins and angle of attack on plume-afterbody flow simulation.
Contract No. DAJA 37-81-C-1213, Annual Technical Report, Febr. 1983.

16
FFA Wind tunnel facilities.
FFA Memorandum 93, Stockholm 1974.

17 Agrell, J.
Danielsson, L.
On the application of Laser-Doppler-Velocimetry for the measurement of velocities in large separated regions bounded by supersonic flow.
Paper presented at the 53rd Meeting of the Supersonic Tunnel Association, 26-28 March 1980, NASA-Ames, Moffet Field, California.

18 Agrell, J. An experimental investigation of supersonic flow over boattails with a centered propulsive jet at angles of attack. FFA TN (Job No. AU-1111 to be published).

19 Agrell, J. An experimental investigation of the influence from controls on supersonic axisymmetric flow over afterbodies with a centered propulsive jet. FFA TN 1982-50, Nov. 1982.

20 Agrell, J. An experimental survey of a separated region on a conical afterbody in a supersonic freestream. FFA TN AU-1187, Dec. 1978.

21 White, R.A. The calculation of supersonic axisymmetric afterbody flow with jet interference and possible flow separation. FFA TN AU-912, 1974.

Table 1. Summary of zero angle of attack test geometries and test parameters[4].

L/D=1.0

M_E	2.01 and 3.27			
M_L	2.0	2.5		
$\beta°$ \ θ_L	20°	0	10°	20°
0°		X		X
4°		X		X[1)]
6°		X		X
8°	X	X	X	X[2)]
10°		X		X

1) also with nozzle extended 0.05 D
2) also with nozzle extended 0.05 D and 0.10 D.

Table 2. Summary of angle of attack test geometries and parameters[18].

M_E	2.0, 3.0										2.0
Jet nozzle	M_L= 2.50; θ_L 20°										
P_L/P_E	Jet off; 1, 3, 6, 9 and 15										
β \ L/D	0.5	1.0	2.0	α	0	3°	4°	6°	8°	10°	15°
Cylin-drical		X			X	X		X		X	X
4°		X	X		X	X		X		X[1)]	X[1)]
8°	X	X			X	X	X[1)]	X	X[1)]	X[1)]	X[1)]

1) Only for L/D = 1

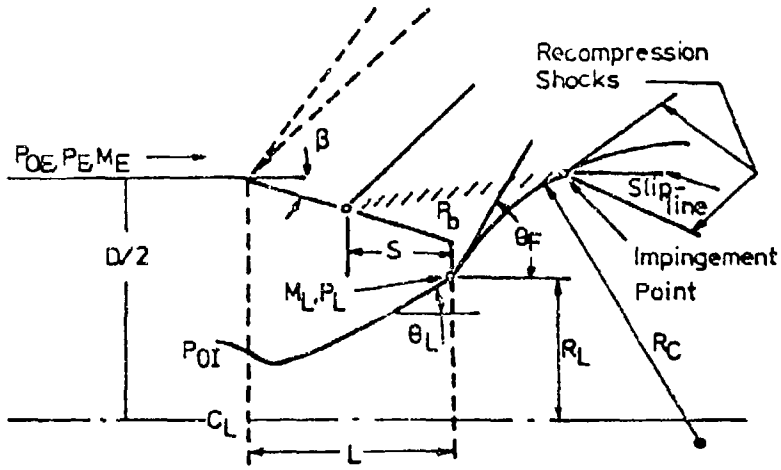

Fig. 1 Flow configuration for plume induced separation from conical afterbody (geometrical and operational parameters identified).

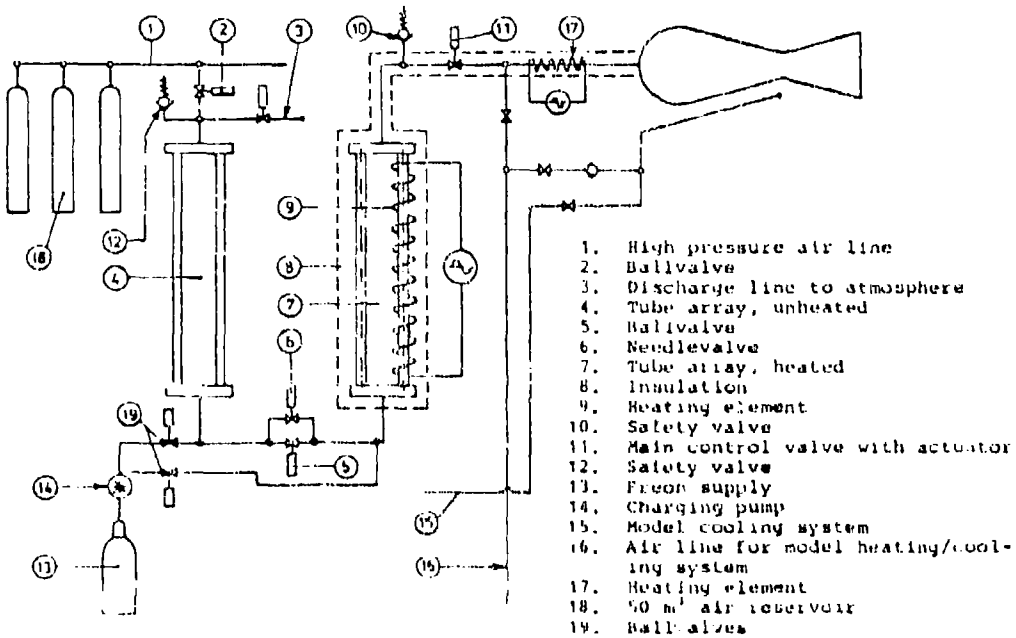

1. High pressure air line
2. Ballvalve
3. Discharge line to atmosphere
4. Tube array, unheated
5. Ballvalve
6. Needlevalve
7. Tube array, heated
8. Insulation
9. Heating element
10. Safety valve
11. Main control valve with actuator
12. Safety valve
13. Freon supply
14. Charging pump
15. Model cooling system
16. Air line for model heating/cooling system
17. Heating element
18. 50 m³ air reservoir
19. Ballvalves

Fig. 2 Annotated schematic of air driver system, Freon heater and Nozzle.

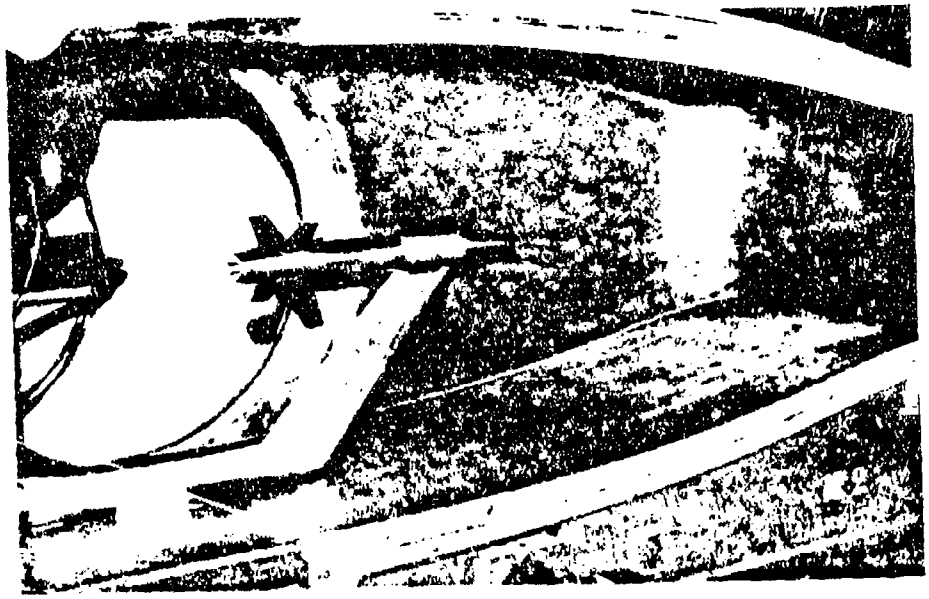

Fig. 3 Model in wind tunnel S5.

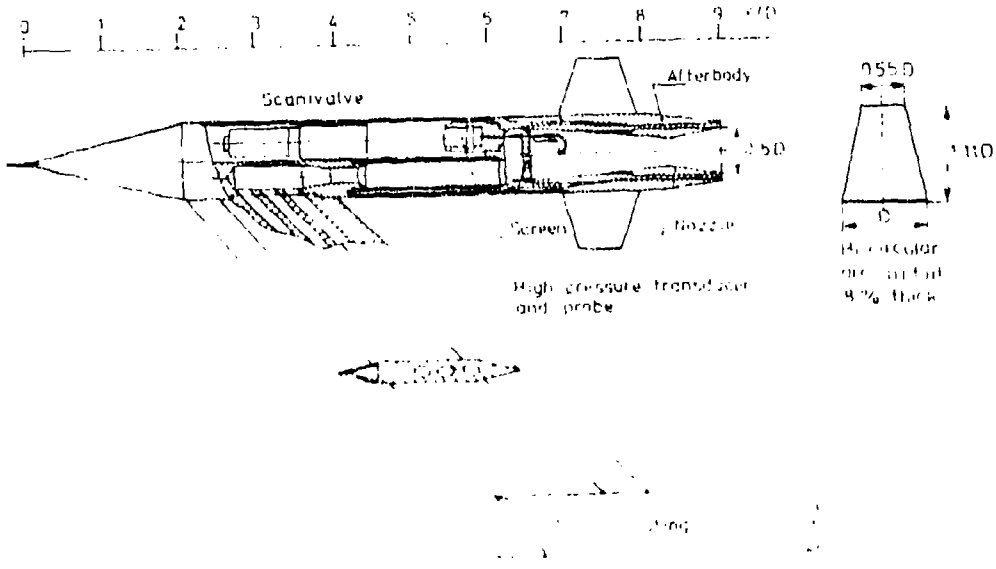

Fig. 4 Sketch of model and strut.

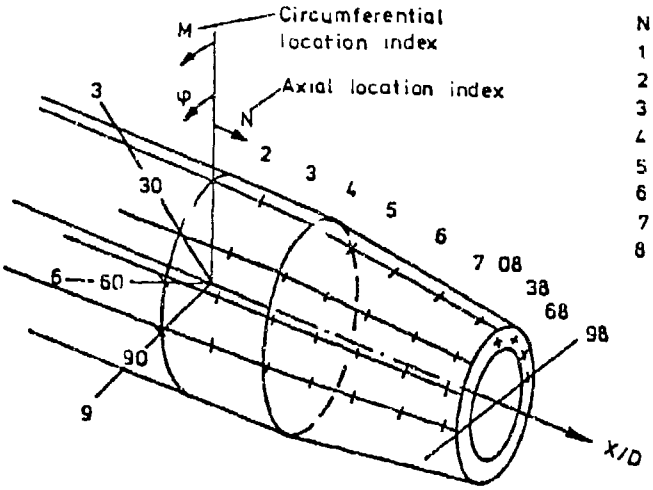

N	X/D
1	8.10
2	8.30
3	8.52
4	8.74
5	8.96
6	9.20
7	9.42
8	9.50

Fig. 5 Location of pressure taps on boattail.

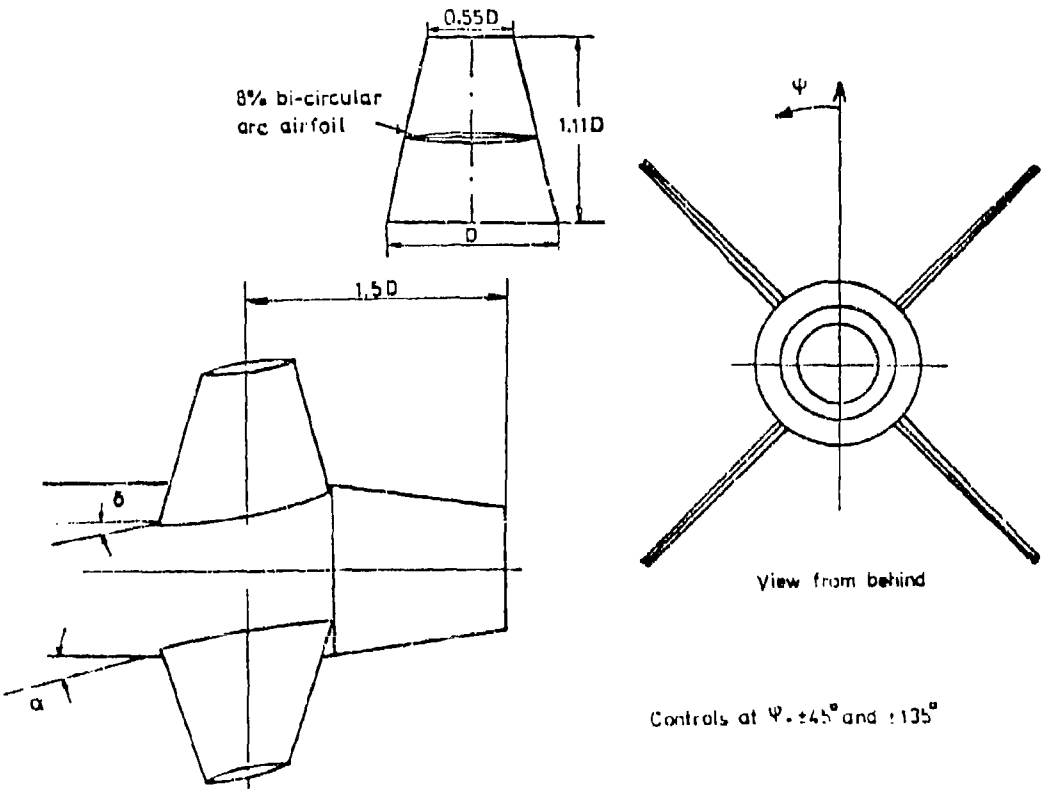

Fig. 6 Control dimensions and definition of control deflection angles.

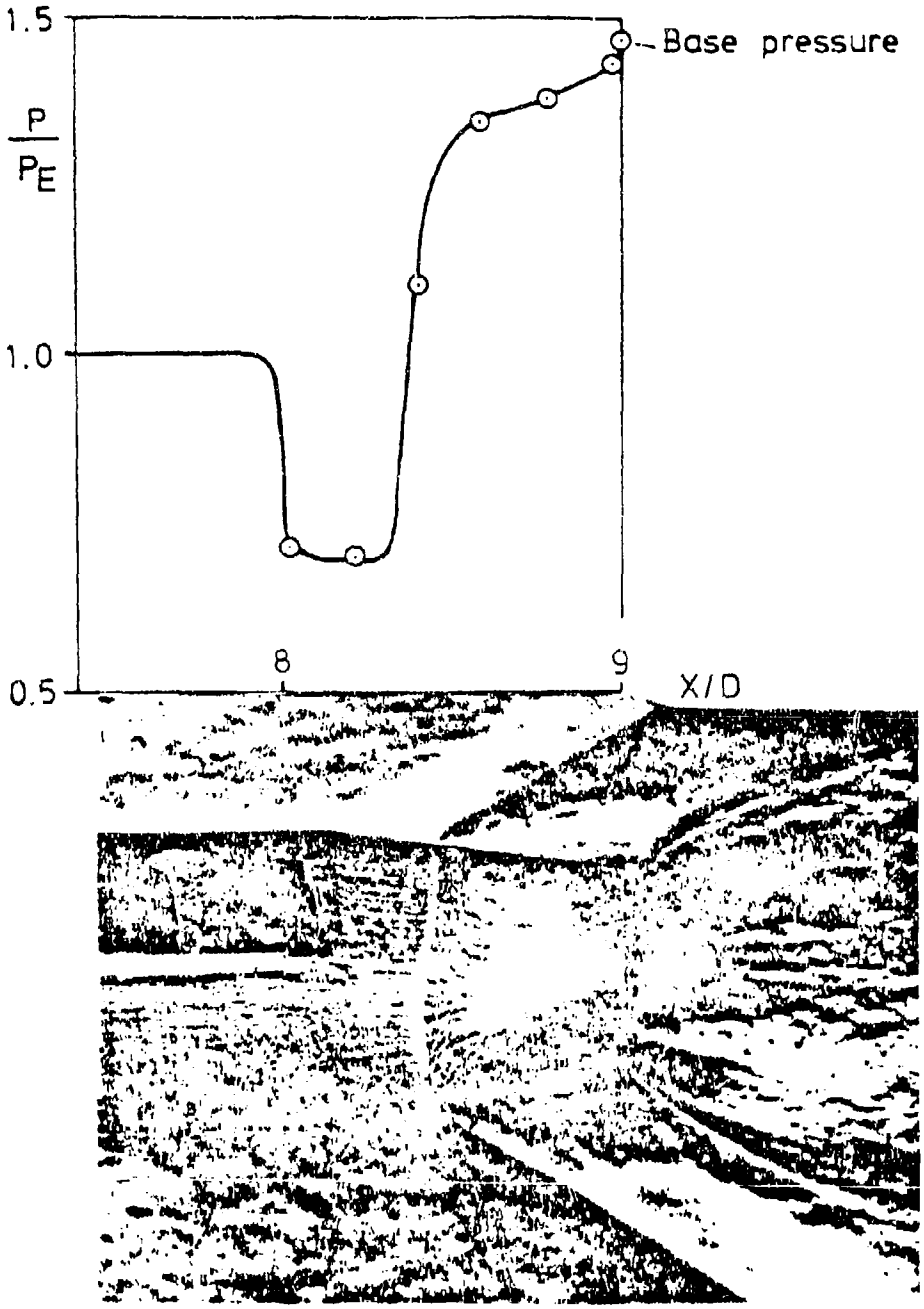

Photomontage of [illegible] flow and [illegible] pressure associated with the corresponding pressure [illegible] $M_1 = 2.01$, [illegible] $M_1 = [illegible]$ [illegible] and $P_1/P_2 = [illegible]$

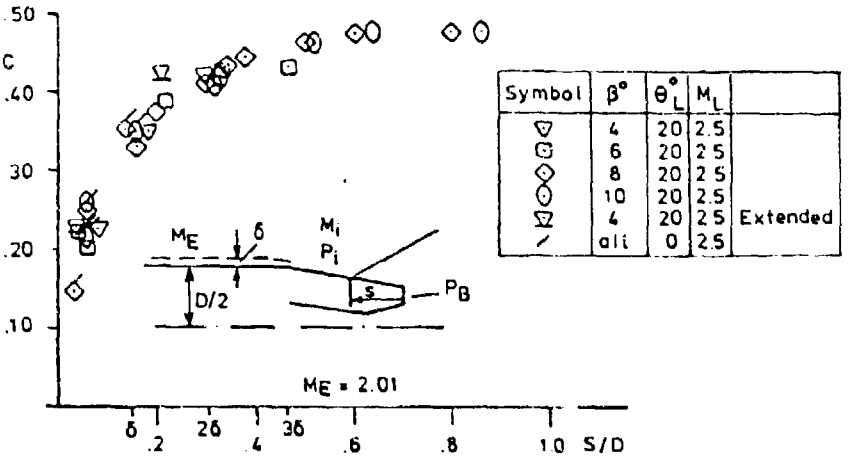

Fig. 8 The pressure rise across the separation as a function of the separation position on the boattail. $P_B/P_i = 1 + C M_i$.

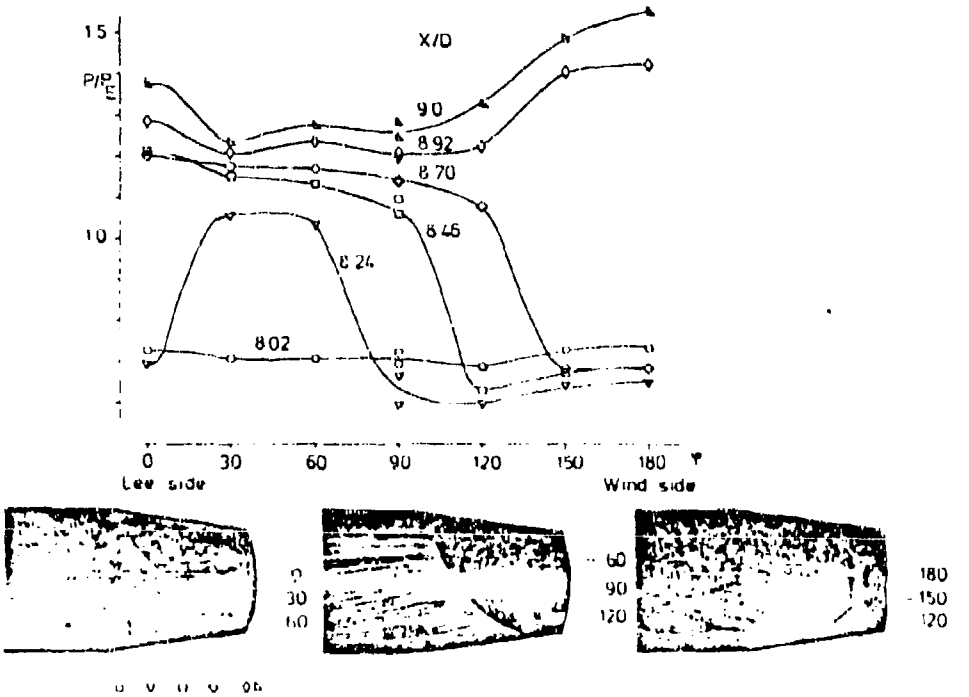

Fig. 9 Pressure distribution on the afterbody with the corresponding oil flow pictures.
$M_F = 2.0$, $L/D = 1$, $\beta = 8^0$, $P_L/P_E = 9$, $\alpha = 6^0$

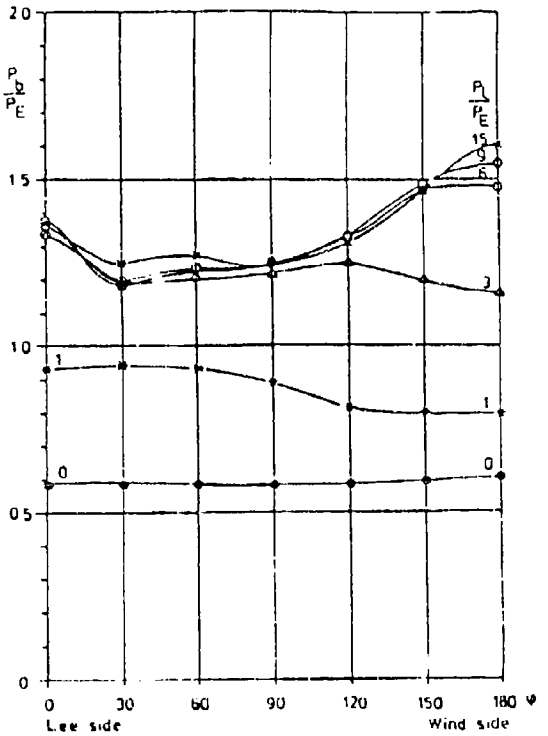

Fig. 10 Dimensionless pressure distribution on base for different jet pressure ratios.
$M_E = 2.0$, $L/D = 1$, $\beta = 8^0$, $\alpha = 6^0$

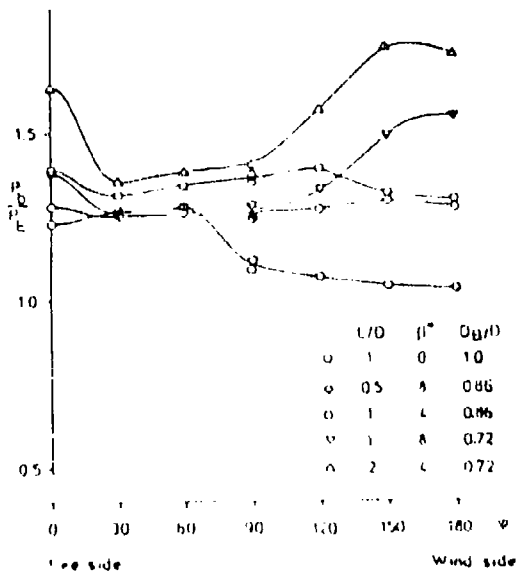

Fig. 11 Dimensionless pressure distribution on base for different ratios of the base to model diameter
$M_E = 2.0$, $P_T/P_E = 9$, $\alpha = 6$

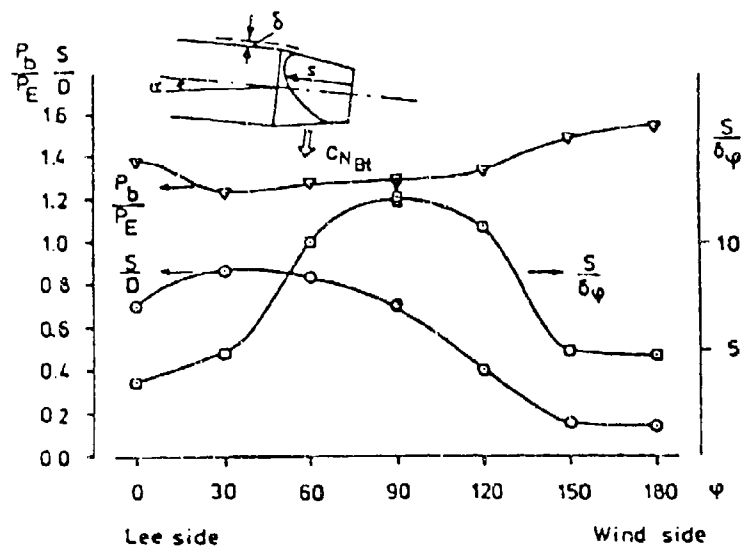

Fig. 12 Separation distance around the afterbody.
$M_E = 2.0$, $L/D = 1$, $\beta = 8^\circ$, $P_L/P_E = 9$, $\alpha = 6^\circ$

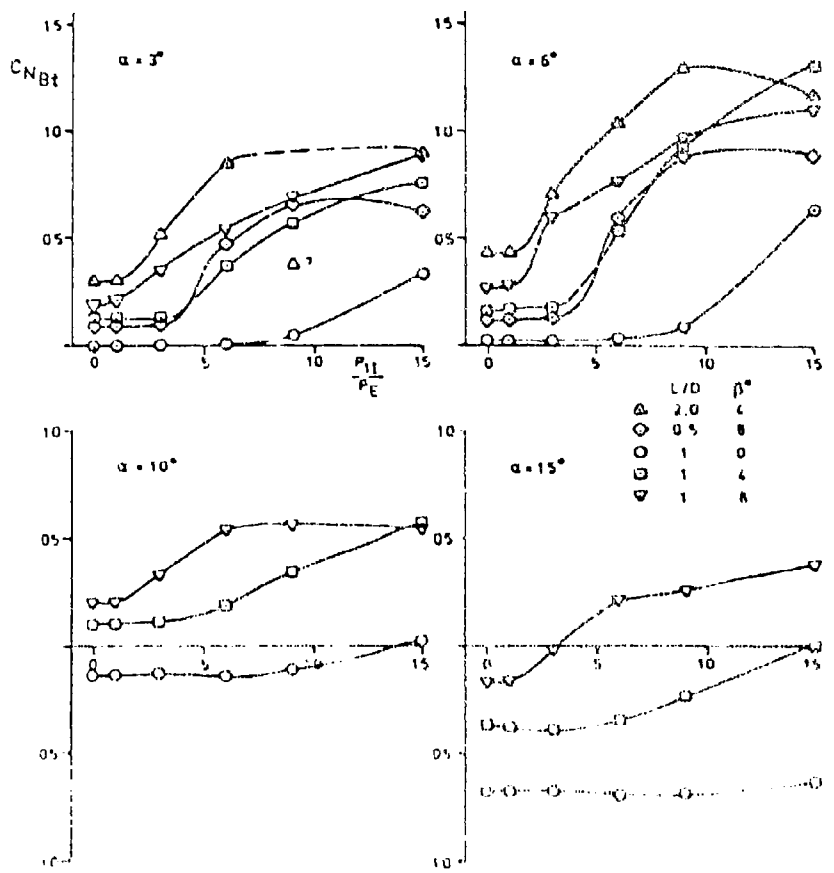

Fig. 13 Boattail normal force coefficient versus jet pressure ratio $M_E = 2.0$

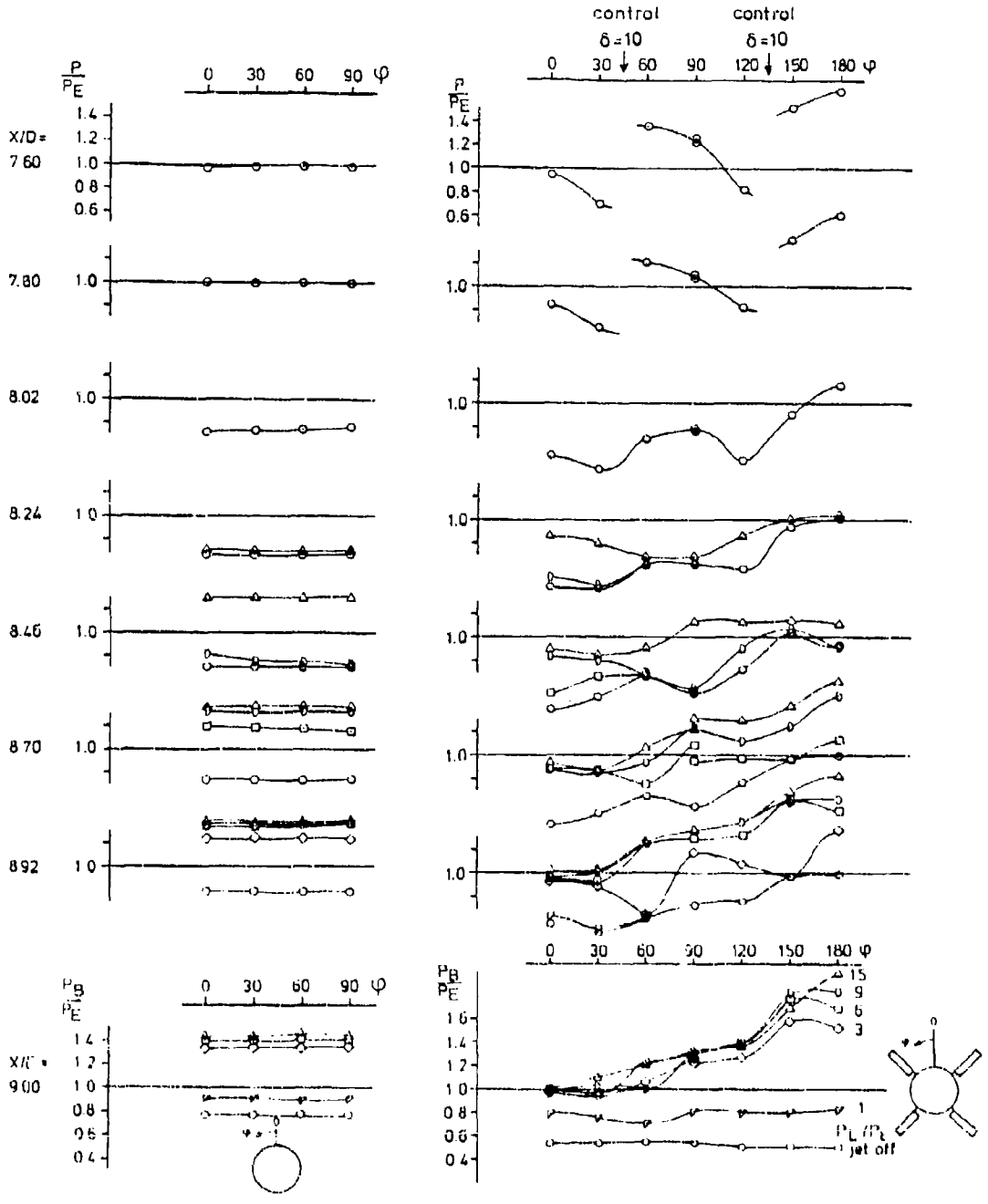

Fig. 14 Surface pressure ratio as a function of φ and P_L/P_E, $\gamma = 8$, $\Delta = (10, -10, -10, 10)$ (For clarity only results, which differ from lower jet pressure ratio results have been plotted).

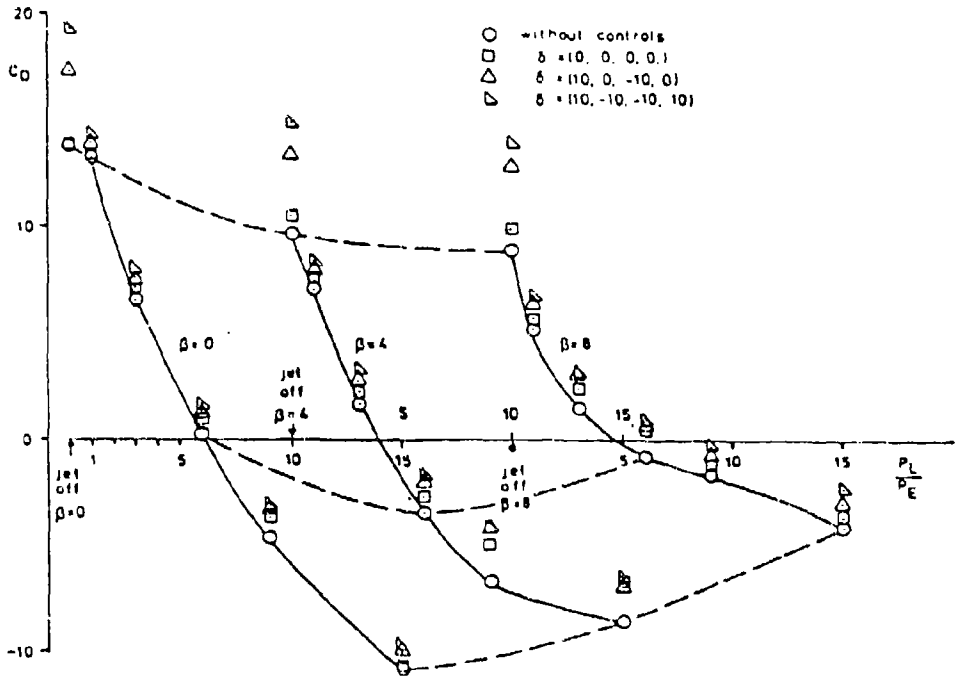

Fig. 15 Total afterbody drag coefficient as a function of jet pressure ratio.

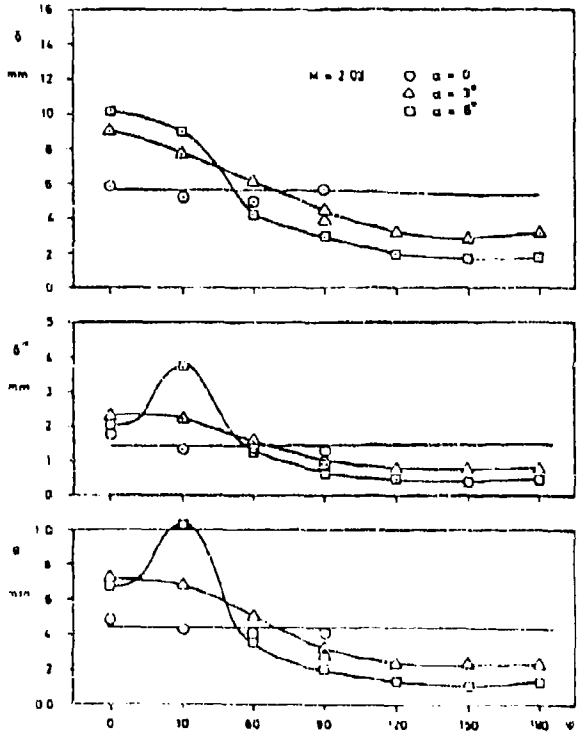

Fig. 16 Boundary layer thickness around the body at X/D = 7.6, M_∞ = 2.03, $Re = 6 \times 10^6$

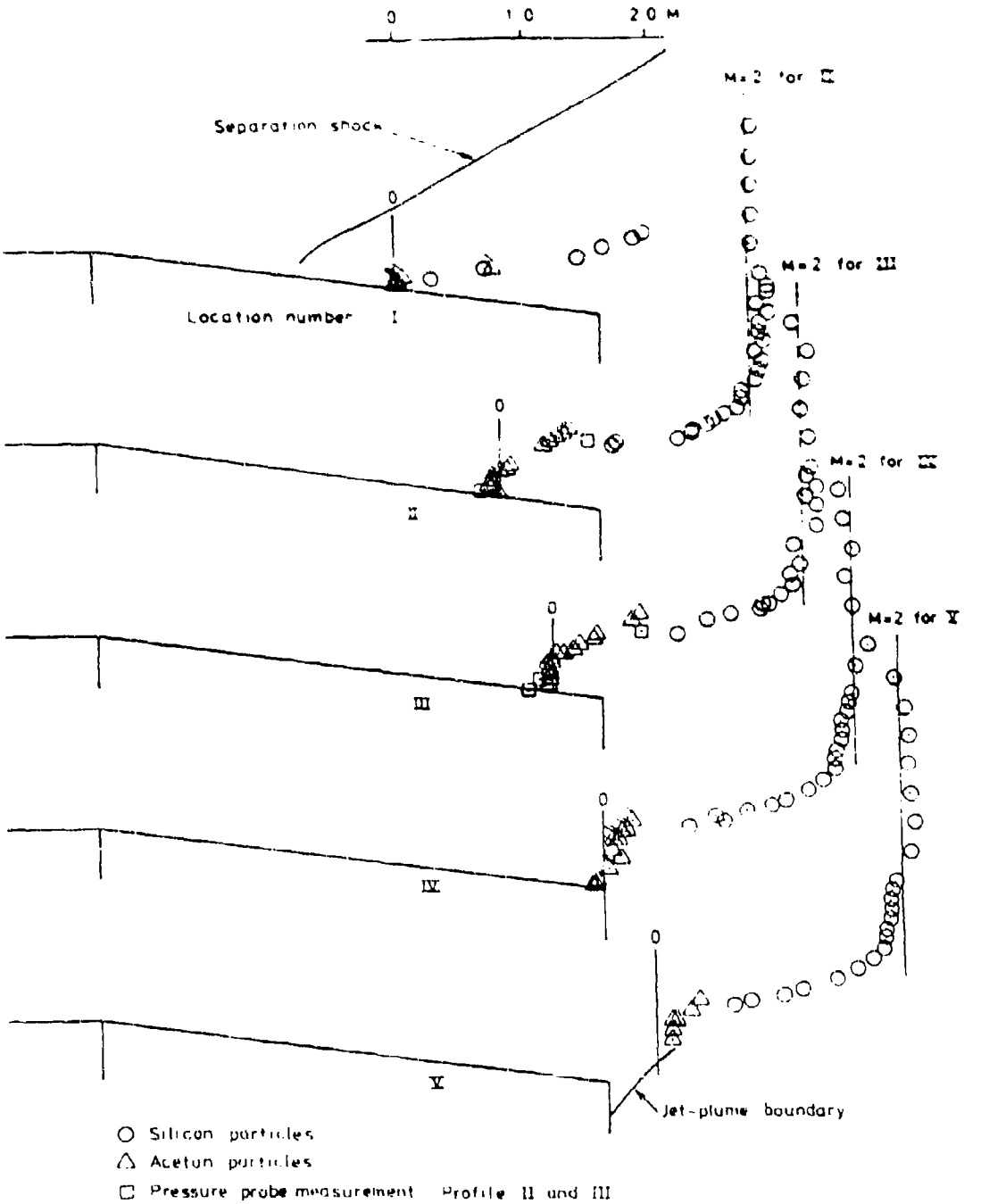

Fig. 17 The measured Mach number distribution over the afterbody at jet pressure ratio 15. $M_\infty = 2.0$.

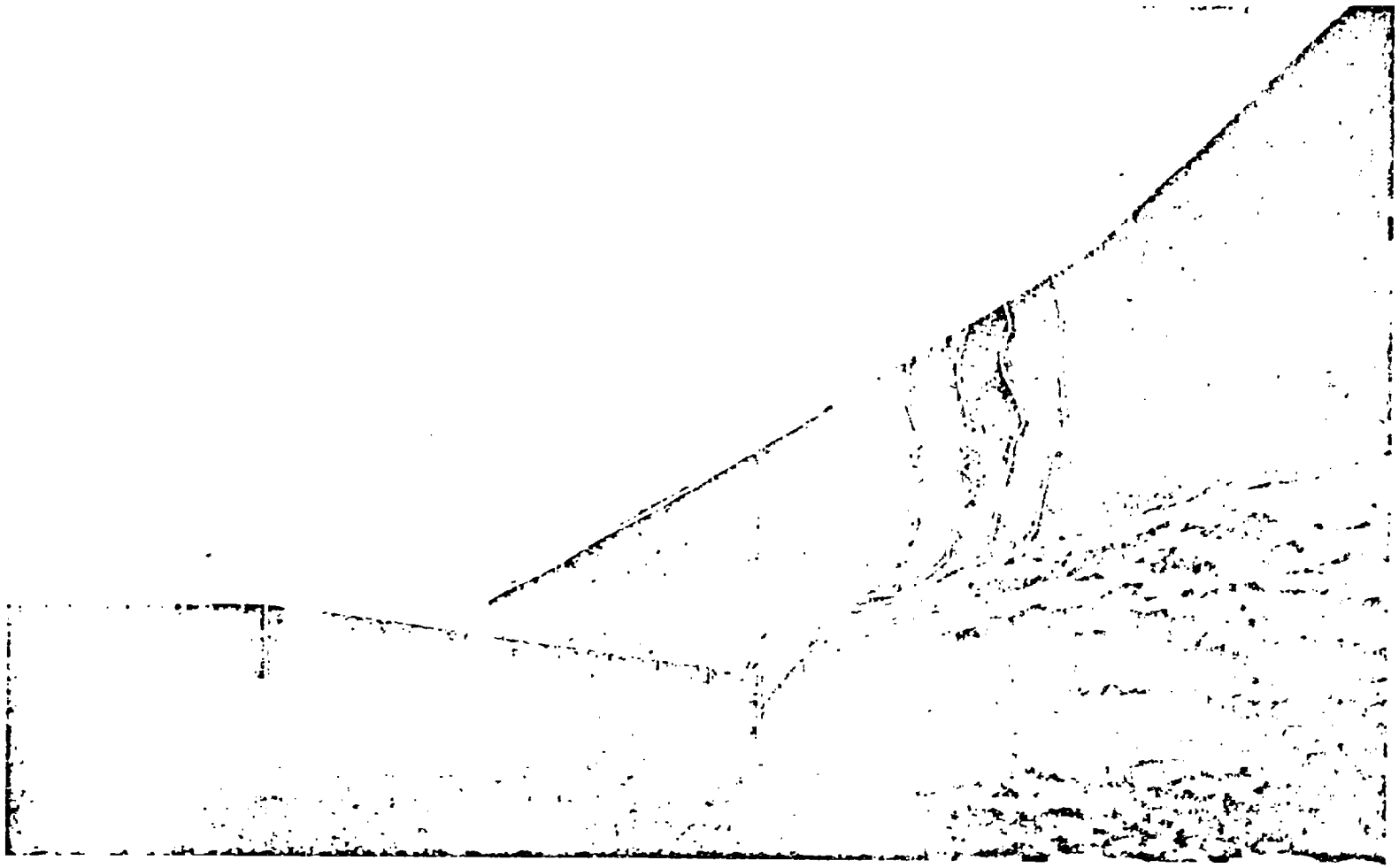

Fig. 18 Schlieren photo and Mach number distribution.
$M_E = 2.03$, $P_L/P_E = 15$

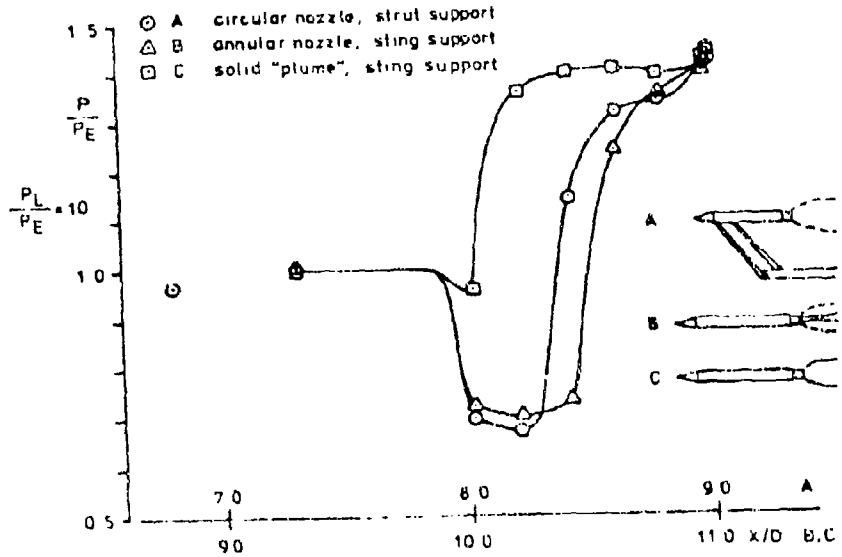

Fig. 19 Afterbody pressure distribution for circular nozzle, annular nozzle and solid plume. $M_E = 2.03$, $\alpha = 0$, $L/D = 1$, $P_L/P_E = 10$. Nozzle exit diameter = 0.7 D.

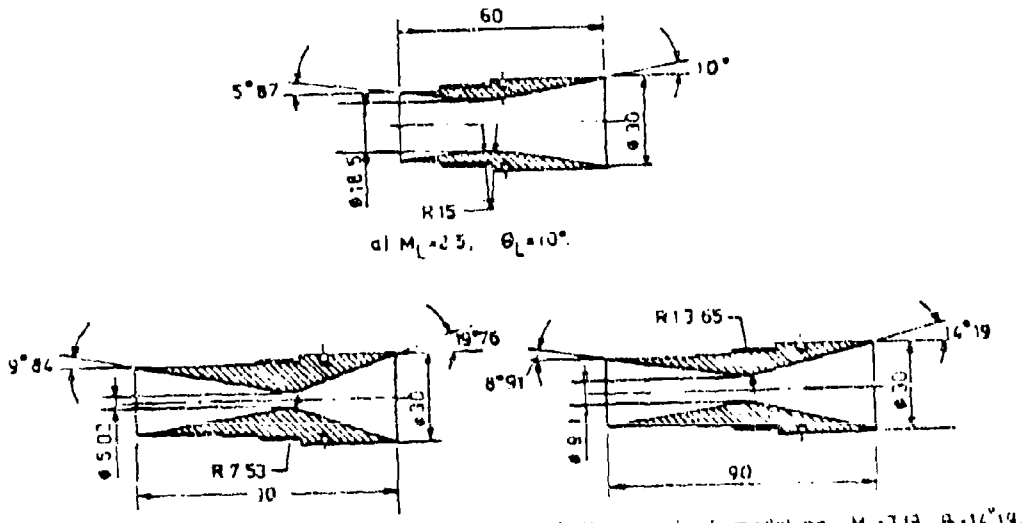

Fig. 20 Nozzles modeling from air to Freon (a) Prototype nozzle (Air, $\gamma = 1.4$). (b,c) Model nozzles (Freon 22, $\gamma_M = 1.16$) (Dimensions are in millimeters)

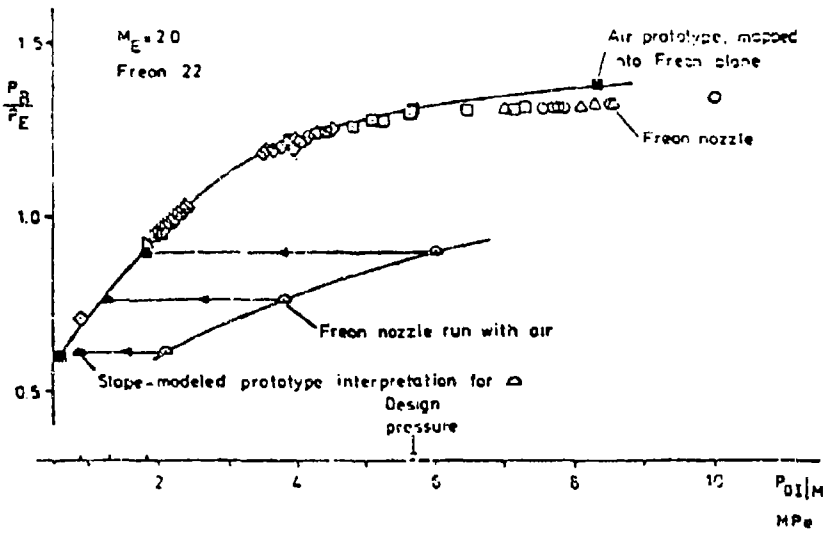

Fig. 21 Base pressure P_B/P_E versus jet stagnation pressure P_{OI} for Freon nozzle (Strong shock modeling).

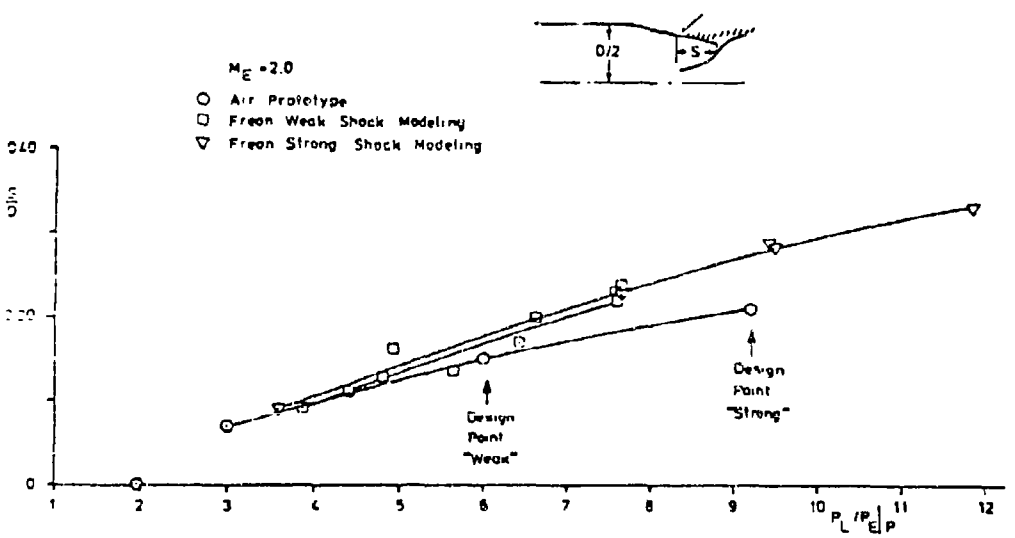

Fig. 22 Separation location vs lip pressure for air (prototype) and Freon (model) nozzles.

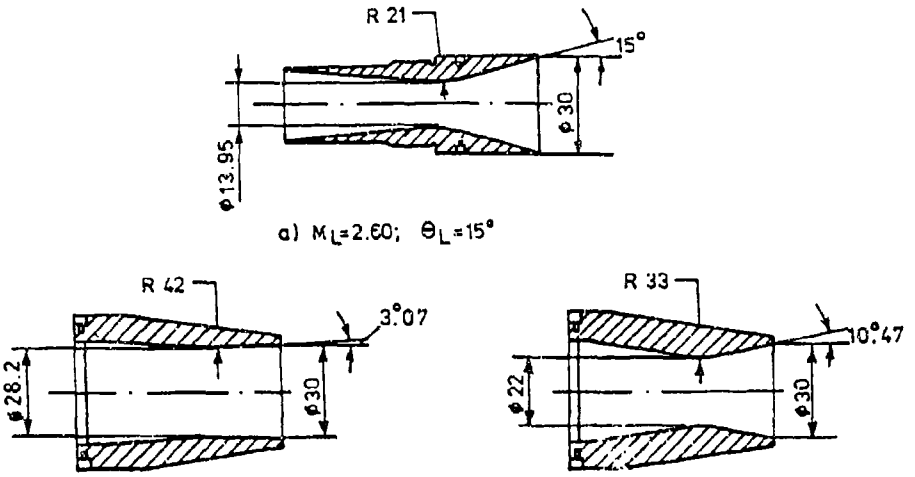

Fig. 23 Nozzles modeling from Freon to air (a) Prototype nozzles (Freon 22, $\gamma_p = 1.16$). (b,c) Model nozzles (Air, $\gamma_M = 1.4$) (Dimensions are in millimeters)

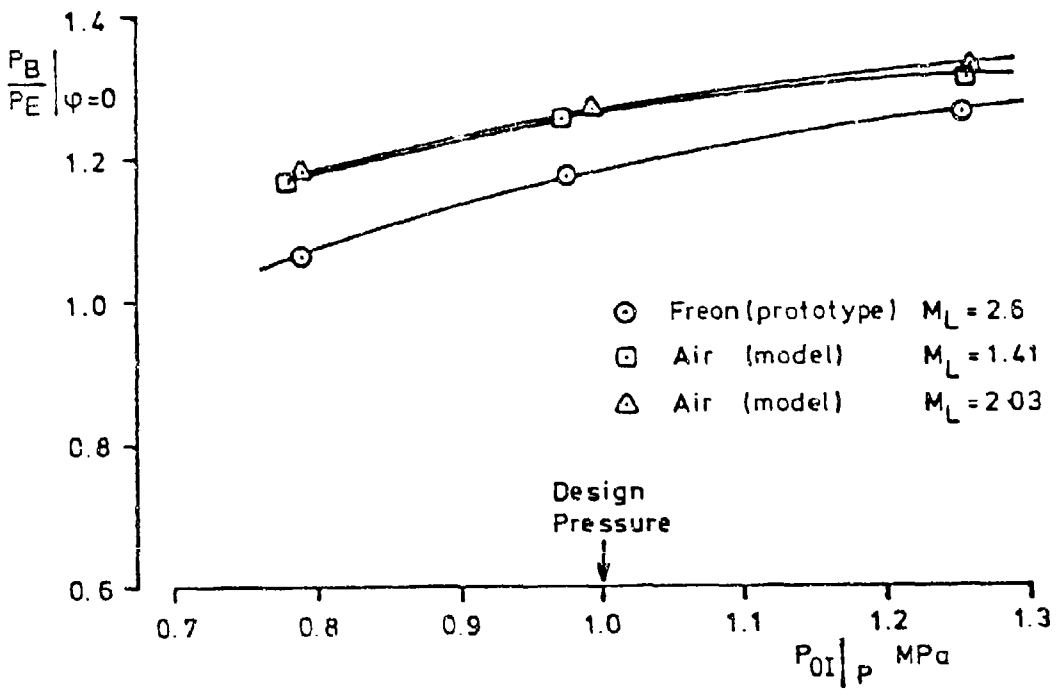

Fig. 24 Base pressure ratio for Freon (prototype) and air (model) versus nozzle stagnation pressure in prototype plane.

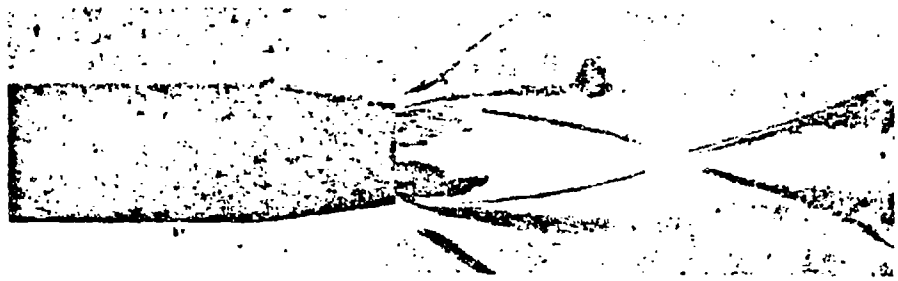

a) Freon (prototype) $M_L = 2.6$

b) Air (model) $M_L = 1.41$

c) Air (model) $M_L = 2.03$

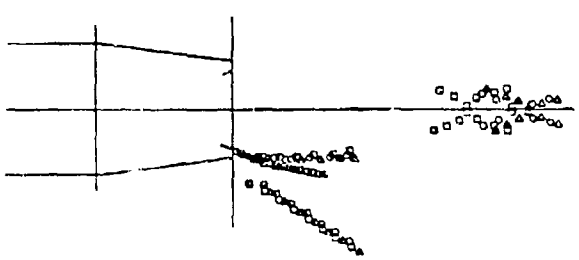

d) Plot overlay

Fig. 25 Schlieren and oil flow pictures from tests at design conditions ($\alpha = 0$; $P_{0I} = 1.0$ MPa).

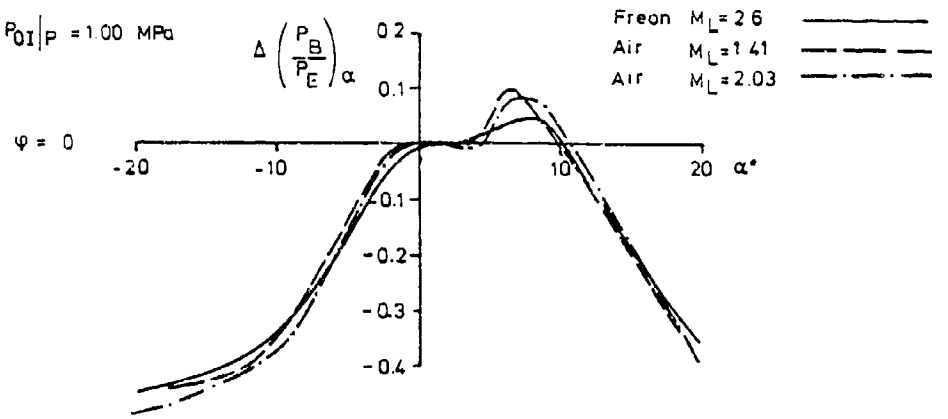

Fig. 26 Effect on base pressure ratio of angle of attack $\Delta(P_B/P_E)_\alpha = (P_B/P_E)_\alpha - (P_B/P_E)_{\alpha=0}$ versus angle of attack α at stagnation pressure $P_{0I}|_P$ = 1.00 MPa = design pressure.

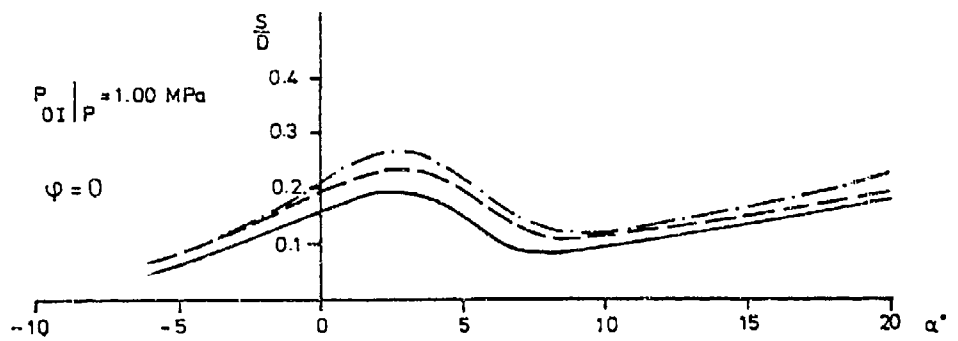

Fig. 27 Separation location S/D at $\varphi = 0$ versus angle of attack α for Freon (prototype) and air (model) nozzles at stagnation pressures $P_{0I|P}$ = 1.00 MPa = design pressure.

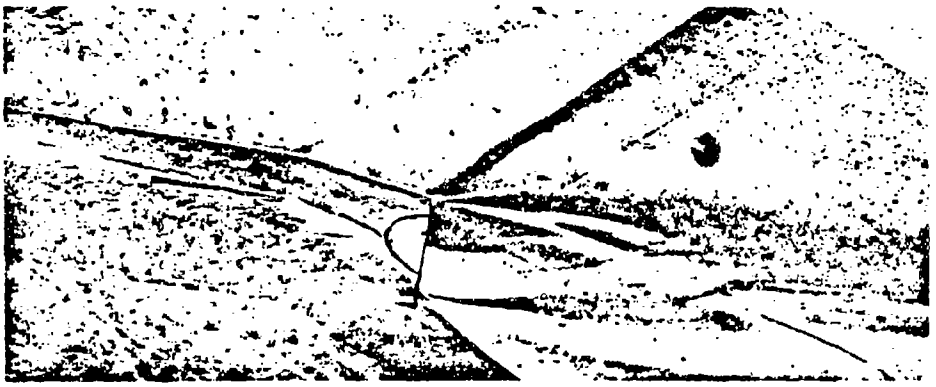

Freon $M_L = 2.6$

Air $M_L = 1.41$

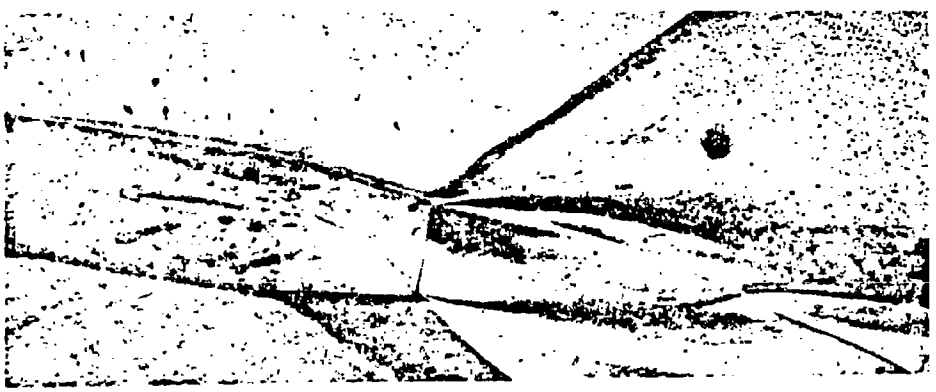

Air $M_L = 2.03$

Fig. 28 Oil flow and Schlieren pictures at $\alpha = 10^{\circ}$ and $P_{OI|P} = 1.00$ MPa for the Freon (prototype) and air (model) nozzles.

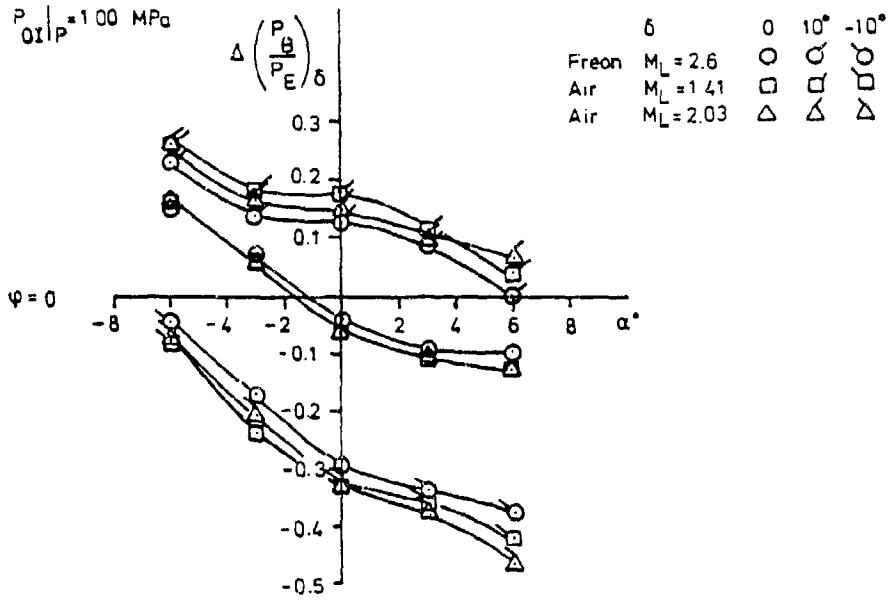

Fig. 29 Effect on base pressure ratio of controls. $\Delta(P_B/P_E)_\delta = (P_B/P_E)_{\text{with controls}} - (P_B/P_E)_{\text{without controls}}$ versus angle of attack α at stagnation pressure $P_{OI}|_P = 1.00$ MPa.

APPENDIX G-1

BASE FLOW AND RELATED MODEL EXPERIMENTS

Paper presented at the

Symposium on Rocket/Plume Fluid Dynamic Interactions

Huntsville, Alabama

April 1983

by

A. L. Addy, V. A. Amatucci, D. W. Kuntz, H. L. Petrie, and M. Samimy

APPENDIX G-1

BASE FLOW AND RELATED MODEL EXPERIMENTS

A. L. Addy[†]
V. A. Amatucci, D. W. Kuntz, H. L. Petrie, and M. Samimy[††]
Department of Mechanical and Industrial Engineering
University of Illinois at Urbana-Champaign
Urbana, Illinois 61801

ABSTRACT

The near-wake flowfield behind the base of a missile is being investigated through a series of small-scale two-dimensional experiments. The primary objective of the research effort is to provide new, extensive, and well-documented data and thus obtain a better understanding of the basic fluid dynamic mechanisms existing in the base flowfield. The two-dimensional experiments concern the growth, development, recompression, and reattachment of a compressible turbulent free shear layer. Also examined are the effects of plume-induced and shock-induced separation of a turbulent boundary layer. The data include laser Doppler velocimeter measurements, extensive static pressure measurements, and flow visualization pictures. The results of preliminary LDV experiments indicate particle size distributions on the order of 1 μm and atomization and insertion of the seed in the wind tunnel plenum chamber as a successful technique. The initial recompression and reattachment data seem to verify two-dimensionality of the wind tunnel flowfields. The development of the LDV system over the past few years is relatively complete and measurements are currently being made in two-dimensional base region flowfields which should provide insight into various component mechanisms.

NOMENCLATURE

Variables

c	Speed of sound
D	Diameter
f_D	Doppler shift frequency
h	Step height
M	Mach number

[†] Professor and Associate Head.
[††] Graduate Research Assistants.

Variables (cont.)

P	Absolute pressure
R	Reattachment location
Re	Reynolds number
T	Absolute temperature
u	Streamwise velocity component
$\vec{V}$	Velocity vector $[\vec{V} = \vec{V}(u,v,w)]$
v	Normal velocity component
w	Spanwise velocity component
x	Physical axial distance
y	Physical normal distance
z	Physical spanwise distance
α	Ramp angle
δ	Boundary layer thickness
κ	Laser beam half-angle after focusing lens
λ	Wavelength
ν	Kinematic viscosity

Subscripts

B	Base
CL	Centerline
g,G	Gas or compressible fluid
j	Inner jet
N	Normal
P	Particle
r	Relative; Reattachment
0	Stagnation condition
1	Upstream of shock wave
2	Downstream of shock wave
∞	Freestream

Superscripts

(')	Fluctuating quantity
$(\overline{\ \ })$	Time averaged quantity

INTRODUCTION

Since the early 1950's, the separated flow region at the base of a missile for flight at supersonic speeds has been studied extensively. The objectives of these studies were to develop an understanding of the mechanisms governing the separated base flow region and to formulate flow models for predicting the base region pressure, temperature, and heat transfer characteristics. The more successful models or methods, judged by their ability to predict base flow conditions in reasonable agreement with experiment, are all combinations of theoretical and empirical components which have been combined to model this complex flow region[1-4]. These methods leave still unanswered many questions regarding the fundamental fluid dynamic nature of the flow mechanisms and interactions within the separated base flow region.

The supersonic turbulent flow which approaches the base of the missile undergoes an expansion process at the geometric corner, a shear layer mixing process between the freestream flow and the recirculating flow, and a recompression and redevelopment process. In each of the components of the base flowfield a number of flow mechanisms exist which are still in need of detailed examination. The flow mechanisms, as indicated in Figure 1, can be broadly categorized as follows:

- Geometric separation of a boundary layer to form a free shear layer. Local expansions or compressions at the separation location are important factors affecting shear layer development, turbulence intensity, and the initialization of the flow entering the base region;

- Effects on shear layer development resulting from modifications of the initial phases of the jet mixing due to adjacent wall geometry and local wake flowfields;

- Shear layer development in the presence of the recirculating base flow. The determination of the local velocity field and the turbulence characteristics of this flow are important to the characterization of the base flow;

- Recompression, reattachment, and redevelopment of the shear flow in the presence of the external and internal flows; and

- Shock wave or aerodynamically induced separation of the body turbulent boundary layer to form a shear layer at locations upstream of the geometric separation location.

These basic flow mechanisms are being investigated through carefully controlled small-scale experiments in an effort to provide well documented new data.

The data obtained from small-scale base flow experiments focus on instantaneous velocity measurements and turbulence information for various features of the base flowfield. The overall objective is to obtain insight concerning the basic fluid dynamic flow mechanisms and the nature of the turbulent transport properties. The data include laser Doppler velocimeter (LDV) measurements, extensive surface pressure measurements, and Schlieren and shadowgraph pictures. The non-intrusive nature of LDV measurements is well suited to the base flowfield, since pressure probe insertion, particularly in the recirculating region, tends to perturb the existing flowfield. The measured data can be statistically analyzed to determine mean velocity, turbulence intensity, Reynolds shear stress, turbulent kinetic energy, and turbulent length scale.

The new base flow data which are obtained from these small-scale experiments will be used to improve the analyses used in the component approach. The research efforts emphasize accurate and reliable data based on an understanding of the phenomena associated with LDV measurements in a supersonic flow and the nature of small-scale experiments. The goal of this paper is to document the measurement and experimental facilities which are currently in use for LDV measurements in two-dimensional, small-scale base flow regions.

WIND TUNNEL FACILITIES

The wind tunnel facilities in the Mechanical Engineering Laboratory of the University of Illinois permit investigation of subsonic, transonic, and supersonic flows through small-scale experiments. The air supply system utilizes high pressure compressors, filters, and dryers to provide clean and dry compressed air for a range of wind tunnel applications. The available mass flowrate of air is at a level which permits, based on model size, either continuous flow or blowdown type small-scale experiments.

The base flow experiments described herein are relatively small scale and generally blowdown mode of operation. The wind tunnels in each case utilize a control valve to supply compressed air into a large cylindrical plenum chamber, where the flow is stagnated. Two-dimensional converging-diverging nozzles are utilized to produce a supersonic, disturbance-free, uniform flow in the test section. The test model is heavily instrumented with pressure taps which allow a survey of the static pressure distribution. The test sections use glass windows in the near-wake region in order to permit LDV measurements to be made. The wind tunnel flow is then exhausted outside the Laboratory to the atmosphere.

LASER DOPPLER VELOCIMETRY

Basic Principles

The fundamental concept of laser Doppler velocimetry (LDV) is that fluid velocity can be measured by mixing the Doppler frequency shifts of scattered laser light. Two intense, coherent laser beams intersect to form an ellipsoidal measurement volume with a set of alternating light and dark fringes. The movement of a seed particle past the resulting fringe pattern will cause some of the incident laser light to be scattered and reflected. The scattered light from the two incident beams reaches the collecting optics and undergoes optical heterodyne mixing in order to produce an output signal. The resulting output signal oscillates at the Doppler shift frequency and is directly proportional to the velocity component normal to the angle bisector of the incident beams and lying in the same plane, $f_D = 2u(\sin\kappa)/\lambda$.

The LDV System

The experimental programs described herein utilize a two component two color LDV system as shown in Figure 2. A 2-W argon ion laser (subsequently replaced by a 5-W argon ion laser) is used as the coherent light source and produces a green beam (λ = 514.5 nm) and a blue beam (λ = 488.0 nm) after passage through the dispersion prism. Each color beam is then split into two parallel beams by its respective beam splitter. The beam splitter components provide equal power in the two partial beams and equal optical path lengths. The intersecting beams form ellipsoidal measurement volumes and permit simultaneous measurement of two velocity components. A dichroic mirror will separate the blue and green scattered radiation and send each to different photomultipliers. The output signal is processed by a DEC PDP-11/03 minicomputer with a dual floppy disk drive.

Frequency shifting is employed by adding a Bragg cell to the optical arrangement in order to handle flow reversals and areas of large turbulence intensity. The size of the measurement volume is affected by the diameter of the incident laser beams and the half-angle between them. Further reduction in the effective size of the measurement volume can be achieved by employing small photodetector apertures and off-axis light collection.

Particle Dynamics and Measurement Bias

The nonintrusive nature of the LDV and its ability to measure velocity components independent of fluctuation intensity make it a very useful tool for examining fluid dynamic flowfields. However, certain problems inherent in the LDV technique, particularly for supersonic flows, require consideration and compensation in the data collection and reduction process. Foremost among these problems are

the effects of the particle dynamics, particularly particle insertion and velocity lag[5-10], and the effects of measurement bias due to the counter-type data processor[11-16].

The problem of particle lag arises when one considers that the velocity of the light scattering particles is actually being measured and not the flow velocity. The choice of particle type and size should focus on the ability of light scattering particles to follow the flow through strong gradients or high frequency fluctuations in velocity. The seed particles should effectively scatter incident light, possess uniformity of particle population, and be available in easily controlled concentrations. Some LDV experiments investigating particle dynamics have been conducted and are discussed in a later section.

The use of a counter-type data processor as a component of the LDV system poses experimental problems regarding the interpretation of data. The effects of velocity biasing and fringe biasing are thoroughly discussed in the literature[11-16] and various correction schemes are proposed and tested herein.

SMALL-SCALE EXPERIMENTS RELATED TO NEAR-WAKE FLOW

Preliminary LDV and Particle Experiments

Numerous LDV experiments were conducted in a small-scale continuous flow supersonic wind tunnel. The objectives of these experiments were as follows:

- To develop, evaluate, and refine procedures and techniques for using LDV in supersonic wind tunnels;
- To determine the number of naturally occurring and compressor generated particles in the flow and to determine their size;
- To evaluate various seed particle generation techniques;
- To estimate seed particle size; and
- To evaluate the abilities and limitations of the equipment making up the total LDV system.

The initial experiments were done without seeding and it was found that no significant number of natural or compressor generated particles in these supersonic flows could produce Doppler signals for which noise did not dominate the results. Results obtained at high system gain levels indicated these types of particles were present but that these particles were too small to produce a good signal. Oil streak lines on wind tunnel windows and rust colored dust on wind tunnel walls also indicated the presence of these particles.

Particle generation methods that were investigated included atomizing silicone oil and atomizing ethanol with monodisperse polystyrene latex particles contained within it. One channel data rates were commonly in excess of 40 kHz for oil seeded flows and approximately 125 times less for the latex/ethanol seeded flows. A coincidence requirement of 0.22 μ s between u- and v-component measurements reduced data rates by up to a factor of 5.

Diameters of particles generated by atomizing silicone oil were estimated by measuring the relaxation of particle velocities downstream of an oblique shock wave. The shock wave was generated by expanding the wind tunnel inlet Mach 2 flow 15° and then turning it 15°, as shown in Figure 3. Static pressure measurements and shock wave angle measurements made from Schlieren photographs indicated that the flow upstream of the shock wave was at Mach 2.58. The theoretical change in the component of velocity normal to the shock wave was 160.7 m/s when T_0 = 296°K.

The velocity relaxation experiments were done using only one LDV channel. Both normal and tangential velocity components were independently measured. The component of velocity tangent to the shock wave was found to change by 0.85 percent or less across the shock wave. The average normal component particle velocities at locations downstream of the shock wave are shown in Figure 4 for oil mist seeded flow. The predicted results obtained using Walsh's[17] empirical drag coefficient for 1 μm and 1.5 μm diameter water droplets are plotted on this figure for comparison. However, the range of relative Mach numbers and Reynolds numbers for the data used in the formulation of this drag coefficient and those occurring downstream of the shock wave, see Figure 5, are quite different. Thus there exists some questions concerning the accuracy of this size estimation.

Experiments were conducted using monodisperse latex particles in order to evaluate the accuracy of Walsh's[17] drag coefficient under the flow conditions of interest. These were done by atomizing a dilute solution of ethanol with latex particles and injecting this either into the wind tunnel plenum chamber or 30 m upstream of the plenum chamber into the supply line. These experiments proved unsuccessful because the ethanol condensed in the expanded supersonic flow of the wind tunnel and produced many ethanol droplets with primarily submicron diameters. These ethanol particles outnumbered and masked the latex particle results. Experiments using Freon-14 as the carrier fluid for the latex particles may be conducted in the future in an attempt to obtain drag coefficient data in this range of flow conditions.

The LDV system, including positioning and alignment hardware, optics, electronics, and computer hardware, performed satisfactorily. The aged 2-W argon ion laser used in these experiments, which operates well below specification output power, has now been replaced by a new 5-W laser. This should allow the use of submicron diameter

latex particles with higher data rates and better signal-to-noise ratios as a result.

Free Shear Layer Formation and Development Experiments

The initialization and growth of the shear layer is being investigated in a series of two-dimensional experiments utilizing LDV measurements. The objectives of these experiments are to obtain a more detailed knowledge of the separation and development process of a compressible turbulent free shear layer and of the potential interactions of flow components occurring in missile base region type flows that may effect the shear layer.

Three basic experiments are planned for the study of compressible free shear layers using LDV. Simultaneous u- and v-component velocity data will be taken with the LDV in all cases. These experiments will be conducted in a blowdown wind tunnel with a supersonic test section inlet that measures 50.8 mm high by 101.6 mm wide. The inlet flow in most of these experiments is at Mach 2.5 with a fully turbulent approach boundary layer. This experimental program will use the three configurations shown in Figure 6 to attain its objectives. The configuration shown in Figure 6(a) will be used to study the development of a constant pressure turbulent free shear layer with a turbulent approach boundary layer and without the effects of a recirculating flow or an expansion or compression at the separation point. This will be achieved by bleeding very low momentum flow through a porous plate, located downstream of the backward facing step, at a rate equal to the shear layer's entrainment rate. The effects of a recirculating flow on the shear layer will be studied using the configuration in Figure 6(b). Note that the approach flow conditions and boundary layer will be the same in all of these experiments. Constant pressure flow, expansion at the separation point, and a weak shock wave at the separation point can be obtained by adjusting the position and angle of the ramp at the right side of Figure 6(b). Figure 6(c) indicates the extreme case of removal of this ramp and will be the strongest expansion to be examined.

The porous plate experiment has been done before[18] but there are good reasons to repeat it. This flowfield is dominated by one component of velocity, has relatively low turbulent intensity, no large accelerations, and no flow reversal. These features make it appealing as our initial LDV effort with compressible turbulent flows. Both the approach flow and bleed flow may or may not be seeded so that the effects of particle concentration gradients can be minimized and also studied. The data from this experiment will be compared with that of the previous study in order to validate the quality of the LDV results. Also this earlier study, which employed hot wires, was unsuccessful in measuring the Reynolds shear stress, $\overline{u'v'}$, and mass flowrate fluctuations, not velocity fluctuations, were measured. The results of this experiment are needed to serve as a basis by

which the results of the other free shear layer experiments will be judged.

The recirculating flow configuration, Figure 6(b), has been used to study shear layer reattachment and redevelopment[19]. However, no effort has been made to examine the shear layer in the presence of recirculation in detail.

Very little detailed knowledge exists concerning the effects of an expansion or weak shock wave at the separation point on free shear layer development. It is expected that the turbulence in the approach boundary layer will be completely quenched in a strong expansion. Thus the turbulent boundary layer remnant will become a laminar rotational layer into which a new initially laminar inner free shear layer grows. Milder expansions will lead to higher levels of turbulence in the boundary layer remnant and the rotational layer should play a more active role in initial shear layer development. A Mach 2 approach flow will be used for the configuration in Figure 6(c). This will be done to reduce the Mach number adjacent to the free shear layer so that it is more nearly equal to the Mach 2.5 flow of the porous plate and recirculating flow experiments.

Free Shear Layer Reattachment and Redevelopment Experiments

The recompression, reattachment, and redevelopment of the turbulent shear layer in the near wake flowfield provides the key component in the overall base flow analysis. The importance of these processes has been cited in the literature[20,21] and a number of empirical models exist[22-27]. In an effort to obtain a better understanding of the basic flow mechanisms of recompression, a research effort is underway to conduct a series of three small-scale two-dimensional experiments. The experiments which are planned are described as follows, noting the configurations shown in Figures 7(a)-7(c):

- Reattachment and redevelopment of a self-similar turbulent supersonic free shear layer on a ramp;
- Reattachment and redevelopment of a developing free shear layer on a horizontal plane; and
- Interaction of two developing free shear layers.

The main objectives of these experiments are to obtain better insight into the reattachment and redevelopment processes of a two-dimensional free shear layer and to evaluate some of the basic assumptions and empirical information of various extensions of the component model. In addition, these data will provide information in order for computational researchers to test different turbulence closure models.

A two-dimensional wind tunnel with a test section 50.8 mm wide and 127.0 mm high has been designed and fabricated. The wind tunnel test section and the test section inlet are adaptable to each of the configurations shown in Figure 7. The test models are heavily instrumented for static pressure measurements and a clear glass test section window exists for LDV measurements in the recompression region.

The initial series of experiments, namely the compression ramp experiments, are characterized by a test model as shown in Figure 7(a). The data which are presented in Figure 8 are for a 15 degree ramp subject to a free shear layer developed from the corner separation of a freestream flow with a Mach number of 2. The turbulent boundary layer is approximately 3.8 mm thick when it separates over a sharp backward-facing step. The resulting free shear layer is approximately 90 mm (24 δ) long when it attaches onto the plane ramp. The angle of the ramp and the distance between the ramp and step have been adjusted so that there are no changes in pressure or flow direction as the boundary layer separates at the step. The typical static pressure distribution for this type of flow is shown in Figure 8(a). In the literature[19,28,29], the necessary length of a free shear layer to achieve self-similarity in terms of mean velocity has been reported to be from 10 to 22 times the incoming boundary layer thickness. The experimental configuration examined here will therefore create an undisturbed self-similar free shear layer with well defined initial conditions for the reattachment process. In general, the compression ramp experiments will be conducted for freestream Mach numbers of 2, 2.5, and 3 using ramps of 15, 17.5, and 20 degrees.

The two-dimensional nature of the flowfield for these experiments was investigated using spanwise surface pressure measurements at a number of stations on the test model. The spanwise pressure survey, again for a Mach 2 freestream and a 15 degree ramp, produced the measurements shown in Figure 8(b). The results seem to indicate that the spanwise surface pressure variation is within the accuracy of the pressure measurements. Further checks will be made by measuring the spanwise velocity component using the LDV. Surface flow pattern visualization methods will also be utilized.

The backward-facing step experiments, depicted in Figure 7(b), will utilize approach Mach numbers of 1.5, 2, and 2.5 in order to produce free shear layers with the same Mach and Reynolds numbers approaching recompression as those of the compression ramp experiments. The free shear layers in these experiments are not expected to reach an equilibrium condition before reattachment occurs. Therefore, the results of self-similar and developing free shear layers with the same approach Mach and Reynolds numbers will be compared.

The two-jet experiments, characterized in Figure 7(c), will examine the interaction between two turbulent, supersonic free shear

layers. Combinations of the Mach numbers 1.5, 2, and 2.5 will be used together with different approach static pressure ratios.

All of the experiments will employ flows which are seeded in the plenum chamber using monodisperse polystyrene latex particles or oil with a mean diameter of 1 micron. Simultaneous u- and v-component velocities as well as time between sample data will be measured. The data will be analyzed in order to determine mean velocities, turbulent intensities, turbulent kinetic energy, Reynolds shear stress, autocorrelation function, turbulence length and time scales, power spectral density, and redeveloping boundary layer thickness parameters.

Shock Wave-Turbulent Boundary Layer Interaction Experiments

The interaction between a shock wave and a supersonic turbulent boundary layer has been the subject of research for well over two decades. Such interactions can occur at a flare on a missile body or on a deflected control surface. In the study of shock wave-boundary layer interactions, three basic configurations are of interest. The first of these is the impinging shock wave, shown in Figure 9(a). In this case an oblique shock wave, generated by an external source, impinges on the boundary layer and is reflected, causing a separation bubble near the impingement point if the wave is strong enough. The second configuration, shown in Figure 9(b), is the compression corner, or ramp. In this flowfield a shock wave is generated as the flow turns and a region of separated flow may exist near the corner depending upon the corner angle and the flow properties. The third configuration, shown in Figure 9(c), is the forward-facing step. A separation region exists upstream of the step and an oblique shock wave is generated near the beginning of the separated region. The location of the separation point will be a function of the flowfield and boundary layer properties.

The scope of these experiments will be limited to experimental studies of the compression corner and forward-facing step flowfields. These two configurations were selected because they most closely represent the separation process that can take place near the base region of a missile in powered flight as a result of flare-induced or plume-induced separation.

A great deal of research effort has been directed at the shock wave-boundary layer interaction problem over the past twenty-five years. Several review papers have been written concerning this research including the work of Zukoski[30], which summarizes forward-facing step experiments, and the work of Adamson and Messiter[31], the most recent of the review papers. Most of the experimental studies done in this area are concerned with measuring mean flow properties. The most thorough of these investigations was performed by Settles[32]. In this work, extensive mean flow measurements of a compression corner flowfield were made. The flowfields were assumed to be

steady,[33] and no instantaneous measurements were taken. Dolling and Murphy used a high frequency response pressure transducer to measure instantaneous wall pressures in a separated compression corner flowfield. The results of this study indicate that the shock structure was not steady but that the shock wave location fluctuated randomly over a significant distance. These results raise questions about the meaning of the mean flow surveys made in the past, and point out the need for more measurements using high frequency response techniques.

The facility to be used in this series of experiments is a 101.6 mm by 101.6 mm supersonic wind tunnel. This tunnel was originally designed with a flexible nozzle assembly which allowed the test section Mach number to be varied from the high subsonic range to approximately three. Although the variable geometry nozzle proved useful in a number of applications, it produced a Mach number distribution within the test section which was less than adequate for this study. As a result, the flexible nozzle assembly has been replaced with a solid nozzle block designed to produce a uniform Mach number within the test section of approximately 2.9. This solid nozzle arrangement is shorter than the flexible nozzle it replaced, allowing the installation of a test section at two different axial locations. Thus it is now possible to conduct experiments at two locations within the constant area section of the tunnel, producing different values of Re_δ due to the different boundary layer thicknesses. These modifications to this wind tunnel have been completed, and tests are currently underway to determine wind tunnel operating characteristics.

The models used in these experimental studies will be heavily instrumented with static pressure taps for determining both flowwise and spanwise pressure distributions. Step heights of 5.08, 10.16, 15.24, and 20.32 mm will be used to obtain data with different ratios of step height to boundary layer thickness. Ramp angles of 8, 12, 16, 20, and 24 degrees will be used with care taken to ensure that the ramps are long enough to simulate infinite ramp conditions. A number of studies have shown that three-dimensionality can be a problem in small-scale wind tunnels. Initially the models will be built to span the 101.6 mm width of the test section. If preliminary measurements indicate that reliable two-dimensional flow is not present near the center of the model, it may prove necessary to reduce the width of the models and install transparent sidewall splitter plates to remove the effects of the wind tunnel side wall boundary layers. These splitter plates would add additional optical surfaces which would increase the difficulty of making accurate LDV measurements.

The primary objective of this study is to use the LDV to measure mean velocities, turbulence intensities, and Reynolds shear stresses throughout the compression corner and forward-facing step flowfields. In addition, mean surface pressure distributions will be measured on all models. A kerosene-graphite technique will be used to determine

separation and reattachment locations, and Schlieren photographs will be used to help visualize the flowfield. The LDV data will be studied closely for the appearance of the unsteady shock wave behavior seen by Dolling and Murphy[33].

Supersonic Power-On Base Flow Experiments

The advent of rocket powered flight initiated many research investigations which attempted to detail the base region flowfield resulting from the interaction between the freestream flow and the rocket exhaust plume[34-36]. The primary goal was to identify and understand the fundamental flow mechanisms and viscous interactions which occurred in the near-wake base flowfield. The interaction of a strongly underexpanded exhaust plume with the freestream flow which initiated separation of the turbulent boundary layer upstream of the physical corner of the base also has drawn considerable interest. The examination of particular flow mechanisms within the power-on base flowfield, including the effects of plume-induced separation, will provide information for extension of the component model to complex geometries and flowfields.

An experimental investigation is being conducted to examine in detail the two-dimensional base flow problem in the presence of an exhaust jet. Special emphasis will be placed on plume-induced afterbody separation with the objective of determining those flow parameters which govern such features as separation point location, recirculating region velocity, and shear layer growth. The data will be LDV measurements, supported by extensive surface pressure measurements and Schlieren and shadowgraph pictures. Most past research focuses on mean velocity determined from pressure distribution data. The use of a two-component, frequency-shifted LDV to measure instantaneous flow velocity, despite its added complexity, has the particular advantage of being nonintrusive in the separated flowfield.

The power-on experiments will utilize a two-dimensional wind tunnel, already constructed, which is 127.0 mm in height and 50.8 mm wide. The freestream and inner jet flows are directed through valves which control the level of stagnation pressure. Continuous-slope converging-diverging nozzles are under design which will produce uniform supersonic flows with turbulent boundary layers at the two-dimensional base. The wind tunnel test section window is approximately 101.6 mm by 184.2 mm and is of adequate size to encompass the entire near-wake flowfield. The test section window port can be utilized with either a clear glass window for LDV measurements or an aluminum port with multiple static pressure taps for a near-wake static pressure survey. The wind tunnel air supply design is readily adaptable for use of high pressure bottled air for the inner jet during the plume-induced separation studies.

The two-dimensional power-on base flow experiments will progress in complexity as follows:

- Preliminary experiments;
- Power-on experiments with separation at the physical corner of the base;
- Power-on experiments with plume-induced afterbody separation upstream of the physical corner of the base; and
- Boattail experiments.

The experiments will be conducted utilizing the wind tunnel in the blowdown mode of operation with a sudden enlargement type diffuser. The data will be LDV measurements in the shear layers and recirculating region and will be reported in the form of velocity profiles, turbulence intensity levels, turbulent kinetic energy, and Reynolds shear stresses.

The preliminary experiments will be conducted in order to verify the two-dimensionality of the flowfield, determine approximate run times, and identify the boundary layer characteristics of the freestream flow just upstream of separation. The two-dimensional nature of the base region will be verified using an oil flow or kerosene-graphite surface visualization technique, and by making spanwise static pressure measurements. Mean velocity profiles will be measured and used to calculate displacement and momentum thicknesses and to ensure a turbulent approaching boundary layer.

The primary power-on experiments, shown in Figure 10(a), will utilize an inner jet with a Mach number of 2.5 in a freestream flow of M_∞ = 2.0, 2.5, and 3.0. The jet-to-base height ratio will cover the range $0.5 \leq h_j/h_B \leq 0.75$ through simple replacement of the splitter plate representing the two-dimensional base. Extensive LDV measurements will be made in the freestream/recirculating flow shear layer, recirculating flow/inner jet shear layer, and the recirculating region. Simultaneous u- and v-component velocity measurements will be made utilizing mono-disperse polystyrene latex particles and oil droplets as seed. Additional seeding in the recirculating region may be necessary in order to produce an adequate data rate. Frequency shifting will be necessary, especially for measurements in the recirculating region and the high turbulence regions, in order to eliminate the directional ambiguity of the velocity components measured by the LDV. The effects of plume-induced afterbody separation, shown in Figure 10(b), will be limited to investigation of the separation zone length, shear layer lengths before the start of recompression, and the correlation of pressure rise to separation with freestream Mach number.

The last series of experiments will incorporate the effects of boattail angle into the flowfield investigation. In this case the

splitter plate will be machined with a slope of 5-10 degrees for the last few base heights. One flow mechanism of particular interest is the modification of the turbulent boundary layer by the expansion at the afterbody/boattail junction as compared to that which occurs at the physical corner of the base. The pressure rise necessary for afterbody separation as the separation region grows will also be examined.

FUTURE PLANS

The complex nature of near-wake base flow experiments requires precision test facilities and state-of-the-art data measurement, acquisition, and analysis systems. The long range goals of this small-scale research effort include ongoing addition of needed experiments and constant upgrading of experimental facilities. The future plans for this base flow research effort thus include new instrumentation and equipment as well as new experiments.

Anticipated instrumentation focuses on the addition of a third velocity component measurement capability to our present two-component LDV system, a 5-W argon ion laser, a super mini-computer base laboratory data system for acquiring and processing LDV and hot-wire anemometer data, and a computer-controlled traverse system to be incorporated with our present manual LDV traverse system. The optical, electronic, and mechanical equipment necessary for three-component LDV capability are being procured and will provide significant new measurement capabilities vital to small-scale experimental research. Plans are also underway to purchase a VAX-11/750 super mini-computer system with a basic magnetic tape subsystem for large data storage. This equipment will greatly facilitate acquisition, processing, analysis, presentation, and storage of LDV data and results. The plans for a computer-controlled modular traverse mechanism system will give us efficient, accurate, and precise LDV measurement volume positioning.

The current extensive two-dimensional base flow experiments will be supplemented in the future with small-scale axisymmetric power-on and power-off experiments. A number of small-scale axisymmetric models already exist and these flowfield measurements would be the natural next step for detailed LDV investigation. Correlation of data for two-dimensional and axisymmetric near-wake flows would provide a useful measurement comparison and lend further insight into the component analysis of the base flowfield.

CONCLUSIONS

The small-scale research effort has produced an introductory level of expertise for making LDV measurements in high-speed flows. The present two component LDV system is operational and is being utilized for studies of particle lag problems and various insertion

techniques. The experience with LDV measurements in supersonic flows is being extended to small-scale two-dimensional near-wake base flowfields. The series of two-dimensional experiments on shear layer development and recompression, shock-induced separation, and plume-induced separation will provide new and more extensive flowfield data. Many of the models now exist and are being tested, while some are still under design. The results of the particle velocity relaxation experiments and the data of the ramp recompression study indicate that careful and accurate LDV measurements can be made in supersonic base flowfields. The new data accumulated from these experiments will contribute to the supersonic power-on base flowfield database.

ACKNOWLEDGMENT

The authors wish to acknowledge the generous support of the U.S. Army Research Office under contracts DAAG 29-79-C-0184 and DAAG 29-83-K-0043. Most of the completed and planned research in the area of base flow experiments described in this paper are being conducted with this funding.

REFERENCES

1. Korst, H. H., Page, R. H., and Childs, M. E., "A Theory for Base Pressures in Transonic and Supersonic Flows," University of Illinois, ME-TN-392-2, March 1955.

2. Korst, H. H., "A Theory for Base Pressures in Transonic and Supersonic Flow," Journal of Applied Mechanics, December 1956, pp. 593-600.

3. Page, R. H., "A Review of Component Analysis of Base Pressure for Supersonic Turbulent Flow," Proceedings of the Tenth International Symposium on Space Technology and Science, Tokyo, Japan, 1973, pp. 459-469.

4. Carpenter, P. W. and Tabakoff, W., "Survey and Evaluation of Supersonic Base Flow Theories," NASA CR-97129, August 1965.

5. Maxwell, B. R. and Seasholtz, R. G., "Velocity Lag of Solid Particles in Oscillating Gases and in Gases Passing Through Normal Shock Waves," NASA TN D-7490, March 1974.

6. Vom Stein, H. D. and Pfeifer, H. J., "Investigation of The Velocity Relaxation of Micron-Sized Particles in Shock Waves Using Laser Radiation," Applied Optics, Vol. 11, No. 2, February 1972, pp. 305-307.

7. Boutier, A., "Laser Anemometry in a Highly Turbulent Supersonic Flow," Proceedings of the Second International Workshop on Laser Velocimetry, Vol. 1, Purdue University, March 1974, pp. 105-112.

8. Mazumder, M. K., Hoyle, B. D., and Kirsch, K. J., "Generation and Fluid Dynamics of Scattering Aerosols in Laser Doppler Velocimetry," Proceedings of the Second International Workshop on Laser Velocimetry, Vol. 2, Purdue University, March 1974, pp. 234-268.

9. Melling, A. and Whitelaw, J. H., "Optical and Flow Aspects of Particles," Proceedings of the LDA-Symposium, Copenhagen, Denmark, 1975, pp. 382-402.

10. Agrell, J. and Danielson, L., "On the Application of Laser-Doppler-Velocimetry to the Measurement of Velocities in Large Separated Regions Bounded by Supersonic Flows," paper presented at the 53rd Meeting of the Supersonic Wind Tunnel Association, Moffett Field, California, March 1980.

11. McLaughlin, D. K. and Tiederman, W. G., "Biasing correction for individual realization of laser anemometer measurements in turbulent flows," The Physics of Fluids, Vol. 16, No. 12, December 1973, pp. 2082-2088.

12. Buchhave, P., "Biasing Errors in Individual Particle Measurements with the LDA-Counter Signal Processor," Proceedings of the LDA-Symposium, Copenhagen, Denmark, 1975, pp. 258-278.

13. Hoesel, W. and Rodi, W., "New biasing elimination method for laser-Doppler velocimeter counter processing," Review of Scientific Instruments, Vol. 48, No. 7, July 1977, pp. 910-919.

14. Dimotakis, P. E., "Single Scattering Particle Laser Doppler Measurements of Turbulence," AGARD-CP-193, Conference on Applications of Non-Intrusive Instrumentation in Fluid Flow Research, Saint-Louis, France, May 1976, pp. 10-1 through 10-14.

15. Kreid, D. K., "Error Estimates for Laser Doppler Velocimeter Measurements in Non-Uniform Flow," Proceedings of the Second International Workshop on Laser Velocimetry, Vol. 1, Purdue University, March 1974, pp. 398-425. (Also Applied Optics, Vol. 13, No. 8, August 1974, pp. 1872-1881.)

16. Karpuk, M. E. and Tiederman, W. G., "Effect of Finite-Size Probe Volume upon Laser Doppler Anemometer Measurements," AIAA Journal, Vol. 14, No. 8, August 1976, pp. 1099-1105.

17. Walsh, M. J., "Influence of Particle Drag Coefficient on Particle Motion in High-Speed Flow with Typical Laser Velocimeter Applications," NASA TN D-8120, February 1976.

18. Ikawa, H. and Kubota, T., "Investigation of Supersonic Turbulent Mixing Layer with Zero Pressure Gradient," AIAA Journal, Vol. 13, No. 5, May 1975, pp. 566-572.

19. Settles, G. S., Baca, B. K., Williams, D. R., and Bogdonoff, S. M., "A Study of Reattachment of a Free Shear Layer in Compressible Turbulent Flow," AIAA Paper No. 80-1408, presented at the AIAA 13th Fluid & Plasma Dynamics Conference, Snowmass, Colorado, July 1980. (Also AIAA Journal, Vol. 20, No. 1, January 1982, pp. 60-67.)

20. Roshko, A. and Thomke, G. J., "Observations of Turbulent Reattachment behind an Axisymmetric Downstream-Facing Step in Supersonic Flow," AIAA Journal, Vol. 4, No. 6, June 1966, pp. 975-980.

21. Bauer, R. C. and Fox, J. H., "An Application of the Chapman-Korst Theory to Supersonic Nozzle-Afterbody Flows," AEDC-TR-76-158, January 1977.

22. Addy, A. L., "Experimental-Theoretical Correlation of Supersonic Jet-on Base Pressure for Cylindrical Afterbodies," Journal of Aircraft, Vol. 7, No. 5, September-October 1970, pp. 474-477.

23. White, R. A., Addy, A. L., and Agrell, J., "An Improved Experimental-Theoretical Base Pressure Correlation for Conical and Cylindrical Afterbodies with Centered Propulsive Nozzle," Proceedings of the Tenth International Symposium on Space Technology and Science, Tokyo, Japan, 1973, pp. 481-488.

24. Page, R. H., Kessler, T. J., and Hill, W. G., Jr., "Reattachment of Two-Dimensional Supersonic Turbulent Flows," ASME Paper No. 67-FE-20, presented at the Fluids Engineering Conference, Chicago, Illinois, May 1967.

25. Carriere, P. and Sirieix, M., "Facteurs d'influence du Recollement d'un Ecoulement Supersonique," Proceedings of the Tenth International Conference of Applied Mechanics, Stresa, Italy, 1960.

26. Carriere, P. and Sirieix, M., "Resultats Recents Dans L'Etude Des Problemes De Melange Et De Recollement," ONERA T. P. 165, 1964.

27. Fox, J. H., "Simple Recompression Model for the Korst Base Pressure Theory," AIAA Journal, Vol. 16, No. 3, March 1979, pp. 311-313.

28. Carriere, P., Sirieix, M., and Delery, J., "Methodes de Calcul des Ecoulements Turbulents Decolles en Supersonique," Progress in Aerospace Sciences, Vol. 16, No. 4, 1975, pp. 385-429.

29. Sirieix, M., Delery, J., and Mirande, J., "Recherches experimentales fondamentales sur les ecoulements separes et applications," ONERA TP No. 520, 1967.

30. Zukoski, E. E., "Turbulent Boundary-Layer Separation in Front of a Forward-Facing Step," AIAA Journal, Vol. 5, No. 10, October 1967, pp. 1746-1753.

31. Adamson, T. C., Jr. and Messiter, A. F., "Analysis of Two-Dimensional Interactions Between Shock Waves and Boundary Layers," Annual Review of Fluid Mechanics, Vol. 12, 1980, pp. 103-138.

32. Settles, G. S., "An Experimental Study of Compressible Turbulent Boundary Layer Separation at High Reynolds Numbers," Ph.D. Thesis, Princeton University, Princeton, New Jersey, 1976.

33. Dolling, D. S. and Murphy, M., "Wall Pressure Fluctuations in a Supersonic Separated Compression Ramp Flowfield," AIAA Paper No. 82-0986, 1982.

34. Alpinieri, L. J. and Adams, R. H., "Flow Separation Due to Pluming," AIAA Journal, Vol. 4, No. 10, October 1966, pp. 1 1866.

35. Fong, M. C., "An Analysis of Plume-Induced Boundary-Layer Separation," Journal of Spacecraft, Vol. 8, No. 11, November 1971, pp. 1107-1113.

36. Addy, A. L., Korst, H. H., White, R. A., and Walker, B. J., "A Study of Flow Separation in the Base Region and Its Effects During Powered Flight," AGARD Conference on Aerodynamic Drag, AGARD-CPP-124, April 1973.

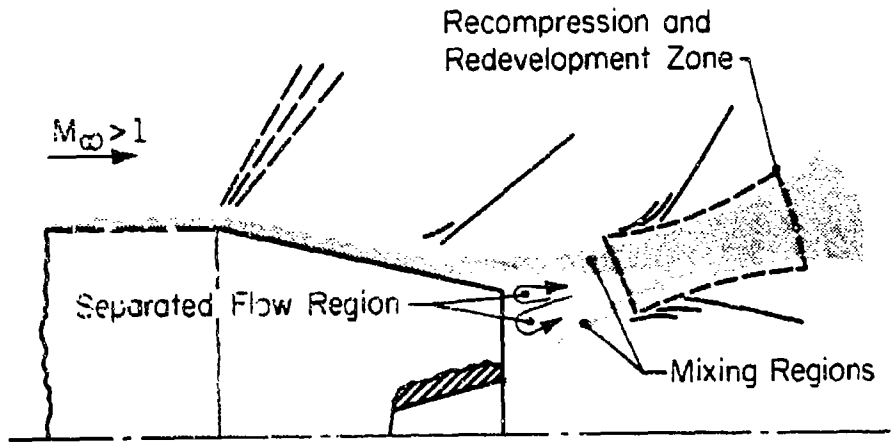

Figure 1(a) Power-on supersonic base flowfield.

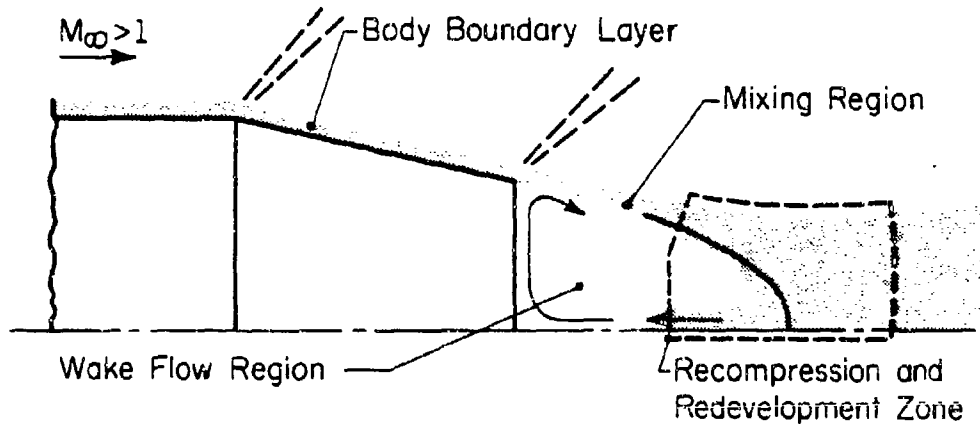

Figure 1(b) Power-off supersonic base flowfield.

Figure 1 Overall schematic indicating important base flow regions.

1. Dispersion prism
2. Polarization rotator
3. Beam splitter (green)
4. Beam splitter (blue)
5. Frequency shifter (blue)
6. Frequency shifter (green)
7. Beam spacer
8. Beam expander
9. Focusing lens
10. Collection lens
11. Dichroic mirror
12. Photodetector (green)
13. Photodetector (blue)

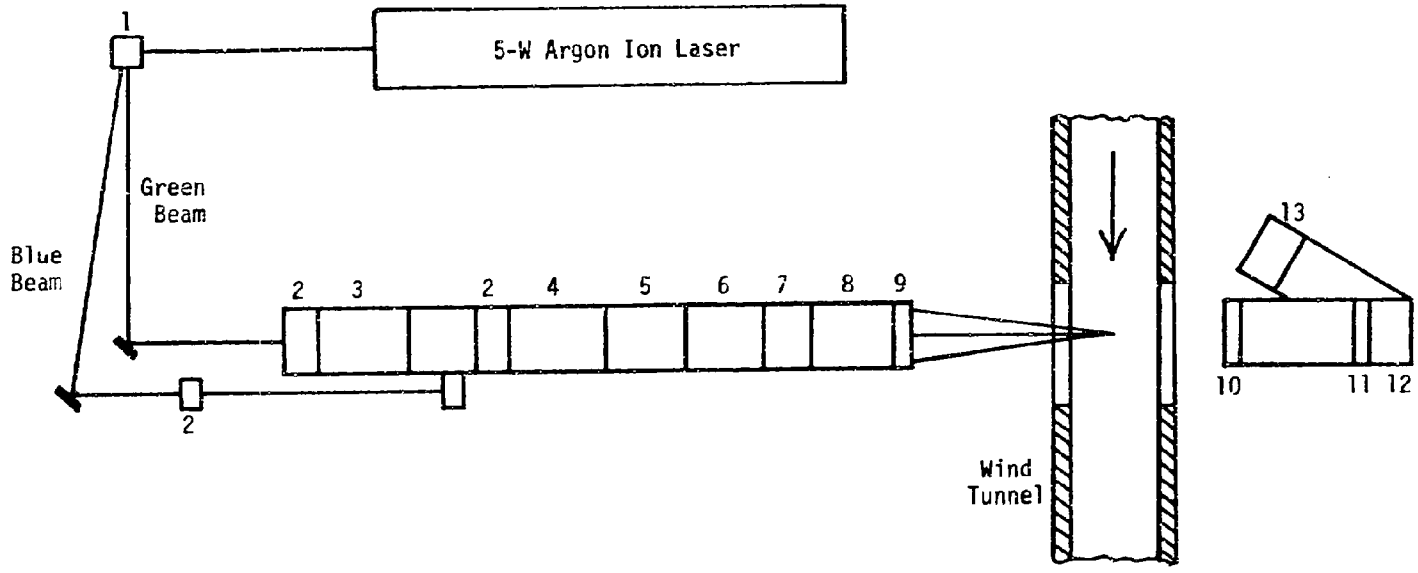

Figure 2 Schematic of the LDV system.

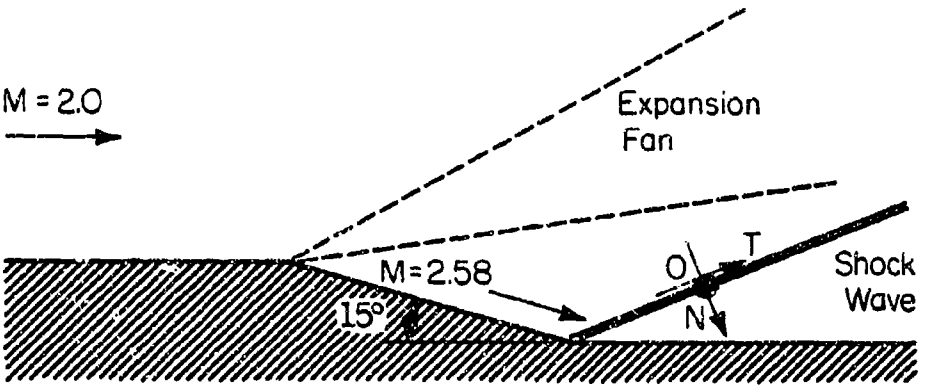

Figure 3 Model configuration for the particle velocity relaxation experiments.

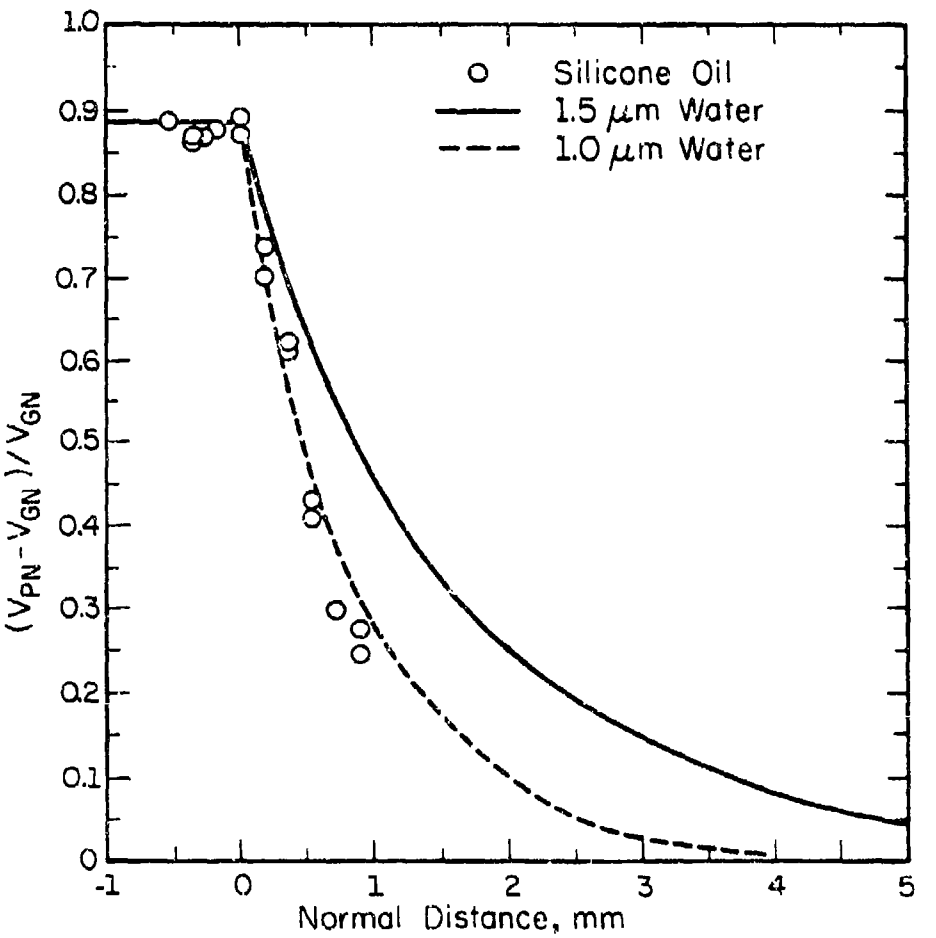

Figure 4 Particle velocity relaxation behind an oblique shock wave at a 15° change in flow direction.

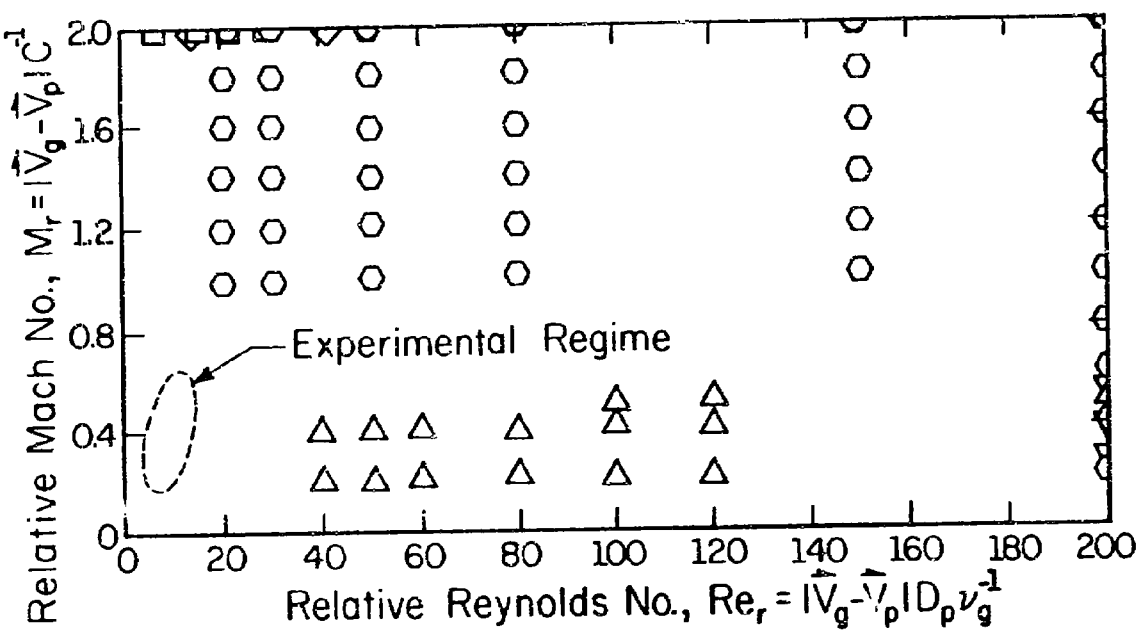

Figure 5 Drag coefficient data indicating current experimental regime.

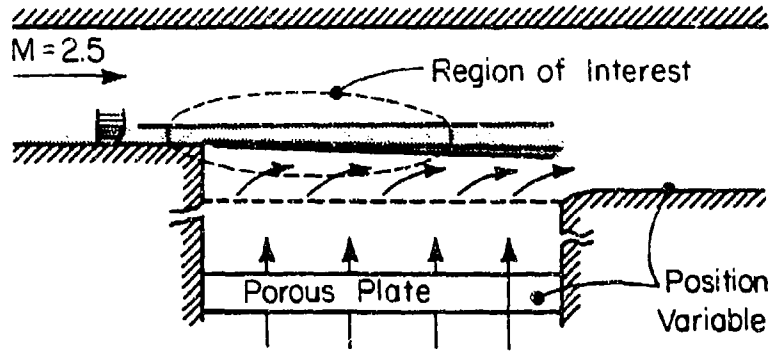

Figure 6(a) Constant pressure shear layer with mass injection.

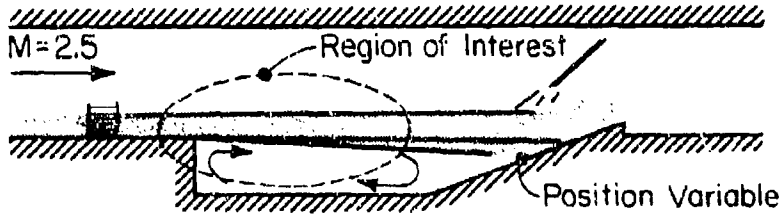

Figure 6(b) Constant pressure shear layer with recirculation.

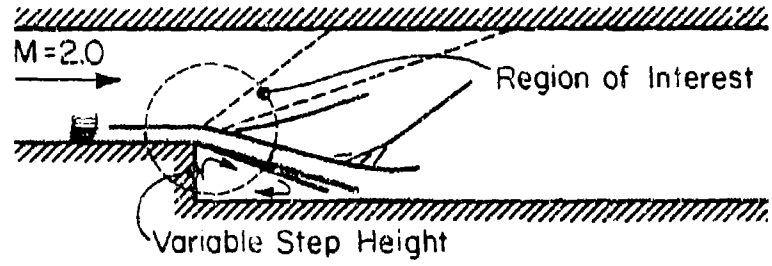

Figure 6(c) Backward-facing step flowfield.

Figure 6 Plane two-dimensional shear layer experiments.

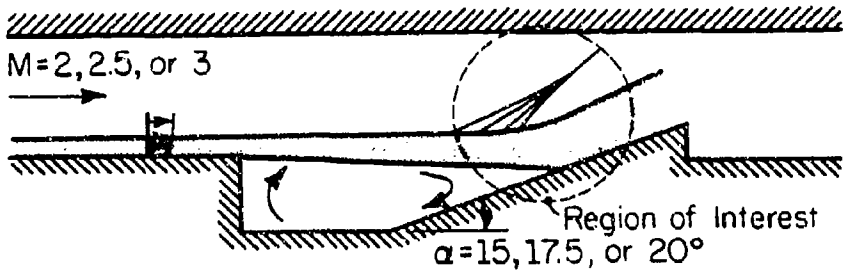

Figure 7(a) Reattachment of a self-similar free shear layer.

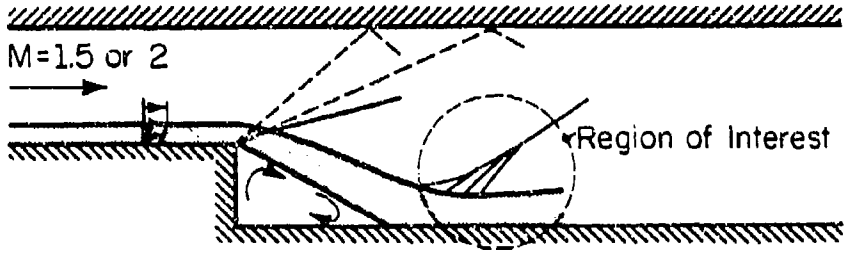

Figure 7(b) Reattachment of a developing free shear layer.

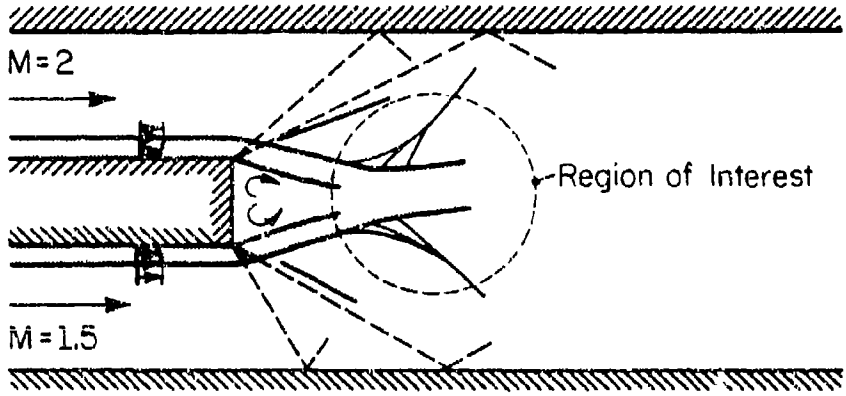

Figure 7(c) Interaction of two free shear layers.

Figure 7 Configurations for two-dimensional recompression, reattachment, and redevelopment experiments.

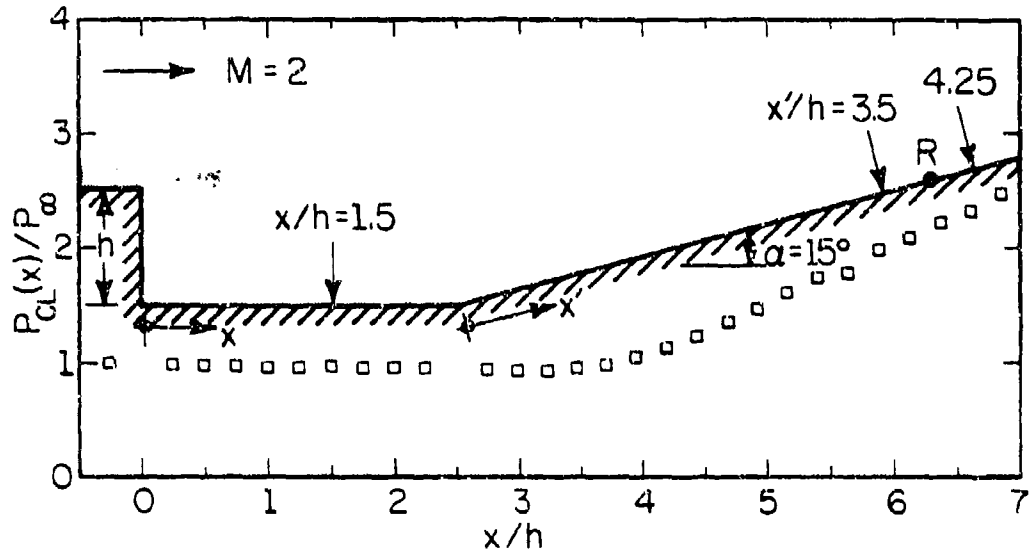

Figure 8(a) Longitudinal static pressure distribution.

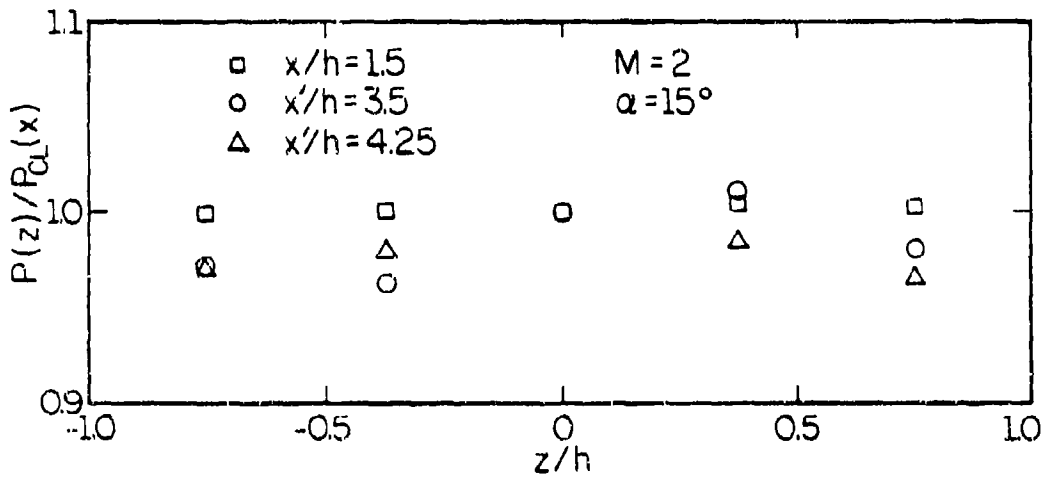

Figure 8(b) Transverse static pressure distribution at three longitudinal locations.

Figure 8 Preliminary results of the two-dimensional recompression experiments using a ramp.

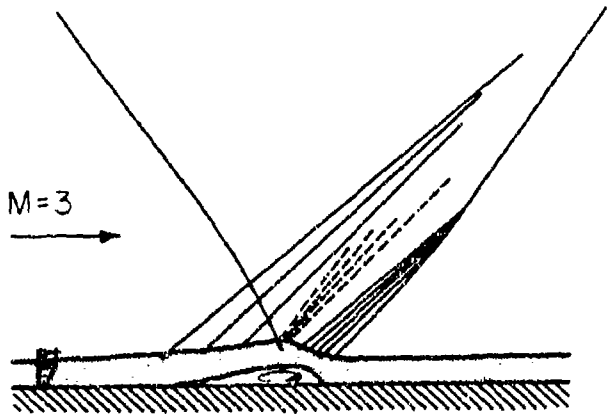

Figure 9(a) Impinging shock wave configuration.

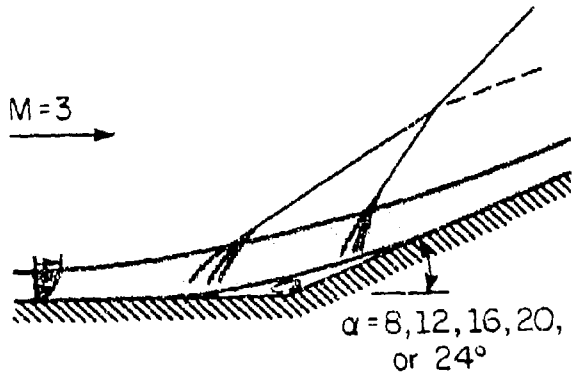

Figure 9(b) Compression corner configuration.

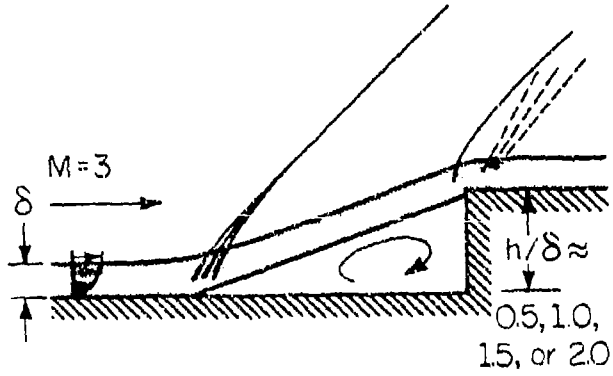

Figure 9(c) Forward-facing step configuration.

Figure 9 Shock wave-boundary layer interaction experiments.

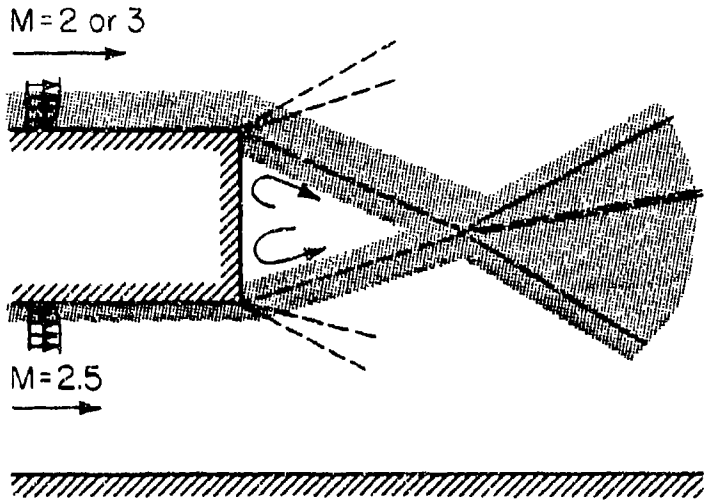

Figure 10(a) Geometric separation at corner of base.

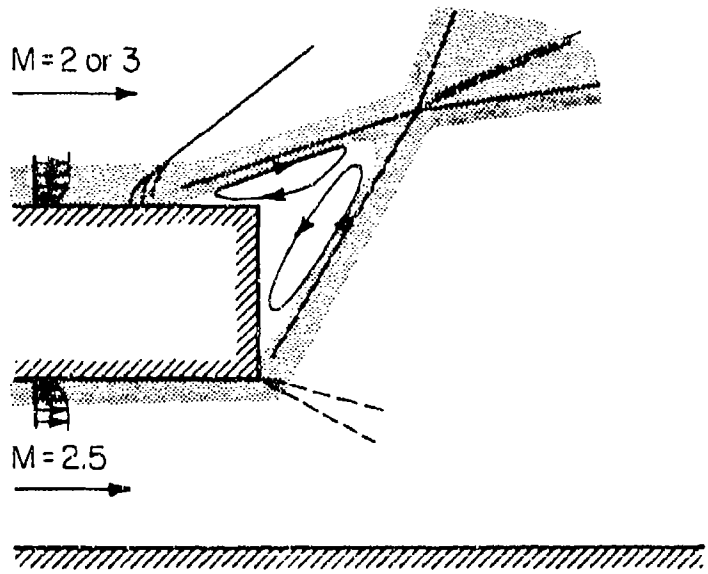

Figure 10(b) Plume-induced separation on afterbody.

Figure 10 Configurations for two-dimensional power-on supersonic base flow experiments.

APPENDIX G-2

SMALL-SCALE MODELS FOR TWO-DIMENSIONAL EXPERIMENTS UTILIZING A LASER DOPPLER VELOCIMETER

(Research effort under the direction of Professor A. L. Addy)

APPENDIX G-2

The photographs included in this appendix show many of the small-scale models of various base flowfield configurations being used for a laser Doppler velocimeter (LDV) study of near-wake phenomena. The experimental research effort is being conducted under the direction of Professor A. L. Addy and is aimed at developing the LDV as an instrument for making accurate velocity measurements in high-speed flows with imbedded separated flow regions. The wind tunnel models depicted herein have been designed and fabricated under ARO sponsorship and are currently being used for near-wake measurements. The details of the planned two-dimensional experiments are described in more detail in Section 4 of this final technical report, under the heading of SMALL-SCALE BASE FLOW EXPERIMENTS UTILIZING A LASER DOPPLER VELOCIMETER. The paper associated with the research effort which utilizes these models was presented by Professor Addy at Huntsville and is included here as Appendix G-1.

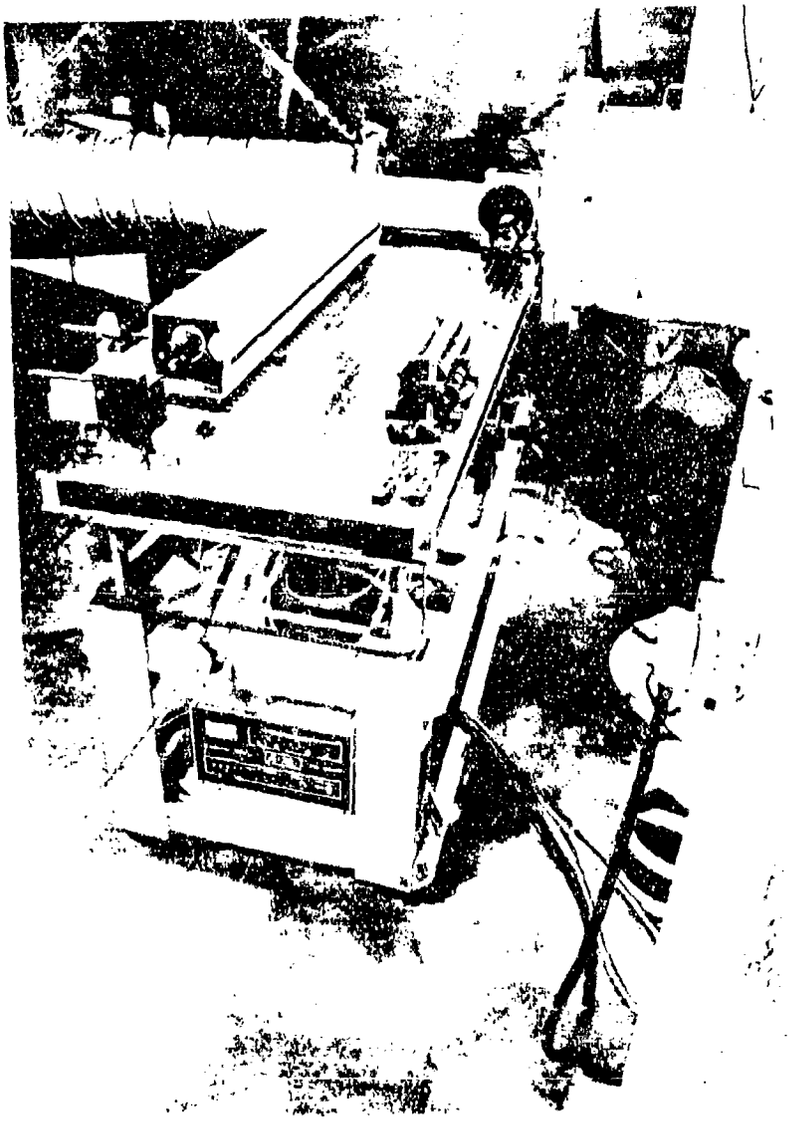

Figure 1 Photograph showing the laser Doppler velocimeter components mounted on the traversing table.

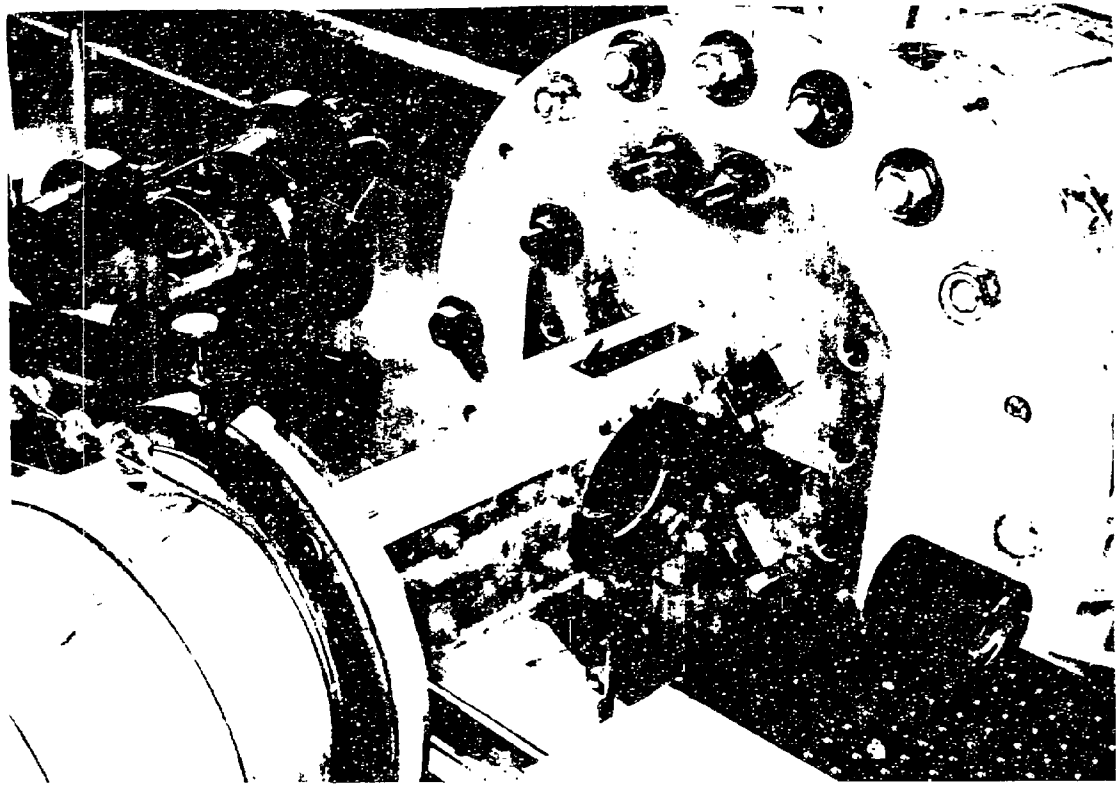

Figure 2 A close view of the LDV collecting optics (photomultipliers) and the particle dynamics experiments test section.

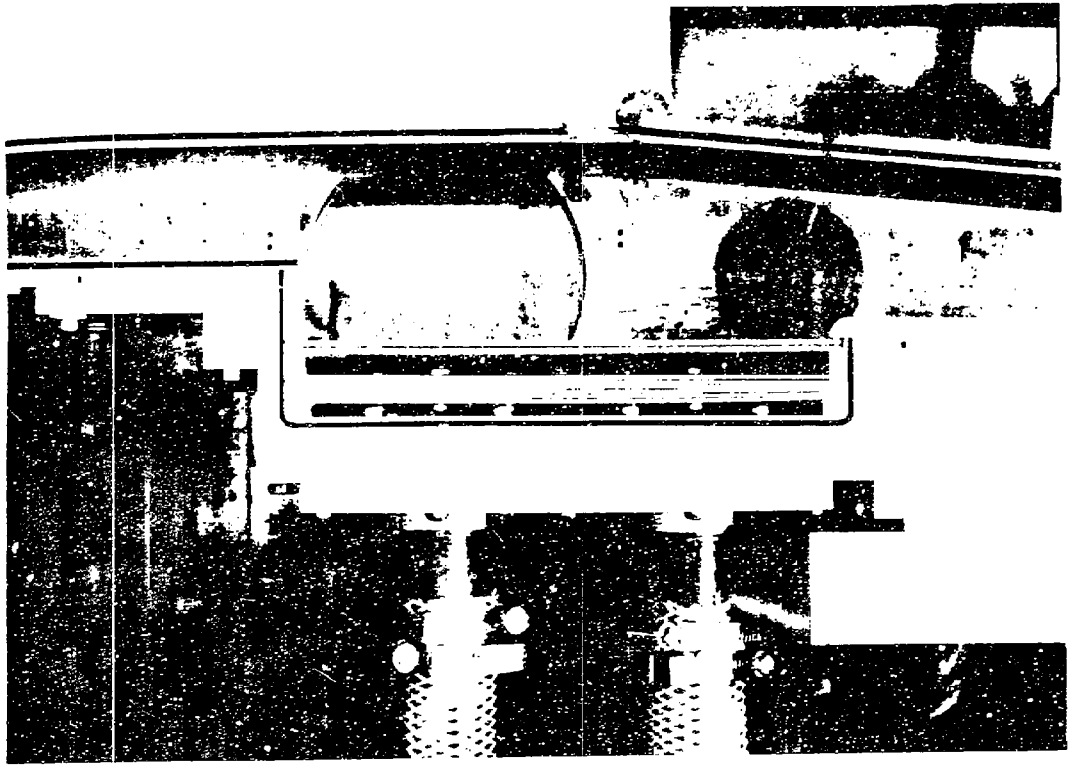

Figure 3 Photograph of the wind tunnel test section for supersonic flow past a backstep with porous plate mass injection in the base region (side wall removed).

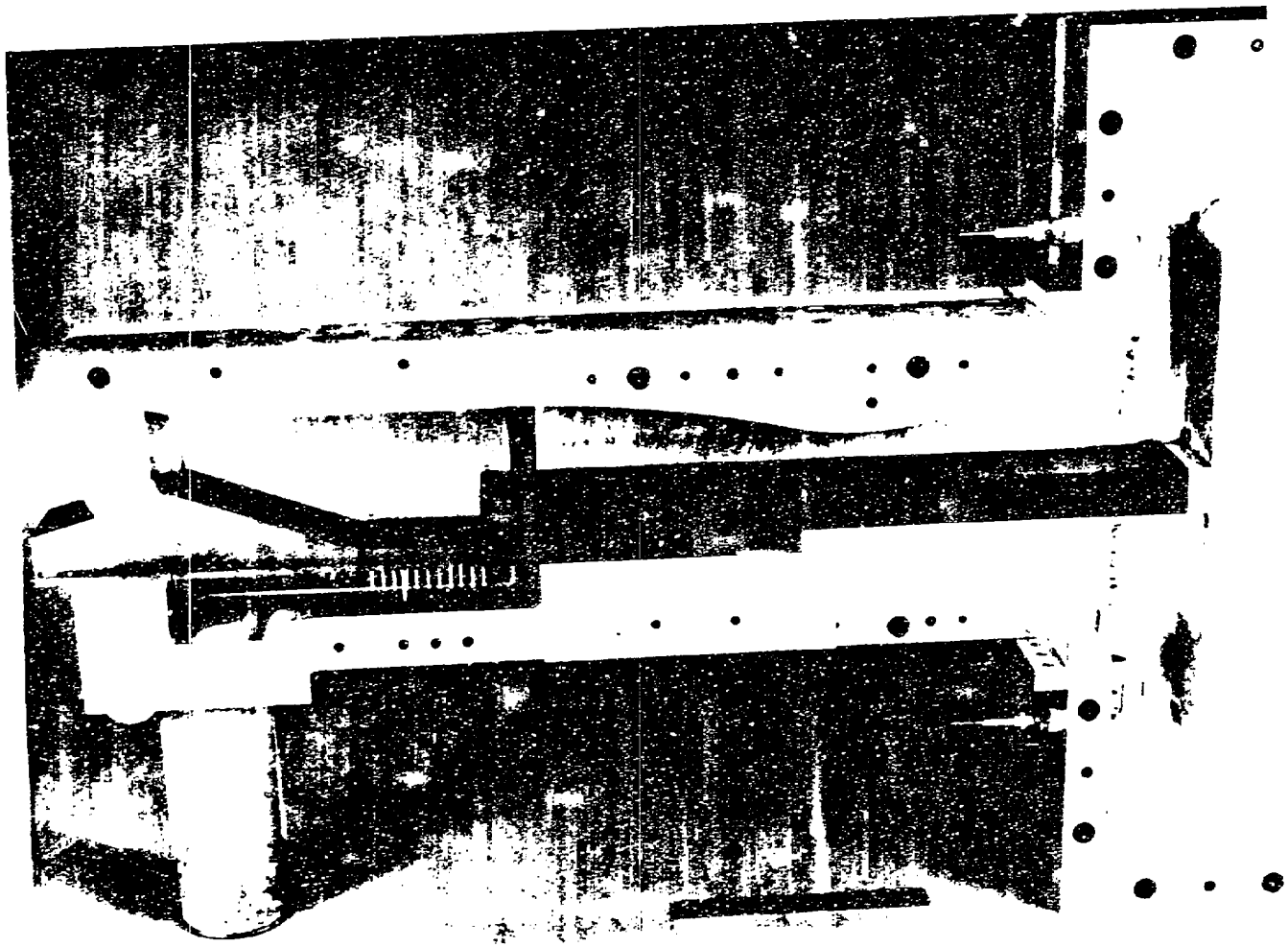

Figure 4 Photograph showing the wind tunnel test section for the ramp recorpression experiments (side wall removed).

Figure 5 Photograph of the supersonic wind tunnel for the investigation of flow over a backstep with recompression on a plane wall (side wall removed).

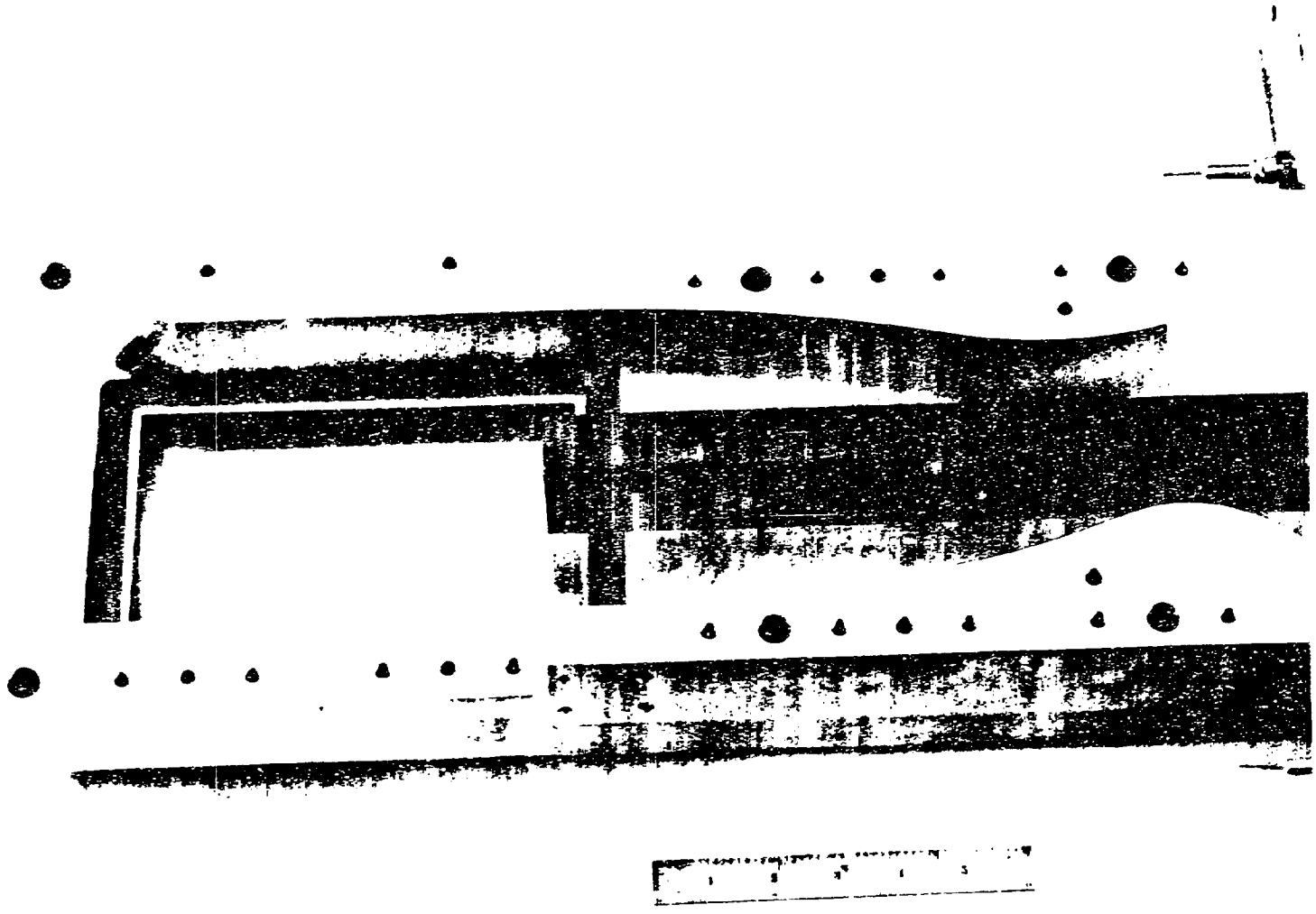

Figure 6 Photograph of the wind tunnel configuration for the investigation of two-stream reattachment recompression (side wall removed).

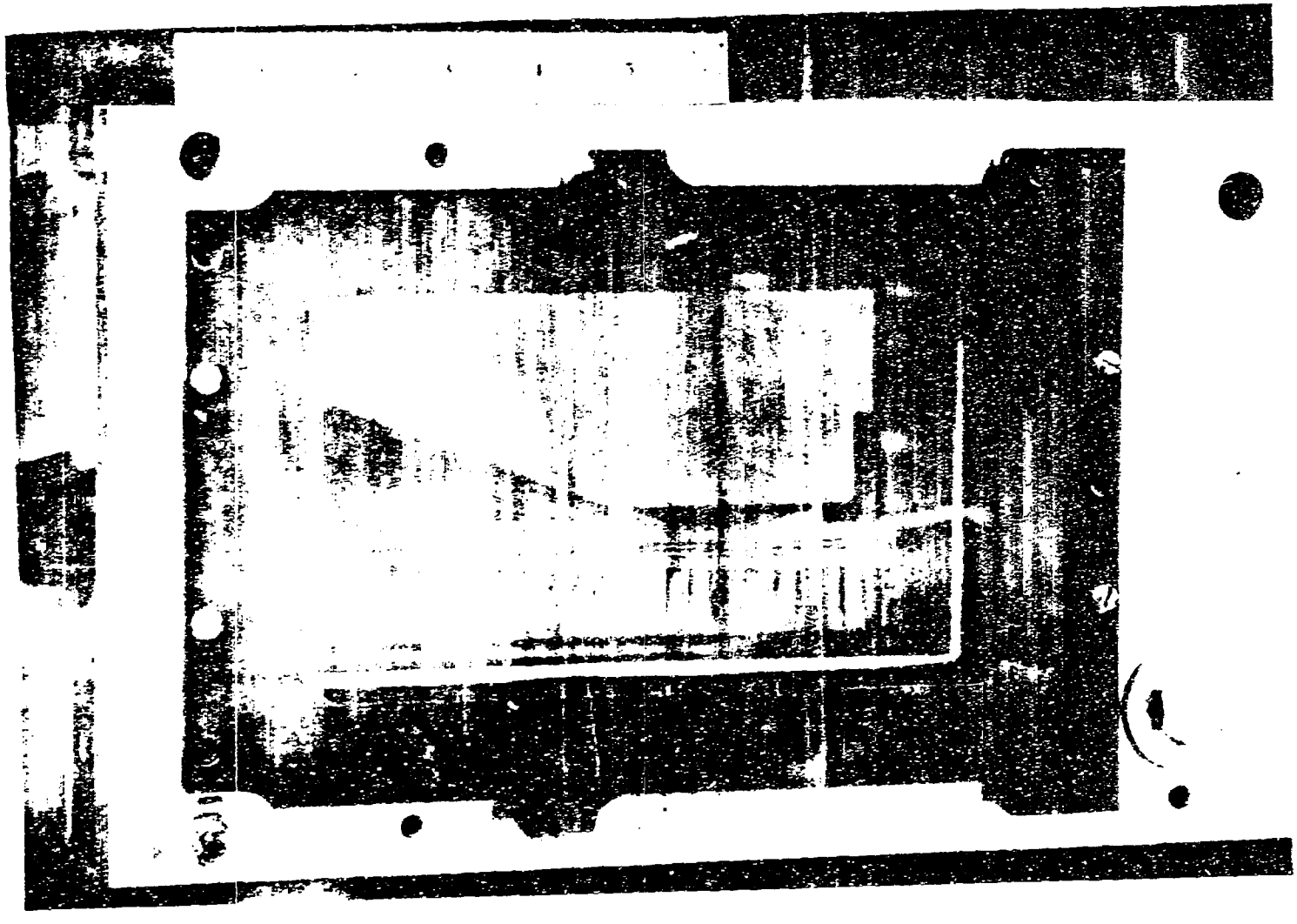

Figure 1. Close-up photograph of the wind tunnel window for supersonic flow past a backstep with reattachment on an inclined ramp. Note the anodized models and extensive static pressure taps.

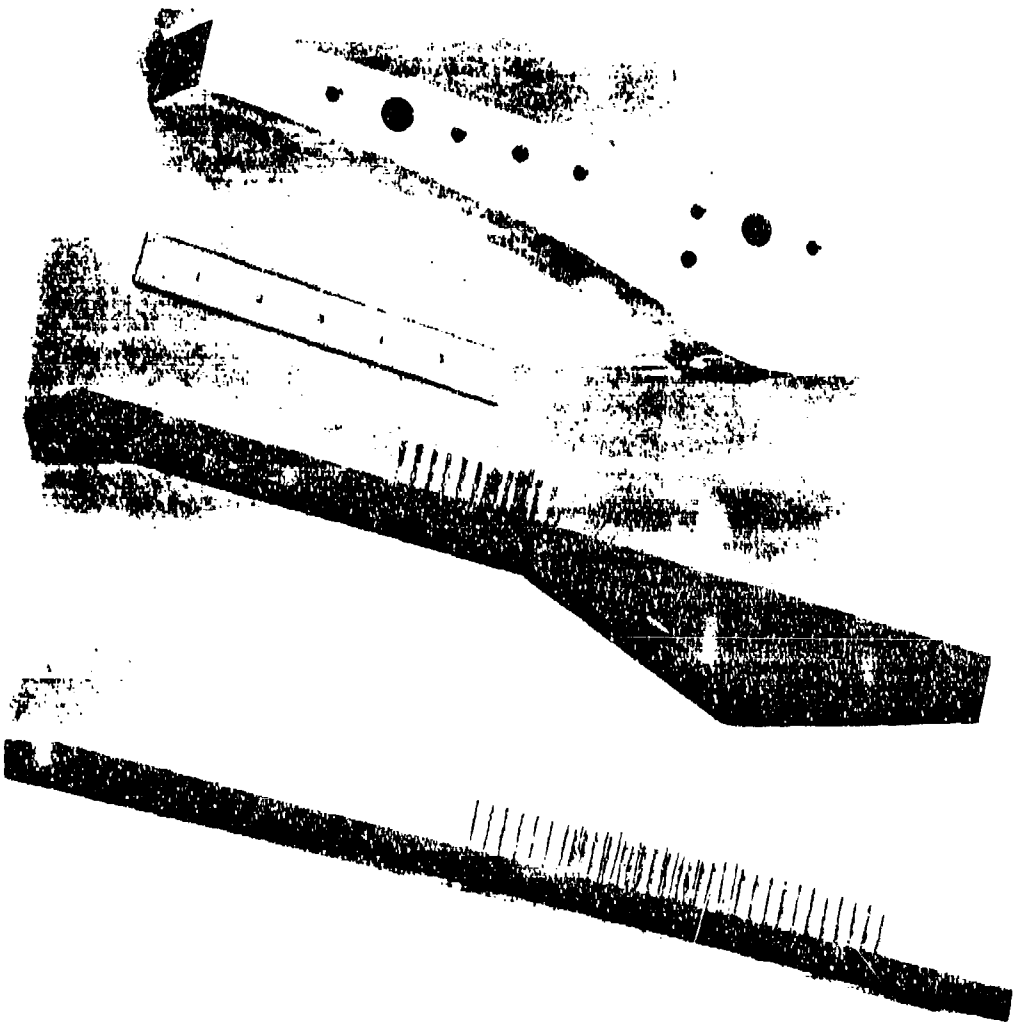

Figure 8 Close-up photograph of the supersonic nozzle block, inclined ramp, and flat surface used for the recompression/reattachment experiments.

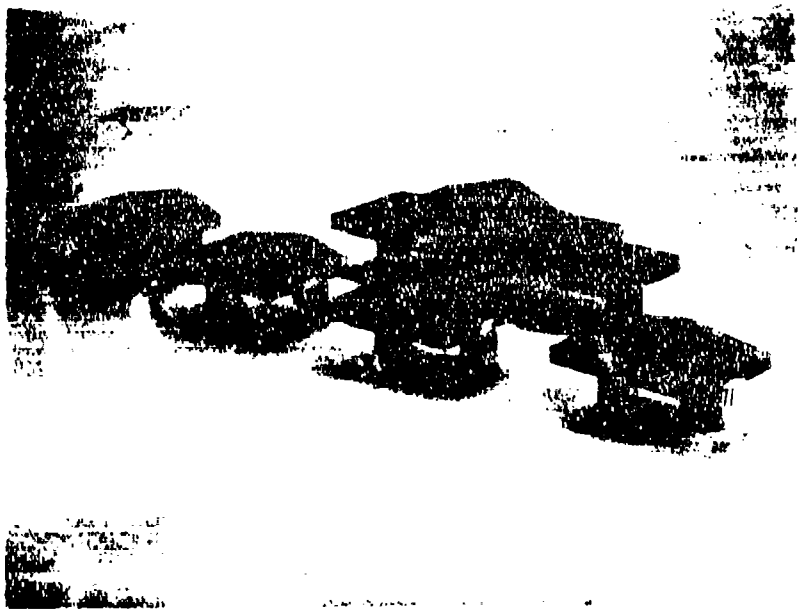

Figure 9 Photograph of the anodized ramp models for the shock-induced separation experiments.

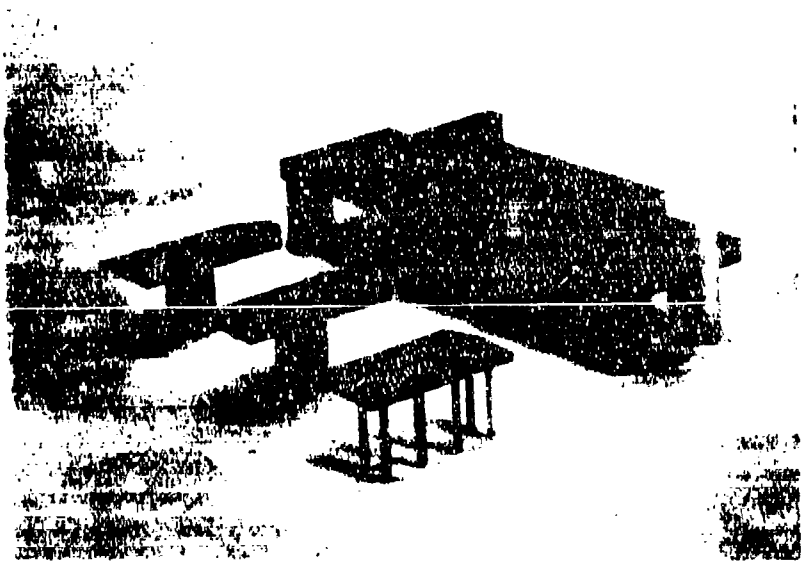

Figure 10 Photograph of the anodized forward-facing step models for the shock-induced separation experiments.

APPENDIX H

THE EFFECT OF EXPANSIONS AND COMPRESSIONS IN A SUPERSONIC FLOWFIELD ON BOUNDARY LAYER MOMENTUM THICKNESS

by

R. A. White and L. P. Hampton

APPENDIX H

THE EFFECT OF EXPANSIONS AND COMPRESSIONS IN A SUPERSONIC FLOWFIELD ON BOUNDARY LAYER MOMENTUM THICKNESS

R. A. White and P. Hampton

Department of Mechanical and Industrial Engineering
University of Illinois at Urbana-Champaign
Urbana, IL 61801

INTRODUCTION

The importance of afterbody boundary layer and wake shear layer development on slipstream separation and base region pressures and temperatures is well established. For plume-induced separation typical of highly accelerating vehicles, the upstream movement of the separation shock and separation pressure rise are known to be effected by both the body geometry and distance from the vehicle base plane [1][†]. Thus, the interaction of the separation shock with afterbody expansion fields such as occur at boattail body junctions also modifies the separation process. Consequently, an investigation of the effects of rapid pressure changes on shear layer characteristics was initiated with the objective of establishing an understanding of their relation to the plume-induced separation problem.

Figure 1 schematically shows the flowfield components for the plume-induced separation process and demonstrates the importance of the shear layer for all portions of the interaction. For more complex interference fields such as occur for vehicles with control surfaces and operating at angle-of-attack, see Figure 2, it will be necessary to rely on wind tunnel testing and modeling techniques for the foreseeable future although detailed information on subcomponents must be sought to provide guidance and understanding in the analysis of this type of problem.

INITIAL CONFIRMATORY STUDIES

A series of initial experiments was undertaken to examine whether published results [2] on the reduction of the separation pressure rise were

---

[†]Numbers in brackets refer to entries in REFERENCES.

related to axisymmetric configurations, in contrast to two-dimensional flows, and on the iteration of separation shocks and afterbody expansions. The results of the experiments on plume-induced separations and resultant separation pressure rise for two-dimensional configurations are shown in Figure 3 along with the axisymmetric results of Reference 2. The agreement is seen to be excellent within the first two boundary layer thicknesses of the base plane. For distances greater than 2δ, the two-dimensional values are slightly less than for the axisymmetric case. The latter may be due to the adverse pressure gradient on axisymmetric afterbodies in contrast to the constant pressure of two-dimensional flows. Favorable pressure gradients further decrease the plateau pressure after separation.

The upstream movement of plume-induced separations is also affected by body generated pressure changes such as occur at body junctions. Thus, the expansion fan at the start of a boattail can be expected to modify the extent of plume-induced separation in conjunction with the engine-to-freestream pressure ratio. The interaction of the separation shock and fan can be expected to delay further upstream migration of the induced separation with increasing engine-to-freestream ratios until the base pressure is sufficiently high to cancel the expansion fan pressure drop. This process is shown in Figure 4 for separations induced by a simulated jet recompression surface. The delay in upstream movement at the expansion corner spans an approximate range of 4 degrees of the reattachment surface corresponding to a change of base pressure of approximately $0.135 < P_B/P_0 < 0.165$.

DETAILED STUDIES OF THE EFFECTS OF SUDDEN COMPRESSIONS AND EXPANSIONS ON SHEAR LAYER MOMENTUM THICKNESS

Since the supersonic external flowfield over typical rocket propelled vehicles contains both expansions (Prandtl Meyer) and compressions (shocks),

particularly in the vicinity of the afterbody and base plane, it is important to be able to determine the effects of these sudden pressure gradients on the boundary layer developing along the missile surface. In particular, for wake solution techniques such as the widely used component approach [1], it can be shown that the approaching boundary layer can be treated as an equivalent mass bleed into the wake. This effective mass bleed is a function of the boundary layer momentum thickness. Consequently, an investigation has been made [3] of the effects of both Prandtl Meyer expansions and separation shocks (not reflected shocks) on the change in a turbulent boundary layer with adjacent supersonic stream.

Analysis

The effects of sudden or rapid pressure gradients on boundary layer parameters have been the subject of a number of studies [4,5]. The primary emphasis has been on reflected shocks in supersonic flow and imbedded shocks in the transonic case. For supersonic flow over missiles, however, the flowfield at separation will have either an expansion or compression (see Figure 1) depending on the engine-to-freestream pressure ratio (here neglecting the apparently trivial case of no pressure change at the separation point).[††] While the stream tube expansion method has been widely used to describe changes due to expansions, it is not applicable to the compression case. Some

[††]It should be noted that while the no pressure change case is apparently an unimportant case in the sense of this study, i.e., $\theta_I = \theta_F$, recent studies [3,6,7] suggest that significant effects can occur due to the laminar sublayer no longer having the turbulence quenching adjacent wall as a boundary condition. Consequently, a new subshear layer appears to form due to transition of the laminar sublayer downstream of separation.

studies have also suggested that in rapid expansions, the layer near the wall may overexpand [6].

In 1965, White [8] suggested that gross features such as momentum thickness of boundary layers subjected to Prandtl-Meyer expansions or separation shocks could be found by integrating the integral momentum equation subject to appropriate assumptions. Such a unified approach is attractive and its confirmation or possible modification was one of the goals of the current study.

The solution given by White is

$$\theta_F/\theta_I = (C_I/C_F)^{2+a}[(C_F^2 - 1)/(C_I^2 - 1)]^{(1/2)[b - (2/(\gamma - 1))]} , \quad (1)$$

where $a = H_i$ and $b = H_i + 1$, H_i being the incompressible form factor for the disturbed flow.

Figure 5 shows a comparison of Eq. (1), using $H_i = 1.20$, to the stream tube expansion method for the effect of a sudden expansion on the momentum thickness. The agreement is seen to be excellent. For compressions, the selection of the approximate H_i value is open to interpretation and Figure 6 shows predicted changes in momentum thickness for two H_i values, one representative of fully developed flows, $H_i = 1.2$, and one representative of separating developed flows, $H_i = 1.8$. The differences are seen to be significant.

Thus an experimental investigation was undertaken to determine the change in boundary layer momentum thickness across sudden compressions and expansions in the Mach number range of 1.5 to 3.0.

Figure 7 is a photograph showing the basic wind tunnel and model configuration. Fixed interchangeable nozzles provided nominal freestream Mach number conditions of 1.5, 2.0, 2.5, and 3.0. Extensive static pressure tap distributions over the model surfaces were used to obtain a clear

determination of the pressure field. The shear layer was probed using a 0.018 in. (height) diameter flattened probe. The probe was manually adjusted in increments of 0.005 inch. Consequently, 40 to 50 points were obtained in each profile. The flow Reynolds numbers were 18×10^6, 25.4×10^6, 30×10^6, and 43.4×10^6 per foot, respectively, for the nominal freestream Mach numbers of 1.5, 2.0, 2.5, and 3.0.

Typical expansion and compression disturbed downstream profiles are shown in Figure 8. The unusual shape of the expansion profile was found to be typical and to have an increasingly distinct knee near the sublayer portion for increasing expansion ratios. A close check of Schlieren photographs, oil flow patterns, and probing nearer the corner showed no indication of a separation bubble. The inner and outer profile nature of the expanded profiles suggests that overexpansion of the laminar sublayer is occurring, followed by redevelopment of this new near wall layer into a quenched lower turbulence outer rotational flow. Such overexpansion has been suggested by previous investigators for separating flows [6] and in association with the lip shock problem. Thus, the boundary layer on afterbodies and its separation characteristics may require a new approach based on the actual boundary layer profile and its description when the flow has experienced a strong and rapid expansion such as occurs at boattail body junctions or for the base pressure problem.

Results and Analysis

The values of the ratio of momentum thickness for both the expansion and compression tests are shown in Figures 9(a) and 9(b) as a function of the pressure ratio across the process. An inversion can be seen to occur between the effects of expansions and compressions depending on the Mach number of the approach flow.

The form of the results suggested that the analysis given by Eq. (1) is correct although the appropriate choice of H_i remains to be determined. A best fit analysis of the data to Eq. (1) using parameter identification by optimization, i.e.,

$$\frac{\partial}{\partial H_i} \sum_j \left[\left(\frac{\theta_F}{\theta_I}\right)_{\text{experimental}_j} - \left(\frac{\theta_F}{\theta_I}\right)_{\text{theoretical}_j}\right]^2 = 0 \qquad (2)$$

was carried out. The values of H_i for the expansion and compression processes as a function of approach Mach number are shown in Figure 10. It is apparent that the H_i values for expansions is approximately 1.0 and for compressions 1.95 and independent of the freestream Mach number over the range of these tests. These H_i values are in the range anticipated in that they are representative of fully developed and separated profiles, respectively. They also point out that the expansion process and compression process lie along different legs of Eq. (1). The latter explains the spreading of the inversion region compared to that of Reference 8 in which a single H_i value was utilized. Figure 11 shows the magnitude of the inversion regions based on Eq. (1) and the experimentally determined H_i values. In Figures 9(a) and 9(b), the test data are also shown along with the fit to Eq. (1). The agreement is seen to be excellent both qualitatively and quantitatively. Thus, the integration of the momentum equation represented by Eq. (1) appears to adequately describe the effects of sudden pressure gradients on attached turbulent boundary layers.

CONCLUSIONS

A detailed experimental study of the effect of rapid expansions and compressions on momentum thickness of the turbulent attached boundary layers has

been carried out. The results of the measurements point to a number of important factors related to boundary layer modifications and development in the presence of rapid pressure gradients. In particular, the following points are of consequence:

(1) Changes in momentum thickness of turbulent boundary layers subjected to sudden expansions and compressions can be correlated and explained by available integral analysis.

(2) The best fit correlation to the formulation of Reference 8 is essentially independent of Mach number over the range tested and are in agreement with fully developed and separated boundary layers.

(3) Excellent qualitative and quantitative agreement exists between the test results and theory.

(4) Apparent sublayer overexpansion occurs for rapid expansions imposed from the outer flow leading to a need for a two profile velocity description downstream of the disturbance.

(5) The effects of rapid expansions on the boundary layer may lead to changes in boundary layer development and separation characterization on boattails.

(6) A detailed laser Doppler velocimeter study of rapidly expanding shear layers is necessary to confirm the effects of sublayer expansion at the corner and in the redevelopment process.

REFERENCES

1. Addy, A. L., Korst, H. H., Walker, B. J., and White, R. A., "A Study of Flow Separation in the Base Region and Its Effects During Powered Flight," AGARD Conference on Aerodynamic Drag, AGARD-CCP-124, April 1973.

2. White, R. A. and Agrell, J., "Boattail and Base Pressure Prediction Including Flow Separation for Afterbodies with a Centered Propulsive Jet and Supersonic External Flow at Small Angles of Attack," AIAA Paper No. 77-958, presented at the AIAA/SAE 13th Propulsion Conference, Orlando, Florida, July 1977.

3. Hampton, L. P., "The Effect of Sudden Expansions and Compressions on Turbulent Boundary Layer Momentum Thickness in Supersonic Flow," M.S. Thesis, Department of Mechanical and Industrial Engineering, University of Illinois at Urbana-Champaign, May 1983.

4. Holden, M. S., "Theoretical and Experimental Studies of Separated Flows Induced by Shock Wave Boundary Layer Interaction," Proc., AGARD Meeting on Separated Flows, AGARD Fluid Dynamics Panel, AGARD CP4(1966) (May 1966); also available as Cornell Aeronautical Laboratory Report AL-1972-A-3, December 1965.

5. Reshotko, E. and Tucker, M., "Effect of a Discontinuity on Turbulent Boundary Layer Thickness Parameters with Application to Shock Induced Separation," NACA TN 3454, May 1955.

6. Gavigilo, J., Dussauge, J.-P., Debieve, J.-F., and Favre, A., "Behavior of a Turbulent Flow, Strongly Out of Equilibrium at Supersonic Speeds," Physics of Fluids, Vol. 20, No. 10, October 1977.

7. Settles, G. S., Williams, D. R., Baca, B. K., and Bogdonoff, S. M., "Reattachment of a Compressible Free Shear Layer," AIAA Paper No. 80-1048, presented at the 13th Fluid and Plasma Dynamics Conference, Snowmass, Colorado, 1980.

8. White, R. A., "Effect of Sudden Expansions or Compressions on the Boundary Layer," AIAA Journal, Vol. 4, No. 12, December 1966, pp. 2232-2234.

FIGURES

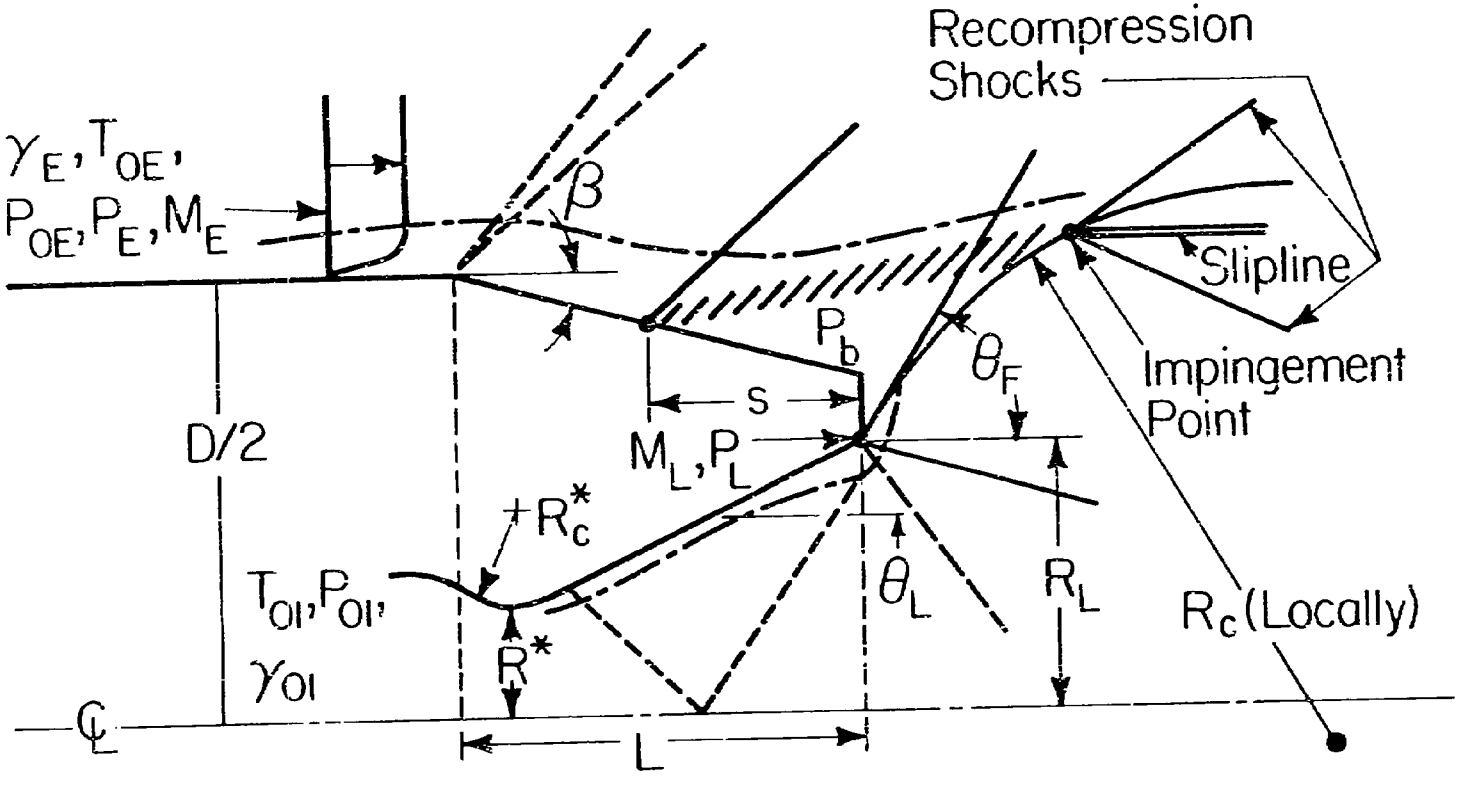

Figure 1 Flow configuration for plume-induced separation from a conical afterbody and identification of geometric and operational parameters.

Figure [illegible] [illegible] photograph of the complex flowfield on the afterbody and in the base region for a typical vehicle with control surfaces at [illegible] and operating at angle-of-attack [illegible]

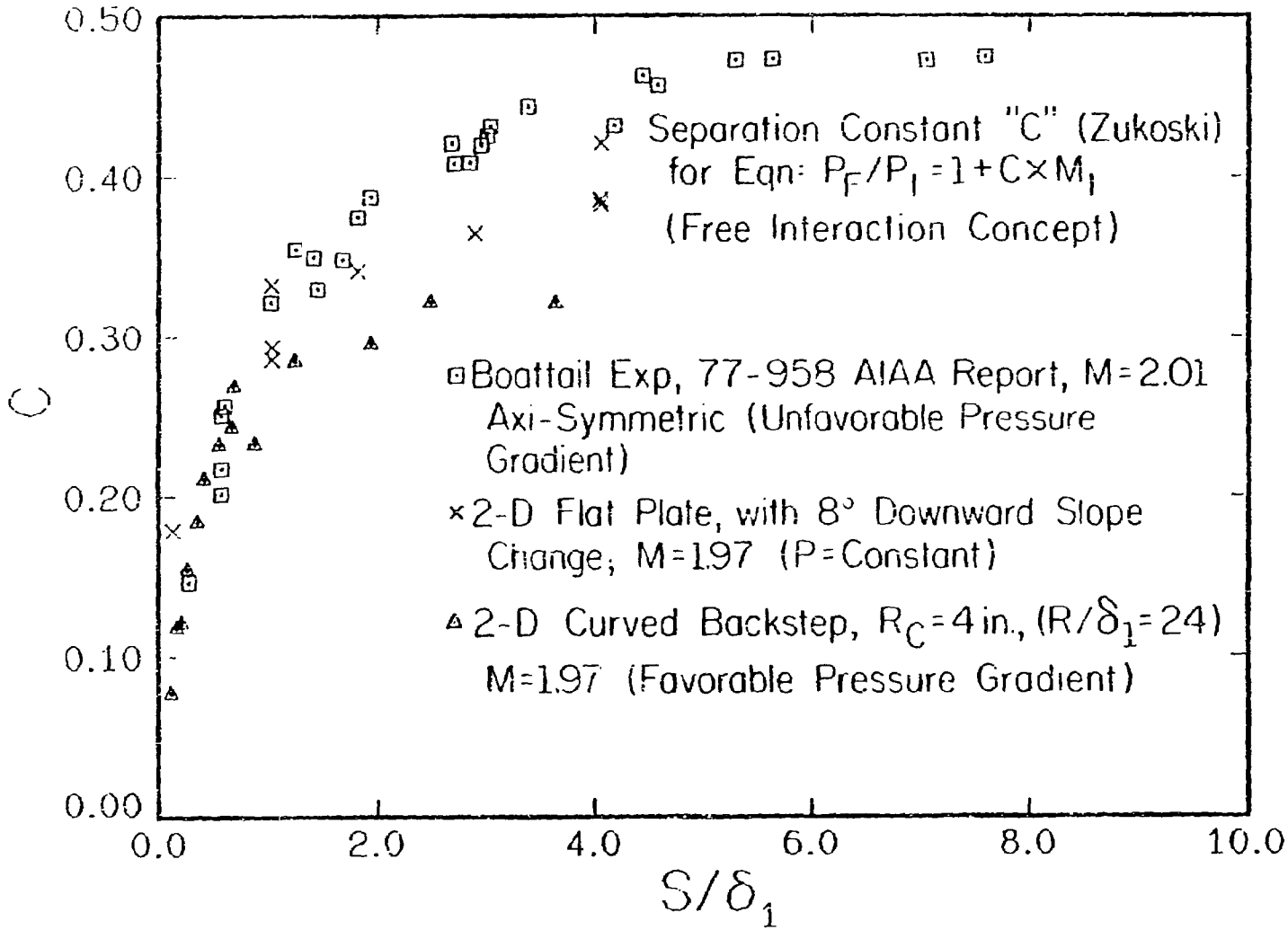

Figure 3 Comparison of the separation pressure rise coefficient (free interaction concept) for different geometries and pressure gradients.

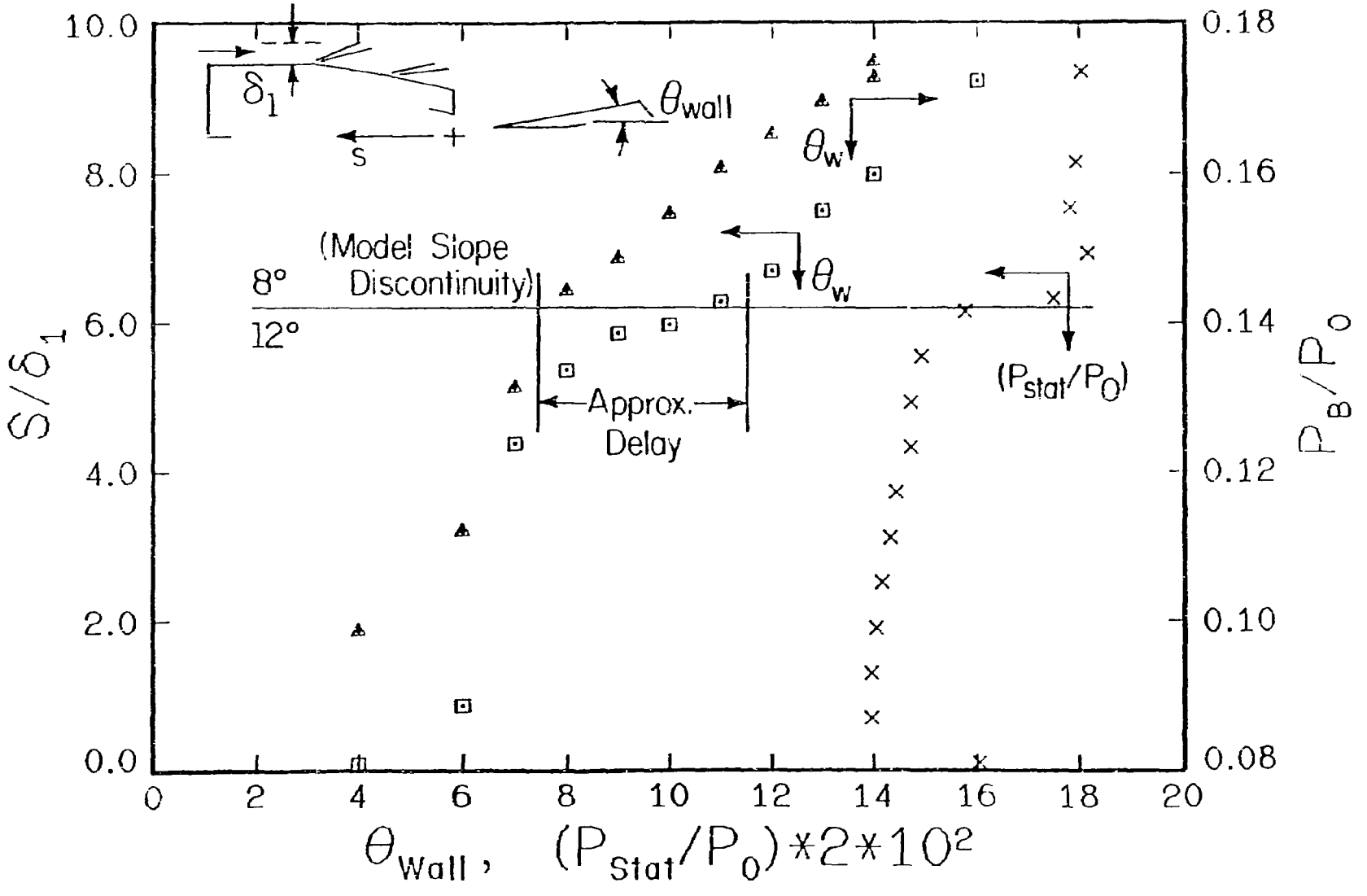

Figure 4 Effect of wall discontinuities (expansion fan) on upstream migration of the induced separation location.

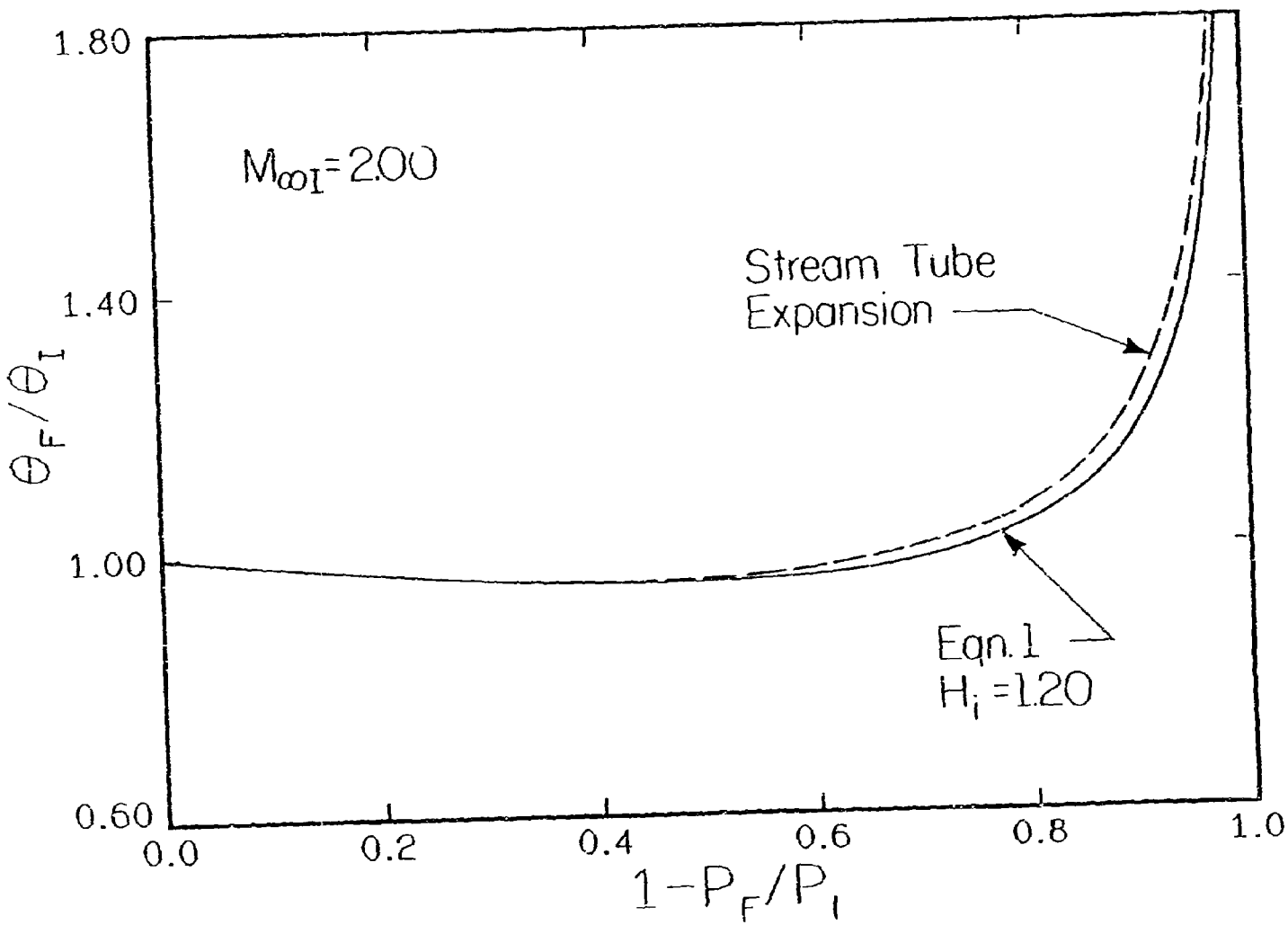

Figure 5 Comparison of the results of Equation (1) with H_i = 1.20 and streamtube expansion method.

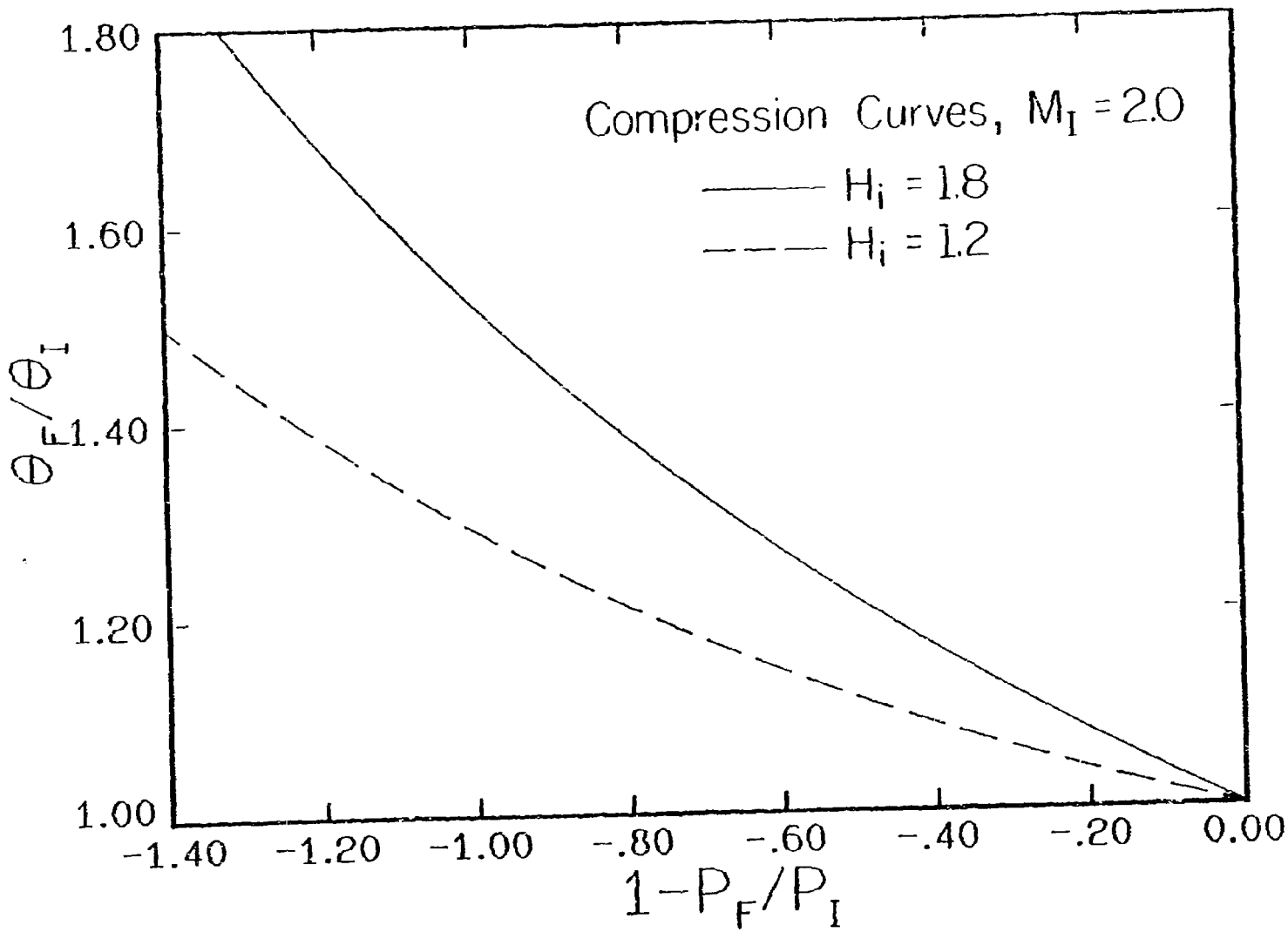

Figure 6 Effect of choice of profile shape parameter on momentum thickness change for sudden compressions.

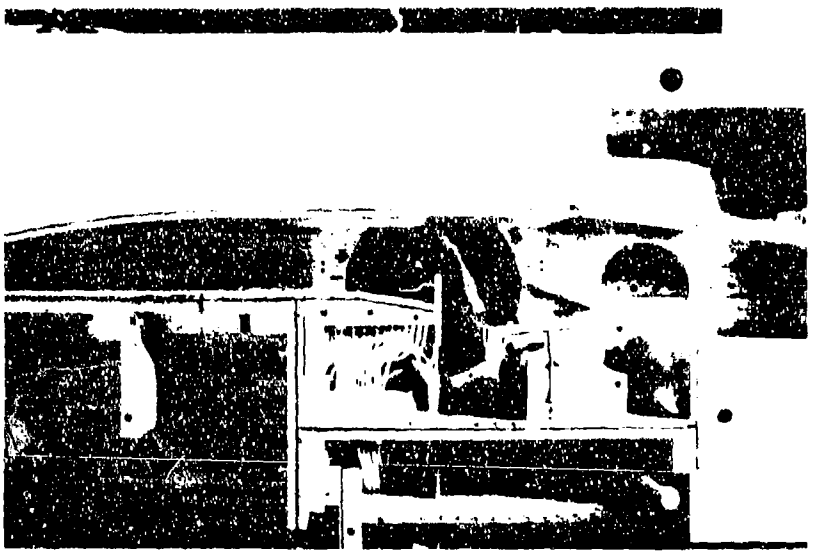

Figure 7 Photograph showing details of the wind tunnel model installation and probe.

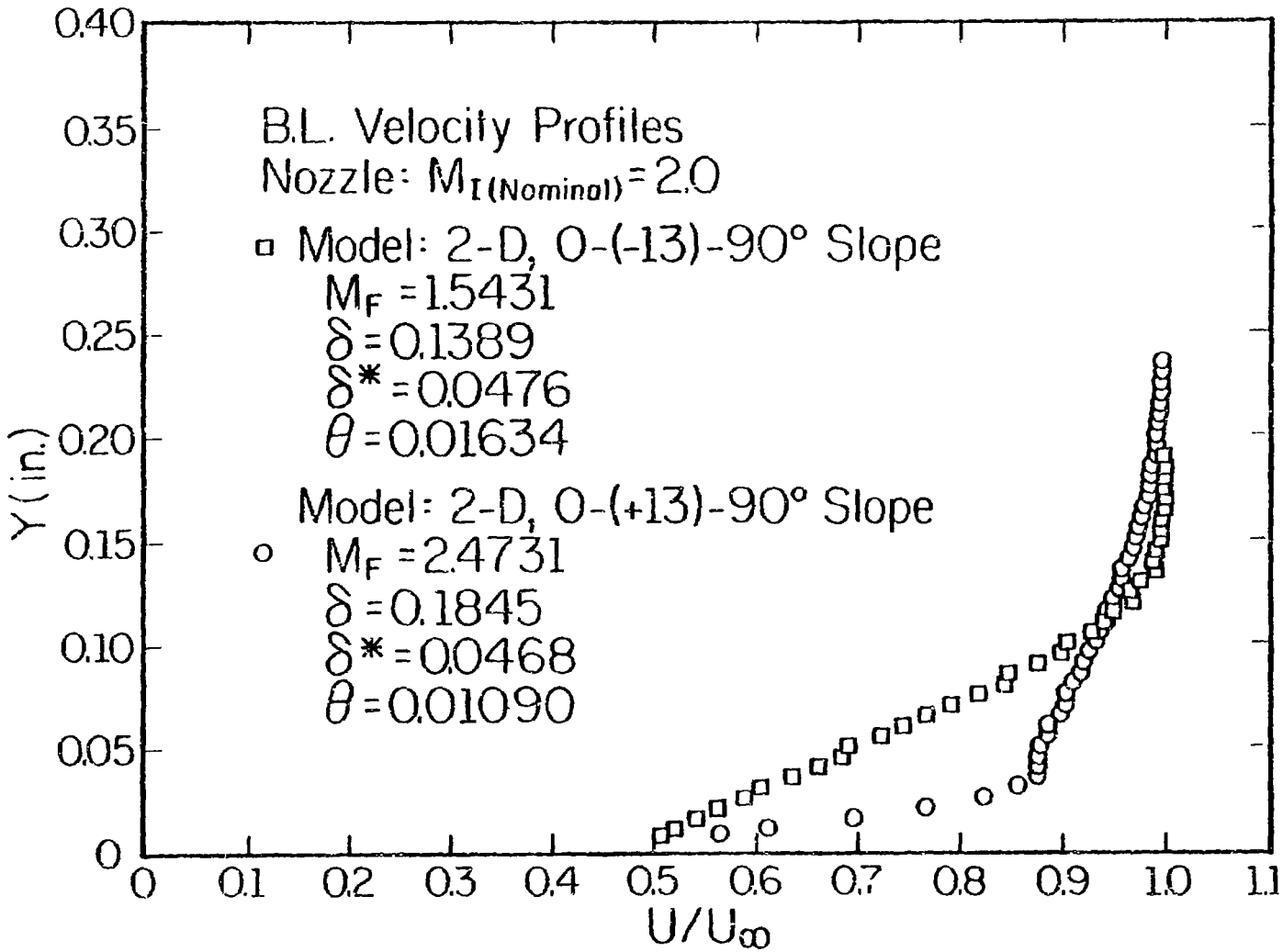

Figure 8 Typical profiles downstream of a sudden expansion and compression for the nominal Mach 2 freestream.

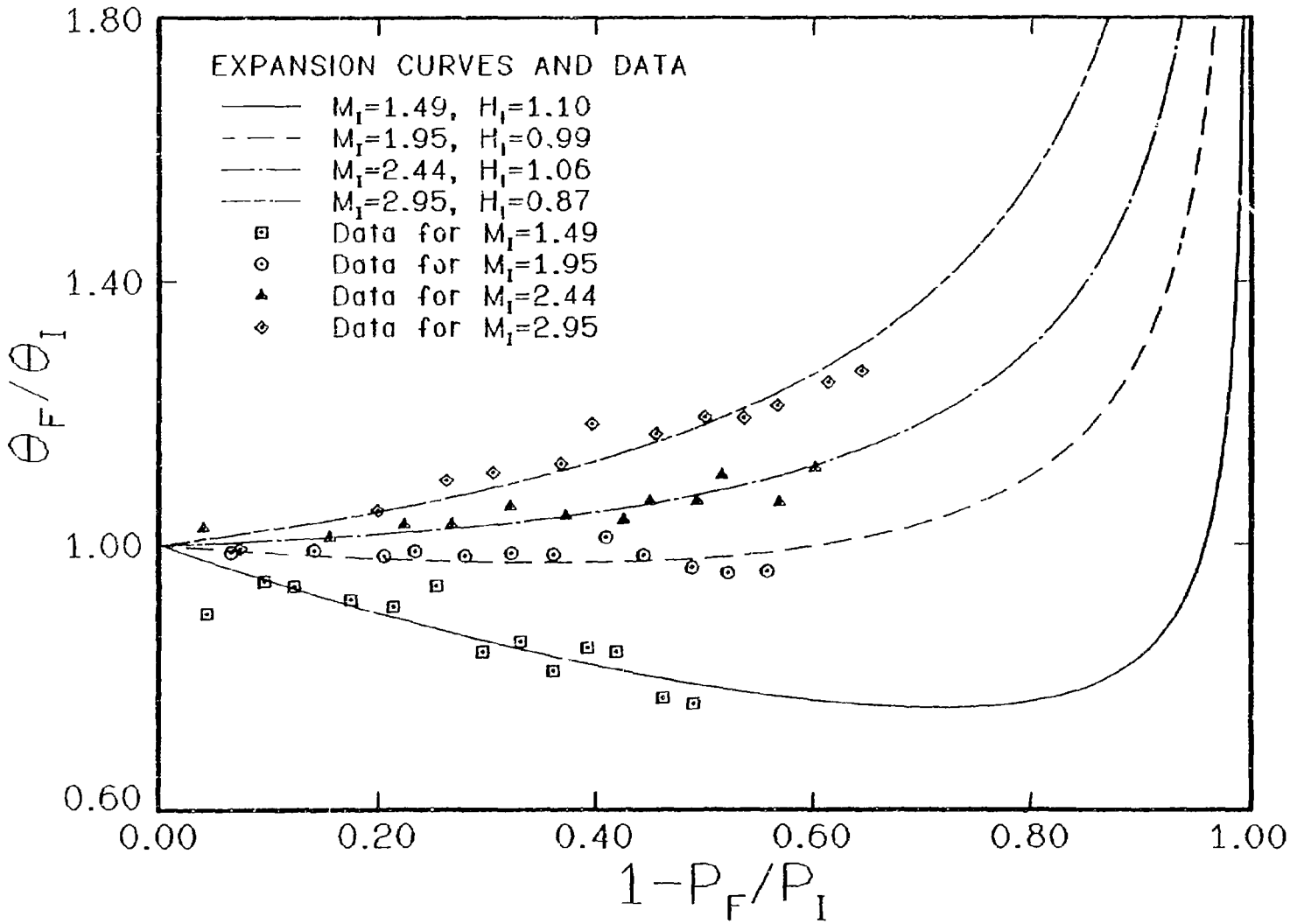

Figure 9(a) Theoretical and experimental momentum thickness ratios for sudden expansions.

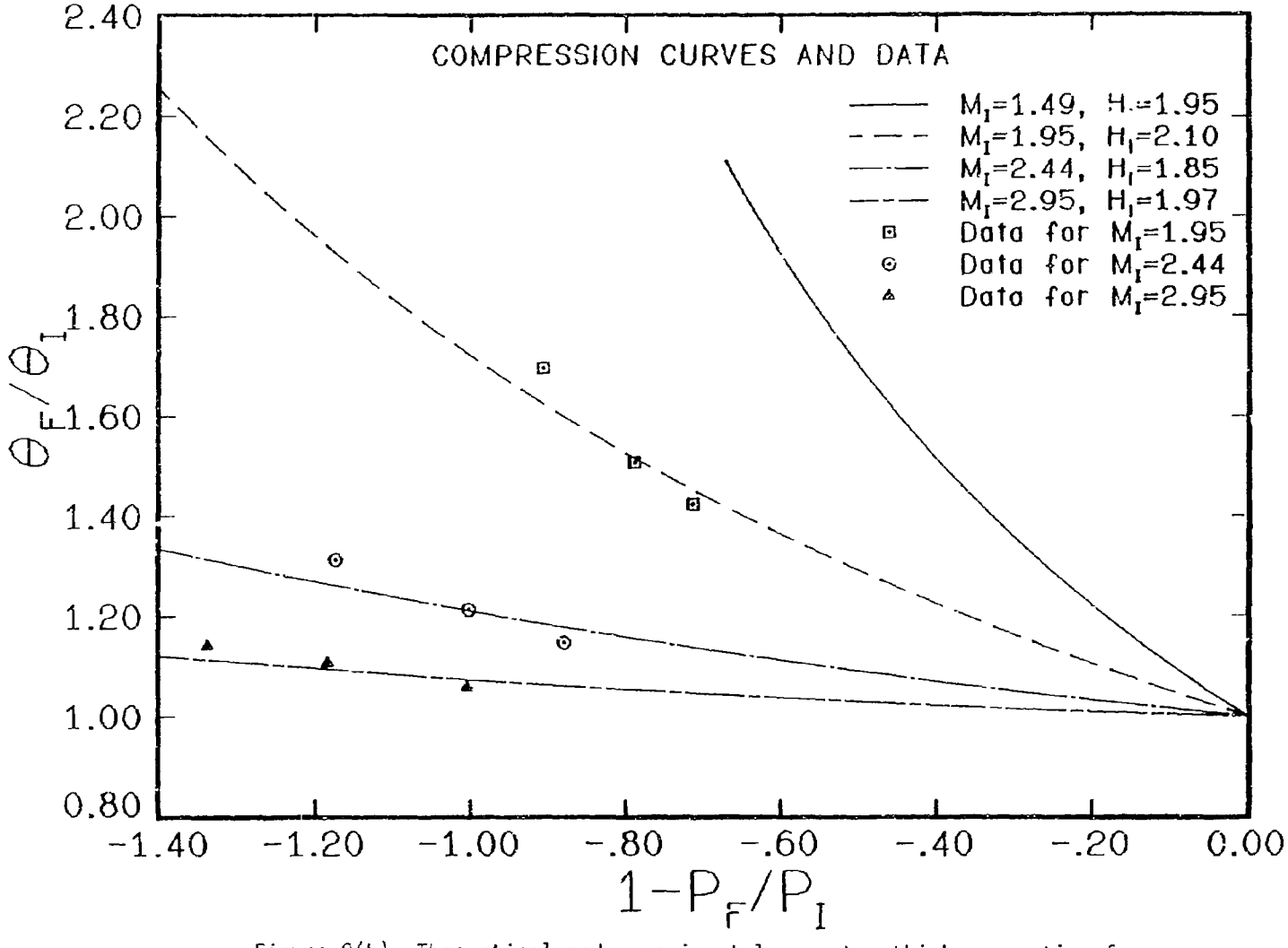

Figure 9(b) Theoretical and experimental momentum thickness ratios for sudden compressions.

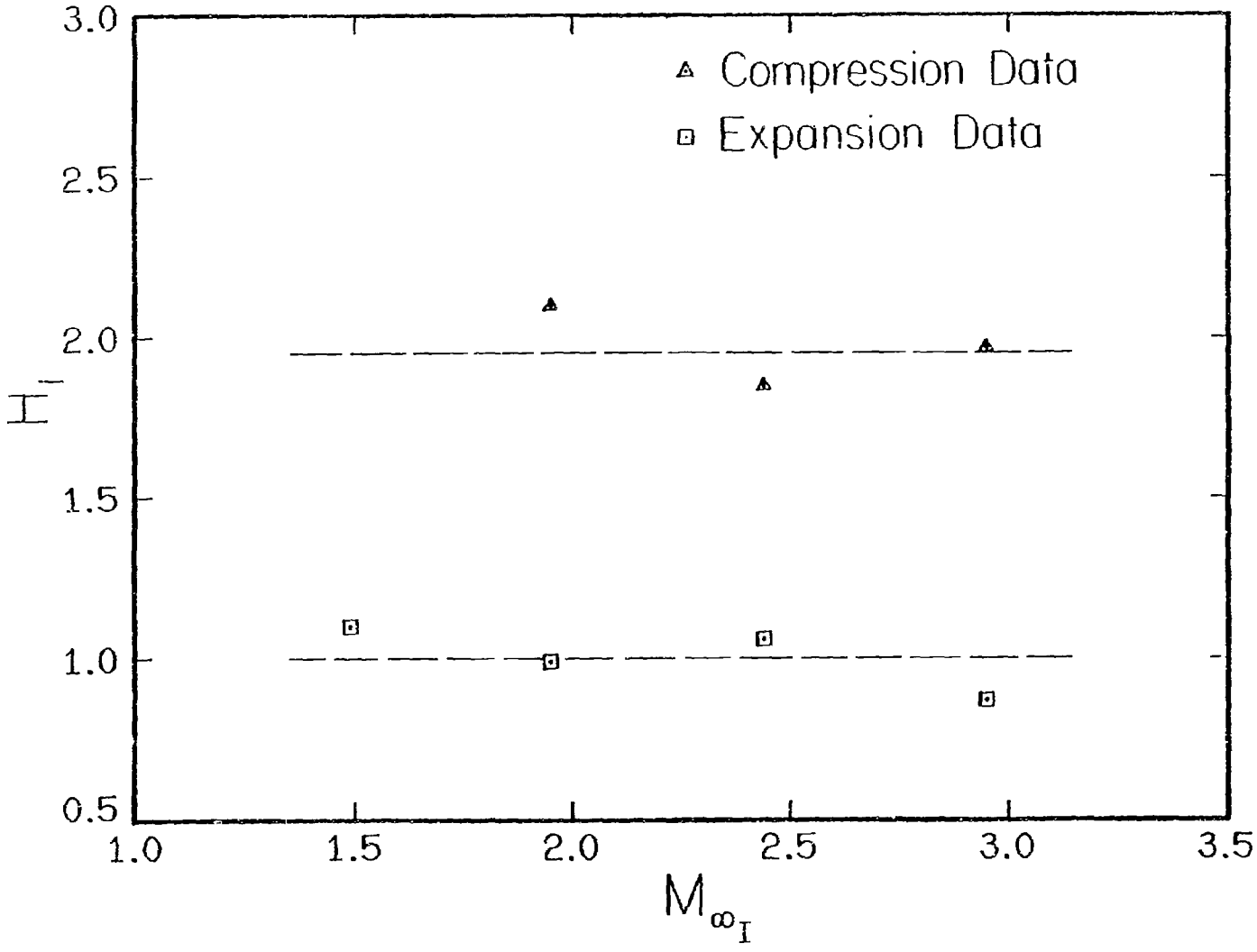

Figure 10 Best fit H_i for Equation (1) to experimental data as a function of initial Mach number.

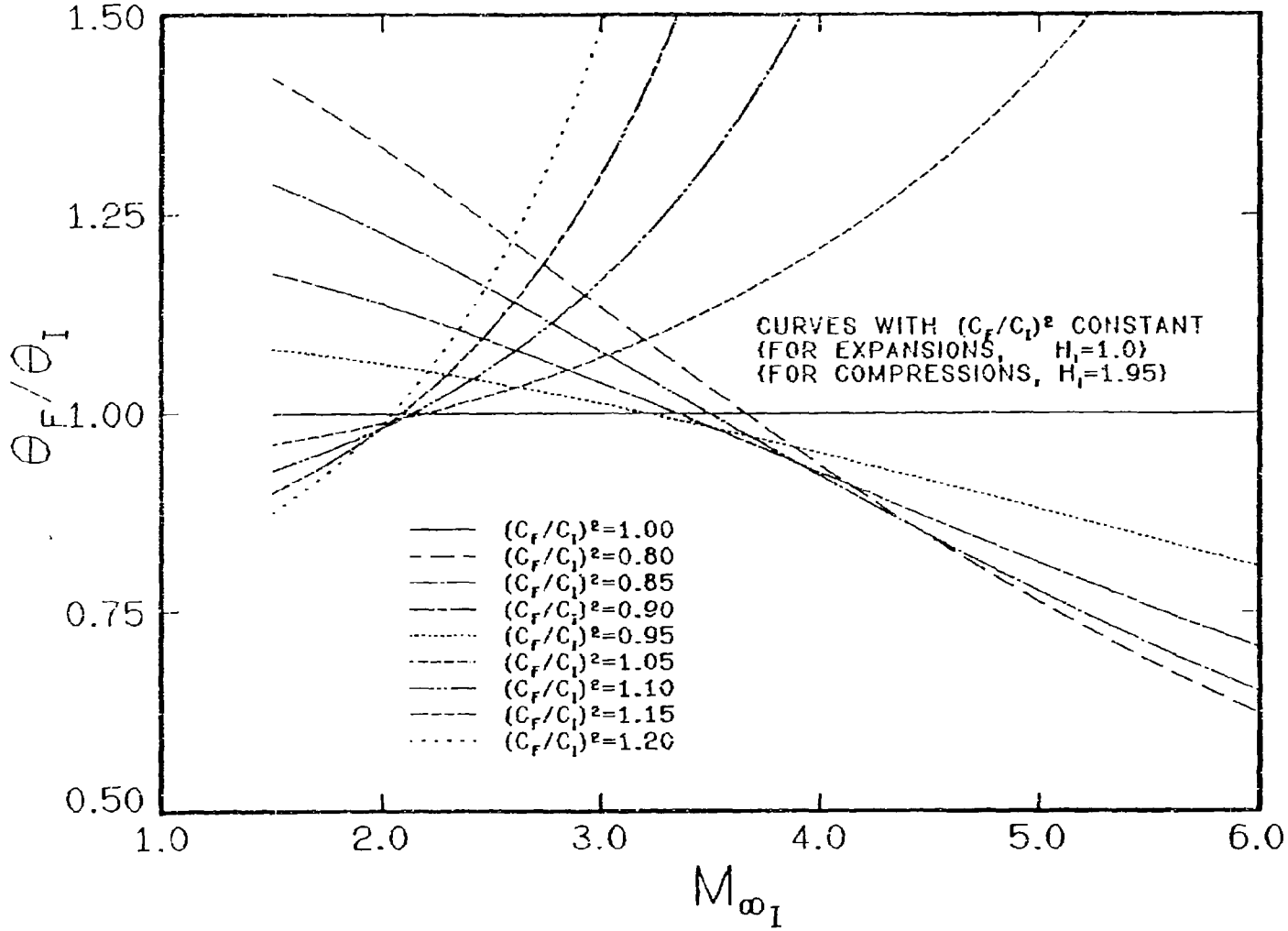

Figure 11 Equation (2), plotted for lines of constant degree of expansion or compression, using best fit H_i values as shown.

APPENDIX I

NEAR WAKE ANALYSIS WITH THE METHOD OF SEQUENTIAL CENTERED EXPANSIONS

by

Professor H. H. Korst

APPENDIX I

NEAR WAKE ANALYSIS WITH THE METHOD OF SEQUENTIAL CENTERED EXPANSIONS

Helmut H. Korst
Professor of Mechanical and Industrial Engineering
The University of Illinois at Urbana-Champaign
Urbana, Illinois

SUMMARY

A wide spectrum of near wake flows is controlled by inviscid and viscid mechanisms in the proximity of the vehicle base. This situation has important implications since it suggests the possibility of simplifying the analysis of the inviscid flow structure while, on the other hand, complicating the viscid mechanisms as they may be strongly influenced by Reynolds number (scale) effects and transitional phenomena.

Since flow component models are based on the separate treatment of inviscid and viscid mechanisms, subject to subsequent integration into an overall system by imposing proper closure conditions at the end of the wake, it is often advantageous and acceptable to utilize an approximate method for dealing with the inviscid wake boundaries. The method of sequential centered expansions becomes quite attractive for jet and/or slipstream boundaries having axisymmetric geometries.

Based on the development of the Potential Equation in the vicinity of a discontinuity in boundary conditions, i.e., slope and curvature, the method originally proposed by Johannesen and Meyer [1] can be extended and adapted to a wide variety of practical problems in supersonic missile flight. In particular, cases involving axisymmetric wakes in both powered and unpowered flight can be analyzed with convenience since both the plume and slipstream boundaries appear in the convenient form of circular shape approximations which accurately represent the initial slopes and curvatures.

Beyond this, however, even problems involving strongly non-axisymmetric vehicle geometries, or flight conditions at high angle-of-attack, can be analyzed by modeling schemes utilizing the method of sequential centered expansions. The only requirement is that the pressure in the near-wake need be reasonably uniform, which is true in many practical cases. The slipstream and jet-plume analysis are carried out in differently oriented polar coordinate systems, as shown in Figures 1 and 2. Consequently, the partial differential equation for the axisymmetric potential flow is as follows:

$$(u^2-a^2)\frac{\partial u}{\partial R} + (v^2-a^2)\frac{\partial v}{R\partial\phi} + uv\left(\frac{\partial v}{\partial R} + \frac{\partial u}{R\partial\phi}\right) - a^2\frac{u}{R} \pm \frac{a^2}{1\pm R\cos\phi}(v\sin\phi - u\cos\phi) = 0$$

where one will distinguish between the cases of the slipstream and the plume by specifying the upper or lower signs, respectively. The series development for the flow in the vicinity of the discontinuity becomes

$$u(R, \phi) = u_0 + u_1(\phi)R + u_2(\phi)R^2 + \ldots$$

$$v(R, \phi) = v_0 + v_1(\phi)R + \ldots$$

$$a(R, \phi) = a_0 + a_1(\phi)R + \ldots$$

which suggests convergence of the solution (pressure distribution along downstream walls or slope and curvature of free jet boundaries) within a region extending one (dimensionless) radius downstream.

After specifying the appropriate boundary conditions, solutions can be found by integration of ordinary differential equations in Region B-1 (flow upstream of the centered expansion, see Figure 3), Region A (modified Prandtl-Meyer fan, see Figure 3), and Region B-2 (flowfield downstream of the centered expansion, see Figure 3).

Even though the initial condition is second order, the solutions can be continued for much larger distances downstream by utilizing the conventional

Method of Characteristics. This explains the success of the mathematical modeling scheme for plumes having dissimilar specific heat ratios.

The method of sequential centered expansions is an integral part of the analyses of the base flowfield which are employed in the published papers which are included in this report as Appendices C, E, F, and K.

REFERENCES

1. Johannesen, N. H. and Meyer, R. E., "Axially-Symmetrical Supersonic Flow near the Centre of an Expansion," The Aeronautical Quarterly, Vol. 2, 1950, pp. 127-142.

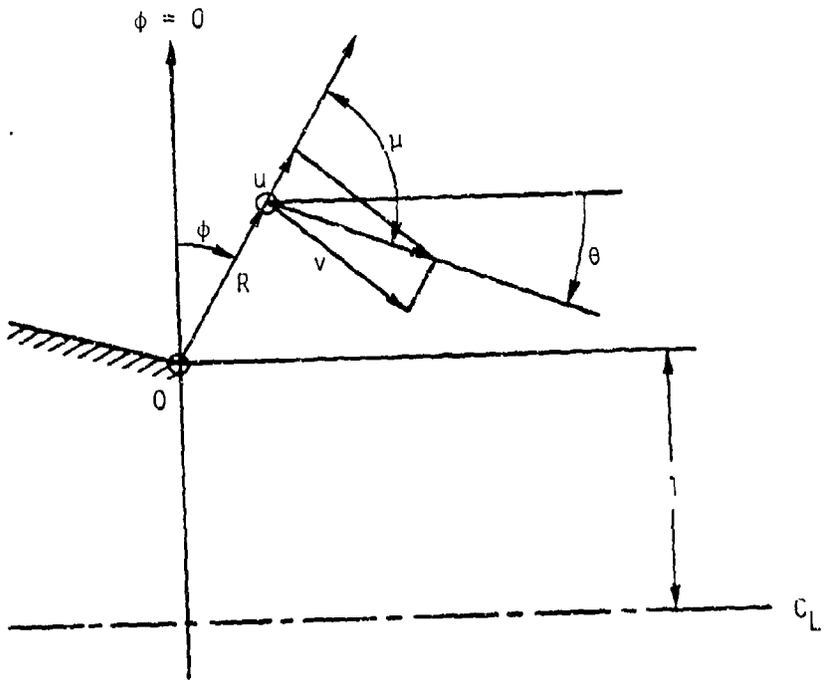

Figure 1 Polar coordinate system for the external slipstream analysis.

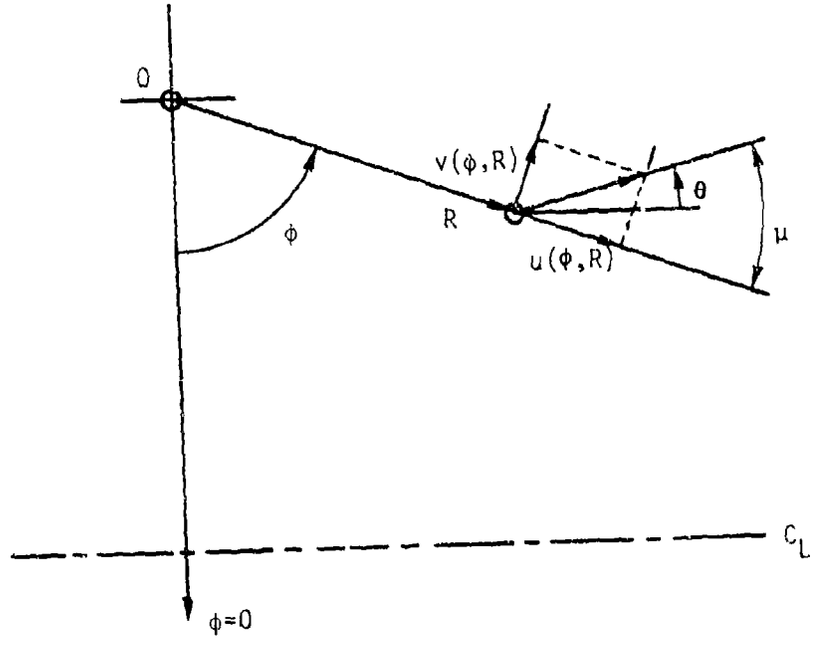

Figure 2 Polar coordinate system for the jet-plume analysis.

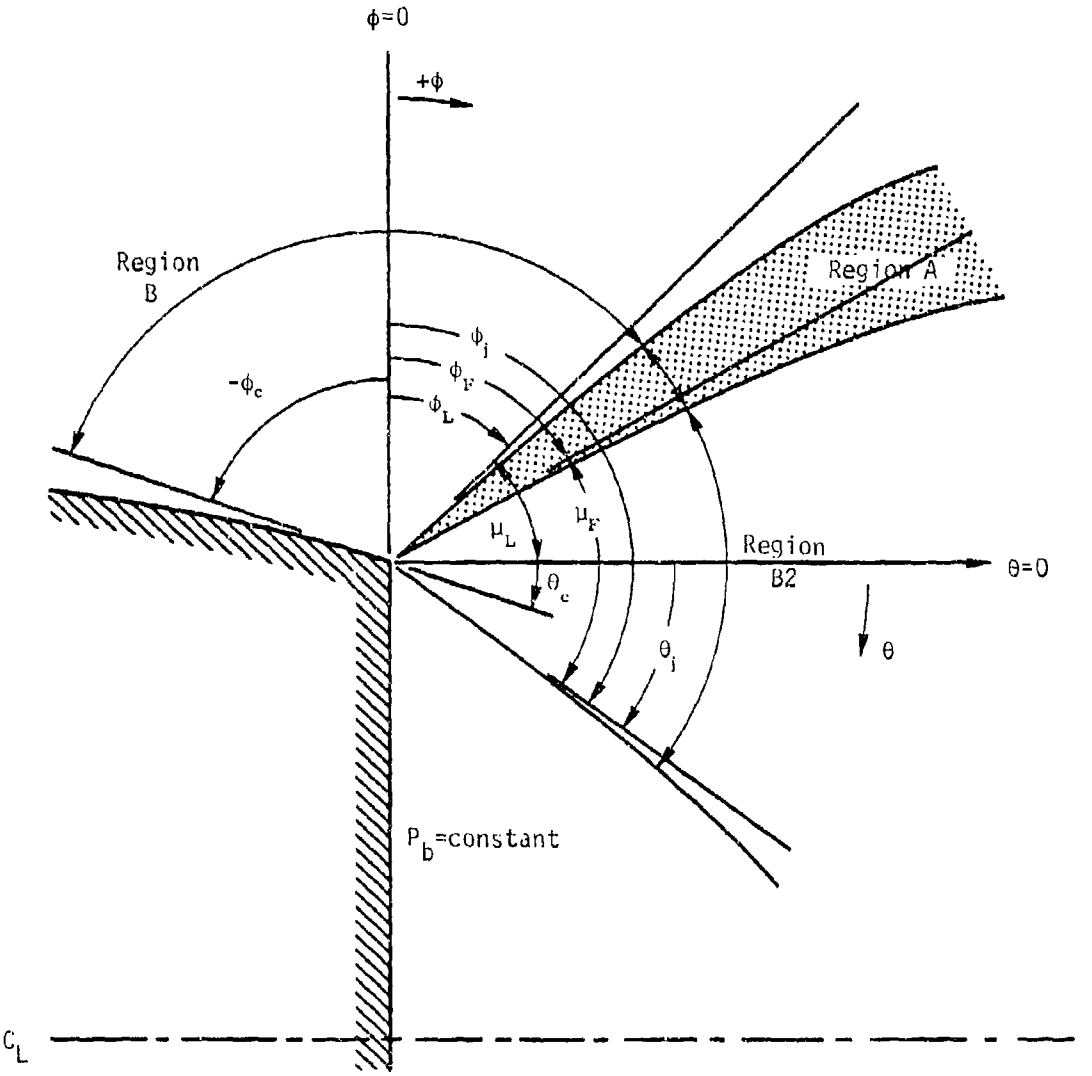

Figure 3(a) Regions of integration of the ordinary differential equations.

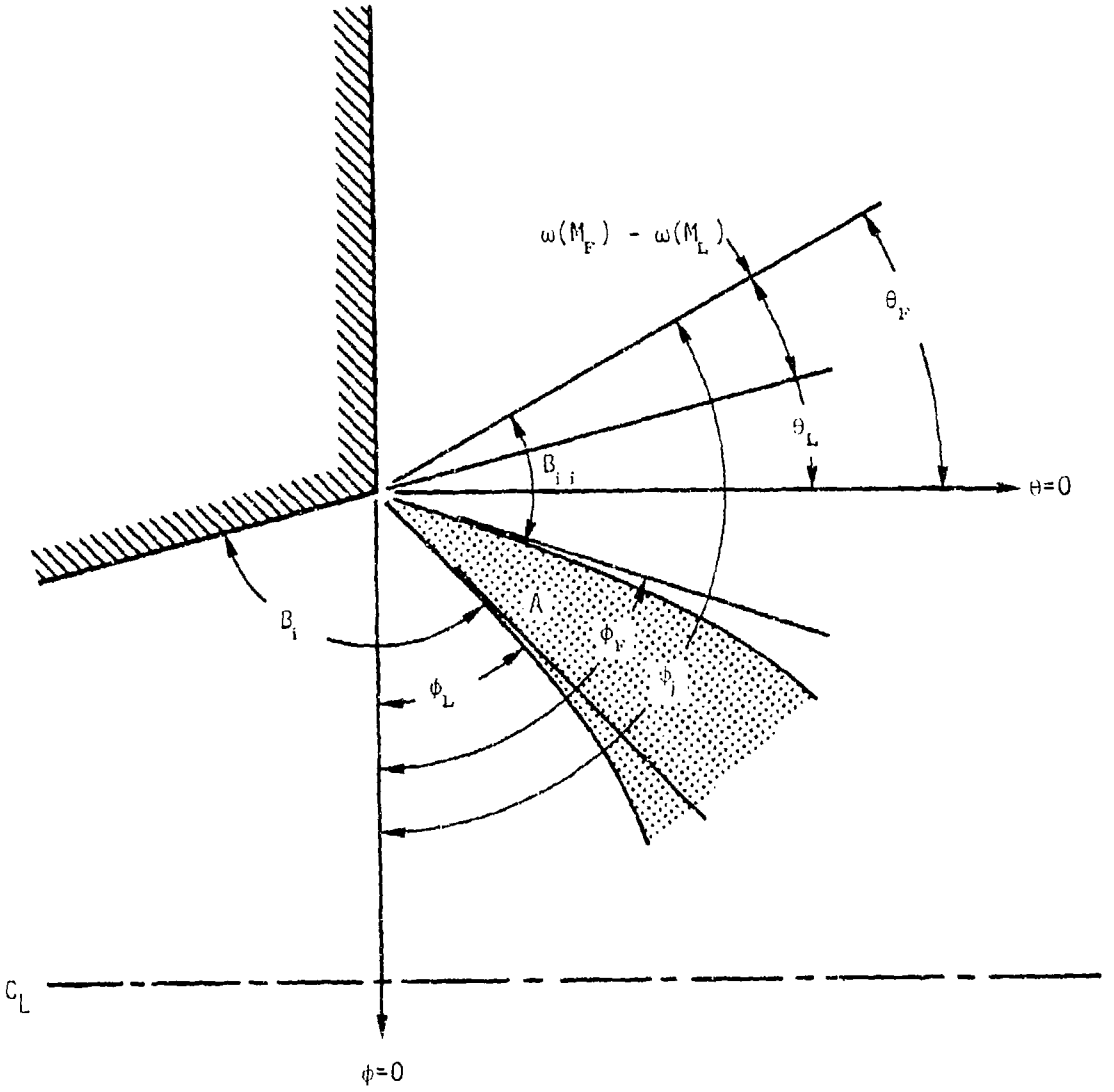

Figure 3(b) Regions of integration of the ordinary differential equations.

APPENDIX J

NON-STEADY PLUME-WALL INTERACTIONS DUE TO FLUIDIC ENTRAINMENT AND CRITICAL OUTFLOW

by

M. J. Marongiu

APPENDIX J

NON-STEADY PLUME-WALL INTERACTIONS DUE TO FLUIDIC ENTRAINMENT AND CRITICAL OUTFLOW

By

Maurice J. Marongiu

B.S., University of Illinois, 1980

THESIS EXCERPTS

Submitted in partial fufillment of the requirements
for the degree of Master of Science in Mechanical Engineering
in the Graduate College of the
University of Illinois at Urbana-Champaign, 1982

Urbana, Illinois

INTRODUCTION

Non-steady phenomena during the early phases of the launch of missiles involving large amplitude pressure waves have been suspected to cause structural failures and generate high impulse noise levels.

Laboratory experiments reported herein have confirmed that unsteady flows may be present and are repeatable under well controlled operating conditions.

Even though unsteady flow has been observed during the starting phases of blowdown wind tunnels [1][†], observation and theoretical modeling of the unsteady plume-launcher interaction have not been reported profusely in the scientific literature with the exception of a related report by Meier, et al. [2]. In their communication, non-steady flow phenomena in two-dimensional and axisymmetric configurations were studied. In all cases, converging nozzles discharged into smooth channels of larger but constant cross-sections, whereas a converging-diverging nozzle was used in the present investigation. It will be shown later that a converging nozzle limits the range of unsteady flow occurrence because a sounding shock wave cannot form in the nozzle.

Meier, et al., reported extensively on the influence of the important geometrical and operational parameters causing flow unsteadiness, employing diverse means such as dynamic and static pressure readings, Schlieren, streak as well as interferometer visualizations, and fast Fourier transform analysis. However, the report does not provide a complete theoretical model to interpret the thorough and extensive experimental data.

[†]Numbers in brackets refer to entries in REFERENCES at end of these excerpts.

Furthermore, their experiments with two-dimensional channels gave rise to asymmetrical flow interactions which are not representative of the scope of this investigation.

Although no satisfactory overall flow model has been proposed offering full understanding of the entire flow phenomena as based on constituent flow components and regions, the literature does provide much detailed information on particular flow components such as fluidic mass entrainment, mixing shear layers, resonating flows past cavities, and choking (critical mass flow rates) in channels and ducts due to irreversibilities (friction or shocks) and/or cross-sectional area reductions.

The objective of this investigation is to propose and test a model based on well established flow components. Both physical and computational aspects of the components and their interactions are introduced and subsequently subject to experimental corroboration.

The configuration germane to the missile launch problem consists, as studied in this case, of a converging-diverging nozzle discharging into a smooth channel of larger but constant cross-section. This channel ends with an adjustable area reduction (secondary constriction or nozzle). Figure 1 shows a sketch of the configuration.

The non-steady operation of such a system can be expected to exhibit the following patterns:

(1) The jet emerging from the nozzle expands forming a plume which impinges on the wall (base flow problem). This will subsequently produce multiple shock wave iterations eventually resulting in subsonic flow at the entrance of the downstream (secondary) nozzle. In spite of the complex nature of the multiple shock interactions, the flow conditions (Mach number) at the entrance of the secondary nozzle will be closely approximated by one-dimensional flow [3].

(2) Since irreversibilities are sustained in the flow, the local stagnation pressures will decrease, thus to maintain a steady flow would require an enlarged secondary throat area that satisfies $A^*_{II}/A^* = P_{OI}/P_{OII}$. If the area ratio of the downstream nozzle is too small, this Mach number cannot be sustained in steady flow and a left-running wave will form.

(3) The difference in the mass flowrates between the choked primary and secondary nozzles will then be stored behind the moving shock.

(4) If the traveling shock proceeds so far upstream that it reaches the end of the wake, the plume impingement is eliminated, and as the jet detaches from the wall, the flow irreversibilities decrease and the stored mass will soon discharge through the secondary nozzle.

(5) The free jet emerging from the nozzle will begin to entrain mass, thus reducing the pressure near the nozzle exit, eventually forming a closed wake with resulting plume expansion and impingement.

If all these events occur, a cyclic system operation will result.

The analysis of the problem has to establish criteria which allow to quantify the geometric and operational parameters in order to arrive at the understanding of under what conditions non-steady operation can be expected and which time scales and pressure amplitudes can be predicted.

An experimental program section will describe the design of the test equipment and instrumentation as well as the data acquisition and processing procedures.

Comparison with analytical and experimental results will then allow to evaluate the merits of the simplified flow model in explaining qualitatively and quantitatively the non-steady flow phenomena as they may occur during the tube-launch of rockets.

CONCLUSIONS

The primary goal for the initial phase of this research endeavor has been to lay down the ground work for more detailed and extensive development of a

theoretical model that would predict, accurately and comprehensively, the conditions (both geometrical and operational) necessary to induce non-steady flow phenomena; and also to describe the system behavior under non-steady operation. Such flow phenomenon can occur during the initial phases of the launch of missiles.

Despite the highly simplified analytical model reported here, the identification of the secondary throat area ($A_{e_{II}}$) as a critical parameter -- provided that the system configuration allows for the development of the fluidic mechanism and near-wake formation and that critical flow prevails through the exit nozzle -- has been possible.

Furthermore, the verification of the base pressure oscillations as being nearly periodical will aid in the prediction of the overall system behavior with regard to oscillation amplitude and frequency.

Detailed modeling of the fluidic entrainment mechanism as a basis for near-wake development as well as accurate experimental data for the changes in base pressure levels during pump-down will be subject to follow-up phases in this research area.

REFERENCES

1. Shapiro, A. H., The Dynamics and Thermodynamics of Compressible Fluid Flow, New York, John Wiley and Sons, Inc. 1953, Vol. 1.

2. Meier, G. E. A., G. Grabitz, W. M. Jungowski, K. J. Witczak, and J. S. Anderson, "Oscillations of the Supersonic Flow Downstream of an Abrupt Increase in Duct Cross-Section," Report No. 65 from the Max-Planck Institute, Goettingen, West Germany, 1978.

3. Korst, H. H., T. L. Butler, and M. B. Briski, "Similation of Jet Plume Interference Effects During the Launch Phase of Missiles," J. of Spacecraft and Rockets, Vol. 18, No. 1, 1981, pp. 24-30.

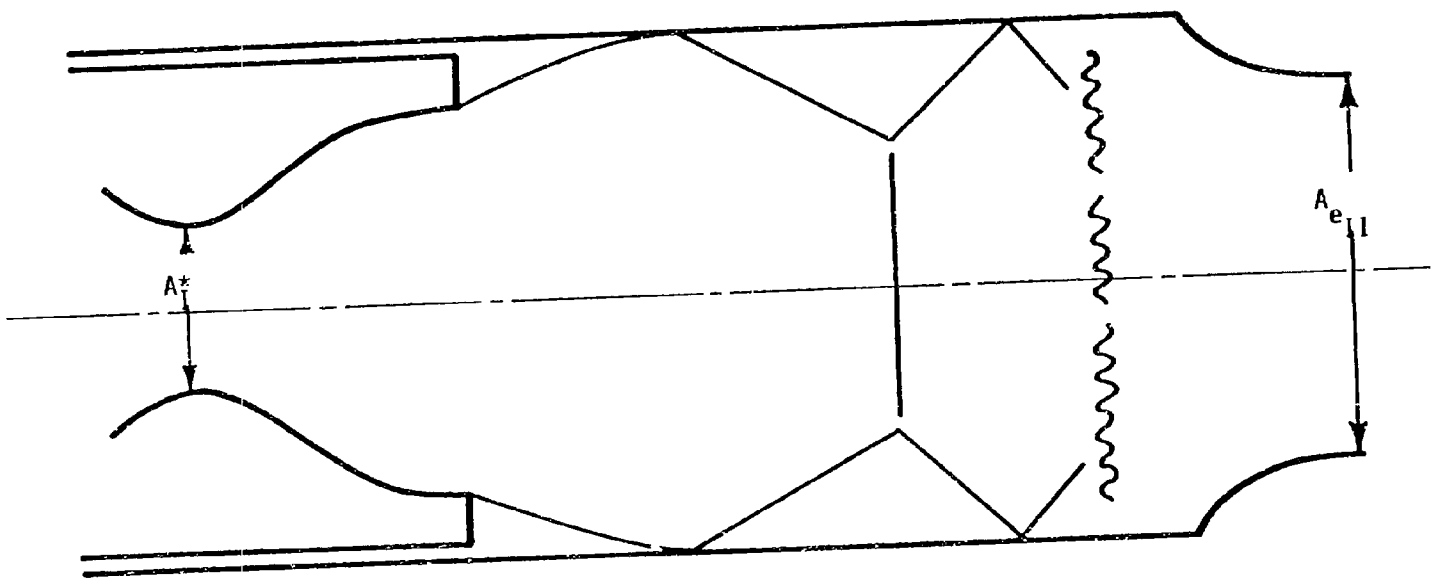

Figure 1 Basic Configuration of Missile Launch-Tube with Outflow Restriction during Initial Launch Phases

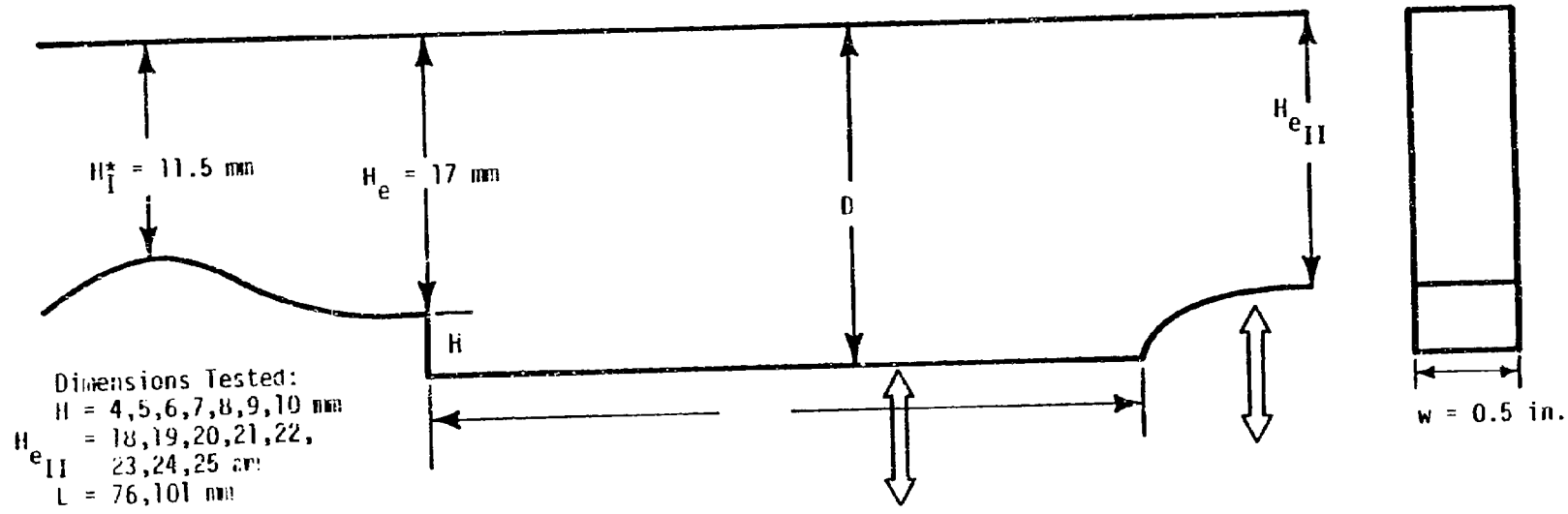

Figure 2 Air Model Configuration showing the Dimensions Tested in this Investigation

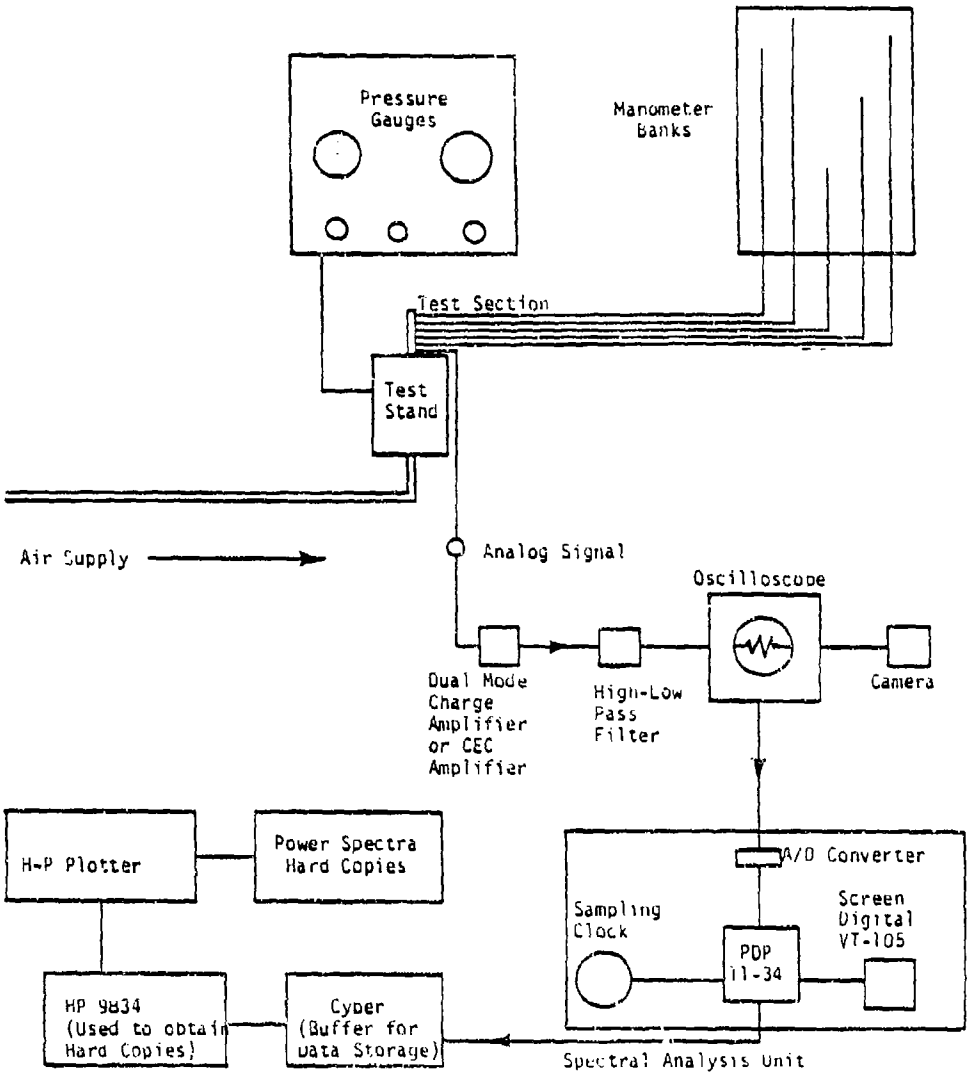

Figure 3 Data Acquisition Flow Diagram

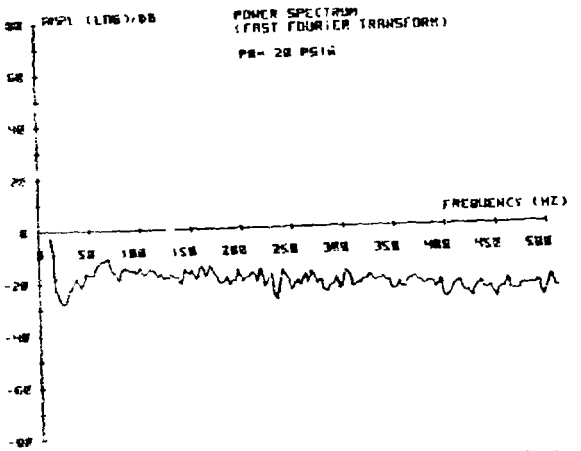

Figure 4(a) Power Spectrum of Base Pressure Oscillations for Case 22 with L = 76 mm

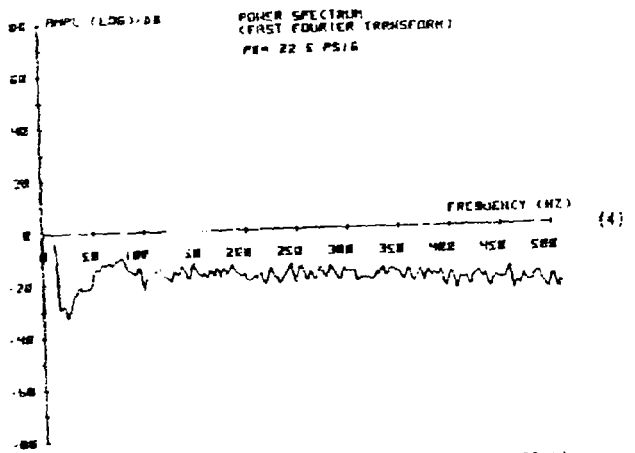

Figure 4(b) Power Spectrum of Base Pressure Oscillations for Case 22 with L = 76 mm

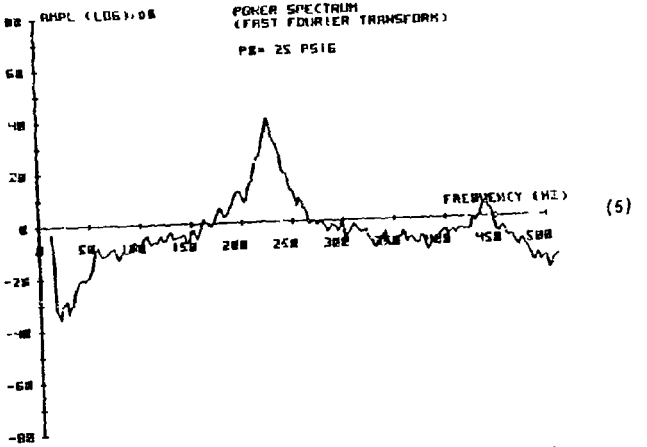

Figure 4(c) Power Spectrum of Base Pressure Oscillations for Case 22 with L = 76 mm

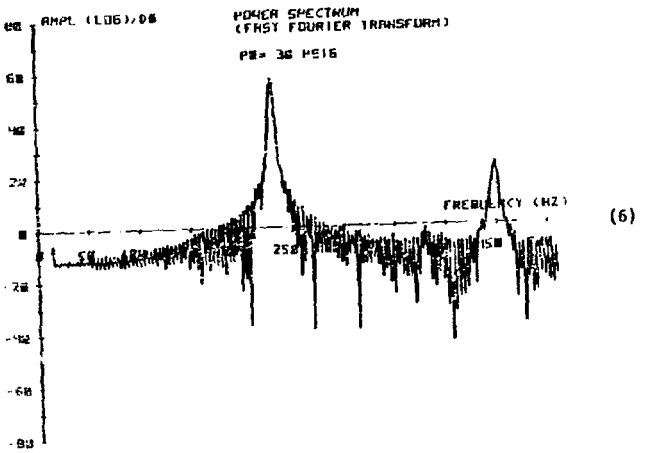

Figure 4(d) Power Spectrum of Base Pressure Oscillations for Case 22 with L = 76 mm

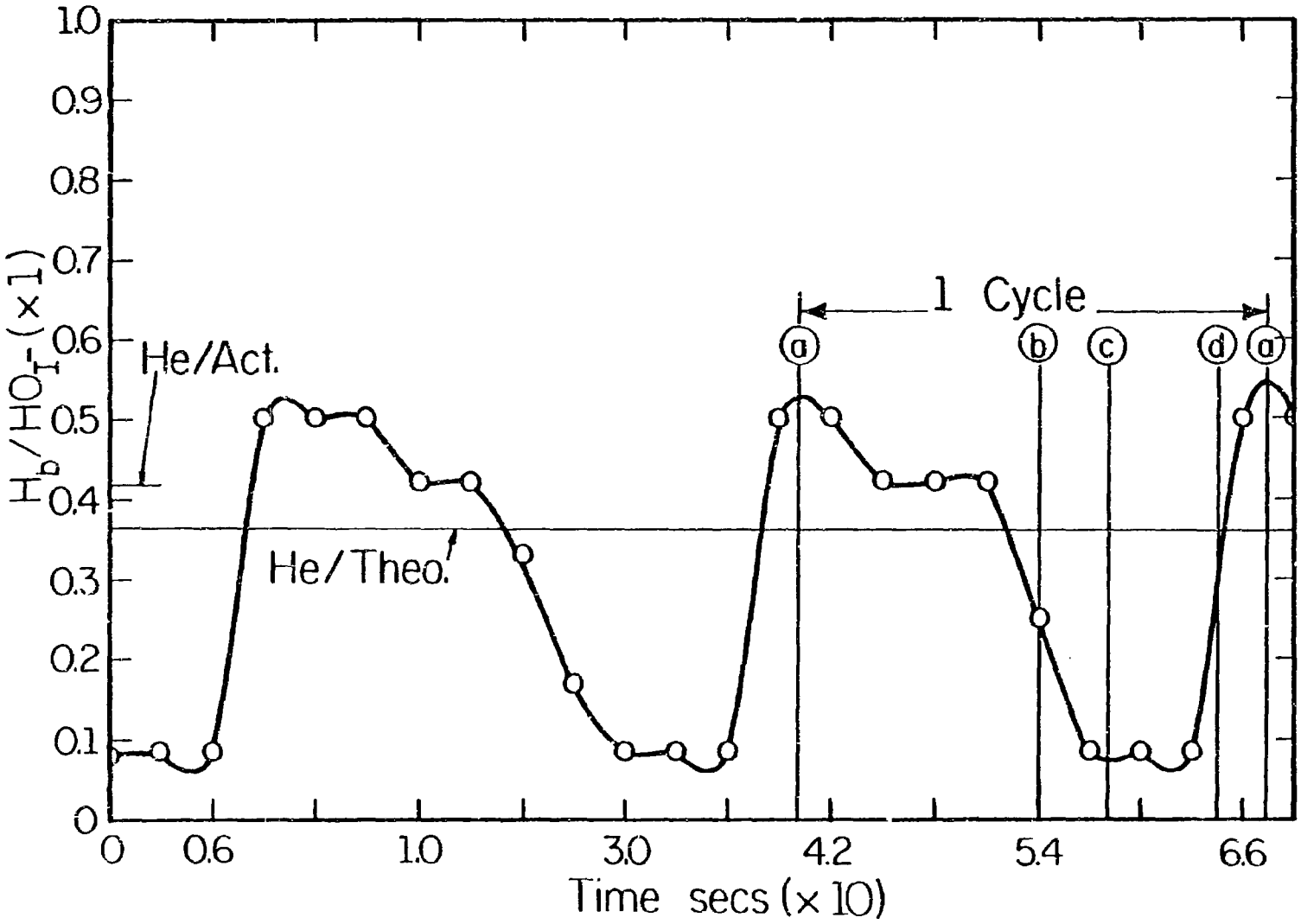

Figure 5 Base Area Water Height (H_b) versus Time on the Water Table Model during Non-Steady Operation

APPENDIX K

THE ANALYSIS OF SECONDARY FLOWS FOR TUBE-LAUNCHED ROCKET CONFIGURATIONS

AIAA Paper No. 81-1222

by

H. H. Korst and J. J. Bertin

APPENDIX A

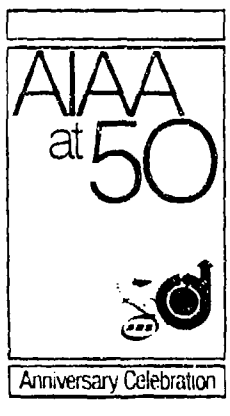

AIAA-81-1222 The Analysis of Secondary Flows for Tube-Launched Rocket Configurations

H. H. Korst, University of Illinois, Urbana-Champaign, IL; and
J. J. Bertin, University of Texas at Austin, TX

AIAA 14th Fluid and Plasma Dynamics Conference

June 23-25, 1981/Palo Alto, California

THE ANALYSIS OF SECONDARY FLOWS FOR TUBE-LAUNCHED ROCKET CONFIGURATIONS*

H. H. Korst+
The University of Illinois at Urbana-Champaign
Urbana, Illinois

and

John J. Bertin++
The University of Texas at Austin
Austin, Texas

Abstract

Theoretical solutions have been computed for the flow fields which exist when an underexpanded nozzle is exhausted into a constant-area launch tube such that the impingement shock wave is relatively weak and the downstream flow remains supersonic. The theoretical flows are compared with experimental data for various nozzle/launch tube configurations. For the test program, unheated air was accelerated to supersonic speed through convergent-divergent nozzles over a wide range of stagnation pressure. In the present paper, an engineering model for the impingement flow-field is presented, the computed flow-field solutions are compared with experimental results, the comparisons are used to verify the validity of the flow model, and solutions are presented to illustrate the effect of γ-variations. The theoretical wall static-pressure distributions in the impingement region and the calculated value for the stagnation pressure for which there is no secondary flow in the annular gap are in good agreement with the experimental data.

Nomenclature

A	Cross-section area
C	Crocco number
d	Diameter
M	Mach number
$\dot{m}$	Mass flow rate
p	Pressure
r	Radius, measured perpendicular to the centerline of the launch tube
R_I	Initial radius of curvature of the inviscid plume boundary
T	Temperature
u	Streamwise velocity component
x	Axial distance along the centerline of the launch tube or streamwise distance (arc length) along the inviscid plume boundary
y	Normal distance to the inviscid plume boundary
γ	Ratio of specific heats
η	Nondimensional shear-layer coordinate
θ	Flow inclination relative to the centerline of the launch tube
ρ	Density
σ	Spreading parameter, defined by equation (1)
ϕ	Dimensionless velocity ratio
ω	Prandtl-Meyer angle

Subscripts

ag	Denotes static properties evaluated at the upstream end of the annular gap
b	Denotes static properties in the base region
d	Discriminating (dividing or stagnating) streamline
ex	Flow through the nozzle exit-plane, i.e., the exhaust flow
F	Free-jet surface (inviscid plume boundary)
i	Denotes properties evaluated at the intersection of the inviscid plume boundary and the launcher wall
j	Zero streamline, i.e., that dividing the exhaust flow from the base air
L	Denotes local conditions at the lip of the nozzle exit-plane
ne	Denotes properties evaluated in the nozzle exit-plane
pit	Pressure measured using a pitot probe collinear with the launch-tube axis
pk	Denotes peak values
r	Outer surface of the rocket
t	Inner surface of the launch tube
t1	Denotes properties evaluated in the stagnation chamber of the simulated rocket
t2	Denotes properties downstream of a normal shock wave
v	Beginning of viscous interaction
1	Mass flow rate given by equation (5)

* The individual research efforts discussed herein were supported by the U.S. Army Research Office through grant DAAG-29-76-G-0209 and by the U.S. Army Missile Command through contract DAAH01-80-C-0116.

+ Professor of Mechanical Engineering, Department of Mechanical and Industrial Engineering, University of Illinois at Urbana-Champaign, Fellow, AIAA

++ Professor, Department of Aerospace Engineering and Engineering Mechanics, The University of Texas at Austin, Associate Fellow, AIAA

Introduction

Various military rockets are launched from tubes. The designer of a tube-launched rocket system must consider the possibility of unbalanced forces acting on the rocket that are caused by flow in the annular gap between the rocket and the launcher wall. As the underexpanded nozzle flow accelerates upon leaving the nozzle, it entrains air from the annular gap forming a shear layer at the plume boundary. The exhaust plume impinges on the wall a short distance downstream of the nozzle exit-plane, creating an impingement shock-wave. When the impingement shock-wave is very weak, a fraction of the entrained air has been given sufficient momentum so that it passes through the impingement shock and the system acts as an ejector. Using the atmosphere at the upstream end of the launcher as its source, a low velocity flow develops in the annular region to supply the mass

flow rate of air that is carried through the shock wave. A fraction of the air entrained by the exhaust plume does not gain sufficient momentum to pass through the shock wave and is turned upstream, creating a separation "bubble" near the launcher wall. Thus, as indicated in the sketch of Fig. 1a, the discriminating (or dividing) streamline can be traced into the annular region between the rocket and the launcher wall.

If the stagnation pressure or the nozzle exit-angle is increased above the values for ejector-type flow, the flow at the plume boundary must turn through a larger angle when it encounters the wall. Thus, although classified as a weak solution, the pressure rise across the shock wave increases. Once the impingement shock-wave becomes sufficiently strong, the resultant adverse pressure gradient causes a fraction of the exhaust flow to be turned upstream into the annular gap, as shown in Fig. 1b. The exhaust that is turned upstream is known as blow-by flow.

When conditions are such that the impingement shock-wave system is strong, massive blow-by occurs. The essential elements of a flow model for this launch-tube flow field have been identified experimentally[1]. A one-dimensional, theoretical, flow-model, which correlates well with the experimental data, has been developed[2]. The pressure gradients and asymmetries resulting from turning a large fraction of the exhaust flow upstream into the annular gap cause unbalanced forces on the rocket. Because the rocket is flying free in the launch tube at this time, these forces can cause the rocket to deviate significantly from its intended flight path. Such deviations in the rocket's trajectory have been observed in flight tests[3], and in cold-gas simulations[4,5]. Therefore, although it is necessary to understand launch-tube flow fields with massive blow-by, they should be avoided whenever possible.

To predict the magnitude and the direction of the flow in the annular gap, one must be able to describe the exhaust plume of the rocket and the viscous/shock-interaction structure that results when the plume encounters the launcher wall. The strength of the impingement shock wave and the characteristics of the viscous interaction at the wall depend on the structure of the exhaust plume and on the geometry of the launch tube. When an underexpanded, supersonic nozzle exhausts into a constant-area tube, the strength of the impingement shock-wave depends on the Mach number of the inviscid flow along the inner edge of the mixing zone at the jet boundary, on the ratio of the specific heats (γ), on the inclination of the impinging flow relative to the launcher wall, and on the velocity profile in the mixing zone.

For a wide range of test conditions, the impingement shock-wave is relatively weak and the downstream flow remains supersonic. For such cases, there is relatively little secondary flow and the pressure in the annular region differs only slightly from the atmospheric value. As a result, unbalanced forces on the missile are relatively small. The Chapman-Korst model[6] can be used to delineate the inviscid and the viscid flow-mechanisms encountered in the plume-impingement flow-field. Once the geometry of the corresponding inviscid plume-boundary is established by an appropriate potential flow analysis, a viscous mixing component is superimposed on the boundary. Wake closure conditions are specified in the form of a modified concept of incomplete

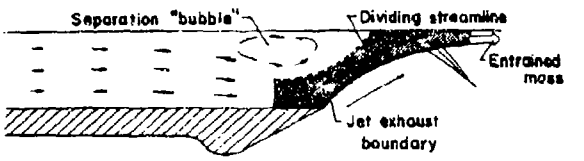

Launcher centerline

Shaded region designates air entrained from the base region which is given sufficient momentum to pass through the impingement shock wave.

(a) System acts as an ejector

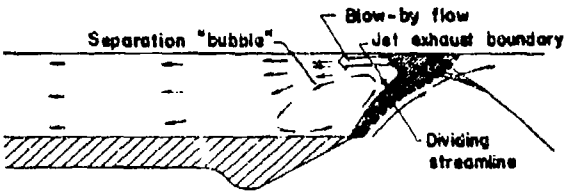

Launcher centerline

Shaded region designates that fraction of the exhaust flow which does not have sufficient momentum to pass through the impingement shock wave.

(b) System produces nominal blow-by flow

Figure 1. - Sketches of possible launch-tube flow fields.

turning of the plume near the point of shear-layer reattachment[7].

Theoretical flow-fields have been calculated for various nozzle/launch-tube configuration using this flow model. The solutions, thus calculated, are compared with experimental data in the present paper. The principal objectives of the present paper are (1) to present an engineering model for the impingement flow-field which is produced when an underexpanded supersonic nozzle is exhausted into a constant-area tube, (2) to compare the computed flow-field solutions with experimental results, and (3) to use the comparisons to establish the validity of the flow model. This final objective is of special importance, since having demonstrated the validity of the flow model, launch-tube flow-fields can be calculated with confidence for other nozzle configurations and/or other specific heat ratios providing the flow satisfies the basic assumptions.

Theoretical Analysis

A component approach for supersonic, turbulent flows, i.e., the Chapman-Korst model[6], forms the basis for the present analysis. It includes the delineation of inviscid and viscid flow-

mechanisms encountered in plume/launcher-wall impingement flows and their subsequent synthesis into an overall systems solution. The geometry of the corresponding inviscid plume boundary is established by an appropriate potential flow analysis. The viscous mixing component is superimposed on the boundary. Wake closure conditions are specified in the form of a modified concept of the incomplete turning of the plume near the point of shear layer reattachment[7]. A number of conceptual simplifications for the plume-impingement flow field, which will be introduced, are justifiable for the conditions of interest.

Since the launching of rockets from straight tubes will generally impose geometric restrictions to blow-by, the present analysis can be simplified by the assumption that the mass flow rates which will be rejected from or entrained into the viscous jet mixing region should be small. It is assumed that the entire system will be operating under essentially isoenergetic conditions, that is, with the stagnation temperature for the entire flow field equal to that of the exhaust gas. This assumption is realistic for most flows under consideration; the exception being if ejector-type flow is induced by the rocket firing.

Since the ratio of the launch-tube diameter to rocket nozzle-exit diameter is usually limited to values ≤ 1.5, the contour of the corresponding inviscid plume boundary can be determined with sufficient accuracy by the second-order potential-flow approximation for axially symmetric, supersonic flow near the center of an expansion[8,9]. The resulting circular-arc configuration is convenient for establishing a simple inviscid-flow-component geometry. On the other hand, it is necessary to treat the nozzle flow in detail in order to define accurately the conditions at, and near, the lip of the exit cross-section. This requires the analysis of the nozzle flow by the method of characteristics (including the effects of characteristics coalescence) as it develops from the transonic flow region near the nozzle throat[10].

The exit-plane conditions near the nozzle lip, will be determined by the local wall-slope, θ_L, the local Mach number, M_L, and the local flow acceleration. With these initial conditions specified, selection of the jet surface Mach number, M_F, will yield a unique solution for the circular-arc approximation of the contour of the inviscid plume boundary in terms of the initial streamline angle, θ_F, and the radius of curvature, R_I[11]. Thus, for a given nozzle configuration and for any jet surface Mach number, M_F, the inviscid flow field will be uniquely determined, see Fig. 2a, with θ_i denoting the inviscid impingement-angle at the cylindrical launcher wall, i.e., at radius r_t. One now has to analyze the viscous flow mechanisms that will provide the closure conditions for determining the actual operating conditions of the system, see Fig. 2b.

The jet mixing characteristics of the free shear-layer at the plume boundary can be approximated by selecting isoenergetic conditions and a linear velocity profile[12]. Use of a self-similar, linear mixing profile does not exclude the study of Reynolds number effects. The effects of the boundary layer along the nozzle wall can be considered, subsequently either in form of an equivalent bleed[7,13] or by analyzing the development of a dissipative shear layer in a rotational but essentially non-dissipative flow field associated

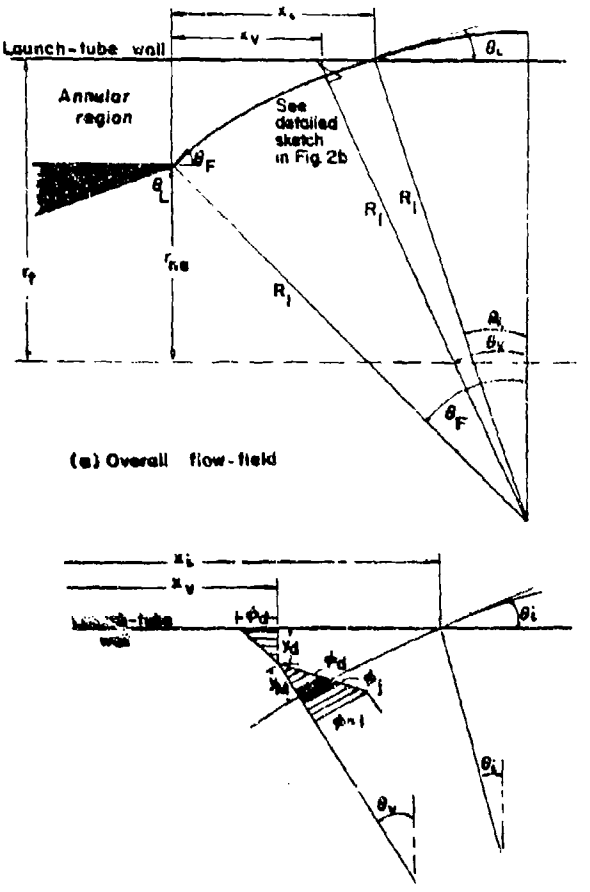

Figure 2. - Sketches of flow model for plume-impingement flow field

with the flow expansions near the nozzle lip. The spread parameter σ shall here be related to the rate of change in slope of the velocity profile[14,15] in the form:

$$\sigma = \frac{\sqrt{\pi}}{u_F} \frac{1}{\frac{\partial}{\partial x}\left[\left(\frac{\partial u}{\partial y}\right)_{max}\right]} \qquad (1)$$

For a linear velocity profile with the conditions at the "inviscid" plume boundary given by u_F and ρ_F, one finds:

$$\phi = \frac{u}{u_F} = \frac{\eta}{\sqrt{\pi}} \qquad (2)$$

where $\eta = \sigma \frac{y}{x}$. The density ratio in the isoenergetic mixing region is:

$$\frac{\rho}{\rho_F} = \frac{1 - C_F^2}{1 - \phi^2 C_F^2} \qquad (3)$$

where use of the Crocco number,

$$C_F = M_F \sqrt{\frac{2}{\gamma - 1} + M_F^2}, \qquad (4)$$

conveniently eliminates the influence of the specific heat ratio on constant-pressure mixing profiles.

Application of the momentum equation to a two-dimensional mixing region allows one to locate the profile with respect to the corresponding inviscid jet boundary in the form:

$$\eta_M = \sigma \frac{y_M}{x} = \sqrt{\pi} \left\{ 1 - \left(\frac{1 - C^2}{C^2} \right) \left(-1 + \frac{1}{2C} \ln \left(\frac{1 + C}{1 - C} \right) \right) \right\} \tag{5}$$

One should note that the application to an axisymmetric, curved plume boundary requires that the length x be interpreted as an arc length and that the use of σ values originally defined for planar mixing zones adds to the inherent uncertainty in making an assessment for the effects of compressibility on the spread parameter. For the present purpose, where the Mach number M_F will seldom exceed 3.5, one may use the simple relationship[16]:

$$\sigma = 12 + 2.56\, M_F$$

The mass-flow-rate per unit depth within the mixing zone up to the streamline $y(\phi)$:

$$\dot{m}_1 = \int_{y=-\infty}^{y(\phi)} \rho\, u\, dy$$

can now be expressed in closed form by:

$$\dot{m}_1 = I_1(\phi, C_F) \frac{x\, u_F\, \rho_F}{\sigma} \tag{6}$$

where

$$I_1(\phi, C_F) = \sqrt{\pi} \frac{\left(C_F^2 - 1 \right)}{2 C_F^2} \left(\ln \left(1 - \phi^2 C_F^2 \right) \right) \tag{6a}$$

The velocity ratio, $\phi = \frac{u}{u_F}$, defines a streamline having the location $y = \frac{x}{\sigma} \left(\eta_M - \frac{\phi}{\sqrt{\pi}} \right)$ measured perpendicular to and outside of the corresponding inviscid plume boundary. The velocity along the zero streamline, which separates the nozzle flow from the air entrained from the base region, is given by:

$$\phi_j = \frac{1}{C_F} \sqrt{1 - \left(1 - C_F^2 \right) \mathrm{EXP} \left(\frac{1}{C_F} \ln \left(\frac{1 + C_F}{1 - C_F} \right) - 2 \right)} \tag{7}$$

The recompression of the plume as it impinges on the cylindrical wall leads to a flow configuration as shown in Fig. 2b. If the stagnating (discriminating or dividing) streamline has a velocity level, ϕ_d, different from that of the zero streamline, ϕ_j, a secondary flow will be established as required for satisfying the conservation of mass in the near wake region. The secondary flow rate will be positive, i.e., ejector-type flow, if $\phi_j > \phi_d$ and negative, i.e., blow-by flow, if $\phi_j < \phi_d$. The secondary flow rate may be approximated as:

$$\dot{m} = 2\pi r_t \frac{x}{\sigma} u_F \rho_F [I_1(\phi_j, C_F) - I_1(\phi_d, C_F)] \tag{8}$$

The condition $\phi_j = \phi_d$ corresponds to an operation without any secondary flow which will be satisfied for the case where the near wake is vented to the atmosphere if:

$$\left. \frac{p}{p_{t1}} \right|_{M_F} = \frac{p_{atm}}{p_{t1}}$$

and for the case where the annular gap is sealed by a tight fitting sabot or by an obturator ring.

As the discriminating streamline, whose velocity ratio is ϕ_d, stagnates at the wall, the process of recompression will be practically isentropic[6,7]. Hence, for a local wall pressure corresponding to an inviscid value of the Crocco number, where $C_d = C_F \phi_d$,

$$\phi_d = \frac{1}{C_F} \sqrt{\frac{C_F^2 - C_d^2}{1 - C_d^2}} \tag{9}$$

Since the reattachment point of this streamline falls into a region where the adjacent inviscid plume flow-field has not yet fully aligned with the solid wall, the concept of an incomplete turning angle will be utilized.

For a linear velocity profile, the correlation proposed by Page et al.[17] for cases involving mass bleed reduces to a remarkably simple expression:

$$C_{L,P} = \frac{\omega(C_F) - \omega(C_d)}{\omega(C_F) - \omega(C_i)} = 0.59 \tag{10}$$

which is valid over a range of inviscid-boundary Mach number from 1 to 5, i.e. $1 \le M_F \le 5$. In equation (10), $\omega(C)$ is the Prandtl-Meyer function (which depends on the Crocco number) and C_i is the Crocco number for the inviscid flow after the impingement of the inviscid jet and its realignment with the launcher wall.

Equations 1 through 10 can be solved to establish the theoretical operating conditions using information about the base pressure, which is approximately equal to the atmospheric value when the annular gap is vented, and the peak reattachment pressure, which is located a distance:

$$x_i = R_1 (\sin \theta_L - \sin \theta_i) \tag{11}$$

from the nozzle exit-plane. For cases where the secondary flow rates are large, equations 1 through 10 must be supplemented by a relationship between the mass flow rate and the pressure drop in the annular gap. This additional relation for the large flow rates in the annular gap is discussed in Ref. 2.

The viscid pressure rise will start near the location:

$$x_v = R_1 \left\{ \sin \theta_L - \sin \theta_v \left(1 + (\theta_L - \theta_v) \frac{\pi}{180} \frac{\eta_M}{\sigma} \right) \right\} \tag{12}$$

as shown in Fig. 2b. The implicit equation for θ_v

$$\theta_v = \cos^{-1} \left\{ \left(\cos \theta_i - \frac{(\theta_L - \theta_v)\sqrt{\pi}}{180\, \sigma} \phi_d \right) \Big/ \left(1 + \frac{(\theta_L - \theta_v)\pi}{180\, \sigma} \eta_M \right) \right\} \tag{13}$$

has to be solved by iteration.

After plume impingement and alignment of the jet surface with the wall by a reversible compression, the pressure distribution for the inviscid flow configuration can again be reasonably approximated by the formal application of the concept of centered expansions. With the new origin of the centered expansion at the impingement point for the inviscid plume, an ordinary differential equation is obtained for M^* along the wall downstream of the impingement and the resulting pressure distribution can be determined. The mathematical approximations inherent in the method-of-centered-expansions restrict the useful range of the calculated wall-pressure distribution to approximately 1.0 r_t downstream of the impingement.

It is of interest to explore the influence of Reynolds number together with an assessment of the nozzle-wall boundary-layer development. The boundary layer in an axisymmetric, convergent/divergent nozzle can be calculated[18,19,20] at the nozzle lip. Then, for a given Mach number, M_E, one can calculate the development of the dissipative shear layer following the expansion from the nozzle exit. After the transition of the thin laminar sublayer, the turbulent mixing layer grows within the rotational shear layer produced by the expanded nozzle boundary-layer until it reaches its inner edge and then crosses into the "free-stream". Calculations for the present test conditions indicate that the velocity ratio for the discriminating streamline in the shear layer is within five percent of the similarity value, as it approaches reattachment. Thus, the test conditions of the current program provide a reasonable simulation for the prototype reattachment pressure rise.

Of greater concern is the behavior of the reattaching flow due to the strong interaction with its boundary layer. Implied with the concept of incomplete turning of the adjacent inviscid stream is the continuation of the pressure rise beyond the stagnation point within the dissipative layer. This will lead to a thickening of the attached boundary layer and may, of itself, cause a pressure overshoot above the level consistent with the full turning of the external flow.

On the other hand, there will also be a communication withi the boundary layer of the rapid expansion following the plume impingement. These mechanisms are expected to modify the pressure distribution across the reattachment region but in opposing fashion. As a result, pressure peaks determined for the corresponding inviscid jet boundary will generally show reasonable agreement with experimental data even though there may be noticeable, albeit explainable, differences between the theoretically determined and the measured pressure distributions.

Experimental Program

The experimental results presented in this paper were obtained at the Rocket Exhaust Effects Facility located at the Experimental Aerodynamics Laboratory (EAL) of the University of Texas at Austin. Simulated rocket exhaust plumes were obtained by accelerating unheated, compressed air (the test gas) through a convergent/divergent nozzle (the simulated rocket). The nozzle flow was exhausted either into quiescent air or into a constant-area launch tube. A sketch of a typical nozzle/launch-tube configuration is presented in Fig. 3. The simulated launch tubes were mounted on a moveable table, so that the location of the launch tube relative to the exit plane of the simulated rocket nozzle could be varied. For all of the runs in the present test program, the axis of the launch tube was collinear with the axis of the simulated rocket nozzle.

The test schedule included three nozzle geometries and three launch tubes which were combined to give nine different configurations. Since the objective of the present paper is to use the experimental data to validate the theoretical flow model and to establish the limits of its validity, only selected data are presented in this paper. For a more complete discussion of the experimental programs, the reader is referred to refs. 21 and 22.

Simulated Rockets

Simulated rocket exhaust flows were produced by accelerating unheated air through convergent/divergent nozzles. Data are presented for two of the nozzle configurations,

1) a 20° conical convergent/divergent nozzle, designated as C3, and
2) a 10° contoured convergent/divergent nozzle, designated as C5.

The geometries of the nozzle configurations studied in the current program are presented in the equations below.

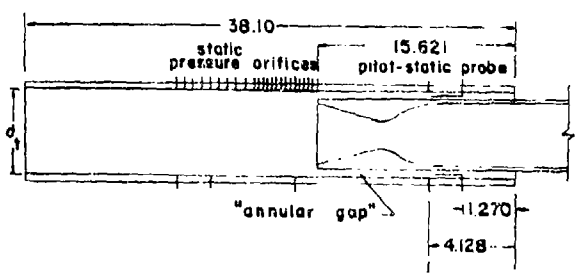

Figure 3. - Sketch of nozzle/launch-tube configurations illustrating the launcher instrumentation (dimensions are in cm).

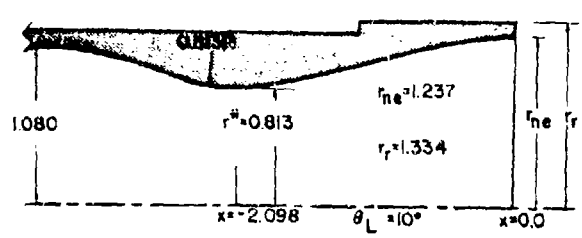

Figure 4. - Sketch of a typical nozzle configuration, C5 nozzle (dimensions are in cm).

The 20° Conical Nozzle, C3:

For $-1.308 \leq x \leq -1.031$:

$$(x + 1.308)^2 + (r - 1.626)^2 = (0.813)^2$$

For $-1.031 \leq x \leq 0.0$:

$$r = 0.759 + 0.364\ (x + 1.308)$$

The 10° Contoured Nozzle, C5:

For $-2.098 \leq x \leq -1.895$:

$$(x + 2.098)^2 + (r - 1.626)^2 = (0.813)^2$$

For $-1.895 \leq x \leq 0.0$:

$$r^2 = 1.530 + 0.434x$$

The equations give the dimensions in centimeters. A sketch of the C5 nozzle is presented in Fig. 4. The throat radius, the nozzle exit-plane radius, and the external radius of the rocket were the same for all nozzles. The cross-section area for all nozzle exit-planes was $A_{ne} = 2.316A^*$. If the acceleration of the flow through the nozzles of this area ratio were isentropic, the Mach number in the nozzle exit-plane would be 2.36 (ref. 23).

Simulated Launch Tubes

The constant-area launch tubes, designated as L1, L2, and L3, were used for the tests (Fig. 3). The inside radius (r_t) for the smooth bored tubes was 1.20 r_{ne} (1.484 cm) for the L1 configuration, 1.275 r_{ne} (1.522 cm) for the L2 configuration, and 1.50 r_{ne} (1.855 cm) for the L3 configuration. Static pressure orifices (0.0635 cm in diameter) were located axially along the tube wall at a spacing of 0.25 r_{ne} (0.309 cm). Additional static pressure orifices spaced 0.50 r_{ne} (0.618 cm) apart were located further downstream.

For each test configuration, i.e., nozzle/launch-tube configuration, two pitot-static probes were located midway between the simulated rocket and simulated launcher wall and 4.128 cm from the upstream end of the launch tube. Static pressure orifices were located in the launch-tube wall at the face of the pitot probes. These pitot-pressure/static-pressure data could be used to "measure" the mass flow rate in the annular gap. The pitot probe was designed so that it could face either upstream or downstream in order to "measure" the mass flow rate in either direction, i.e., ejector flow or blow-by flow.

The Mass Flow Rate

The mass flow rates were calculated using the pressure data from the pitot-static probes located at the upstream end of the annular gap. If one assumes one-dimensional, isentropic flow in the annular gap, and perfect gas properties, then the dimensionless mass flow rate is given by:

$$\frac{\dot{m}_{ag}}{\dot{m}_{ex}} = M_{ag}\sqrt{\frac{T_{t1}}{T_{ag}}}\,\frac{p_{ag}}{p_{t1}}\left\{\frac{(r_t^2 - r_r^2)}{\sqrt{\frac{2}{\gamma+1}}\left(\frac{2}{\gamma+1}\right)^{\frac{1}{\gamma-1}}(r^*)^2}\right\} \qquad (1)$$

For those runs where blow-by occurred, p_{ag} was assumed to be the atmospheric value and the measured pitot pressures were used to calculate M_{ag}. For the ejector flow calculations, the pitot pressures were assumed to be the atmospheric value while measured value of p_{ag} was used in the calculation of the Mach number in the annular gap.

Obturator Rings

For some of the runs, obturator rings were used to seal the base region so that there could be no flow in the annular gap. The obturator ring fit snugly into the annular gap at an x of approximately -1.270 cm i.e., upstream of the nozzle exit plane.

Discussion of Results

Solutions of the theoretical flow-fields have been computed from the transonic region of the nozzle throat, through the nozzle, and through the impingement of the jet-exhaust plume on the launcher-wall. Computed solutions have been obtained both for the C3 and for the C5 nozzles. Thus, the theoretical solutions of the rocket exhaust flow-field represent the effects of the actual nozzle geometries on the overall flow-field. The theoretical solutions will be compared with the experimental data. In some cases, two theoretical solutions representing vary degrees of rigor were generated. In such cases, the theoretical solutions will be compared with each other.

Nozzle Flow Field

The static pressures were measured along the wall of the divergent section of the C5 nozzle for stagnation pressures from 0.7×10^6 N/m^2 to 8.8×10^6 N/m^2. For stagnation pressures of 3.4×10^6 N/m^2, or greater, the values for the ratio p/p_{t1} were a function of position only. The nondimensionalized static-wall-pressure measurements are compared in Fig. 5 with the theoretical values computed using the method of characteristics.

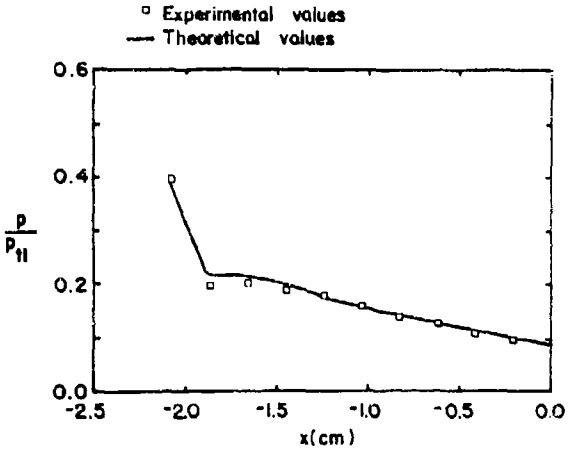

Figure 5. - The static-wall-pressure distribution for the C5 nozzle.

The agreement between the theoretical and the experimental distributions is excellent.

The radial pitot-pressure distributions which result when unheated air is accelerated from a reservoir where p_{t1} is 8.715×10^6 N/m^2 through the C3 nozzle and exhausts into quiescent air are presented in Fig. 6. The theoretical values of p_{t2}/p_{t1} are compared with experimental pitot-pressures for the nozzle exit-plane ($x = 0.0\ r_{ne}$) and for the plane at $x = 0.5\ r_{ne}$. The theoretical values of the pitot pressures were calculated using the local Mach number, which is computed using an isentropic method-of-characteristics solution, to define the stagnation pressure ratio across a normal shock wave (p_{t2}/p_{t1}). The effect of the local flow inclination was not included in the calculation procedure. The effect on the theoretical stagnation pressure ratios presented in Fig. 6 for $x \leq 0.85\ r_{ne}$ should be small, since, as Pope and Goin[24] note, a pitot probe "will be insensitive to angle of attack up to 10 deg for an orifice diameter of only 10 percent of the outside diameter and up to 15 deg for one 98 percent of the outside diameter." The theoretical total-pressure distributions in the nozzle exit-plane are in very good agreement with the experimentally-determined distributions. Referring to the tabulated values of Ref. 23, the total pressures that the Mach number varies from 2.13 near the axis to 2.48 near the wall of the nozzle. Recall that if one assumes that the flow undergoes a one-dimensional acceleration from the sonic throat to the stream tube of the exit-plane, the Mach number would be 2.36. Thus, although the C3 is a conical nozzle, the flow in the nozzle exit-plane is not conical.

For $x = 0.5\ r_{ne}$, the pitot-pressures measured in the internal region are in reasonable agreement with the theoretical values. The theoretical model even predicts the variation which occurs near $r = 0.5\ r_{ne}$. For $r > 0.965\ r_{ne}$, the measured pitot-pressures decrease rapidly with increasing r until near the plume boundary. These data illustrate that since the Mach number is constant along an "inviscid plume boundary", the local Mach number is a maximum at a point between the edge of the core region and the plume boundary.

The theoretical values outside of the core region are calculated using the relations for an axisymmetric Prandtl-Meyer expansion and those are in very good agreement with the experimentally-determined distributions. Referring to the tabulated values of Ref. 23, the total

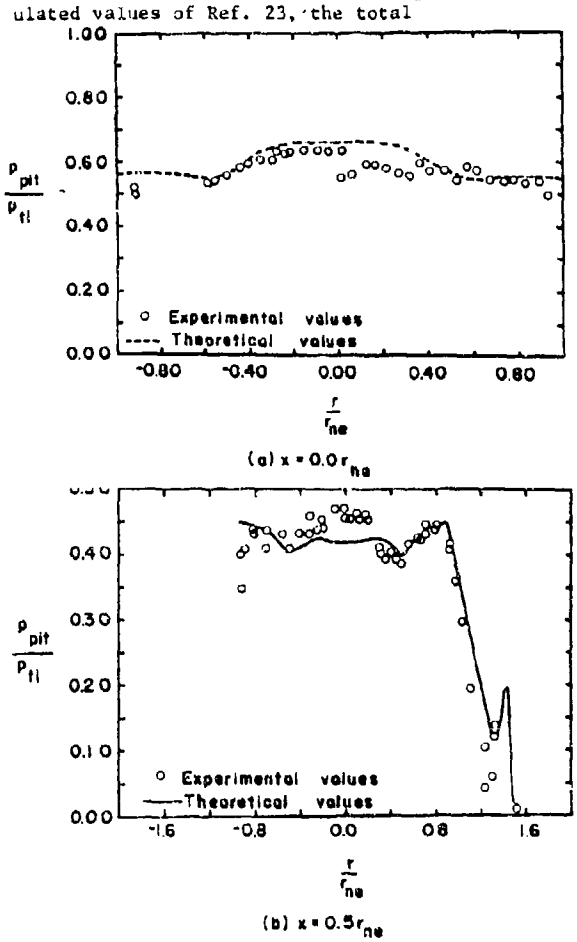

Figure 6. - Radial pitot-pressure distributions for the C3 nozzle exhausting into quiescent air, $P_{t1} = 8.715 \times 10^6$ N/m^2

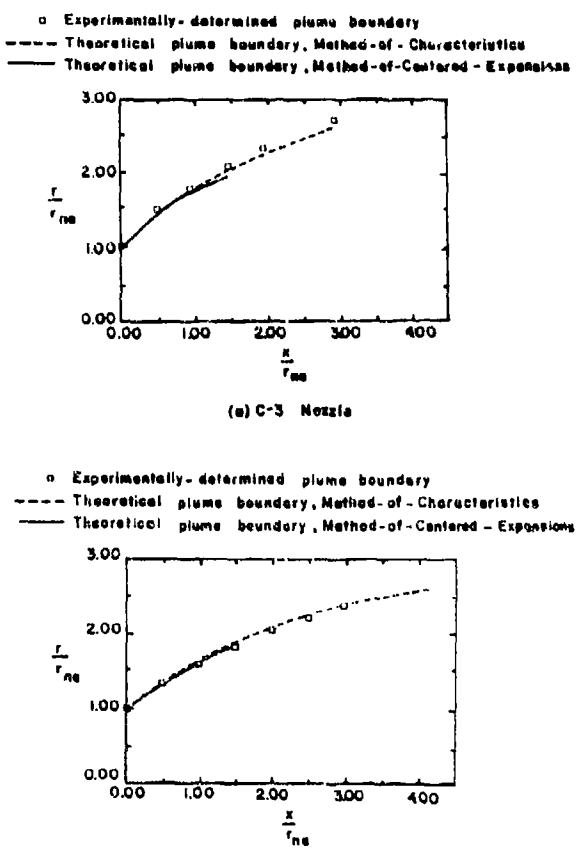

Figure 7. - A comparison of the computed and experimentally-determined plume boundaries.

for a linear velocity variation in the mixing layer. Local flow inclinations as great as 37° cause the theoretical values which do not account for the local flow inclination to exceed the measured values. Note also that the jet mixing region is narrow, leading to uncertainty in the correlations in a high gradient region. Nevertheless, the correlation between the theoretical and the experimental values is considered good.

When the stagnation pressure is 8.715×10^6 N/m^2, the static pressure in the nozzle exit-plane is roughly six times the atmospheric value. Thus, as the exhaust gases leave the nozzle, they accelerate rapidly until the pressure along the plume boundary is equal to the static pressure of the surrounding gas. The plume boundaries for the C3 (20° conical) and for the C5 (10° contoured) nozzles, as calculated using the method-of-characteristics, are presented in Fig. 7. The plume boundaries computed using the method-of-characteristics are in excellent agreement with those observed in the schlieren photographs of the nozzle exhausting into quiescent air. This is true for both of these nozzles, which are of considerably different geometries.

The correlation between the theoretical and the experimentally-determined flow-fields indicates that the nozzle-exhaust flow-field can be well modeled analytically. Thus, the method-of-characteristics for axisymmetric flow provides an acceptable tool even when no direct provisions are made for the occurence of internal shocks. As will be seen, the plume impingement and the initial wall-pressure rise will be described with sufficient accuracy by the method-of-characteristics followed by plane shock relations.

The internal radii of the launch tubes used in the present test program are from 1.2 r_{ne} to 1.5 r_{ne}, depending on the launch-tube configuration. Since the developing shear layer is relatively short, the ensuing viscous/shock-interaction structure at the wall is very dependent on the expansion process as the flow leaves the nozzle.

For the relatively small values of r_t/r_{ne} of interest in tube-launched-rocket applications, it is necessary to model the plume boundary only for a short distance. Thus, the calculation of the inviscid plume boundary by a technique which provides quick but reasonable contours becomes attractive. The theoretical plume boundaries have been calculated using the method-of-centered-expansions[8,9]. These approximate plume boundaries are compared with those calculated using the more rigorous method-of-characteristics and with the data in Fig. 7. Note that the plume boundary calculated using the method-of-centered-expansions is very close to the actual boundary for both nozzles. Thus, the inviscid plume boundaries calculated using the method-of-centered-expansions provide a close approximation of the actual plume boundaries, making the method attractive for use in generating quick calculations of the plume impingement flow. However, at a given x-location, the local flow angle at the plume boundary calculated using the method-of-centered-expansions is slightly less than the actual flow angle which will affect the subsequent correlations.

Launch-Tube Flow-Fields

When a highly underexpanded supersonic nozzle exhausts into a constant-area tube, the viscous/shock-wave interaction due to the impinging flow is subject to a boundary condition in the base region. If the annular gap between the rocket and the launch-tube wall is open, i.e., vented, the atmospheric pressure at the forward end of the vented annular gap forms the boundary condition. The direction and the magnitude of the secondary flow which is usually generated by the impingement interaction is controlled by this boundary condition. If the mass flow rate of the secondary flow in the annular gap is relatively low, the pressure will vary only slightly along the annular gap. Thus, the static pressure in the base region will be approximately equal to the atmospheric value. However, if the annular gap is sealed, the pressure in the base region will assume a value such that the viscous/shock-wave interaction at impingement creates a "constant-mass" recirculating flow in the base region.

Pressure distributions for the launch-tube flow-fields with the annular gap sealed by an oburator ring. - Over a wide range of stagnation pressure, the ratio p_b/p_{t1} is essentially independent of the stagnation pressure when the annular gap is sealed. That the pressure ratio p_b/p_{t1} should be constant for a given configuration for a fully developed supersonic flow is well documented, e.g., refs. 22, 25, and 26. Korst et al[27] have shown that the equilibrium (or steady-state) value of the base pressure is governed by the viscous shear-layer at the boundary of the nozzle exhaust plume that bounds the "dead-air" base-flow region and by the physical geometric

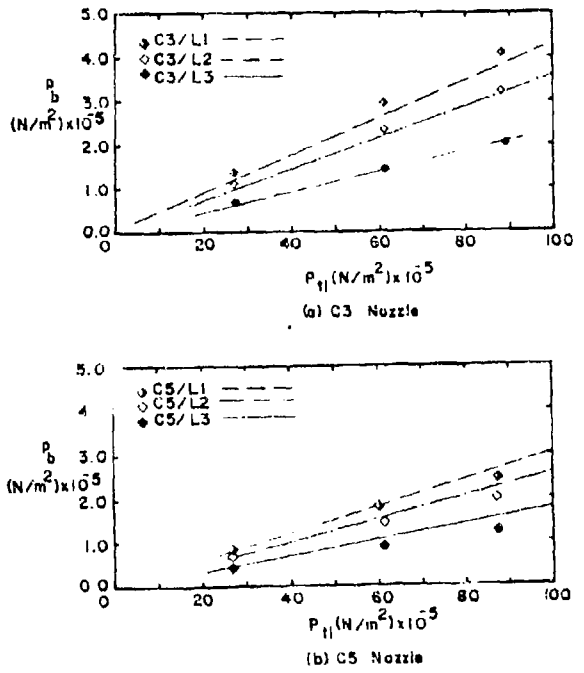

Figure 8. - A comparison of the theoretical and the experimental base pressure with the base region sealed by an obturator ring (i.e., $\dot{m}_{ag} = 0$)

constraints. The theoretical values of the base pressure are presented for the C3 and the C5 nozzles in Fig. 8 for all three launch tubes for stagnation pressures from 2.5 x 10^6 N/m^2 to 8.8 x 10^6 N/m^2.

The experimental values of the static wall-pressure vary only slightly with x in the region between the obturator ring (small negative x-coordinate) and the intersection of the exhaust plume with the launcher wall, reaching a minimum just before the impingement-induced pressure rise. This is illustrated by the data presented in Figs. 9 and 10. For the purposes of the present paper, the static wall-pressure sensed by the orifice located at x = 0.0 r_{ne} (i.e., in the plane of the nozzle exit) is designated as the base pressure.

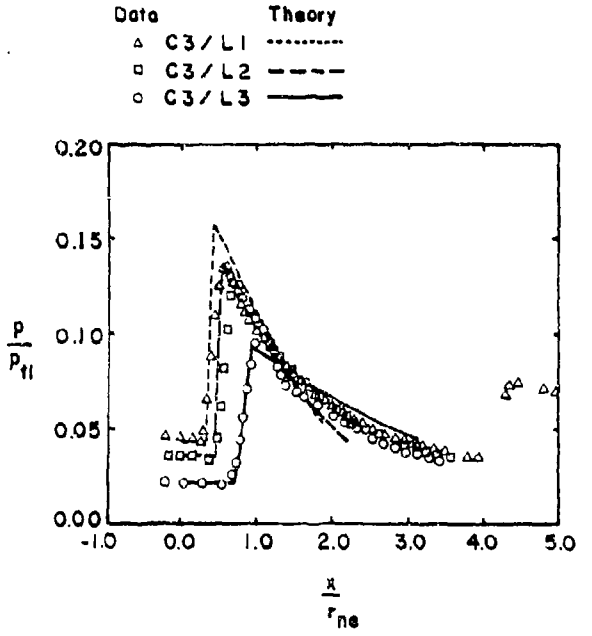

Figure 9. - The effect of launch-tube radius on the static wall-pressure distributions, C3 nozzle with an obturator ring, p_{t1} = 8.715 x 10^6 N/m^2.

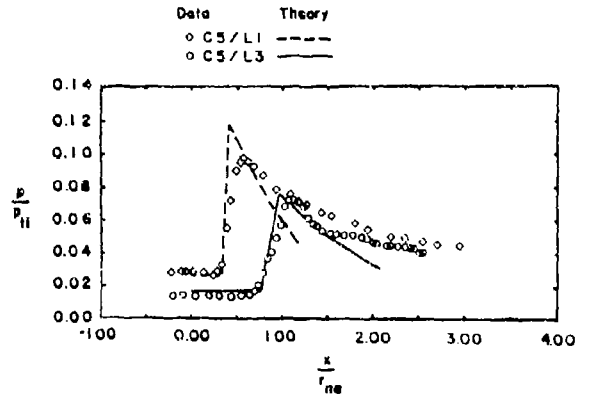

Figure 10. - The effect of launch-tube radius on the static wall-pressure distributions, C5 nozzle with an obturator ring, p_{t1} = 8.715 x 10^6 N/m^2.

The experimental values of p_b are presented in Fig. 8. Since they are a linear function of p_{t1}, the ratio p_b/p_{t1} is constant for a given configuration. Furthermore, they compare very well with the theoretical values for both nozzles.

The static-pressure distributions in the vicinity of the plume impingement have been computed for flows with the annular gap sealed by an obturator ring. The pressure distributions for unheated air accelerating from a reservoir where p_{t1} is 8.715 x 10^6 N/m^2 through the C3 nozzle into the constant-area launch-tubes are presented in Fig. 9. Similar solutions for the C5 nozzle are presented in Fig. 10. The theoretical solutions are compared with experimental data for these nozzle/launch-tube configurations. Note, that as the tube radius is increased from 1.20 r_{ne} (the L_1 tube) to 1.50 r_{ne} (the L3 tube), the base pressure decreases and the location of the peak pressure moves further downstream of the nozzle exit-plane. However, as the base pressure decreases, the angle through which the plume boundary expands at the nozzle exit-plane increases. As a result, the pressure ratio across the impingement shock-wave (i.e., the peak static-pressure divided by the base value) increases as r_t increases.

For both nozzles, the theoretical value of the peak pressure in the impingement region is significantly greater than the corresponding experimental value for the L1 launch-tube. Because of the small difference between r_t and r_{ne}, the free-shear layer at the plume boundary is relatively short and the flow deceleration associated with the impingement process significantly modifies the viscous/shock-wave interaction. The modification is not reflected in the theoretical flow model and, thus, the peak pressure is overestimated by the theory. However,

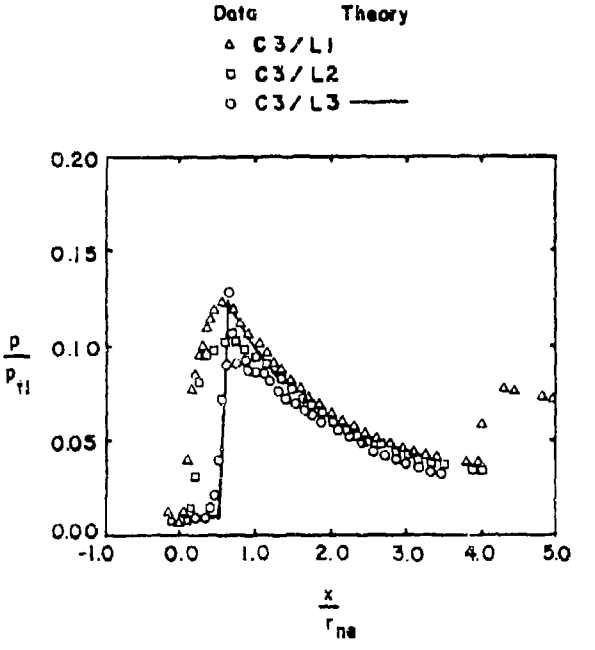

Figure 11. - The effect of launch-tube radius on the static wall-pressure distributions, C3 nozzle without an obturator ring, p_{t1} = 8.715 x 10^6 N/m^2. (note: blow-by occurs)

the agreement between the theoretical and the experimental values is much better for the L3 launch-tube. The improvement in the correlation for the larger-radius launch-tube is attributed to compensating effects of approximations in the theoretical flow model.

Pressure distributions for the launch-tube flow-fields with a vented annular gap. - As noted earlier, if the mass flow rate of the secondary flow in the annular gap is relatively low, the pressure will vary only slightly along the annular gap. Since the static pressure in the nozzle exit-plane (p_{ne}) is directly proportional to the stagnation pressure, while the base pressure (p_b) remains roughly constant, the jet pressure ratio (p_{ne}/p_b) varies with p_{t1}. Thus, the viscous/shock-wave interaction depends on the stagnation pressure as well as the nozzle/launch-tube configuration.

The effect of the launch-tube is indicated by the pressure distributions presented in Figs. 11 and 12 for the largest value of p_{t1}. Since the base pressure is approximately constant, the shape of the plume boundary would be independent of the launch-tube radius, if the flow were inviscid. If the shape of the plume boundary were indeed independent of the launch-tube radius, as r_t decreased, the intersection of the plume boundary and the wall would be nearer the nozzle exit. Thus, the impingement shock-wave would move upstream and increase in strength as r_t decreases.

These trends are substantiated by both the theoretical and the experimental pressure distributions for the nozzle/launch-tube configurations using the C5 nozzle, which are presented in Fig. 12. As was the case for the flow fields with the obturator ring, the correlation between theory and experiment is better for the larger radius launch-tube, the L3. As before, the theoretical model of the shear layer does not reflect the interaction between the approaching free shear-layer and the pressure rise of the impingement shock-wave. However, as was shown in Fig. 7, the method-of-centered-expansions, which is used to provide the approximate inviscid plume boundary, yields plumes for which the local flow angle at the plume boundary is slightly less than the actual flow angle. Because these two flow-model approximations tend to compensate each other, the theoretical values of the peak pressure are in very good agreement with the data for these flow/geometry conditions.

Although experimental pressure distributions are presented for all three C3/launch-tube configurations, a theoretical distribution is presented only for the C3/L3. Theoretical solutions were not possible for the C3/L1 or for the C3/L2 configurations with the present flow model, since the local flow inclination at the plume boundary intersection with the launcher wall exceeds the value which can be turned through a weak shock-wave. This contrasts the flow fields for the sealed annular gap. Recall that theoretical pressure distributions were presented in Fig. 9 for all three launch tubes when the annular gap was sealed by an obturator ring. As shown in Fig. 8a, the base pressure is considerably greater than the atmospheric value, when the annular gap is sealed, and the expanding flow turns through a smaller angle as it leaves the nozzle. Therefore, with an obturator ring in place, the local flow inclination of the impinging plume is such that the impingement shock wave is weak.

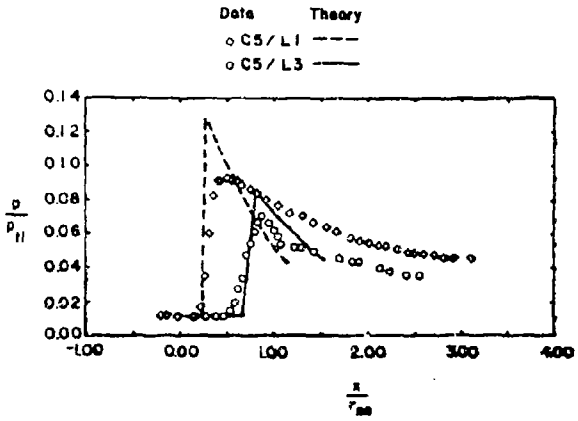

Figure 12. - The effect of launch-tube radius on the static wall-pressure distributions, C5 nozzle without an obturator ring, $p_{t1} = 8.715 \times 10^6$ N/m^2. (note: blow-by occurs)

Although the theoretical solutions indicate the weak impingement shock-waves are not possible for the C3/L1 or the C3/L2 configurations, the maximum measured values of the pressure are not large enough to indicate the presence of a strong shock-wave. Thus, these pressure distributions indicate a relatively strong interaction between the impingement shock-wave and the free-shear layer at the plume boundary. For the two smaller-radius tubes, the streamwise pressure-gradient along the launcher wall is not constant in the impingement region. As was discussed in ref. 22, the relatively strong viscous/shock-wave interaction which occurs for this nozzle/launch-tube configuration at high stagnation pressures produces significant blow-by flow.

Secondary flows. - As the rocket exhaust entrains base-region air, a free-shear layer develops along the plume boundary, accelerating air from the base-region and decelerating exhaust gas. When this free-shear layer encounters the adverse pressure

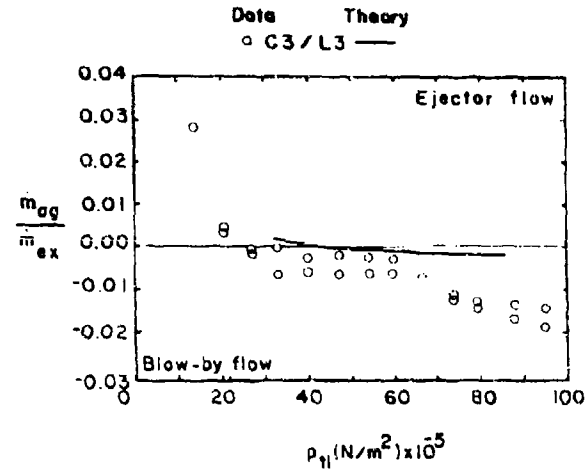

Figure 13. - The mass flow rate in the annular gap ($\dot{m}_{ag}$) as a function of stagnation pressure for C3 nozzle.

gradient associated with the impingement shock-wave, some of the flow passes through the shock wave, some of it is turned back. As discussed in Fig. 1, if the stagnation pressure is relatively low, the system acts as an ejector with some of the entrained air passing through the impingement shock-wave. As the stagnation pressure is increased, the ratio p_{ne}/p_b increases and the flow expands through a larger angle as it leaves the nozzle. As a result, the strength of the impingement shock increases. Once the impingement shock is sufficiently strong, the resultant adverse pressure gradient causes a fraction of the exhaust flow to be turned upstream (blow-by flow).

Theoretical and experimental values of the secondary flow rates are presented as a function of the stagnation pressure in Figs. 13 and 14. For all three configurations, theory provides a good prediction of the stagnation pressure for which there is no flow in the annular gap. However, the theory provides reasonable estimates of the secondary flow rates only for relatively low flow rates. This is evidenced by the comparison between data and theory for the C3/L3 configuration, which deteriorates as p_{t1} increases above 6×10^6 N/m^2.

This result should not be surprising. As has been often noted, the theoretical model of the shear layer does not reflect the interaction between the approaching free shear-layer and the pressure rise of the impingement shock-wave. Both of these approximations contribute to the limitation of the flow model to the prediction of the lower secondary flow rates. As the model is presently formulated, the secondary flows are only carried between streamlines within the linear mixing profile. Thus, the model is not applicable to high secondary flow rates.

For the C5/L1 configuration, the theory provides a reasonable approximation of the crossover value of the stagnation pressure but does not come close to the blow-by flow rates, as shown in Fig. 14. Part of the difference may be experimental. Since

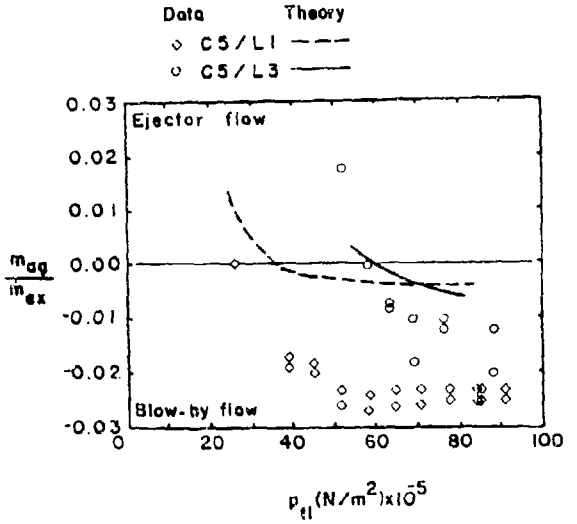

Figure 14. - The mass flow rate in the annular gap ($\dot{m}_{ag}$) as a function of stagnation pressure for C5 nozzle.

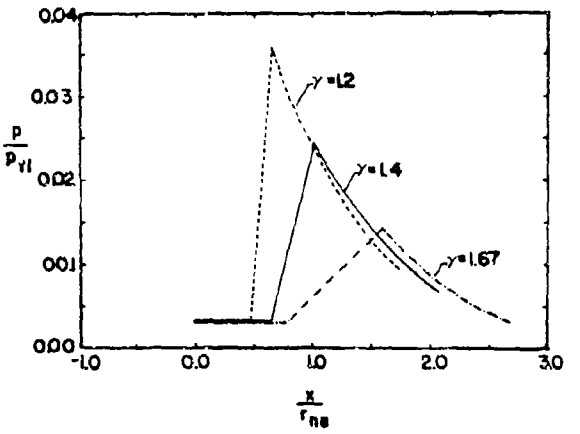

Figure 15. - The effect of γ on the static wall-pressure distribution.

the diameter of the pitot probe was approximately 50% of the width of the annular gap for the L1 tube configuration, inaccuracies in the total pressure measured by the pitot probes may contribute to significant experimental errors. Nevertheless, the theoretical flow model provides a reasonable estimate of the stagnation pressure required for zero secondary flow.

The correlation between the computed solutions and the experimental data demonstrates that the flow model provides a reasonable approximation for exhaust flows where the impingement shock wave is relatively weak and the downstream flow remains supersonic. Thus, the computed solutions can be used to investigate the relation between the launch-tube flow-field and various flow parameters. The effects of the nozzle configuration and of the stagnation pressure (or Reynolds number) on the impingement flow-fields have already been discussed. The effect of the specific-heat ratio on the static-pressure distribution along the launcher wall is illustrated by the computed solutions presented in Fig. 15. These solutions are for a conical nozzle (θ_l = 12.4° and M_{ne} = 1.8) exhausting into a launch tube for which $r_t = 1.47\ r_{ne}$. The computed solutions indicate that the peak value of the impingement-induced pressure rise is sensitive to the specific-heat ratio.

Concluding Remarks

An engineering model has been developed to describe the impingement flow field which is produced when an underexpanded supersonic nozzle exhausts into a constant-area tube. Solutions of the theoretical flow-fields have been computed from the transonic region of the nozzle throat, through the nozzle, and through the impingement of the exhaust plume on the launcher wall. The theoretical solutions have been compared with experimental data. Based on the correlations between the data and the theory, the following conclusions are made.

1. The corralations between the theoretical and the experimentally-determined flow-fields in the nozzle and of the free exhaust plume indicate that the nozzle-exhaust flow-field can be well modeled analytically.

2. With the annular gap sealed by an obturator ring, the theoretical model closely predicts the static pressure in the "dead-air" base region. The theoretical and the experimental static wall-pressure distributions in the impingement region are in reasonable agreement, with the best correlation for the relatively large-radius tube.

3. For the vented annular-gap configurations, the theoretical wall-static pressure distributions in the impingement region again are in reasonable agreement with the data, providing the impingement shock-wave can be calculated using the weak, oblique, shock-wave relations.

4. The theoretical flow model provides a reasonable estimate of the reservoir (stagnation) pressure for which there is no secondary flow in the annular gap. However, the theoretical flow model represents the actual flow-field only when the secondary flow can be accomodated within the linear mixing profile.

References

1. J.J. Bertin, and J.L. Batson, "Comparison of Cold-Gas Simulations and Rocket-Launch Data for Constrictive Launchers," Journal of Spacecraft and Rockets, Vol. 13, No. 11, Nov. 1976, pp. 684-691.

2. H.H. Korst, T.L. Butler, and M.B. Briski, "Simulation of Jet Plume Interference Effects During the Launch Phase of Missiles", AIAA Paper No. 79-1292, presented at the AIAA/SAE/ASME 15th Joint Propulsion Conference, Las Vegas, June 1979.

3. Staff, "Non-Tipoff Tube Launcher Flight Test Program," Report Number 7-52100/3R-61, LTV Aerospace Corp., Michigan Div., Dec. 1973.

4. W.H. Appich, Jr., and E.D. Tipping, "Free-Rocket Trajectory Errors from Plume-Induced Loading During Tube Launch," Journal of Spacecraft and Rockets, Vol. 14, No. 10, Oct. 1977, pp. 614-620.

5. D.W. Barnette, J.J. Bertin, and J.L. Batson, "Free-Flight Rocket's Initial Trajectory as Affected by Massive Blow-by", Journal of Spacecraft and Rockets, Vol. 15, No. 6, Nov.-Dec. 1978, pp. 334-340.

6. H.H. Korst, "A Theory for Base Pressures in Transonic and Supersonic Flow", Journal of Applied Mechanics, Vol. 23, 1956, pp. 593-600.

7. P. Carriere, M. Sirieix, and J. Delery, "Methodes de Calcul des Ecoulements Turbulents Decolles en Supersonique" Progress in the Aerospace Sciences, Pergamon Press, Vol. 16, No. 4, 1975, pp. 385-429.

8. N.H. Johannesen and R.F. Meyer, "Axially-Symmetrical Supersonic Flow Near the Centre of an Expansion", The Aeronautical Quarterly, Vol. 2, Aug. 1950, pp. 127-142.

9. H.H. Korst, "Analytical Concepts for the Modeling of Propulsive Jet Plume Interference Effects", ULIU ENG 77-4010, Sept. 1977, The University of Illinois Experiment Station.

10. J.R. Kliegel and J.N. Levine, "Transonic Flow in Small Throat Radius of Curvature Nozzles", AIAA Journal, Vol. 7, No. 7, July 1969, pp. 1375-1378.

11. H.H. Korst and R.A. Deep, "Modeling of Plume Induced Interference Problems in Missile Aerodynamics", AIAA Paper No. 79-0362, presented at the 17th Aerospace Sciences Meeting, New Orleans, Jan. 1979.

12. P.M. Gerhart and H.H. Korst, "On the Free Shear Layer Downstream of a Backstep in Supersonic Flow", Journal of Fluids Engineering, ASME, Vol. 95, Series 1, No. 3, 1973, pp. 361-366.

13. R.A. White, "Effect of Sudden Expansions or Compressions on a Turbulent Boundary Layer", AIAA Journal, Vol. 4, No. 12, Dec. 1966, pp. 2232-2234.

14. H.H. Korst and W.L. Chow, "Non-Isoenergetic Turbulent (Pr_t = 1) Jet Mixing Between Two Compressible Streams at Constant Pressure", CR-419, Apr. 1966, NASA.

15. H.H. Korst and W.L. Chow, "On the Correlation of Analytical and Experimental Free Shear Layer Similarity Profiles by Spread Rate Parameters", Journal of Basic Engineering, Trans. ASME, Series D, Vol. 93, 1971, pp. 377-382.

16. W. Tripp and H.H. Korst, "The Pressure on a Blunt Trailing Edge Separating Two Supersonic Two-Dimensional Air Streams of Different Mach Numbers and Stagnation Pressures, but Identical Stagnation Temperatures", Proceedings, 5th Midwestern Conference on Fluid Mechanics, University of Michigan, Ann Arbor, 1967.

17. R.H. Page, W.G. Hill, and T.J. Kessler, "Reattachment of Two-Dimensional Supersonic Turbulent Flow", ASME Paper 67-FE-20, 1967.

18. D.R. Bartz, "Turbulent Boundary Layers in Cooled, Convergent-Divergent Nozzles, ASME Transactions, Vol. 75, pp. 1235-1245, 1955.

19. H.H. Korst, "Effect of Turbulent Boundary Layer in Cooled C-D Nozzles on Plume Modeling", Final Report for Task Order 76-207, University of Illinois at Urbana-Champaign, Feb. 1976.

20. T.L. Butler, "Simulation of Jet Plume Interference in Cases of Dissimilar Specific Heat Ratio", M.S. Thesis, Department of Mechanical and Industrial Engineering, University of Illinois at Urbana-Champaign, 1976.

21. J.J. Bertin, S.J. Sutter, Jr., D.P. Dannemiller, and D.L. Booker, "A Comparison of Theoretical and Experimental Flow Fields for an Underexpanded Rocket Exhaust", AIAA Paper 79-0340, presented at the 17th Aerospace Sciences Meeting, New Orleans, Jan. 1979.

22. J.J. Bertin, E.S. Idar, and D.L. Booker, "Secondary Flows for a Tube-Launched Rocket Configuration", AIAA Paper 80-0372 presented at the 18th Aerospace Sciences Meeting, Pasadena, Ca., Jan. 1980.

23. Staff, "Equations, Tables, and Charts for Compressible Flow", Report 1135, 1953, NACA.

24. A. Pope and K.L. Goin, High-Speed Wind Tunnel Testing, J. Wiley and Sons, 1965, New York.

25. J. Fabri and R. Siestrunck, "Supersonic Air Ejectors", Advances in Applied Mechanics, Vol. V, Academic Press, Inc., 1958, New York, pp. 1-34.

26. R.C. German, R.C. Bauer, and J.H. Panesci, "Methods for Determining the Performance of Ejector-Diffuser Systems", Journal of Spacecraft and Rockets, Vol. 3, No. 2, Feb. 1966, 193-200.

27. H.H. Korst, W.L. Chow, and G.W. Zumwalt "Research on Transonic and Supersonic Flow of a Real Fluid at Abrupt Increases in Cross-Section (With Special Consideration of Base Drag Problems -- Final Report", Report No. ME-TN-392-5, Dec. 1959, The University of Illinois.

APPENDIX L

LAUNCH-TUBE FLOWFIELD TECHNOLOGY BASED ON COLD-GAS SIMULATIONS, FLIGHT TEST MEASUREMENTS AND THEORETICAL MODELS

Paper presented at the

Symposium on Rocket/Plume Fluid Dynamic Interactions

Huntsville, Alabama

April 1983

by

J. J. Bertin and H. H. Korst

APPENDIX L

LAUNCH-TUBE FLOW-FIELD TECHNOLOGY BASED ON COLD-GAS SIMULATIONS, FLIGHT-TEST MEASUREMENTS AND THEORETICAL MODELS

John J. Bertin
Bettie Margaret Smith Professor of Engineering
The University of Texas at Austin
Austin, Texas

and

Helmut H. Korst
Professor of Mechanical and Industrial Engineering
The University of Illinois at Urbana-Champaign
Urbana, Illinois

SUMMARY

Since there are a wide variety of tube-launched military rockets, the designer needs to have a basic understanding of the flow-field produced when a highly underexpanded nozzle exhausts into a tube. To understand the resultant flow field, one must be able to model the viscid/inviscid interactions that take place because the exhaust plume is confined by the launcher walls. Important parameters for modeling the exhaust plume include: the nozzle-exit angle, the nozzle-exit Mach numbers, γ of the gas, the jet expansion ratio, and the radius of curvature of the plume.

The impingement shock-wave may be weak (oblique with the downstream flow remaining supersonic) or strong (normal with the downstream flow becoming subsonic). When the impingement shock-wave is weak, there is relatively little blow-by flow. The large adverse pressure gradient associated with the strong shock wave causes a significant fraction of the exhaust gas to be turned upstream into the annular gap between the rocket and the launch-tube wall. This "massive blow-by" flow can produce significant asymmetric pressure forces that markedly alter the trajectory of the rocket.

In many designs, the launch tube is not of constant area. Rails, frangible bore riders, or different diameter tubes may be used to constrain the missile while it builds up speed and angular momentum. These constrictions to the exhaust flow in a nontipoff launch tube may radically alter the flow field. Important geometry parameters for a nontipoff launch-tube include: the geometry of the constriction, the aft-tube radius, the forward-tube radius, the length of the aft tube, and the length of the forward tube. The constrictive area ratio has a significant influence on the impingement shock-structure. If the aft-tube cross section is smaller than a second throat, the exhaust flow is choked by the constriction and a strong impingement shock wave follows the nozzle-exit motion.

The forward-facing surface in a nontipoff launch-tube can produce significant "transients" in the flow field. "Puffs" of blow-by can

occur as the exhaust splashes back from the obstruction. As the missile moves away from the step (or constriction), the flow field is similar to that for an isolated step in a supersonic stream.

The present paper reviews the launch-tube flow-fields that result when a highly underexpanded supersonic nozzle exhausts into a launch tube. Data from a wide variety of cold-gas simulations and from two flight-test programs are used to develop flow models for a wide variety of design applications.

NOMENCLATURE

The following are the commonly used symbols of this paper. The reader should refer to the cited reference for the meaning of symbols to which only a single reference is made.

A	Cross-section Area
d	Diameter
f	Friction factor
L	Length
M	Mach number
$\dot{m}_{ag}$	Mass flow-rate in the annular gap
$\dot{m}_{ex}$	Exhaust mass flow-rate (also $\dot{m}_{ne}$)
p	Pressure
r	Radius, measured perpendicular to the centerline of the launch tube
R_1	Initial radius of curvature of the inviscid plume boundary
T	Temperature
u	Streamwise velocity component
x	Axial distance along the centerline of the launch tube, measured from the change in cross section
$\bar{x}$	Axial distance along the centerline of the missile (or launch tube), measured from the nozzle exit plane
γ	Ratio of specific heats
ε	Flow inclination relative to the centerline of the launch tube
ζ	Dimensionless velocity ratio

Subscripts

aft	Aft tube of the launcher
ag	Denotes static properties evaluated at the upstream end of the annular gap
b	Denotes static properties in the base region
d	Discriminating (dividing or stagnating) streamline
eq	Equivalent passage diameter
ex	Flow through the nozzle exit-plane, i.e., the exhaust flow
F	Free-jet surface (inviscid plume boundary)
for	Forward tube of the launcher
g	Gage location
i	Denotes properties evaluated at the intersection of the inviscid plume boundary and the launcher wall
j	Zero streamline, i.e., that dividing the exhaust flow from the base air or relating to the jet boundary
L	Denotes local conditions at the lip of the nozzle exit-plane
ne	Denotes properties evaluated in the nozzle exit-plane
pit	Pressure measured using a pitot probe collinear with the launcher-tube axis
pk	Denotes peak values
r	Outer surface of the rocket
t	Inner surface of the launch tube or stagnation temperature
t1	Denotes properties evaluated in the stagnation chamber of the simulated rocket
t2	Denotes properties downstream of a normal shock wave
v	Beginning of viscous interaction or vent
2s	Static conditions downstream of a weak shock wave

Superscript

*	Sonic flow conditions

This page is blank.

INTRODUCTION

Various military rockets are launched from tubes. The designer of a tube-launched rocket system must consider the possibility of unbalanced forces acting on the rocket that are caused by flow in the annular gap between the rocket and the launcher wall. Barnette et al.[1] have shown that the trajectory of a tube-launched rocket can be significantly affected by the unbalanced forces associated with this secondary flow. To predict the magnitude and the direction of the flow in the annular gap, one must be able to describe the exhaust plume of the rocket and the viscous/shock interaction structure that results when the plume encounters the launcher wall. The strength of the impingement shock wave and the characteristics of the viscous interaction at the wall depend on the structure of the exhaust plume and on the geometry of the launch tube.

When there is negligible secondary flow, the pressure in the annular region between the rocket and the launcher wall varies only slightly and is approximately equal to the atmospheric value. The pressure downstream of the weak, impingement shock wave is much greater than the pressure at the forward end of the launch tube (i.e., the atmospheric value). Thus, pressure in the impingement region is greater than that at the forward end of the launcher. Nevertheless, experimental measurements[2] obtained in the Rocket Exhaust Effects Facility at the University of Texas at Austin indicate that, when the stagnation pressure is relatively low, air from outside of the launcher can be drawn into the annular region toward the exhausting jet. Thus, at these conditions, the exhaust gases have sufficient momentum and the shock is sufficiently weak so that the system acts as an ejector. This is true even when the pressure downstream of the shock wave is approximately five times the base pressure. A sketch of a possible flow model for the ejector-type performance of the system is presented in Fig. 1a. As the underexpanded nozzle flow accelerates into the straight launch tube it entrains air from the base region. A fraction of the entrained air is given sufficient momentum so that it passes through the impingement shock wave. Using the atmosphere at the upstream end of the launcher as its source, a low velocity flow develops in the annular region to supply the mass flow-rate of air that is carried through the shock wave. Note, the static pressure in the annular region is below the atmospheric value. A fraction of the air entrained by the exhaust plume does not gain sufficient momentum to pass through the shock wave. When this fluid encounters the adverse pressure gradient associated with the impingement process, it is turned upstream and recirculates in a separation "bubble" near the launcher wall. Thus, as indicated in the sketch of Fig. 1a, the dividing streamline may be traced into the annular region between the rocket and the launcher wall.

As the stagnation pressure is increased, the ratio P_{ne}/P_b increases and the flow expands through a larger angle as it leaves the nozzle. As a result, the Mach number of the exhaust flow and the angle at which it encounters the wall increase, causing the impinge-

ment shock wave to become stronger. Once the impingement shock wave becomes sufficiently strong, the resultant adverse pressure gradient causes a fraction of the exhaust to be turned upstream, as shown in Fig. 1b. The exhaust that is turned upstream is known as blow-by flow. Since the flow in the annular gap originates at the shock impingement and exhausts to the atmosphere at the upstream end of the launcher, the static pressure in the annular gap is greater than the atmospheric value.

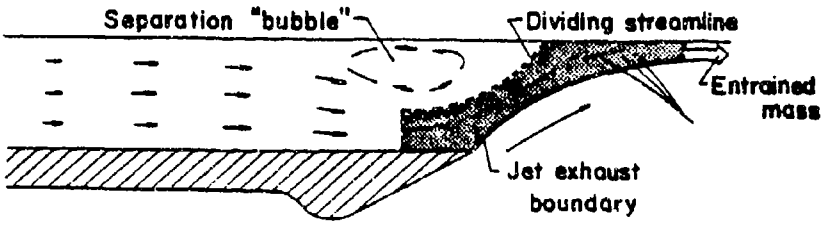

Launcher centerline

Shaded region designates air entrained from the base region which is given sufficient momentum to pass through the impingement shock wave.

(a) System acts as an ejector

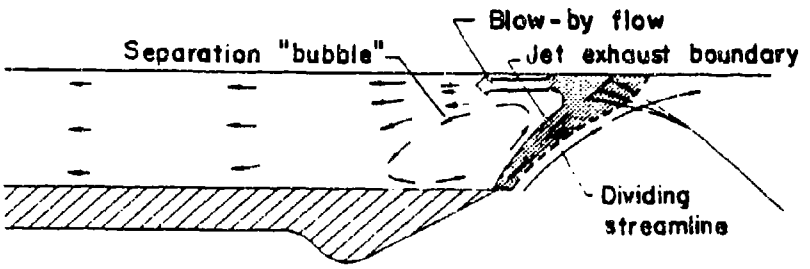

Launcher centerline

Shaded region designates that fraction of the exhaust flow which does not have sufficient momentum to pass through the impingement shock wave.

(b) System produces nominal blow-by flow

Figure 1. - Sketch of the viscid/inviscid interaction flow-fields for a weak impingement shock wave.

For both of these flows, the flow downstream of the impingement shock wave accelerates and the static pressure at the wall decreases until the shock wave, generated when the jet exhaust impinges on the wall, crosses the launch tube and strikes the opposite wall. Across the reflected shock wave, there is a sudden increase in the static wall pressure and a sudden decrease in the Mach number and in the total pressure. As the shock wave reflects back and forth across the tube, it becomes progressively weaker. The distance between the impingement points decreases (since the shock wave angle increases as the Mach number just upstream of the shock wave decreases). Since the mass flow rate in the annular gap ($\dot{m}_{ag}$) is a relatively small fraction of that exhausting through the nozzle ($\dot{m}_{ex}$) for the two cases represented in Fig. 1, the flow in the annular gap shall be termed a "secondary flow".

The stagnation pressure can be increased until the Mach number of the exhaust flow and the angle at which it encounters the wall are such that a weak shock wave cannot exist. For these conditions, the impingement shock wave is strong, and the flow downstream of the shock wave is subsonic, as shown in Fig. 2. The very large adverse pressure gradient associated with the strong shock wave can cause over 10 percent of the exhaust flow to be turned upstream into the annular gap[3]. The large pressure gradient required to change the flow direction of a large fraction of the exhaust gases in a relatively short distance "magnifies" the inherent asymmetries in the exhaust flow field. Thus, massive blow-by flow may cause large pressure differentials to act on the missile. Since these pressure differentials are relatively large and act near the nozzle-exit plane, they create a very large moment about the center of gravity. As a result, the missile pitches in an oscillatory motion during that portion of the launch when the missile is in free flight in the launch tube.

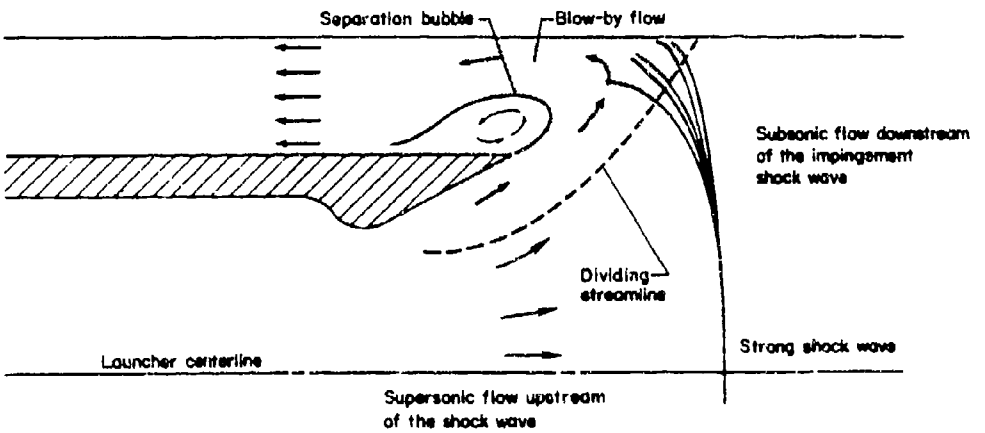

Figure 2. - Sketch of the viscid/inviscid interaction flow field for a strong impingement shock wave.

When an underexpanded, supersonic nozzle exhausts into a constant-area tube, the strength of the impingement shock wave depends on the Mach number of the inviscid flow along the inner edge of the mixing zone at the jet boundary, on the ratio of specific heats, on the inclination of the impinging flow relative to the launcher wall, and on the velocity profile in the mixing zone. However, many launch tubes are such that their cross-section area does not remain constant. The presence of rails, frangible bore riders, and changes in the cross-section serve as constrictions to the exhaust flow. Constrictions located in the exhaust flow downstream of the nozzle can produce dramatic changes in the launch-tube flow field. If the reduction in cross-section area due to the constriction is relatively large, the constriction (or the constrictive section) may serve as a second throat, choking the exhaust flow in the launch tube. Thus, the mass flow-rate that can pass through the constriction is limited and additional exhaust gases must flow upstream into the annular gap between the rocket and the launcher wall, i.e., significant blow-by flow occurs. For these flows, a strong shock wave is generated when the plume impinges on the wall, producing a large pressure gradient that turns a significant fraction of the flow upstream into the annular gap. The resultant flow is similar to that depicted in Fig. 2. Choking of the exhaust flow by a constrictive change in cross-section has been observed both in cold-gas tests at the University of Texas at Austin[1] and in flight tests at the White Sands Missile Range[4].

THE PLUME CHARACTERISTICS

The uncertainties involved in modeling the plume-related flowfields (especially those for complex configurations where the flow past the missile affects the exhaust plume) encourage the engineer to use experimental techniques to define the flow field. Experimental programs require proper plume simulation, including geometrically congruent inviscid jet contours, correct pressure-rise/jet-boundary deflection (plume stiffness), and mass-entrainment characteristics along the wake boundaries[5,6]. Nyberg et al.[6] note further: "Thus, modeling with gaseous plumes is needed and normally involves dissimilar specific heat ratios." Pindzola[7] notes that "on the basis of existing data, the jet pressure ratio is shown to have the greatest effect on performance characteristics. Certain characteristics are affected by conditions in the immediate vicinity of the base. These conditions in turn are shown to be affected most by the initial inclination angle of the jet. Characteristics affected by downstream jet conditions are seen to be dependent upon the parameters $\gamma_j M_j^2/\beta_j$ and $(RT)_j$ and the jet momentum."

Korst and Deep[8] note that: "Whatever the velocity distribution in the nozzle, the plume shape in the vicinity of the nozzle exit, especially for strongly underexpanded nozzles, will mainly depend upon the local approach conditions to the nozzle lip." It is then possible to determine the nozzle-exit conditions in terms of the Mach number and the nozzle divergence angle at the nozzle lip, which will geometrically duplicate the jet contour produced by a gas with different specific heat ratios as it expands from the nozzle. The

simulation parameters are[5]:

$$\theta_{F,M} = \theta_{F,P} \text{ and } R_{C,M} = R_{C,P}$$

where the subscripts M and P are for the model and for the prototype, respectively.

Simulated Rockets

Simulated rocket exhaust flows were produced by accelerating unheated air through convergent/divergent nozzles[9,10]. Data are presented for two of the nozzle configurations,

1) a 20° conical convergent divergent nozzle, designated as C3, and

2) a 10° conical contoured convergent divergent nozzle, designated as C5.

The geometries of the nozzle configurations studied in the current program are presented in the equations below.

The 20° Conical Nozzle, C3:

For $-1.308 \leq \tilde{x} \leq -1.031$:

$$(\tilde{x} + 1.308)^2 + (r - 1.626)^2 = (0.813)^2$$

For $-1.031 \leq \tilde{x} \leq 0.0$:

$$r = 0.759 + 0.364\ (\tilde{x} + 1.308)$$

The 10° Contoured Nozzle, C5:

For $-2.098 \leq \tilde{x} \leq -1.895$:

$$(\tilde{x} + 2.098)^2 + (r - 1.626)^2 = (0.813)^2$$

For $-1.895 \leq \tilde{x} \leq 0.0$:

$$r^2 = 1.530 + 0.434\tilde{x}$$

The equations give the dimensions in centimeters. A sketch of the C5 nozzle is presented in Fig. 3. The throat radius, the nozzle exit-plane radius, and the external radius of the rocket were the same for both nozzles. The cross-sectional area for the nozzle exit-plane was $A_{ne} = 2.316A^*$ for both nozzles. If the acceleration of the flow through nozzles of this area ratio were isentropic, the Mach number of the nozzle exit plane would be 2.36 (ref. 11).

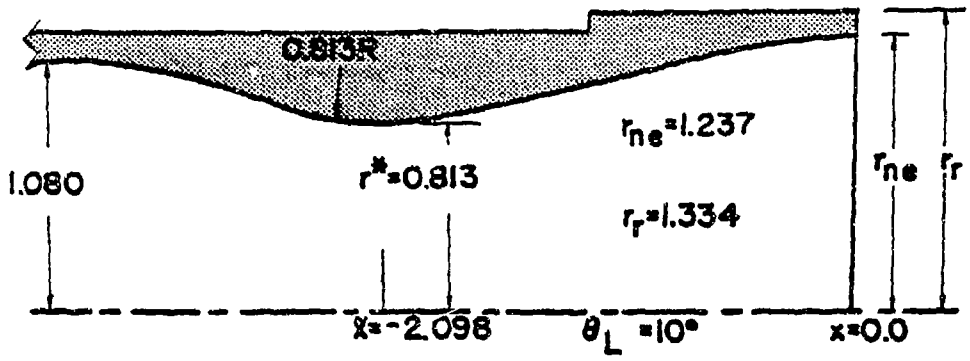

Figure 3. - Sketch of the C5 nozzle.

When the stagnation pressure is 8.715×10^6 N/m^2, the static pressure in the nozzle exit-plane is roughly six times the atmospheric value. Thus, as the exhaust gases leave the nozzle, they accelerate rapidly until the pressure along the plume boundary is equal to the static pressure of the surrounding gas. The plume boundaries for the C3 (20° conical) and for the C5 (10° contoured) nozzles, as calculated using the method-of-characteristics are presented in Fig. 4. The plume boundaries computed using the method-of-characteristics are in excellent agreement with those observed in the schlieren photographs of the nozzles exhausting into quiescent air. This is true for both of these nozzles, which are of considerably different geometries.

The correlation between the theoretical and the experimentally-determined flow-fields indicates that the nozzle-exhaust flow-field can be well modeled analytically. Thus, the method-of-characteristics for axisymmetric flow provides an acceptable tool even when no direct provisions are made for the occurrence of internal shocks. As will be seen, the plume impingement and the initial wall-pressure rise will be described with sufficient accuracy by the method-of-characteristics followed by plane shock relations.

The internal radii of the launch tubes used in the present test program are from 1.2 r_{ne} to 1.5 r_{ne}, depending on the launch-tube configuration. Since the developing shear layer is relatively short, the ensuing viscous/shock-interaction structure at the wall is very dependent on the expansion process as the flow leaves the nozzle.

For the relatively small values of r_t/r_{ne} of interest in tube-launcher/rocket applications, it is necessary to model the plume boundary only for a short distance. Thus, the calculation of the inviscid plume boundary by a technique which provides quick, but reasonable contours becomes attractive. The theoretical plume boundaries have been calculated using the method-of-centered-expansions[12,13]. These approximate plume boundaries are compared with those calculated using the more rigorous method-of-characteristics and with the data in Fig. 4. Note that the plume boundary calculated using the method-

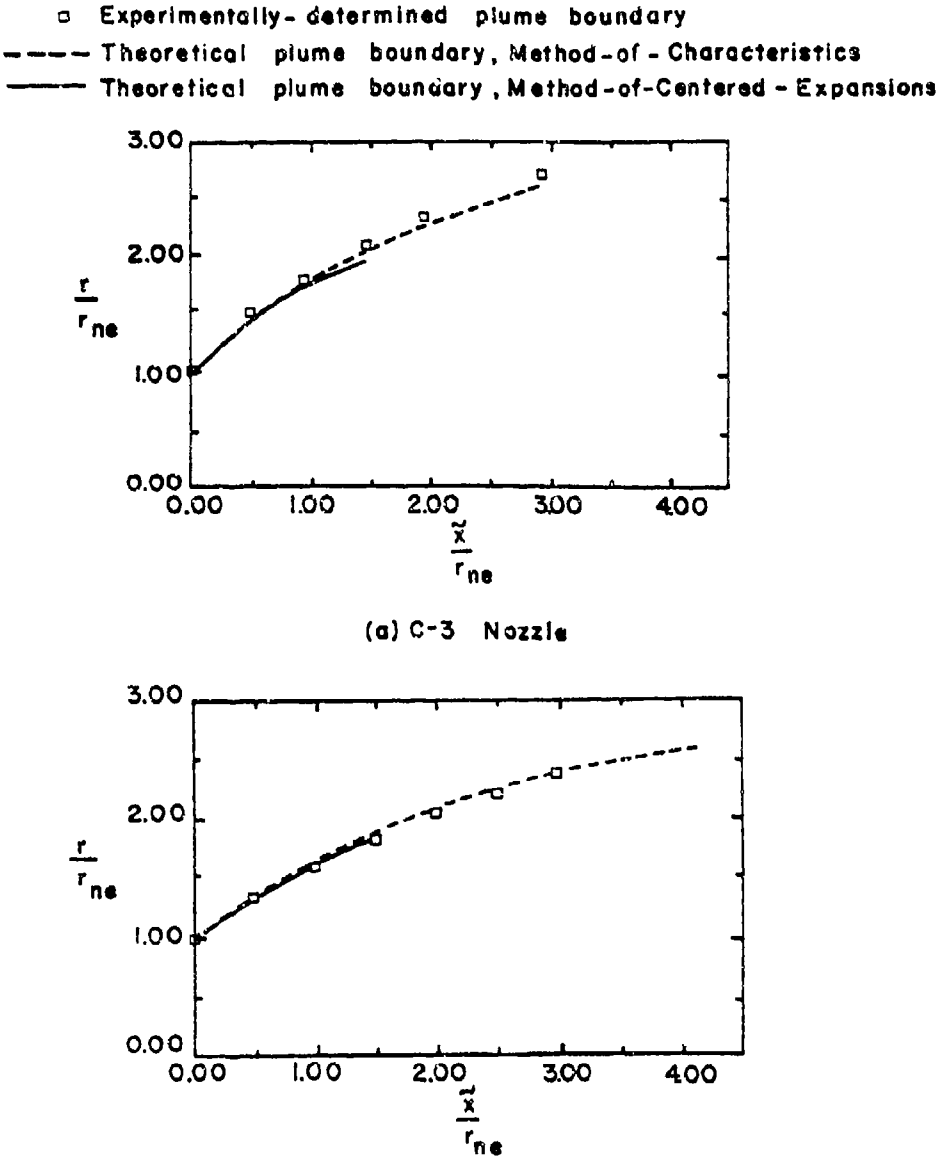

Figure 4. - Plume boundaries for the C3 and for the C5 nozzles exhausting into quiescent air (p_{t1} = 8.715 x 10^6 N/m^2 = 86 atmospheres).

of-centered-expansions is very close to the actual boundary for both nozzles. However, at a given x-location, the local flow angle at the plume boundary calculated using the method-of-centered-expansions is slightly less than the actual flow angle. As will be seen, this difference contributes to a discrepancy between the calculated impingement shock strength and the measured strength. Nevertheless, the inviscid plume boundaries calculated using the method-of-centered-expansions provide a reasonable approximation of the actual plume boundaries, making the method attractive for use in generating quick calculations of the plume impingement flow.

In addition to the jet pressure ratio and the nozzle exit conditions, the effects of the properties of the exhaust gas have been considered by many researchers. The selection of the test gas was a major element in the design of a jet simulation test facility for use with the FFA $0.25m^2$ and $1.0m^2$ wind tunnels. Korst et al.[5] report: "After an examination of the alternatives, Freon-22 was chosen. Cost and chemical stability--which allows it to be heated to sufficiently high temperatures without chemical breakdown--were major factors in its selection." Experience with Freon-22 as a test gas was reported by Nyberg et al.[6]: "The Freon plume shapes have been found to be in close agreement with those of the corresponding air test supporting the suggested modeling methodology and design procedures."

Galigher et al.[14] reported: "The cold jet technique can be used to match either the initial inclination angle or the maximum diameter of the inviscid plume boundary of the hot jet. However, viscous interaction effects for a cold jet differ from those for a hot jet since mixing between the nozzle exhaust and local external flow depends largely on temperature and velocity gradients." They also observed: "The differences obtained in boattail pressure drag between the cold jet simulation and hot jet duplication results were significant at nozzle pressure ratios representative of turbofan and turbojet engines at subsonic Mach numbers. Adjusting the cold jet nozzle ratio to correct for the changes in the exhaust plume specific heat ratio with temperature did not account for the differences observed."

Since the blow-by flow is caused by the adverse pressure gradient associated with the impingement shock, the static pressure in the nozzle exit-plane (p_{ne}) must be significantly greater than the static pressure between the rocket and the launcher wall at the nozzle exit-plane (p_b), i.e., $p_{ne} > p_b$. Note that this pressure (p_b) is equivalent to the ambient pressure of the atmosphere for a stationary nozzle exhausting into still air. The primary variables which define the characteristics of the exhaust plume include:

(a) the divergence angle of the conical nozzle, θ_{ne},

(b) the Mach number in the nozzle exit-plane, M_{ne},

(c) the ratio of specific heats, γ, and

(d) the jet pressure ratio, p_{ne}/p_b.

When an underexpanded jet exhausts from a nozzle into still air, the degree of expansion which occurs is a function of M_{ne}, γ, and p_{ne}/p_b. The initial inclination of the jet boundary (δ_j) increases as γ decreases and as p_{ne}/p_b increases. In addition, increases in the divergence angle of the nozzle by the amount $\Delta\theta$ increases δ_j by the

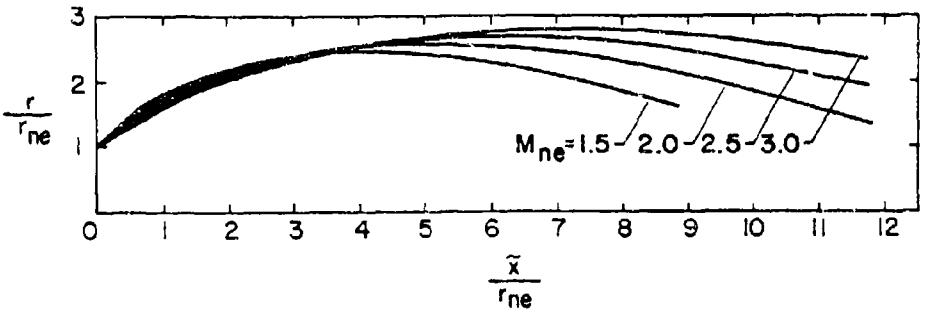

(a) Effect of M_{ne}

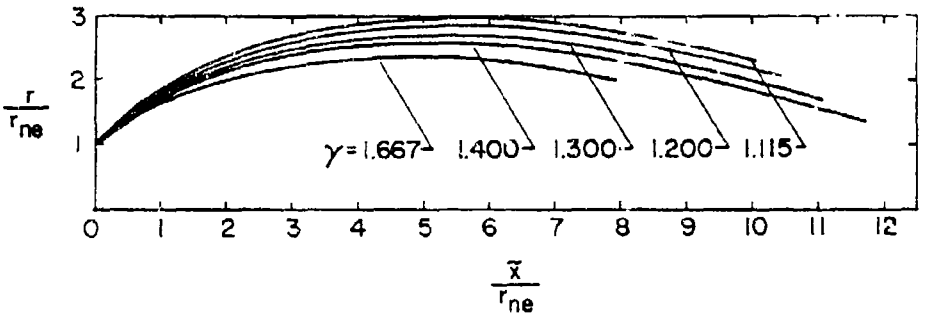

(b) Effect of γ

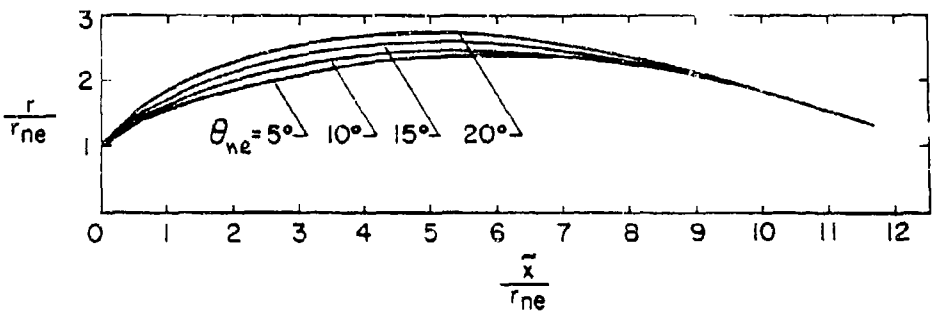

(c) Effect of θ_{ne}

Figure 5. - Example of the effects of jet Mach number, ratio of specific heats of the jet, and nozzle divergence angle upon the shape of the jet boundary. $p_{ne} = 5p_b$.

same amount. The effect of these variables on the shape of a free jet is illustrated in the curves in Fig. 5, which are taken from ref. 15, for a jet pressure ratio (p_{ne}/p_b) of 5. The correlations, which are considered typical, indicate that the effect of increasing M_{ne} is to decrease the initial inclination of the boundary, to increase the maximum diameter of the free jet, and to move the maximum diameter farther away from the nozzle exit-plane. The effect of increasing γ is to decrease the initial inclination of the boundary, to decrease the maximum diameter of the free jet, and to move the maximum diameter closer to the nozzle exit-plane. The effect of increasing θ_{ne} is to increase the initial inclination of the boundary, to increase the maximum diameter of the jet, and to move the maximum diameter closer to the nozzle exit-plane.

This discussion of the plume characteristics has ignored the interaction between the external flow over the missile and the exhaust plume. This viscous/inviscid interaction is neglected because the velocity of the rockets considered in the present study as they leave the launch tube is relatively low. Furthermore, the velocity of the exhaust gas is roughly 20 times the velocity of the rocket as it clears the launcher.

LAUNCH-TUBE FLOW-FIELDS BASED ON COLD-GAS SIMULATIONS

When a highly underexpanded supersonic nozzle exhausts into a constant-area tube, the viscous/shock-wave interaction due to the impinging flow is subject to a boundary condition in the base region. If the annular gap between the rocket and the launch-tube wall is open, the atmospheric pressure at the forward end of the vented annular gap forms the boundary condition. The direction and the magnitude of the secondary flow which is usually generated by the impingement interaction is controlled by this boundary condition. If the mass flow-rate of the secondary flow in the annular gap is relatively low, the pressure will vary only slightly along the annular gap. Thus, the static pressure in the base region will be approximately equal to the atmospheric value. However, if the annular gap is sealed, the pressure in the base region will assume a value such that the viscous/shock-wave interaction at impingement creates a "constant-mass" recirculating flow in the base region.

Simulated Launch Tubes

Constant-area launch tubes, designated as L1, L2, and L3, were used for the tests as described in ref. 10. The inside radius (r_t) for the smooth bored tubes was 1.20 r_{ne} (1.484 cm) for the L1 configuration, 1.275 r_{ne} (1.522 cm) for the L2 configuration, and 1.50 r_{ne} (1.855 cm) for the L3 configuration. Static pressure orifices (0.0635 cm in diameter) were located axially along the tube wall at a spacing of 0.25 r_{ne} (0.309 cm). Additional static pressure orifices spaced 0.50 r_{ne} (0.618 cm) apart were located further downstream.

For each test configuration, i.e., nozzle/launch-tube configu-

ration, two pitot-static probes were located midway between the simulated rocket and simulated launcher wall and 4.128 cm from the upstream end of the launch tube. Static pressure orifices were located in the launch-tube wall at the face of the pitot probes. These pitot-pressure/static-pressure data could be used to "measure" the mass flow-rate in the annular gap. The pitot probe was designed so that it could face either upstream or downstream in order to "measure" the mass flow-rate in either direction, i.e., ejector flow or blow-by flow.

Transients and Quasi-Steady Flows

Most of the experimental data described in this paper were obtained in blow-down facilities, where an unheated test gas was exhausted through a convergent/divergent nozzle. For the Rocket Exhaust Effects Facility at the University of Texas at Austin, the simulated rocket exhaust is of several seconds duration with the exhaust air being released through the supply chamber/nozzle assembly from the external storage tanks by means of a rapidly opening valve. The test is terminated by closing the valve. Thus, the stagnation pressure increases from the atmospheric value to the test value in approximately two seconds at the beginning of the test. The stagnation pressure returns to the atmospheric value during the shutdown process, which is of similar duration. Extremely low pressures were measured[16] on the wall of the L1 launch tube as the stagnation pressure builds up during the initial phase and as it decreases during the terminal phase of the test. The low pressures result because the system acts as an ejector at the low stagnation pressures. The strong ejector action produced during the start up and the shutdown processes is evident in all of the pressure histories presented in Figs. 6 and 7. The pressure data presented in Fig. 6 were obtained at an orifice located just downstream of the nozzle exit-plane ($\tilde{x}_g = 0.04\ r_{ne}$) but upstream of the impinging exhaust for most stagnation pressures. The pressure data presented in Fig. 7 were obtained at an orifice located in the annular gap far from the nozzle exit plane ($\tilde{x}_g = -\ 7.15\ r_{ne}$).

As can be seen in the data, the low static pressure associated with the ejector action was followed by a transient overshoot before reaching the "steady-state" value for the particular test conditions. It is believed that this transient behavior occurs as the flow tries to expand from the nozzle to the temporarily, low base pressures creating a rather strong impingement shock wave. The resultant pressure rise across the impinging shock interacts with the base pressure causing it to increase, which would act to reduce the turning angle and, therefore, decrease the strength of the impingement shock wave. The process is complicated by the fact that the stagnation pressure is increasing simultaneously. Since the "overshoot" precedes the high negative ejector pressures during the shutdown process, the process appears to be a complex interplay between the rapidly changing stagnation pressure and the viscous interaction of the impingement process.

Consider now the effect of the stagnation pressure on the wall pressure just downstream of the nozzle exit-plane, i.e., the data of

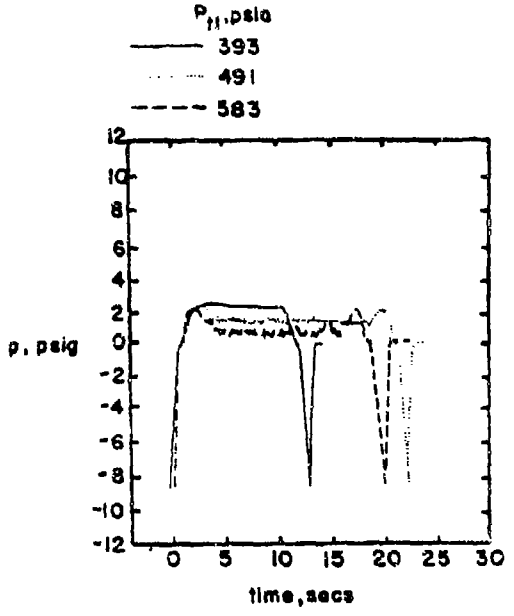

(a) Relatively low stagnation pressures.

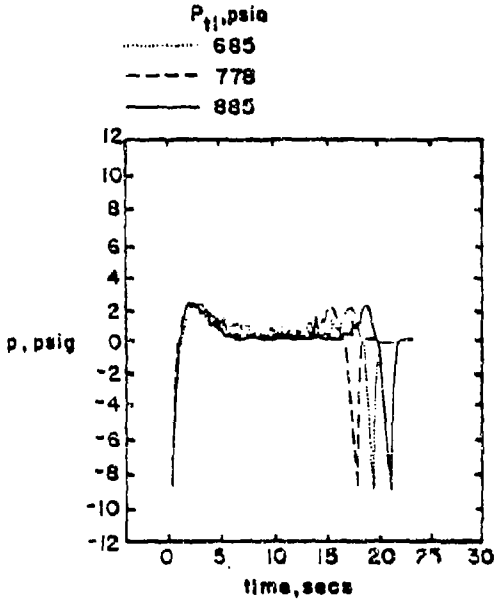

(b) Mid-range stagnation pressures.

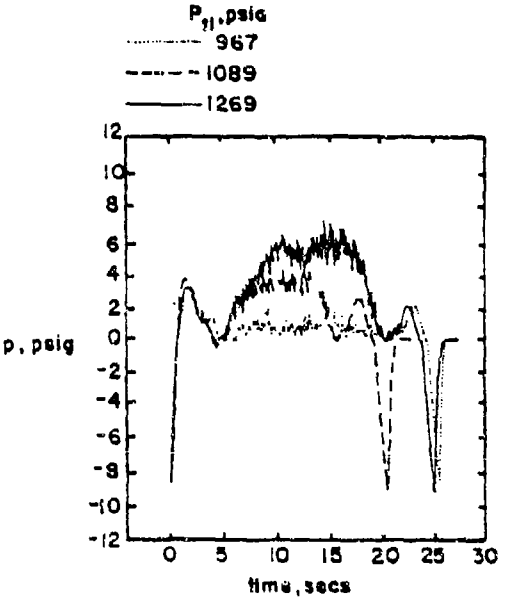

(c) Relatively high stagnation pressures.

Figure 6. - Static wall-pressure measurements from an orifice located just downstream of the nozzle exit-plane, $\tilde{x}_g = 0.04\ r_{ne}$.

Fig. 6. The steady-state value of the static wall-pressure for $\tilde{x}_g = 0.04\ r_{ne}$ decreases with stagnation pressure for $p_{t1} < 1089$ psia. These relatively low pressures indicate that the entrainment process at the plume boundary appears to be a dominant factor in the wall pressures in this region. Thus, for $p_{t1} < 1089$ psia, the wall static pressure is greatest for the lowest value of the stagnation pressure (i.e., $p_{t1} = 393$ psia). For $p_{t1} \geq 1089$ psia, the rapid increase in the pressure in this region begins to reflect the impingement of the plume's shear layer. Since p_{ne} is proportional to p_{t1}, the exhaust expands through a larger angle as the stagnation pressure increases. Thus, the "location" of the exhaust impingement on the wall moves nearer to the exit plane (and, therefore, this orifice) as p_{t1} is increased. Furthermore, the impinge-

ment shock wave should be stronger as the stagnation pressure increases. The wall-pressures should also increase.

Wall-pressure measurements from the annular gap are presented in Fig. 7. The steady-state pressures that were measured in this region were essentially independent of position. The "steady-state" values of the static wall pressure usually increase with p_{t1}. Since the blow-by flow in the annular gap originates at the plume impingement and exhausts to the atmosphere at the upstream end of the launch tube, the pressure in the annular gap should indeed be greater than the atmospheric value. At the higher values of p_{t1}, the pitot-pressure measurements from the annular gap[17] indicate that the flow is nearly choked. This explains why the corresponding pressures are well above

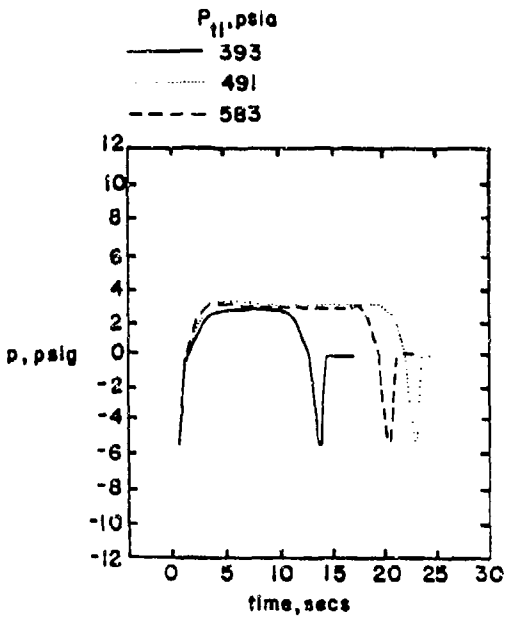

(a) Relatively low stagnation pressures.

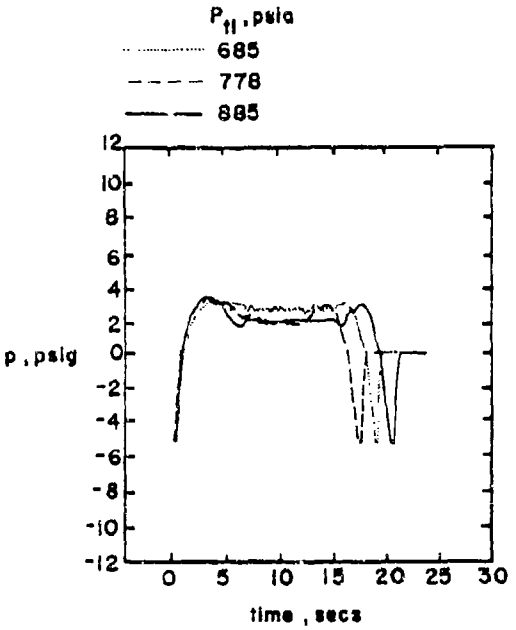

(b) Mid-range stagnation pressures.

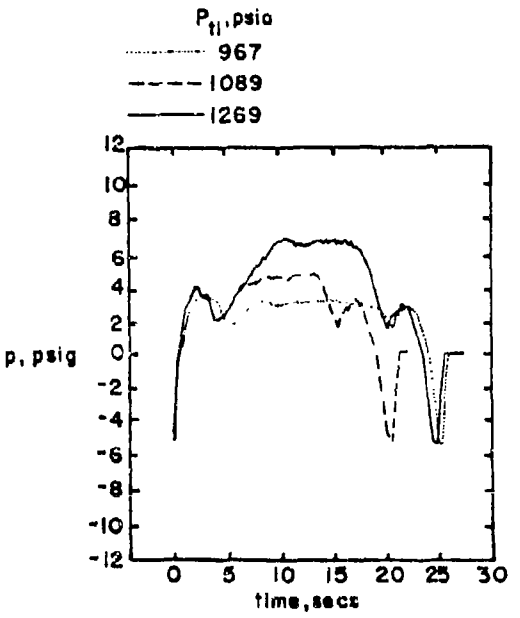

(c) Relatively high stagnation pressures.

Figure 7. - Static wall-pressure measurements from an orifice located in the annular gap, $\tilde{x}_g = -7.15\, r_{ne}$.

the atmospheric value.

Similar results were observed in the data obtained during a flight test program in which an anti-tank rocket was launched from a tube. At the time of ignition, large negative gage pressures were recorded for orifices located on the wall. Thus, the system acted as an ejector. Hence, because the base pressure was relatively low, the exhaust expanded through a relatively large angle, creating a strong shock wave as it impinged on the wall. As the rocket motor came up to pressure (i.e., as the stagnation pressure increased to its steady-state value), massive blow-by occurred initially, producing choked flow and extremely high pressures in the annular gap. In response to this transient peak in the base pressure, the expanding exhaust turned through a smaller angle and the strength of the impingement shock wave was reduced dramatically. Thus, the resultant "steady-state" pressures in the launch tube were lower than the transient peak values.

For the prototype configurations considered in the present study, the time from ignition until the rocket cleared the launch tube was less than one second. The flow-field simulations made using the Rocket Exhaust Effects Facility were of the order of 20 seconds. Thus, questions may exist as to the validity of the cold-gas simulations of the prototype flows. Batson[18] found that the static wall-pressure distributions in a constant-area tube obtained during a cold-gas test program were qualitatively similar to those obtained when a stationary rocket was exhausted into a constant-area tube. Batson and Bertin[19] examined the tube-wall static-pressure distributions which were obtained when a rocket accelerated through an instrumented tube. The static wall pressures from these dynamic rocket firings were qualitatively similar to the corresponding data from the static rocket firings of ref. 18. Thus, a quasi-steady flow analysis should provide a reasonable model of the actual flow field produced by a tube-launched rocket.

Relatively-Low (Secondary) Flow Rates in the Annular Gap

For a wide range of flow conditions, the impingement shock-wave is relatively weak and the downstream flow remains supersonic. For such cases, there is relatively little secondary flow and the pressure in the annular region differs only slightly from the atmospheric value. As a result, unbalanced forces on the missile are relatively small. The Chapman-Korst model[20] can be used to delineate the inviscid and the viscid flow-mechanisms encountered in the plume-impingement flow-field. Once the geometry of the corresponding inviscid plume-boundary is established by an appropriate potential flow analysis, a viscous mixing component is superimposed on the boundary. Wake closure conditions are specified in the form of a modified concept of incomplete turning of the plume near the point of shear-layer reattachment[21].

A number of conceptual simplifications for the plume-impingement flow field, which will be introduced, are justifiable for the conditions of interest. Since the launching of rockets from straight tubes will usually impose geometric restrictions to blow-by, the

present analysis can be simplified by the assumption that the mass flow-rates which will be rejected from or entrained into the viscous jet-mixing region should be small. This, in turn, allows the adoption of a linear velocity profile in the mixing region[22]. It is also assumed that the entire system will be operating under essentially isoenergetic conditions, that is, with the stagnation temperature equal to that of the exhaust gas. This assumption is realistic for most flows under consideration; the exception being ejector-type flow generated by an actual rocket firing.

Since the ratio of the launch-tube diameter to rocket nozzle-exit diameter is limited to values ≤ 1.5, the contour of the corresponding inviscid plume boundary can be determined with sufficient accuracy by the second-order potential-flow approximation for axially symmetric, supersonic flow near the center of an expansion[12,13]. The resulting circular-arc configuration is convenient for establishing a simple inviscid-flow-component geometry. On the other hand, it is necessary to treat the nozzle flow in detail in order to define accurately the conditions at, and near, the lip of the exit cross-sec-

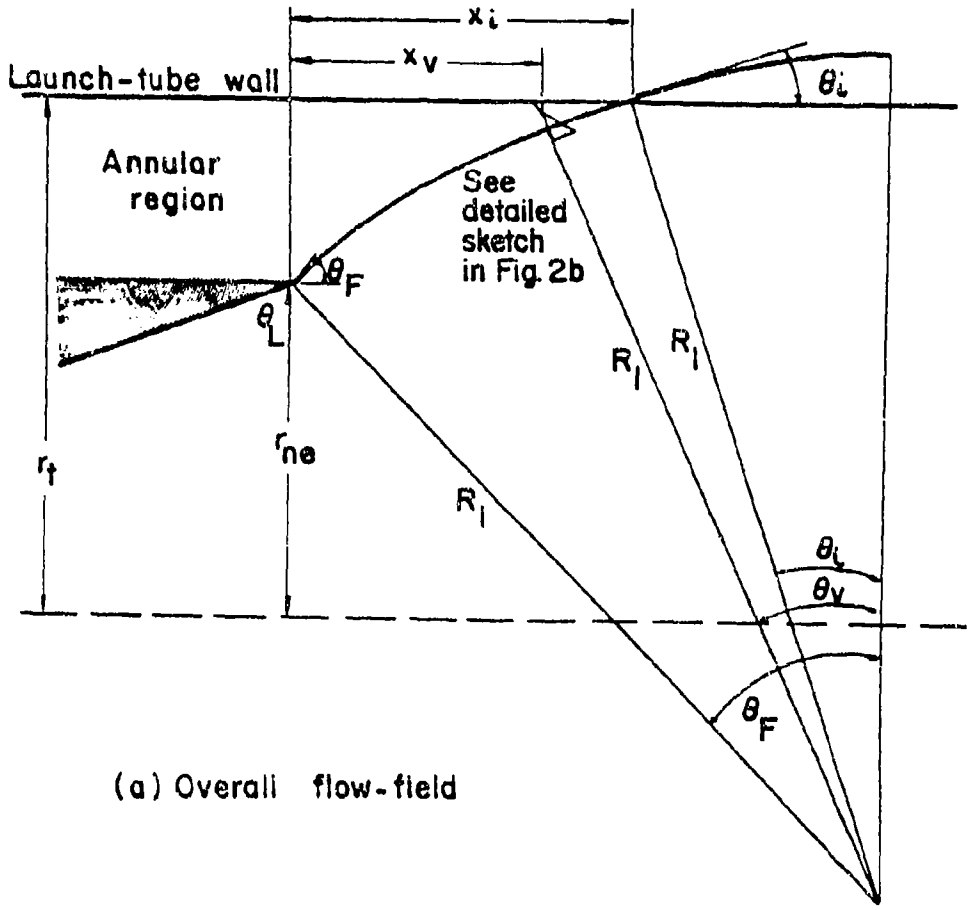

Figure 8. - Sketch of the impingement flow model.

tion. This requires the analysis of the nozzle flow by the method-of-characteristics (including the effects of characteristics coalescence) as it develops from the transonic flow region near the nozzle throat[23].

The exit-plane conditions near the nozzle lip will be determined by the local wall-slope, θ_L, the local wall-curvature, the local Mach number, M_L, and the local flow acceleration. With these initial conditions specified, selection of the jet surface Mach number, M_F, will yield a unique solution for the circular-arc approximation of the contour of the inviscid plume boundary in terms of the initial streamline angle, θ_F, and the radius of curvature, R_1[8].

Thus, for a given nozzle configuration and for any jet surface Mach number, M_F, the inviscid flow field will be uniquely determined, see Fig. 8, with θ_i denoting the inviscid impingement angle at the cylindrical launcher wall, i.e., at radius r_t. The jet mixing characteristics of the free shear layer at the plume boundary and the recompression of the plume as it impinges on the cylindrical wall were discussed in ref. 24. The spreading parameter σ is related to the change in slope of the velocity profile[25,26].

The recompression of the plume as it impinges on the cylindrical wall leads to a flow configuration as shown in Fig. 8b. If the stagnating (discriminating) streamline has a velocity level, ϕ_d, different from that of the zero streamline, ϕ_j, a secondary flow will

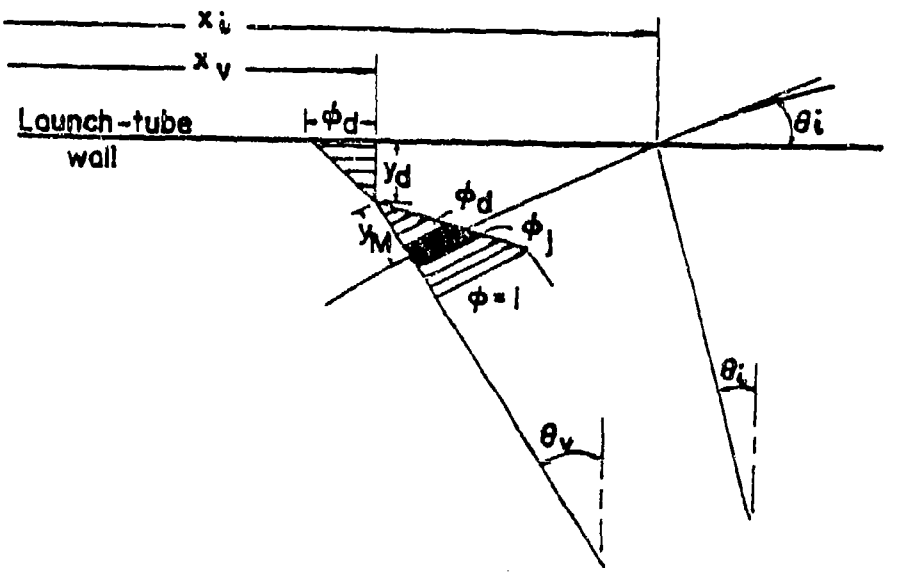

(b) Details of impinging shear-layer for ejector-type flow ($\phi_i > \phi_d$, ■ secondary flow)

Figure 8. - Concluded.

be established as required for satisfying the conservation of mass in the near wake region. The secondary flow rate will be positive, i.e., ejector-type flow, if $\phi_j > \phi_d$ and negative, i.e., blow-by, if $\phi_j < \phi_d$.

As the discriminating streamline, whose velocity ratio is ϕ_d, stagnates at the wall, the process of recompression will be practically isentropic[20,21]. After plume impingement and alignment of the jet surface with the wall by reversible compression, the pressure distribution for the inviscid flow configuration can again be treated with reasonable approximation by the formal application of the concept of centered expansions. With the new origin of the centered expansion at the impingement point for the inviscid plume, an ordinary differential equation is obtained for M* along the wall downstream of the impingement and the resulting pressure distribution can be determined. The mathematical approximations inherent in the method-of-centered-expansions restricts the useful range of the calculated wall-pressure distribution to approximately 1.0 r_{ne} downstream of the impingement.

It is of interest to explore the influence of Reynolds number together with an assessment of the nozzle-wall boundary-layer development. The boundary layer in axisymmetric, convergent/divergent nozzles can be calculated[27,28,29] at the nozzle lip. Then, for a given Mach number, M_E, one can calculate the development of the dissipative shear layer following the expansion from the nozzle exit-plane. After the transition of the thin laminar sublayer[30], the turbulent mixing-layer grows until its inner edge reaches and then crosses into the "free-stream" within the rotational shear layer produced by the expanded nozzle boundary layer. The developing mixing layer proceeds toward, but usually does not reach, self-similar mixing profiles. Calculations for the present test conditions indicate that the velocity along the dividing streamline is within five percent of the similarity value. Thus, the test simulations of the current program provide a reasonable simulation for the prototype reattachment pressure rise.

Of greater concern is the behavior of the reattaching flow due to the strong interaction with its boundary layer. Implied with the concept of incomplete turning of the adjacent inviscid stream is the continuation of the pressure rise beyond the stagnation point within the dissipative layer. This will lead to a thickening of the attached boundary layer and may, by itself, cause a pressure overshoot above the level consistent with the full turning of the external flow.

On the other hand, there will also be a communication within the boundary layer of the rapid expansion following the plume impingement. These mechanisms are expected to modify the pressure distribution across the reattachment region, but in opposing fashion. As a result, pressure peaks determined for the corresponding inviscid jet boundary will generally show reasonable agreement with experimental data even though there may be noticeable, albeit explainable,

differences between theoretically determined and measured pressure distributions.

Pressure distributions for the launch-tube flow-fields with the annular gap sealed by an obturator ring. - Over a wide range of stagnation pressure, the ratio p_b/p_{t1} is essentially independent of the stagnation pressure when the annular gap is sealed. That the pressure ratio p_b/p_{t1} should be constant for a given configuration for a fully devel-

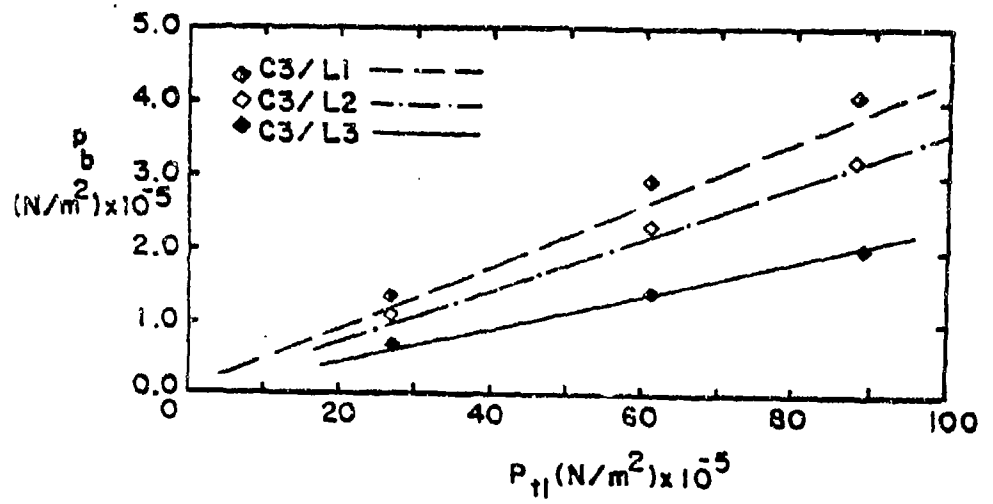

(a) C3 Nozzle

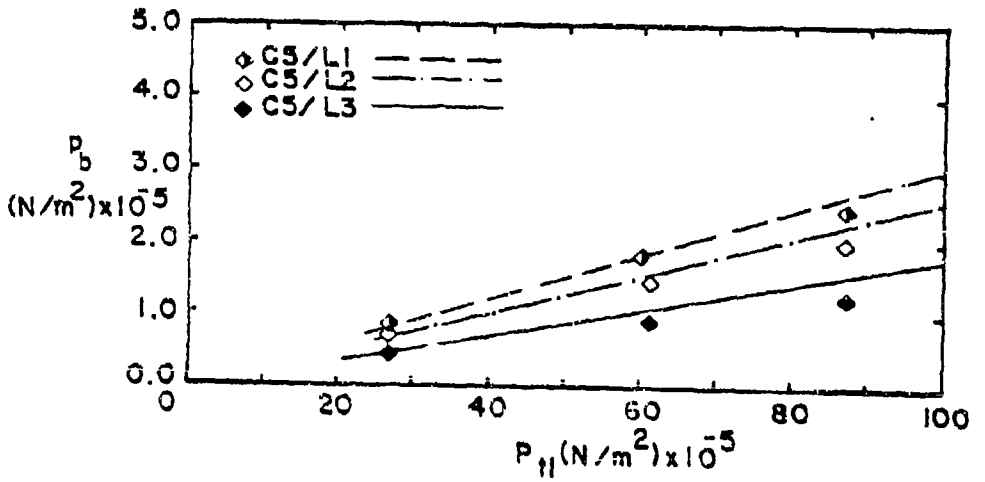

(b) C5 Nozzle

Figure 9. - A comparison of the theoretical and the experimental base pressure with the base region sealed by an obturator ring, i.e., $\dot{m}_{ag} = 0$.

oped supersonic flow is well documented, e.g., refs. 10, 31, and 32. Korst et al[33] have shown that the equilibrium (or steady-state) value of the base pressure is governed by the viscous shear-layer at the boundary of the nozzle exhaust plume that bounds the "dead-air" base-flow region and by the physical geometric constraints. The theoretical values of the base pressure are presented for the C3 and the C5 nozzles in Fig. 9 for all three launch tubes for stagnation pressures from 2.5×10^6 N/m^2 to 8.8×10^6 N/m^2.

The experimental values of the static wall-pressure vary only slightly with $\tilde{x}$ in the region between the obturator ring (small negative $\tilde{x}$-coordinate) and the intersection of the exhaust plume with

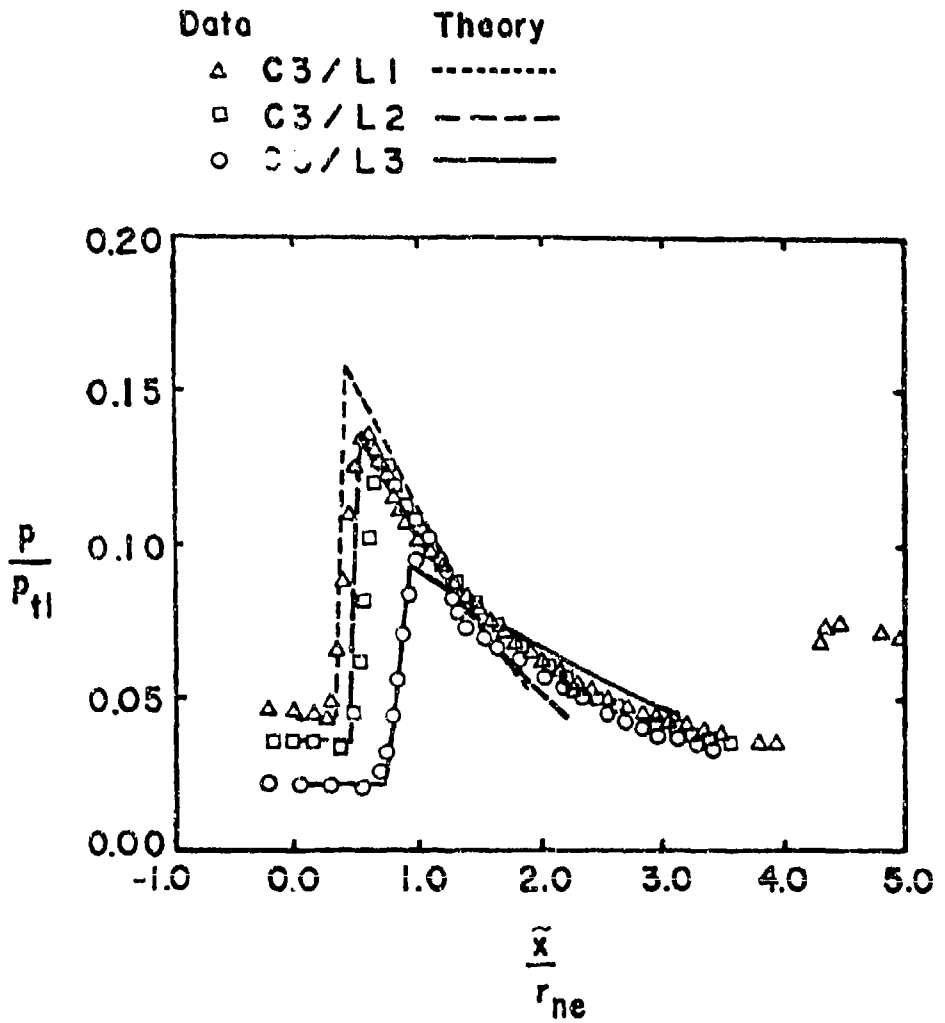

Figure 10. - The effect of launch-tube radius on the static wall-pressure distributions for the C3 nozzle with an obturator ring, $p_{t1} = 8.715 \times 10^6$ N/m^2.

the launcher wall, reaching a minimum just before the impingement-induced pressure rise. This is illustrated by the data presented in Figs. 10 and 11. Recall that relatively low pressures upstream of the impinging jet were also observed in the transient pressure data presented in Fig. 6. For the purposes of the present paper, the static wall-pressure sensed by the orifice located at $\tilde{x} = 0.0\ r_{ne}$ (i.e., in the plane of the nozzle exit) is designated as the base pressure. The experimental values of p_b are presented in Fig. 9. Since they are a linear function of p_{t1}, the ratio p_b/p_{t1} is constant for a given configuration. Furthermore, they compare very well with the theoretical values for both nozzles.

The static-pressure distributions in the vicinity of the plume impingement have been computed for flows with the annular gap sealed by an obturator ring. The pressure distributions for unheated air accelerating from a reservoir where p_{t1} is 8.715×10^6 N/m^2 through the C3 nozzle into the constant-area launch-tubes are presented in Fig. 10. Similar solutions for the C5 nozzle are presented in Fig. 11. The theoretical solutions are compared with experimental data for these nozzle/launch-tube configurations. Note, that as the tube radius is increased from 1.20 r_{ne} (the L1 tube) to 1.50 r_{ne} (the L3 tube), the base pressure decreases and the location of the peak pressure moves further downstream of the nozzle exit-plane. However, as the base pressure decreases, the angle through which the plume

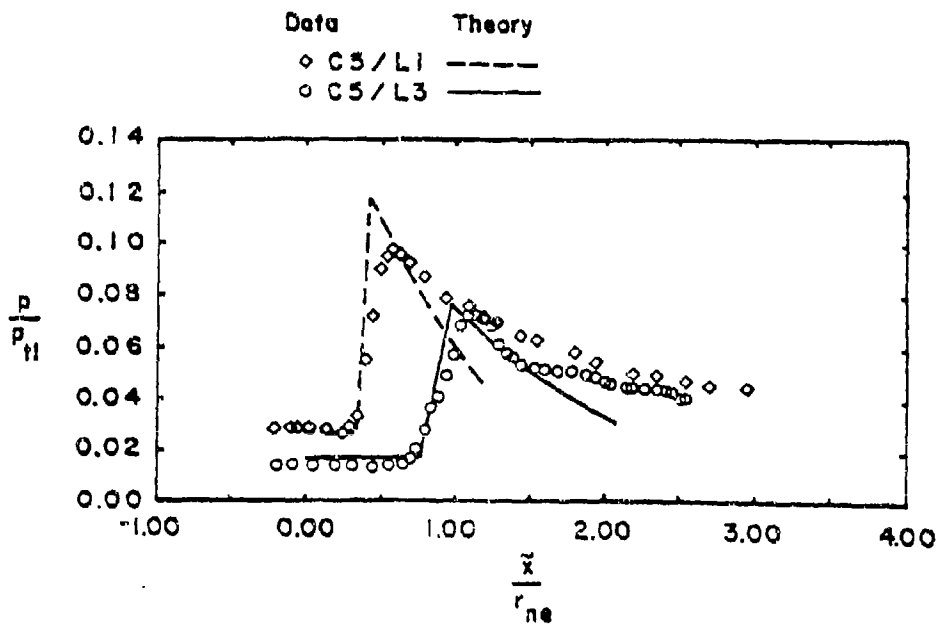

Figure 11. - The effect of launch-tube radius on the static wall-pressure distributions for the C5 nozzle with an obturator ring, $p_{t1} = 8.715 \times 10^6$ N/m^2.

boundary expands at the nozzle exit-plane increases. As a result the pressure ratio across the impingement shock wave (i.e., the peak static-pressure divided by the base value) increases as r_t increases.

For both nozzles, the theoretical value of the peak pressure in the impingement region is significantly greater than the corresponding experimental value for the L1 launch-tube. Because of the small difference between r_t and r_{ne}, the free-shear layer at the plume boundary is relatively short and the flow deceleration associated with the impingement process significantly modifies the viscous/shock-wave interaction. This modification is not reflected in the theoretical flow model, and thus, the peak pressure is overestimated by the theory. The agreement between the theoretical and the experimental values is much better for the L3 launch-tube. The improvement in the correlation for the larger-radius launch-tube is attributed to compensating effects of approximations in the theoretical flow model.

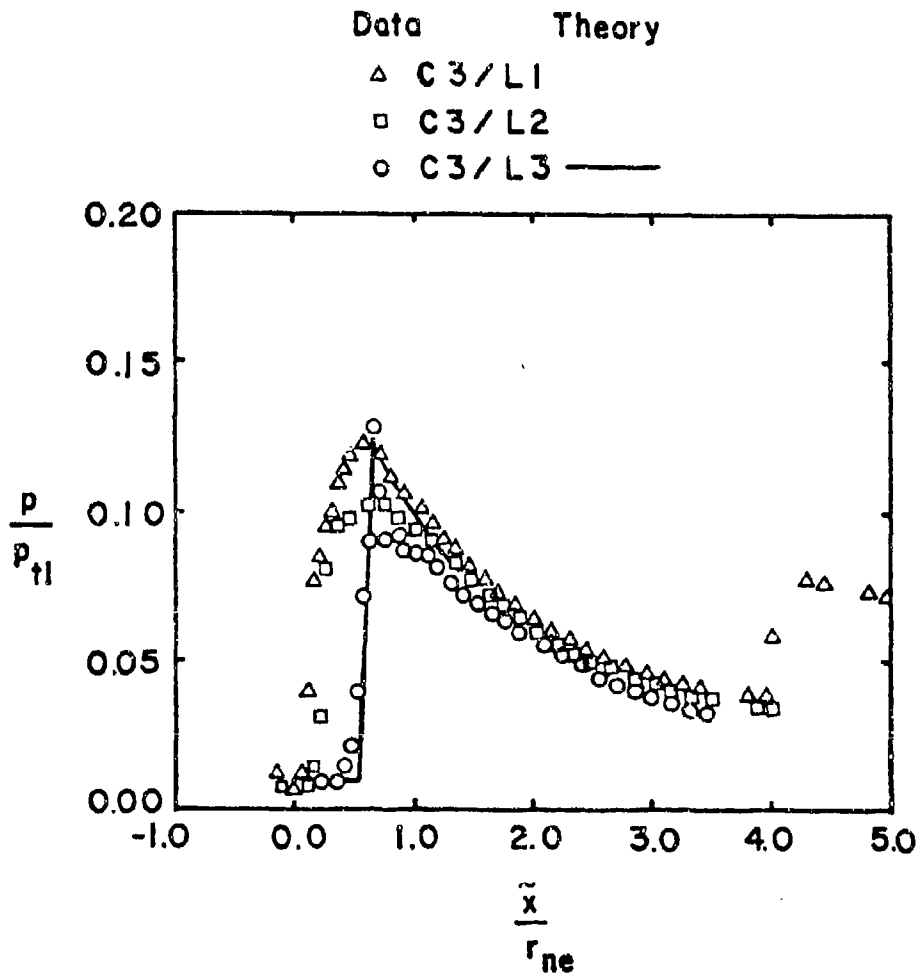

Figure 12. - The effect of launch-tube radius on the static wall-pressure distributions, C3 nozzle without an obturator ring, $p_{t1} = 8.715 \times 10^6$.

Pressure distributions for the launch-tube flow-fields with a vented annular gap. - As noted earlier, if the mass flow-rate of the secondary flow in the annular gap is relatively low, the pressure will vary only slightly along the annular gap. Since the static pressure in the nozzle exit-plane (p_{ne}) is directly proportional to the stagnation pressure, while the base pressure (p_b) remains roughly constant, the jet pressure ratio (p_{ne}/p_b) varies with p_{t1}. Thus, the viscous/shock-wave interaction depends on the stagnation pressures as well as the nozzle/launch-tube configuration.

The effect of the launch-tube radius is indicated by the pressure distributions presented in Figs. 12 and 13 for the largest value of p_{t1} tested. Since the base pressure is approximately constant, the shape of the plume boundary would be independent of the launch-tube radius, if the flow were inviscid. If the shape of the plume boundary were indeed independent of the launch-tube radius, the intersection of the plume boundary and the wall would be nearer the nozzle exit as r_t decreased. Thus, the impingement shock-wave would move upstream and increase in strength as r_t decreases.

These trends are substantiated by both the theoretical and the experimental pressure distributions for the nozzle/launch-tube configurations using the C5 nozzle, which are presented in Fig. 13. As was the case for the flow fields with the obturator ring, the correlation between theory and experiment is better for the larger radius launch-tube the L3. As before, the theoretical model of the

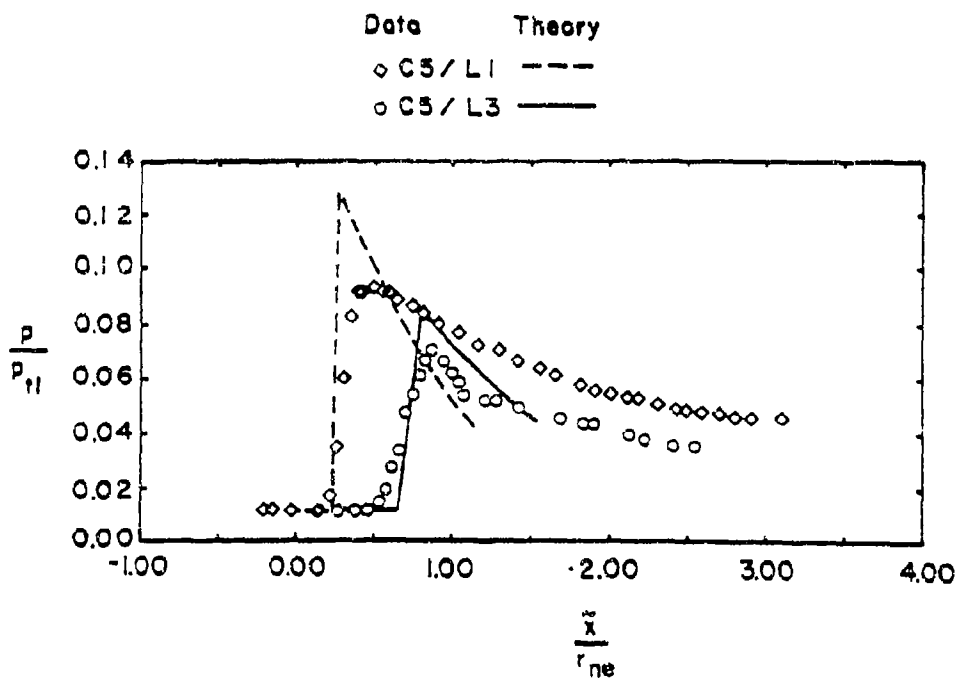

Fig. 13. - The effect of launch-tube radius on the static wall-pressure distributions, C5 nozzle without an obturator ring, $p_{t1} = 8.715 \times 10^6$.

shear layer does not reflect the interaction between the approaching free shear-layer and the pressure rise of the impingement shock-wave. However, as was shown in Fig. 4, the method-of-centered-expansions, which is used to provide the approximate inviscid plume boundary, yields plumes for which the local flow angle at the plume boundary is slightly less than the actual flow angle. Because these two flow-model approximations tend to compensate each other, the theoretical values of the peak pressure are in very good agreement with the data for these flow/geometry conditions.

Although experimental pressure distributions are presented for all three C3/launch-tube configurations, only for the C3/L3 is the theoretical distribution presented in Fig. 12. Theoretical solutions were not possible for the C3/L1 or for the C3/L2 configurations with the present flow model, since the local flow inclination at the plume boundary intersection with the launcher wall exceeds the value which can be turned through a weak shock-wave. This contrasts the flow fields for the sealed annular gap. Recall that theoretical pressure distributions were presented in Fig. 10 for all three launch tubes when the annular gap was sealed by an obturator ring. As shown in Fig. 9a, the base pressure is considerably greater than the atmospheric value, when the annular gap is sealed, and the expanding flow turns through a smaller angle as it leaves the nozzle. Therefore, with an obturator ring in place, the local flow inclination of the impinging plume is such that the impingement shock-wave weak.

Although the theoretical solutions indicate the weak impingement shock-waves are not possible for the C3/L1 or the C3/L2 configurations, the maximum measured values of the pressure are not large enough to indicate the presence of a strong shock-wave. Thus, these pressure distributions indicate a relatively strong interaction between the impingement shock-wave and the shear layer at the plume boundary. For the two smaller radii tubes, the stream-wise pressure-gradient along the launcher wall is not constant in the impingement region. As was discussed in ref. 10, the relatively strong viscous/shock-wave interaction which occurs for this nozzle/launch-tube configuration at high stagnation pressures produces significant blow-by flow.

Secondary flows. - As the rocket exhaust entrains base-region air, a free-shear layer develops along the plume boundary, accelerating air from the base-region and decelerating exhaust gas. When this free-shear layer encounters the adverse pressure gradient associated with the impingement shock-wave, some of the flow passes through the shock wave, some of it is turned back. As discussed in Fig. 1, if the stagnation pressure is relatively low, the system acts as an ejector with some of the entrained air passing through the impingement shock-wave. As the stagnation pressure is increased, the ratio p_{ne}/p_b increases and the flow expands through a larger angle as it increases. Once the impingement shock is sufficiently strong, the resultant adverse pressure gradient causes a fraction of the exhaust flow to be turned upstream (blow-by flow).

Theoretical and experimental values of the secondary flow rates

are presented as a function of the stagnation pressure in Figs. 14 and 15. For all three configurations, theory provides a good prediction of the stagnation pressure for which there is no flow in the annular gap. However, the theory provides reasonable estimates of the secondary flow-rates only for relatively low flow rates. This is evidenced by the comparison between data and theory for the C3/L3 configuration, which deteriorates as p_{t1} increases above 6 x 10^6 N/m^2.

This result should not be surprising. Furthermore, as has been often noted, the theoretical model of the shear-layer does not reflect the interaction between the approaching free-shear layer and the pressure rise of the impingement shock-wave. Both of these approximations contribute to the limitation of the flow model to the prediction of the lower secondary flow rates. As the model is presently formulated, the secondary flows are only carried between streamlines within the linear mixing profile. Thus, the model is not applicable to high secondary flow-rates.

For the C5/L1 configuration, the theory provides a reasonable approximation of the crossover value of the stagnation pressure but does not come close to the blow-by flow-rates, as shown in Fig. 15. Part of the difference may be experimental. Since the diameter of the pitot probe was approximately 50% of the width of the annular

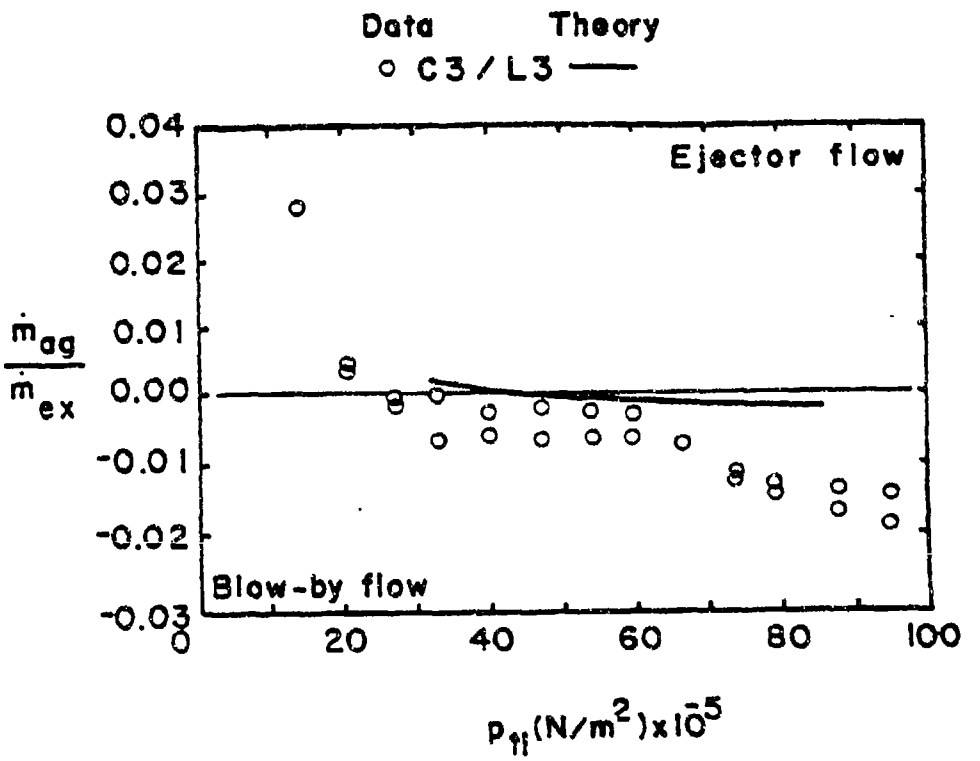

Figure 14. - The mass flow-rate in the annular gap as a function of the stagnation pressure for the C3 nozzle.

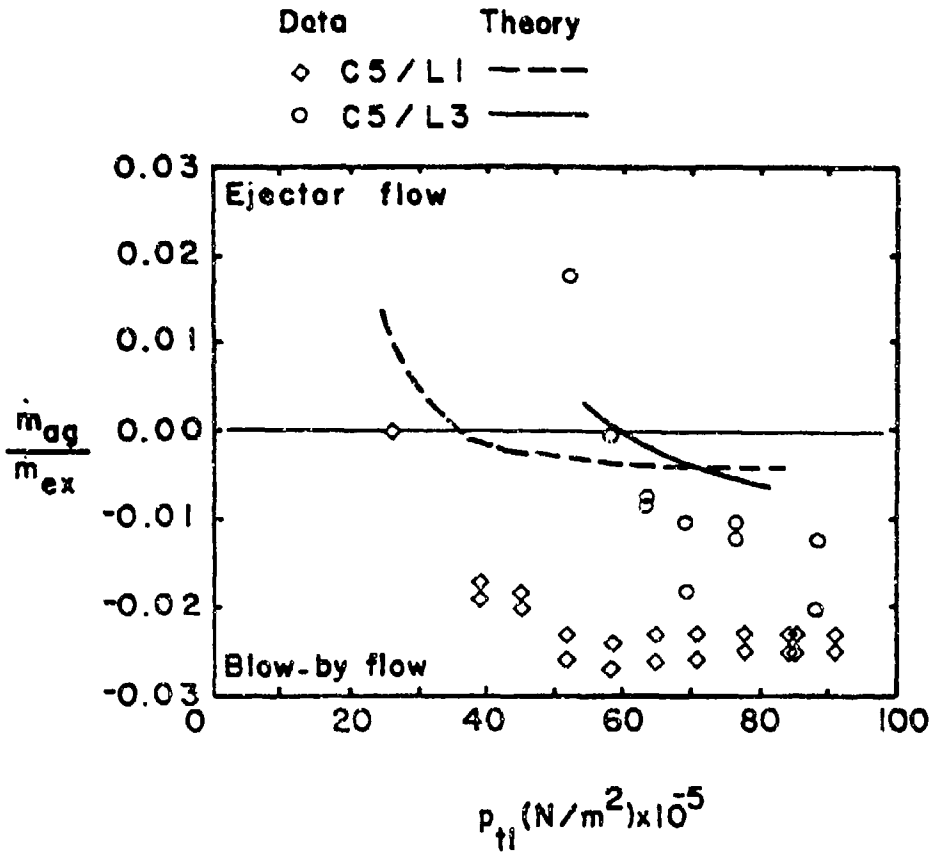

Figure 15. - The mass flow-rate in the annular gap as a function of the stagnation pressure for the C5 nozzle.

gap for the L1 tube configuration, inaccuracies in the total pressure measured by the pitot probes may contribute to significant experimental errors. Nevertheless, the theoretical flow model provides a reasonable estimate of the stagnation pressure required for zero secondary flow.

The effects of nozzle stagnation pressure on the impingement shock strength can be seen in the data[34] presented in Fig. 16. Note that the impingement shock strength is defined as the pressure ratio across the impingement shock-wave (p_{pk}/p_b); p_{pk} is the peak static wall-pressure and p_b is the base pressure, which is the static pressure measurement for the $\bar{x}_g = 0.0\ r_{ne}$ orifice. (The divergent portion of the C4 nozzle is conical with a 10° half-angle.) The experimental values in these figures are compared with corresponding theoretical values computed using the rotational method-of-characteristics (RMOC) code to describe the impinging exhaust, neglecting the shear layer that develops at the plume boundary. In Fig. 16a the curves representing the theoretical solutions for the C3/L1 and the C3/L2 configurations terminate at stagnation pressures of 5.5×10^6 N/m^2 (800 psia) and 6.3×10^6 N/m^2 (920 psia) respectively, since the computed solutions

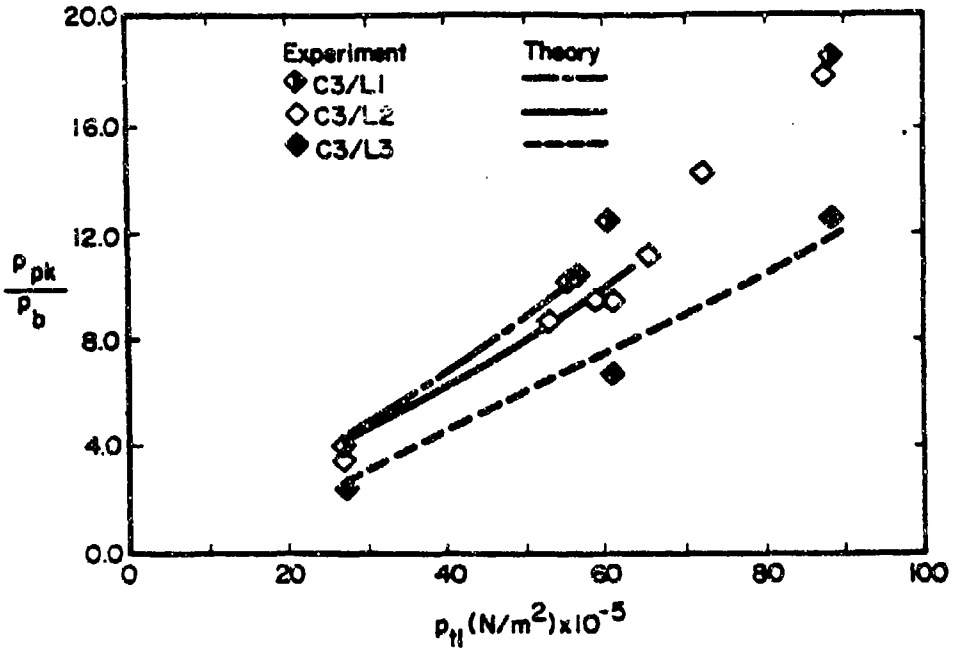

(a) C3 nozzle

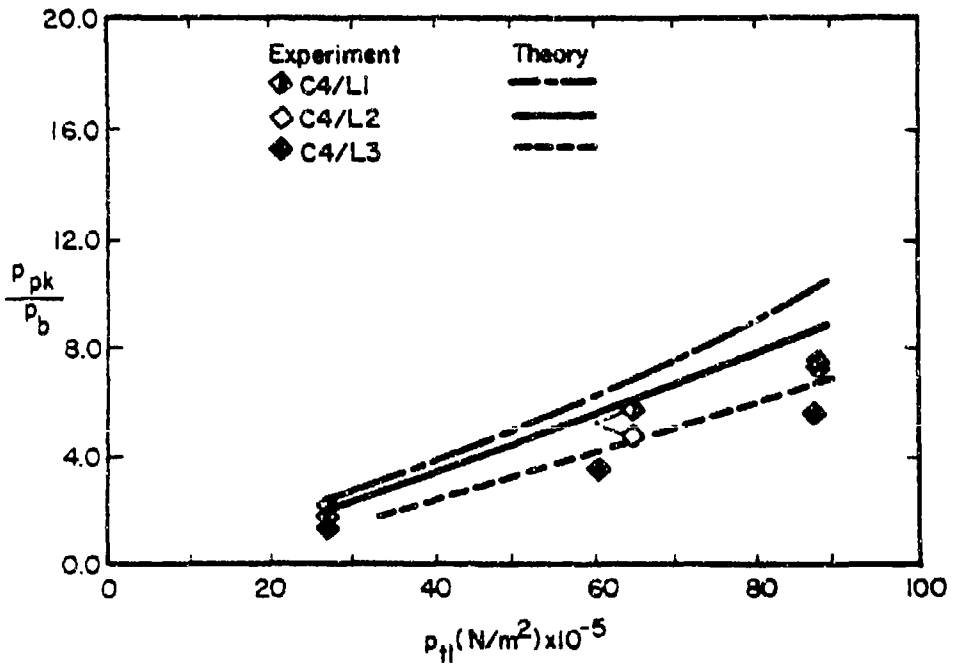

(b) C4 nozzle

Figure 16. - Pressure ratio across the impingement shock-wave as a function of the stagnation pressure (no obturator ring).

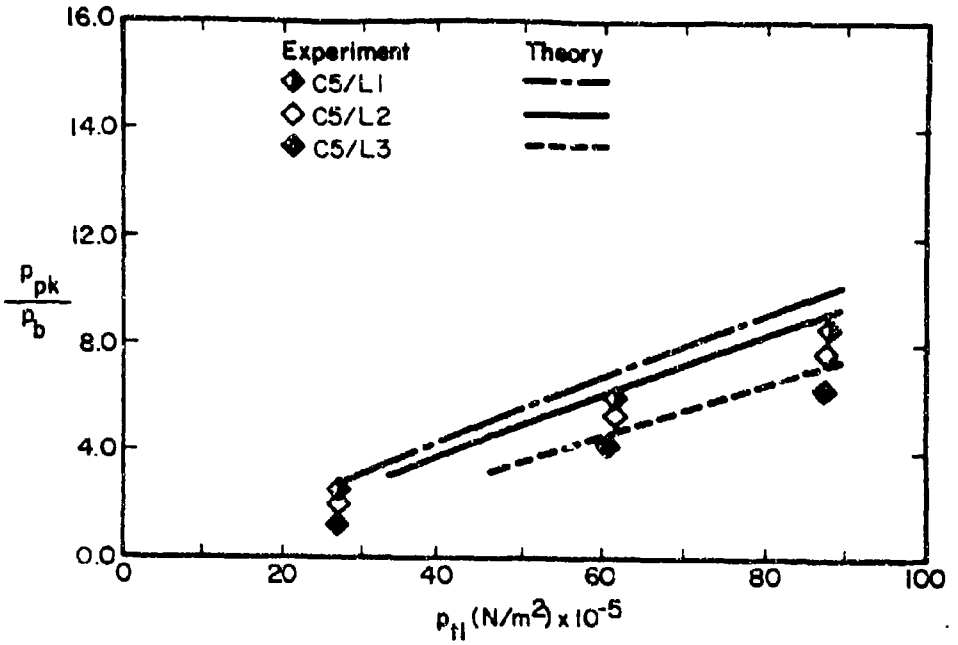

(c) C5 nozzle

Figure 16. - Concluded.

indicate that the impinging exhaust flow could not be turned through a weak shock wave if the stagnation pressure were higher. Therefore, neglecting the viscous effects of the shear layer at the plume boundary, the cutoffs in the theoretical curves indicate the lowest value of the stagnation pressure where one would expect the impingement process to generate a strong shock wave. The experimental values for these two nozzle/launch-tube configurations indicate higher impingement shock strengths for a p_{t1} of approximately 8.85 x 10^6 N/m^2 (1269 psia) than would be expected from an extrapolation of the theoretical solutions. Note also that, at these conditions, the static wall-pressure distributions (refer to Fig. 12) indicate significant viscous interactions at the plume boundary in the impingement region. Nevertheless, although these impingement shock strengths are comparatively strong, they do not indicate the presence of strong, "normal" shock waves. Thus, for the stagnation pressures where the weak-shock solution is no longer possible, the experimental values do indicate a transition region where the impingement shock-wave becomes significantly stronger, but not truly "strong". For all the other nozzle/launch-tube configurations, the theoretical solutions predicted the existence of weak shock waves throughout the range of nozzle stagnation pressures that were tested. In general, the experimental data show reasonable agreement with the theory and, as expected, the theory overpredicts the impingement shock strengths due to neglecting interaction of the viscous shear layer.

As evident in the data presented in Fig. 16, for a given nozzle, the impingement shock strength increases with decreasing tube radius.

The following logic is offered to explain this trend. For the present test conditions, where the mass flow-rates in the annular gap are relatively small, the base pressure is essentially constant. Therefore, unless the impingement process produces significant viscous interactions (which did occur for some test conditions), the plume boundary for a given nozzle/stagnation-pressure condition is independent of the launch-tube radius. Thus, when the nozzle exhausts into a smaller tube, the radial coordinate where the plume intersects the wall decreases and the impingement angle, i.e., the angle at which the nozzle flow intersects the wall, increases. This requires that the impingement shock wave become stronger since the flow must be turned through a greater angle. Also, for a given tube configuration, the impingement shock-wave was significantly stronger for the C3 nozzle than for either the C4 or C5 nozzle. This occurs because the nozzle exit-angle (θ_{ne}) is greater for C3 (20°) than for C4 or C5 (10°) and, therefore, so is the impingement angle.

For the launch-tube flow-field without an obturator ring, a data correlation was obtained[35] that relates the mass flow-rate ratio

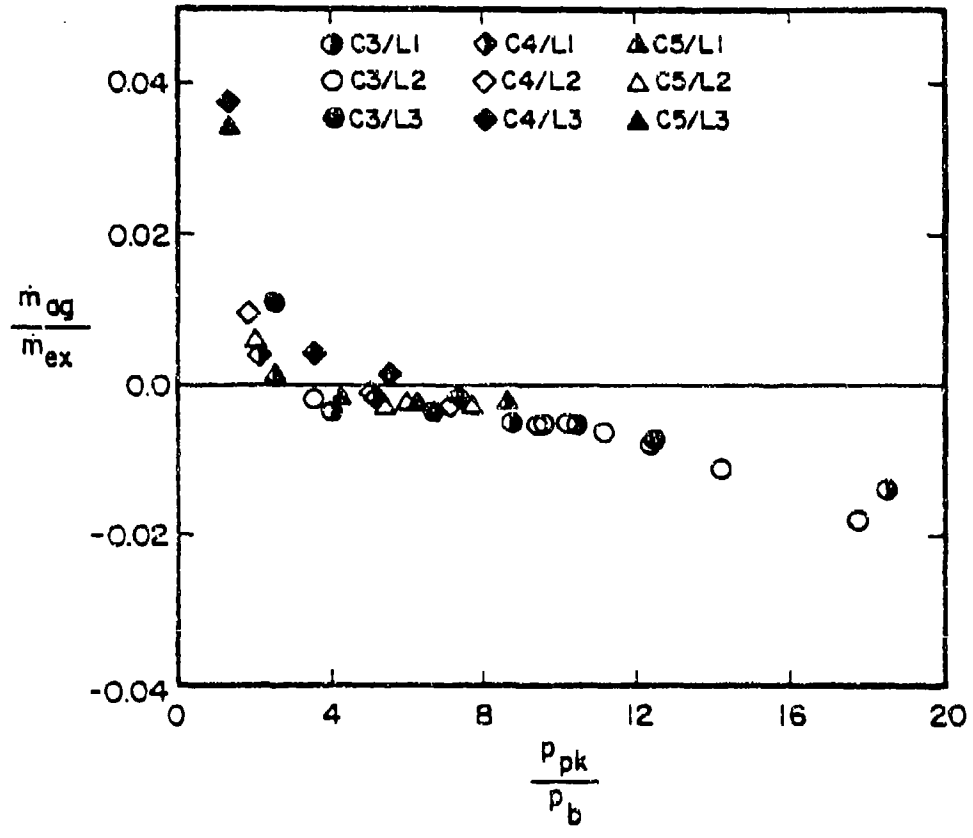

Figure 17. - The mass flow-rate in the annular gap as a function of the impingement shock strength.

($\dot{m}_{ag}/\dot{m}_{ex}$) in the annular gap to the measured value for the impingement shock-wave strength (p_{pk}/p_b), as shown in Fig. 17. Note that the mass flow-rate in the annular gap is essentially a function of the impingement shock strength over the range of nozzle/launch-tube configurations studied in the present program. Although there is some variation, a single curve can be faired through all of the data to provide the designer of a straight-tube-launched rocket system with a reasonable estimate of the mass flow-rate that will occur in the annular gap if the approximate value of the impingement shock strength is known.

Theoretical values for the pressure ratio across the weak shock wave which is generated when an inviscid, underexpanded jet impinges on the wall of a straight tube ($r_t = 1.549\ r_{ne}$) are presented in Fig. 18. The theoretical solutions, which were generated using the method-of-characteristics relations (neglecting the shear layer at the plume boundary) to calculate the isentropic flow upstream of the shock wave, were obtained for

	$\gamma = 1.18$			$\gamma = 1.40$		
p_{ne}/p_b	15.07	7.54	5.13	15.07	7.54	5.13
p_b/p_{t1}	0.00482	0.00963	0.01416	0.005	0.010	0.0147

where M_{ne} was 2.338 for both gases, i.e., both values of γ. The righthand limit of the curves indicates (approximately) the largest divergence angle of the nozzle at which the impingement shock is still weak for that pressure ratio. If the divergence angle of the nozzle were larger than this value, the impingement shock-wave would be strong. As the jet pressure ratio decreases, larger divergence angles are possible before the shock wave becomes strong. This is true because as the jet pressure ratio decreases, the jet expands less (i.e., the initial inclination of the jet boundary is less) and, therefore, the angle through which the flow is turned at the wall is less.

Massive Blow-By Flow in the Annular Gap

As has been noted , if the impingement shock-wave is strong, the resultant, large adverse pressure-gradient can turn a significant fraction of the exhaust flow upstream into the annular gap. A strong impingement shock-wave is produced when the inclination of the impinging jet exceeds a critical angle or when the exhaust flow encounters a constrictive change in cross section, i.e., the forward end of the launch tube has a larger cross section than the aft end (or ignition end). Note also that not every constrictive change in cross section causes massive blow-by. As will be discussed, the reduction in cross section must be large enough to choke the flow. Although massive blow-by has been observed in straight tubes, the subsequent discussion will focus on launch tubes with a constrictive change in cross section, since this is a feature of "nontipoff" launch tubes. In a nontipoff launch tube, the missile is constrained while it builds up speed and angular momentum. The front and the rear supports of the missile are released simultaneously in an attempt to minimize mal-launch effects. The presence of rails, frangible bore riders, and

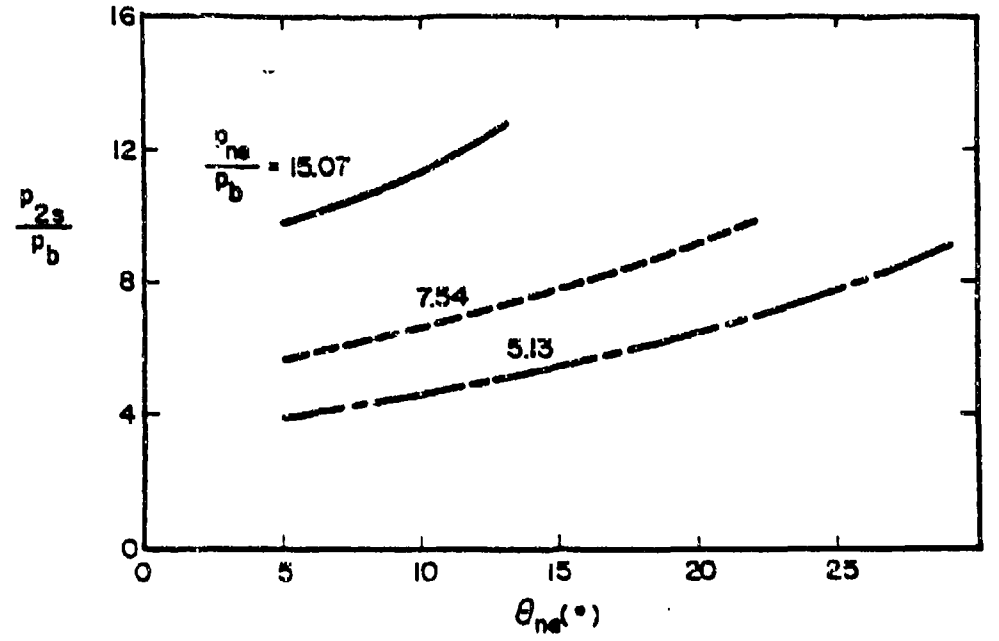

(a) γ = 1.18

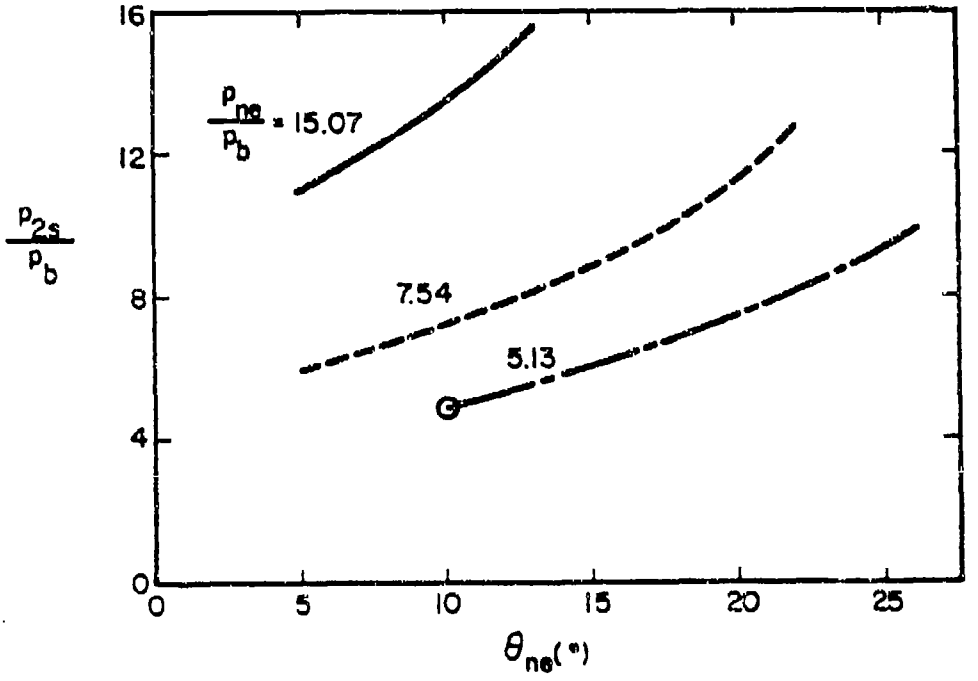

(b) γ = 1.40

Figure 18. - The pressure ratio across a weak, impingement shock-wave, $r_t = 1.549\ r_{ne}$.

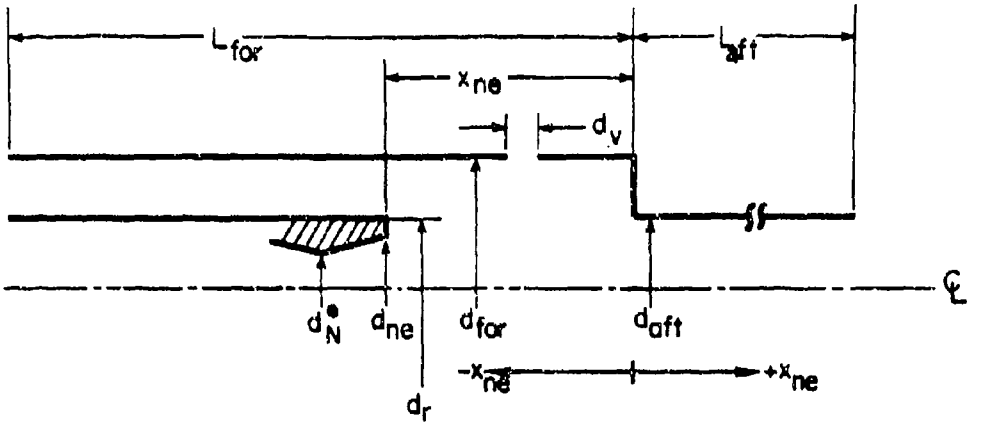

Figure 19. - The geometry and its nomenclature for a rocket/nontipoff-launch-tube configuration.

smaller-diameter cylindrical aft-tubes serve to constrict the flow of the exhaust gas. Measurements of the pressure differentials acting on the aft end of simulated rockets [1,36] clearly show that these blow-by flows can be a significant error source.

The subsequent discussion will focus on flows where the nozzle exit-plane is at least $4r_{ne}$ into the forward tube, i.e., $x_{ne} \leq -4r_{ne}$. Furthermore, d_{aft}/d_{for} is sufficiently small that flow is choked by the constriction. The geometry nomenclature is illustrated in Fig. 19.

When the parameters of the rocket exhaust flow field and the launch-tube geometry are such that the impingement shock-wave is strong and the flow is choked by the constriction, the flow field in the launch tube is similar to that depicted in Fig. 20. The relative dimensions of nozzle-exit radius (r_{ne}): aft-tube radius (r_{aft}): forward-tube radius (r_{for}) are to scale. The axial dimensions are not to scale. Thus, whereas the impingement shock-wave is sketched as a normal shock wave extending almost from wall to wall, oblique shock waves associated with the initial turning of the flow probably extend over a longer distance than indicated in the sketch. The extent over which the pressure rise occurs would be a measure of the interaction between the viscous shear layer and the complex shock-wave structure. The essential features of the flow model include: (1) the underexpanded flow in the nozzle exit-plane (designated by the subscript ne), (2) the supersonic flow just upstream of the impingement shock-wave (designated by the subscript us), (3) the subsonic flow just downstream of the strong impingement shock-wave (designated by the subscript ds), (4) the reverse, or blow-by, flow (i.e., that fluid in the viscous shear layer which cannot overcome the adverse pressure gradient generated by the interaction between the impingement shock and the viscous flow), (5) the region at the base of the constrictive change in cross section (i.e., the step) where some of the fluid which has passed through the shock system stagnates, (6) the subsonic flow at the entrance of the small-diameter, aft tube (designated by the subscript ati), and (7) the sonic

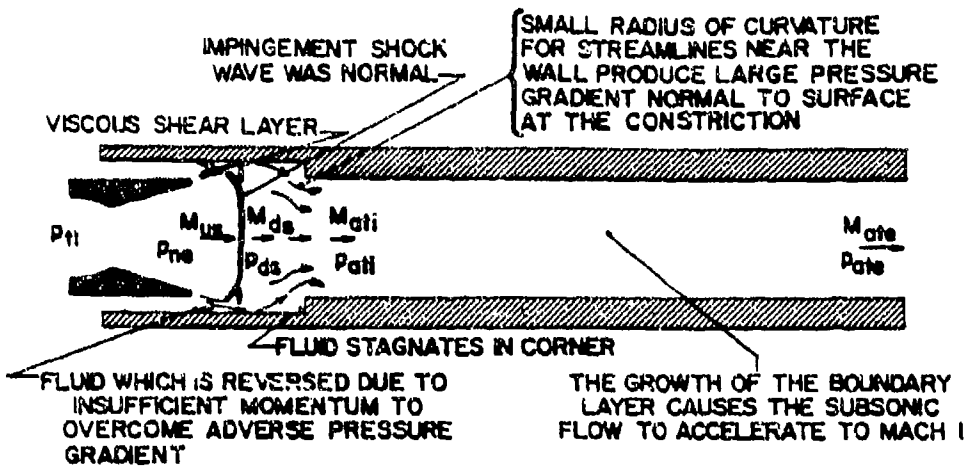

Figure 20. - Sketch of the flow model for the choked exhaust flow in a constrictive launcher.

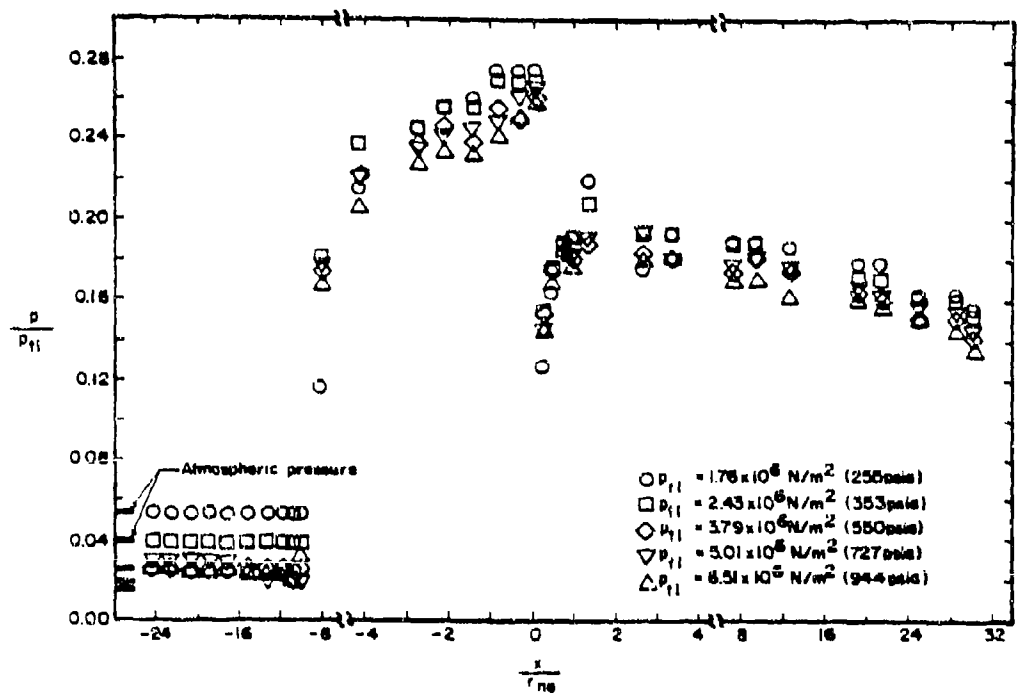

Figure 21. - The static wall-pressure distribution for unheated air exhausting into the 0.2-scale Rip-Zap launcher, $x_{ne} = -10.41\ r_{ne}$.

flow at the exit plane of the small-diameter, aft tube (designated by the subscript ate).

To substantiate the validity of the flow model for the choked flow in a constrictive tube, consider the experimental pressures of Fig. 21. These data were obtained with the nozzle exit-plane 10.41 r_{ne} from the constriction for which $A_{aft} = 0.595A_{for}$. In the subsequent discussion, the experimental pressures will be compared to approximate, theoretical values based on a one-dimensional flow incorporating the phenomena of Fig. 20. The one-dimensional exhaust flow is assumed to accelerate isentropically from the sonic conditions at the throat to the conditions just upstream of the shock. Since A_{for} was 5.302A*, M_{us} would be 3.237 (Ref. 11). Downstream of the normal shock-wave, the theoretical Mach number (M_{ds}) is 0.4626 and the theoretical static pressure (p_{ds}) is 0.2147 p_{t1}. The theoretical value for the static pressure is in reasonable agreement with the experimental values of Fig. 21, since the corresponding experimental values are approximately 0.22 p_{t1}. The theoretical stagnation-pressure downstream of a normal shock-wave (0.2676 p_{t1}) is in reasonable agreement with the pressures measured at the base of the rectangular step. Thus, there is reasonable agreement between the experimental data and the theoretical values for this relatively simple flow model. Furthermore, it was observed [3,37] that the location of the normal shock-wave is fixed with respect to the nozzle exit-plane and that the choked blow-by flow rate is independent of nozzle-exit location. These three observations support the conclusion (as illustrated in Fig. 20) that the fluid which constituted the blow-by flow did not pass through the shock system.

The pressure data indicate that the flow accelerates through the constriction and is, therefore, subsonic. The subsonic flow immediately downstream of the shock wave in the forward tube ($M_{ds} = 0.4626$) would accelerate to sonic conditions (for a one-dimensional, isentropic flow) if A* were 0.6933 A_{for}. But A_{aft} is only 0.595 A_{for}. Thus, the aft tube is approximately 14% smaller in cross section than the sonic throat-area for the upstream flow. It was noted[37] that the fraction of the exhaust flow which is turned upstream ($\dot{m}_{ag}/\dot{m}_{ex}$) is approximately 15%. Thus, once the critical value of reservoir pressure (or mass flow-rate) has been exceeded, the large reduction in area (from A_{for} to A_{aft}) causes the flow to choke at the constriction. (The reader is reminded that the other parameters, such as the characteristics of the shock impingement, are of extreme importance. In analyzing the Rip-Zap flight test data[38] the apparently anomalous behavior of the Flight-12 data was attributed to probable "differences in the plume characteristics".) Adjustments took place in the internal flow field, so that the flow in the exit plane of the aft tube is sonic, i.e., $M_{ate} = 1$. The model for the resultant flow in the aft tube appears to be that described by Shapiro[39] as choking due to friction. That the flow in the exit plane of the aft tube is indeed sonic was indicated by the static pressure measurements, presented in Fig. 21. Assuming that the fluid near the center of the launcher accelerates isentropically from "ds", the static pressure at the sonic location would have been 0.5283 p_{t2} or 0.1414 p_{t1}. This value for the theoretical static pressure at the sonic location is essentially equal to the static-pressure measurements from near the exit plane of the aft tube.

Using a one-dimensional flow model to represent the choked flow in a constrictive launch-tube provides a reasonable correlation with the experimentally-determined static pressure distribution along the launcher wall. Thus, this reasoning will be used to calculate the onset of blow-by. The following assumptions were made regarding the flow model.

(1) The exhaust flow expands isentropically from the nozzle exit-plane until it encounters the wall. For a given γ, the Mach number of the flow just upstream of the impingement shock-wave can be determined using the area ratio of the cross section of the forward tube to the throat area, or equivalently, d_{for}/d^*.

(2) A normal shock wave occurs at the impingement location.. Therefore, given the upstream Mach number and γ, the downstream Mach number can be calculated.

(3) The small-diameter aft tube acts as a second throat. Given the Mach number downstream of the normal impingement shock-wave, γ, and the area of the forward tube, one can calculate the minimum area through which the subsonic flow can be accelerated, which is a sonic throat for the shocked flow. Thus, the constrictive area ratio for the launcher,

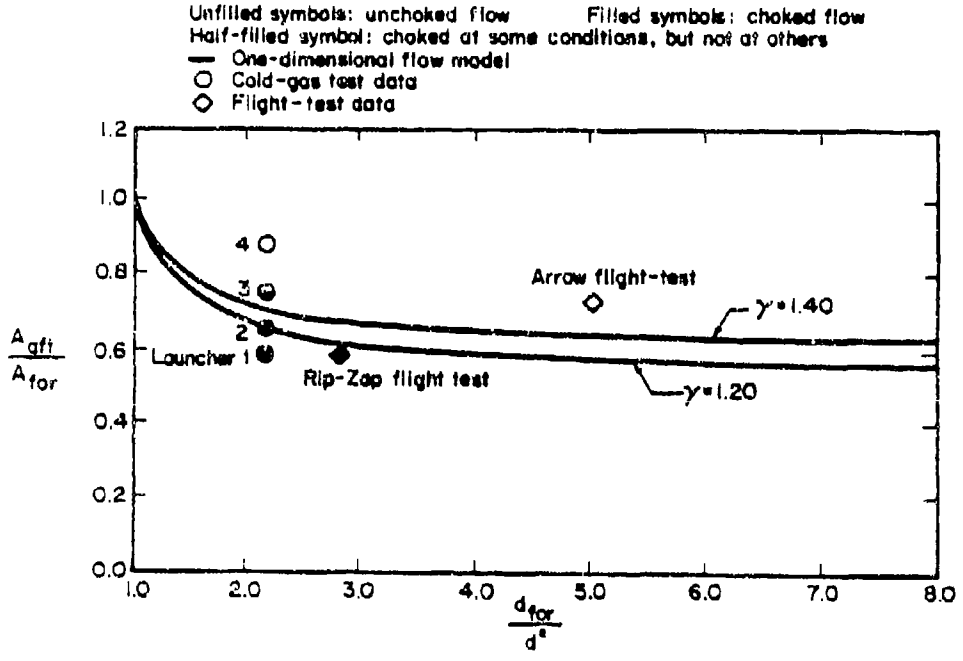

Figure 22. - The minimum constrictive area ratio through which the rocket exhaust gas can pass without choking the flow.

A_{aft}/A_{for}, can be calculated. If the area of the aft tube is less than this area for a second throat, then a substantial fraction of the exhaust flow must be turned upstream.

The minimum constrictive area ratio, A_{aft}/A_{for}, through which the exhaust flow can pass without significant blow-by flow occurring is presented in Fig. 22 as a function of d_{for}/d^*.

The correlations based on this simple flow model are compared with data from the cold-gas test programs conducted at the University of Texas at Austin[37,40] and from flight-test programs[41,42]. The correlation predicts choking in Launcher 1 (A_{aft}/A_{for} = 0.595, see Ref. 37) and in Launcher 2, which was verified by the experiments. The correlation predicts that the constrictive area ratio for Launcher 3 (A_{aft}/A_{for} = 0.735) is just above that for choking. As was noted in Ref. 40, in some cases the flow did choke; in others, it did not. It is assumed that the differences were due to the presence of the boundary layer and viscid/inviscid interactions that reduced the effective cross section. Flow in Launcher 4 did not choke, which is as expected. Data from the Rip-Zap flight test programs[3,38] indicated that the flow choked, as would be expected from the correlation. The correlation indicates that the flow should not choke in the Arrow launcher. Again, the flight-test data[3,41] were consistent with the correlation.

The reader is cautioned against using the correlation casually. To be valid, the flow in the nozzle exit-plane must be considerably underexpanded. The growth of the viscous boundary-layer would change the effective cross-sectional area of the tube and, therefore, influence the minimum values of A_{aft}/A_{for}. Other parameters which cause losses in the total pressure of the flow, e.g., the presence of spin vanes, would also produce significant changes in the correlation. Furthermore, changing the base-region boundary conditions, such as by sealing the annular gap to prevent secondary flow, would affect the actual correlation. For the second-throat ejector-diffuser systems, the constriction-induced shock wave causes the cell pressure to increase, which in turn causes the jet to expand through a lesser angle reducing the strength of the shock. This compensating interrelation (which allows second-throat diffuser ejectors to "start" for very low constrictive area ratios) does not occur for the launch-tube flows. Instead, the constriction-induced shock wave promotes blow-by flow. Empirical correlations developed by Jones et al.[43] and verified by German et al.[32] indicate that second-throat ejector-diffuser systems would start for constrictive area ratios at which massive blow-by occurs for the launch-tube flow fields.

A quantitative model incorporating the flow mechanisms described in Figs. 20-22 has been developed[44]. The nomenclature for this model is presented in Fig. 23. It is also assumed:

(1) that the flow is quasi-steady,

(2) that the interaction mechanism in the forward tube becomes established within a few nozzle-exit diameters as the afterbody alights from the aft tube[37], and

(3) that the very complex viscid/inviscid interaction mechanism upstream of the constrictive diameter can be treated as one-dimensional[32].

Recall that the detailed pressure data of Fig. 21 indicates highly curved streamlines at the constriction. Furthermore, a variety of constrictive geometries have been represented in different phases of the research[38,41,42]. Depending upon the shoulder geometry and the effect of the shock pattern and/or the adverse pressure gradient along the upstream wall, the flow entering the aft tube may be subject to a contraction, decreasing the effective one-dimensional entrance cross section (vena contracta). The presence of a vena contracta is indicated by experimental data showing a localized pressure drop just downstream of the entrance cross section in the constriction. While exact solutions for such contractions can be derived for potential flow by means of hodograph methods, it is evident that the actual approach and downstream conditions preclude the usefulness of such concepts. A parametric study of contracting flows by one-dimensional compressible flow modeling suggests that even the lower limit (producing initial conditions in a "free sonic throat") will not result in a substantial modification of both Mach number and stagnation pressure as the entrance condition for the Fanno flow component so that an isentropic relation may be assumed to relate the flow conditions in cross sections 2' and 3.

Based on the same reasoning as above, entrance into the front tube can then also be considered to be isentropic, generated by a stagnation condition p_b, T_t prevailing near the nozzle base.

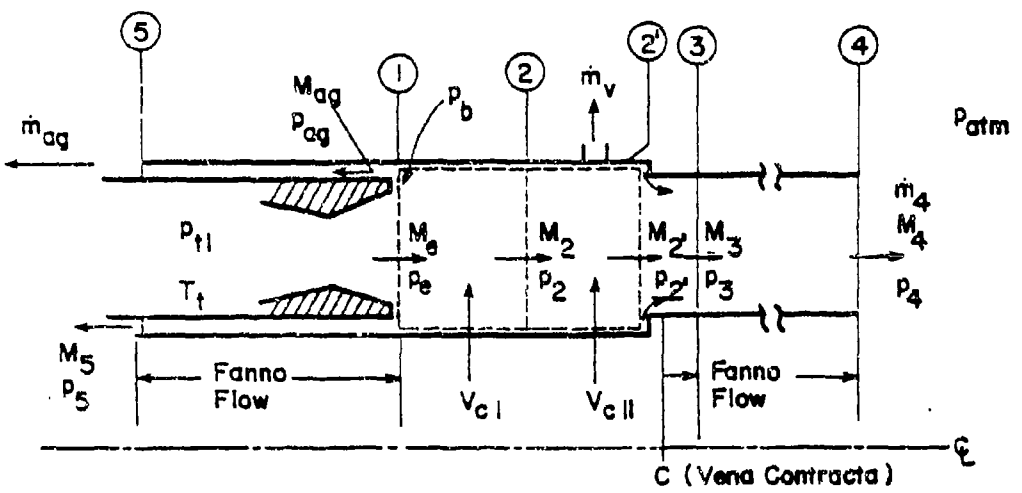

Figure 23. - Nomenclature and one-dimensional flow-field model for choked flow in a constrictive, nontipoff launch-tube.

Flows through the aft tube as well as in the (generally eccentric) annular region between missile body and launcher fore-tube shall be treated as Fanno line problems[39]. This is certainly an approach suggested by convenience which can, however, be justified by close scrutiny of experimental data obtained with flows individually discharged through either one of the conduits. Use of the functional relationship between entrance and exit Mach numbers is expressed with the help of the auxiliary function $[f\ L_{max}/d_{eq}]$ where d_{eq} is the equivalent passage diameter ($d_{eq} = d_3$ for the aft tube and $d_{eq} = d_2 - d_r$ for the forward tube)[39]. The friction factor, $f = f(Re_{d_{eq}}, e/d_{eq})$, can be calculated from Colebrook's equation[45] (small changes in Reynolds number along the passages not being significant):

$$1/(f^{1/2}) = -0.86\ \ell n[e/(3.7\ d_{eq}) + 2.51/[Re_{d_{eq}}\ (f^{1/2})]$$

Use of this equation (originally derived for circular pipes and incompressible flow) is justified in view of the limited annular eccentricity of the forward tube[46] and the fact that the flow is subsonic in both passages. More questionable is the assumption of fully-developed turbulent flow in the aft tube. Nevertheless, experimental evidence seems to support such a treatment. Pressure distributions along Fanno lines can be evaluated with the help of the auxiliary functions $(f\ L/d_{eq})(k,M)$ determining location and $(p/p^*)(k,M)$ determining the local pressure levels[39].

The individual flow-model components are linked together and a unique solution for the entire system can be found by an iterative computational procedure following this brief outline. Assuming first critical outflow from both forward and aft tubes, a base pressure ratio corresponding to a normal shock in the nozzle-exit cross section, and choosing a reasonable value for the friction coefficients, one finds, for a given geometry, first values for M_{ag} and M_3. This, in turn, allows one to find $M_{2'}$ and in the absence of, or ignoring initially, the flow through the vent ports, M_2. Consequently, p_2/p_{t1} can be found. The calculations are carried downstream (along both aft and forward tubes) having established first approximations for pressure levels and temperature levels, so that Reynolds numbers and friction factors can be found. Thus, flow rates through aft and forward tubes and vent ports can be determined. Exit conditions both for aft and forward tubes are then examined and the entire procedure repeated until subsequent iterations for p_b/p_{t1} agree within a prescribed limit.

A comparison between the pressure distributions computed based on this flow model and the corresponding experimental pressures from Ref. 37 is presented in Fig. 24. As can be seen, the quantitative agreement is quite good for this case with a rocket nozzle-exit position -8.41 nozzle radii upstream of the cross-sectional constriction. The relative insensitivity of pressure ratios to absolute nozzle stagnation pressure levels is also borne out by the computer solution. The existence of a vena contracta downstream of the constriction is evident from the experimental data but quick recovery to Fanno-line type flow is also observed.

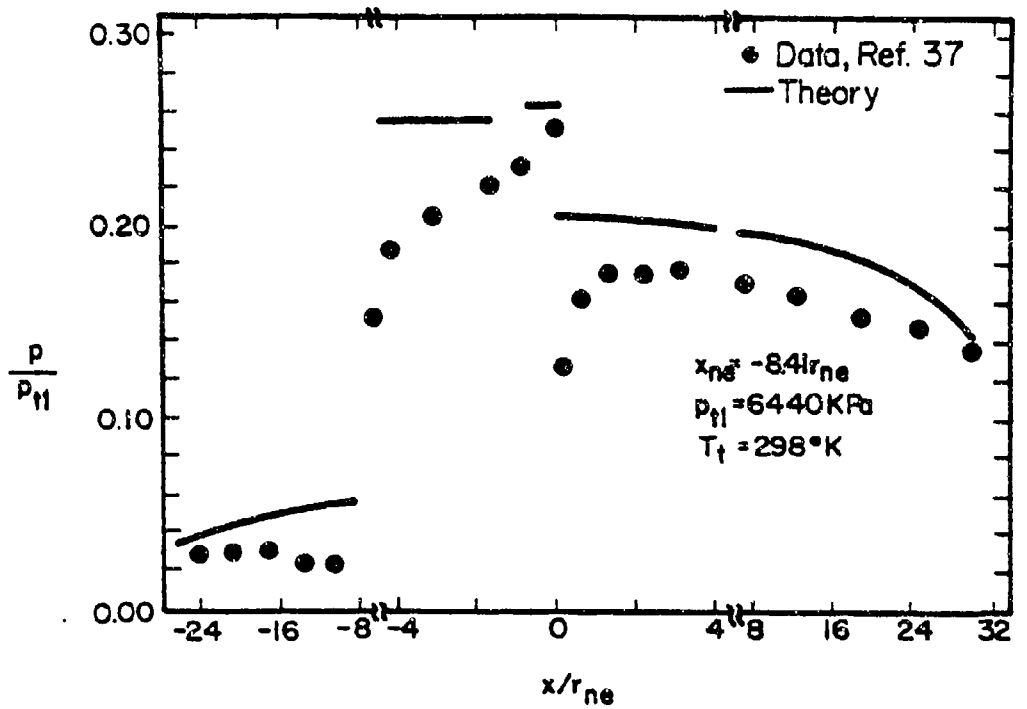

Figure 24. - Comparison of experimental and theoretical static wall-pressure distributions for the 0.2-scale Rip-Zap launch-tube, $x_{ne} = -8.41\ r_{ne}$.

A comparison between calculated and experimentally determined[37] blow-by mass flow-rates is presented in Fig. 25. Both the level and the dependence upon nozzle stagnation pressure show good agreement. By using the computer option for vent-port effectiveness, the predicted blow-by rates for different "equivalent diameter" vent ports are also shown.

As an alternative to vent ports, an increase in aft-tube diameter can also be considered as a means for controlling blow-by[47]. The result of theoretical calculations indicates the elimination of significant blow-by for aft-tube diameters such that the area ratio A_3/A_2 (i.e., A_{aft}/A_{for}) is in excess of 0.79. This agrees well with the predictions and the experimental evidence presented in Fig. 22.

It has been suggested[42,47,48] and is supported by the limited data obtained in free-flight testing[42] that the simulation of hot propellants by cold-air-flow experiments not only offers qualitative information but also shows reasonable quantitative correlation of pressure ratios. Implied in this statement is the retention of all geometrical parameters, except a scale factor[42] and, in addition, the practical insensitivity with respect to the specific heat ratio. Obviously, the quasi-steady analysis does not account for the acceleration of the propellant gas. However, it can be shown that the effects of non-steady gas motion are relatively unimportant, at least for the initial stages of the launch process. By contrast, one expects that differences

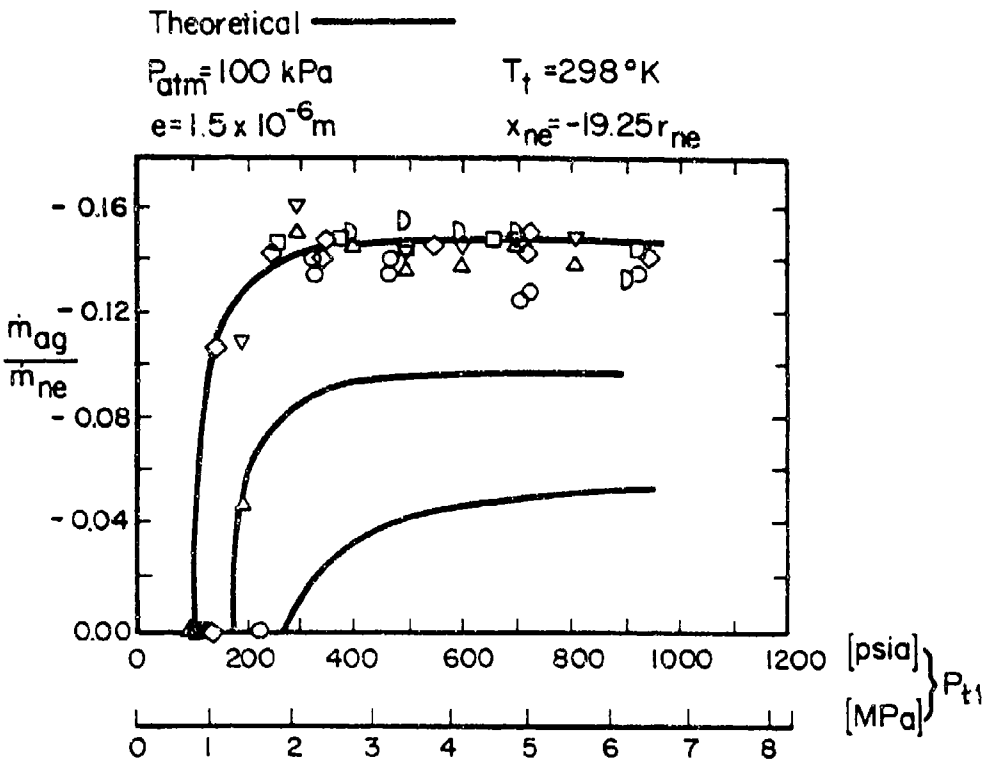

Figure 25. - Comparison of experimental and theoretical blow-by flow rates for 0.2-scale Rip-Zap launch-tube, x_{ne} = -19.25 r_{ne}.

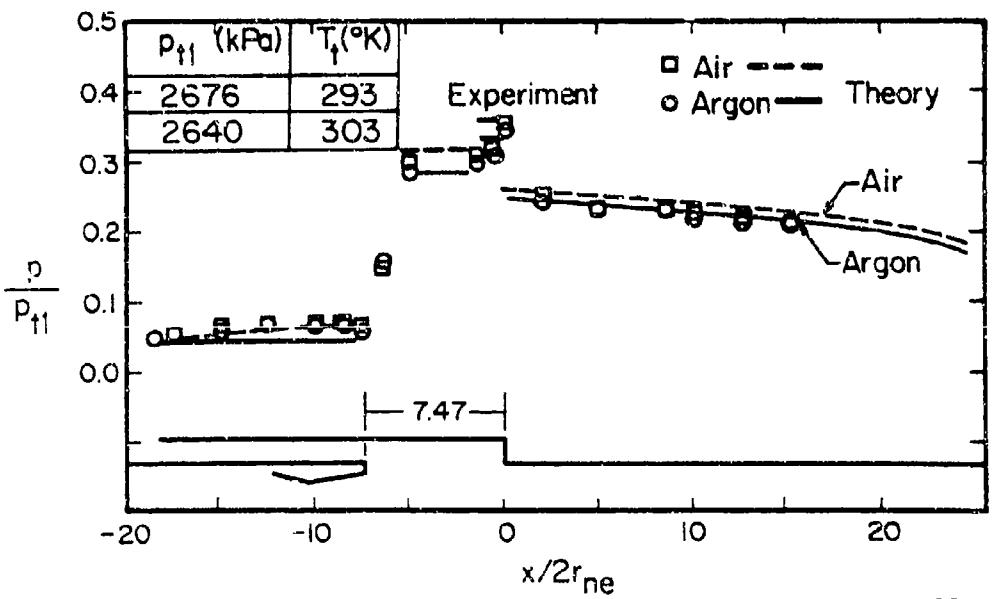

Figure 26. - Comparison of experimental and theoretical static wall-pressure distributions for air and for Argon.

caused by the use of dissimilar gases and scale effects have to be carefully examined. This requires the study of the influence of specific heat ratio and Reynolds number dependency. The isolated parametric influence of the specific heat ratio (retaining gas constant and viscosity coefficients for air) was explored using the computer program available at the University of Illinois[49]. A sweeping appraisal of this factor, extending to γ values near unity, showed no appreciable effects; neither for pressure distributions nor for blow-by mass rate ratios.

The availability of the Argon blowdown facility[50] made it attractive to conduct experiments to clarify the influence of the specific heat ratio while practically eliminating scale (Reynolds number) effects. Comparison between experimental and theoretical pressure levels showed excellent agreement, as shown in Fig. 26. Even though the nozzle-exit Mach numbers for air and for Argon were different and all gas-dynamic functions appearing in the analysis are affected by the specific heat ratios, the dimensionless pressure levels for the two gases are in good agreement.

ANALYSIS OF FLIGHT TEST DATA

The basic nomenclature and exhaust flow-field phenomena for tube-launched rockets have been presented in the previous sections using primarily theoretical flow-field models and experimental data obtained through cold-gas simulations. These basic precepts will now be incorporated into the analysis of wall pressure measurements obtained during two flight-test programs[1,3,4,38,41,42] that used nontipoff launch tubes.

In a nontipoff launcher, the cross section is varied so that the rocket is constrained immediately after ignition but, once it has sufficient velocity, it flies free of any tube support for a short distance as it emerges from the tube. The use of the term "constrictive change in cross section" indicates that the radius of the aft tube is smaller than the radius of the forward tube. Thus, in addition to the parameters which characterize the underexpanded supersonic exhaust flow, the resultant flow field depends on the geometry of the launch tube. The geometric variables for the launch-tube configuration include the aft-tube radius, the forward-tube radius, the geometry of the constriction, the length of the forward tube, and the length of the aft tube.

A sketch of the launch sequence is presented in Fig. 27. The flow of the rocket's high temperature and high pressure exhaust gas in these nontipoff launch tubes is particularly complex because of the presence of the constriction. Initially, the rocket is constrained while the linear and the angular momentum of the rocket increase. Once the exit plane of the nozzle reaches the change in cross section, the mechanisms that constrain the rocket (such as sabots) are released. Thus, the sabots located at the forward end of the rocket are thrown free as the nose emerges from the tube. The constraints located at the aft end are released simultaneously, so that although a significant portion of the missile is still in the launcher, it flies free of constraints.

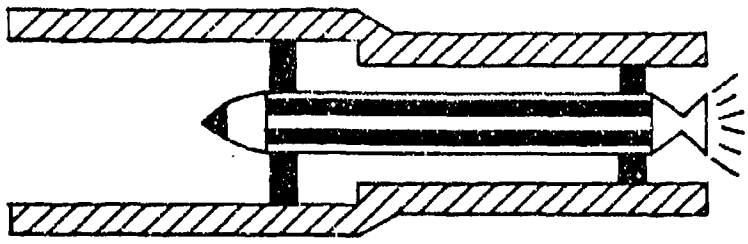

(a) Ignition (rocket initially constrained)

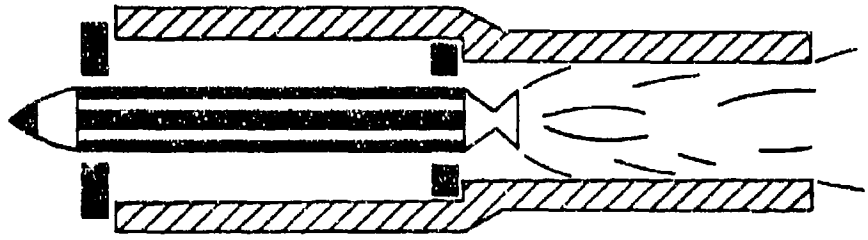

(b) Simultaneous release of sabots

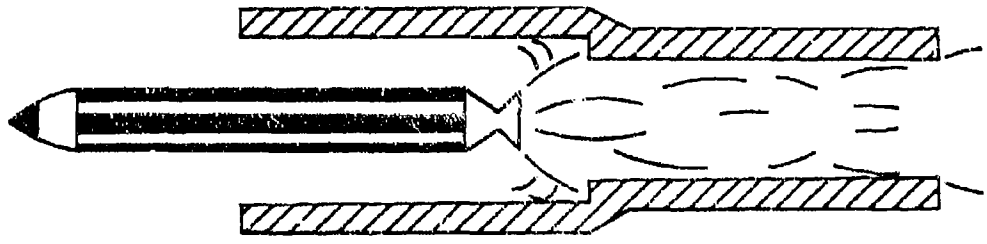

(c) Free flight

Figure 27. - Sketch of the launch sequence in a constrictive, nontipoff launch-tube.

During the time interval immediately after ignition when the rocket exhausts directly into the aft tube, the flow fields correspond to those already described for a straight-tube launcher. Significant blow-by flow rates would occur only if the nozzle divergence angle, the Mach number in the exit plane, the ratio of specific heats, and the jet pressure ratio were such that the impingement shock-wave would be strong. However, as will be discussed, the pressure measurements for both programs indicate that the impingement shock-wave was weak as long as the nozzle exhausted into the aft tube.

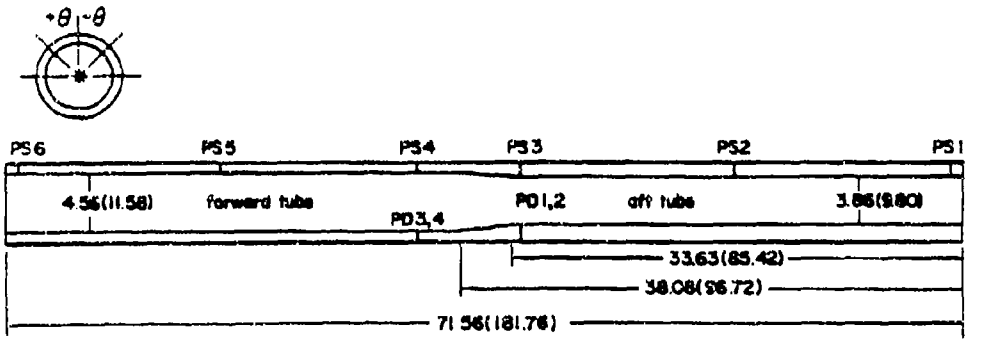

(a) Arrow launch-tube

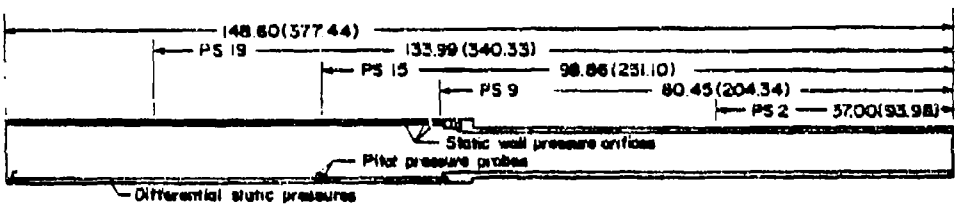

(b) Rip-Zap launch-tube

Figure 28. - Sketches of flight-test launch-tubes and their instrumentation. Dimensions in inches (centimeters).

As the nozzle exit-plane enters the forward tube, i.e., as $x_{ne} < 0$, shock waves can occur not only as the exhaust from the underexpanded jet encounters the wall but also as the flow encounters the constriction. As indicated by the data presented in Fig. 22, the exhaust flow was choked by the constriction in one program, i.e., the Rip-Zap configurations, but not in the other program, i.e., the Arrow configuration. Sketches of the launch-tubes and their instrumentation are presented in Fig. 28. Note that A_{aft} is 0.717 A_{for} for the Arrow launch-tube but is 0.595 A_{for} for the Rip-Zap configurations. As discussed in Refs. 3 and 38, two different geometries were used to accomplish the constrictive change in cross section for the Rip-Zap configurations. However, the constrictive geometry had only a second-order effect on the exhaust flow-field, once the nozzle exit-plane had moved a few diameters from the constriction into the forward tube.

When the nozzle exit-plane first enters the forward tube, i.e., $-1.5\ r_{ne} < x_{ne} < 0$, the exhaust from the underexpanded jet impinges directly on the constriction. The pressure rise which results depends on whether the reduction in the cross-section area is accomplished abruptly by a rectangular step or gradually by a ramp configuration (for examples of constrictive geometries, refer to Ref. 42). If the impinging exhaust flow encounters a relatively high rectangular step, a curved shock wave which is essentially normal near the wall develops. At this instant, a large pressure gradient from the constriction ($x = 0$) to the forward end of the launcher causes a significant portion

of the exhaust flow to be turned upstream, i.e., reversed. The reverse flow generated when the exhaust splashes onto the constriction will be termed "splashback". Significant splashback can produce significant (transient) increases in the pressure in the annular gap, as will be evident in the Rip-Zap measurements. However, negligible splashback was observed[3] during the Arrow flight-test program in which a rocket was launched from a tube for which A_{aft} was 0.717 A_{for} and the change in cross section was accomplished by a 4° ramp. Thus, the geometry of the constriction as well as constrictive area ratio has a marked effect on the magnitude of the splashback flow rate.

Pressure Measurements from the Arrow Program

It has been noted that, when the nozzle exhausted directly into the aft tube, the impingement shock-wave and the reflected shock waves were weak. This is true for both flight-test programs. Thus, under the quasi-steady-flow assumption, the shock-wave structure and the static wall-pressure distribution at any instant in time would be similar to that presented in Fig. 29. These data were obtained during static firings into a constant-diameter launch tube[19].

In the flight-test programs, the missile gradually accelerates through the launch-tube. Thus, one can view the flow as corresponding to the situation where a point on the wall moves away from the nozzle exit-plane. To interpret the flight-test data in terms of the pressure distribution presented in Fig. 29, imagine that a pressure gage moves axially, experiencing temporarily high pressures as it passed through the impingement shock-wave and its reflections.

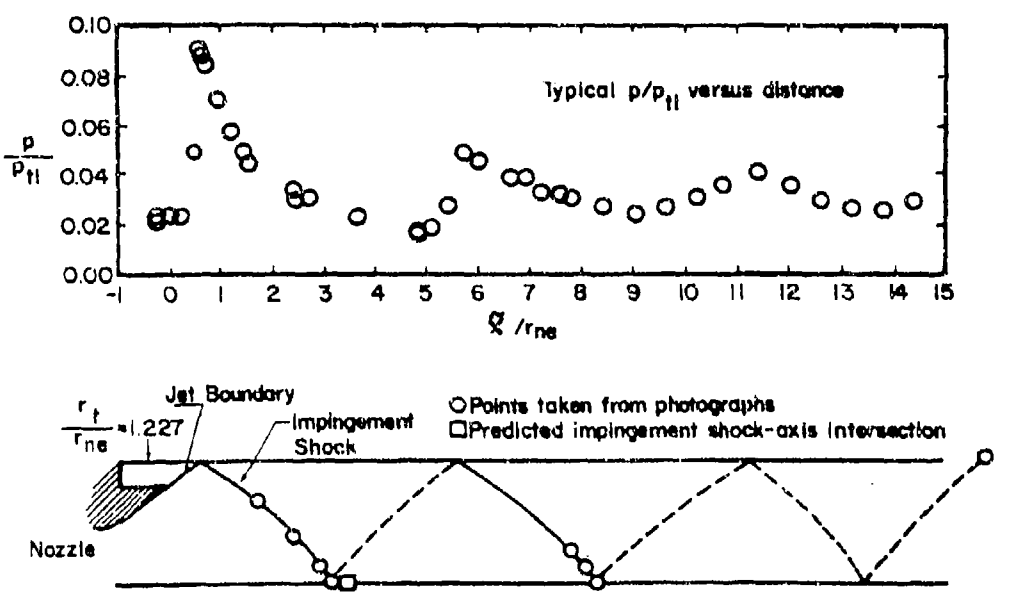

Figure 29. - Sketch of typical pressure distribution and shock structure for supersonic flow in a constant-area launch-tube.

The static wall-pressure measurements for PS1, which was located in the small-diameter, aft tube and which was the first gage to be exposed to the rocket exhaust (see Fig. 28a), are presented as a function of time in Fig. 30a. This pressure history which was measured during Flight 110 is typical. The pressure data are presented in dimensionless form as the ratio, p/p_{t1}, i.e., the static pressure divided by the stagnation pressure of the rocket motor. Since the reservoir stagnation pressure was not measured, it was assumed to be the nominal value for the Arrow motor, 8.97×10^6 N/m^2 (1300 psia). While the rocket exhausted directly into the aft tube, the pressure periodically rose suddenly (due to a shock impinging on the wall) then decreased gradually. The period became shorter as the rocket accelerated away from the gage. These data

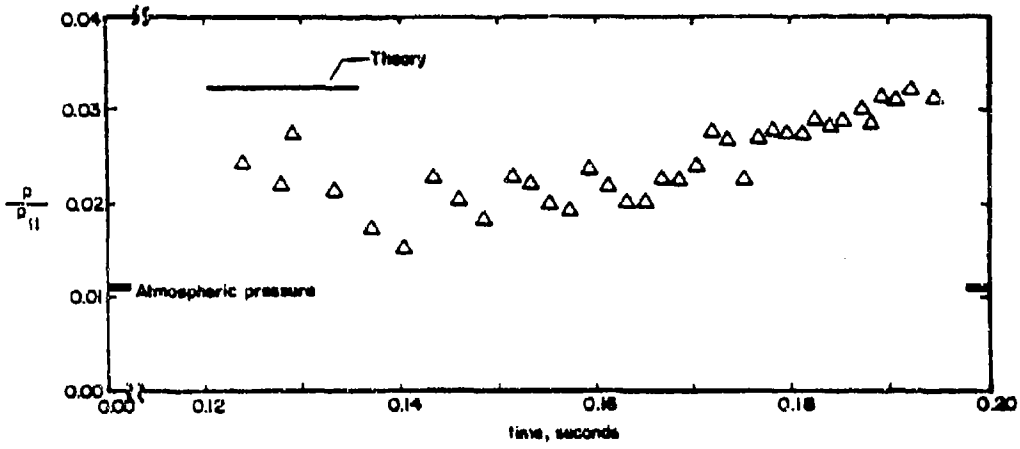

(a) As a function of time for Flight 110

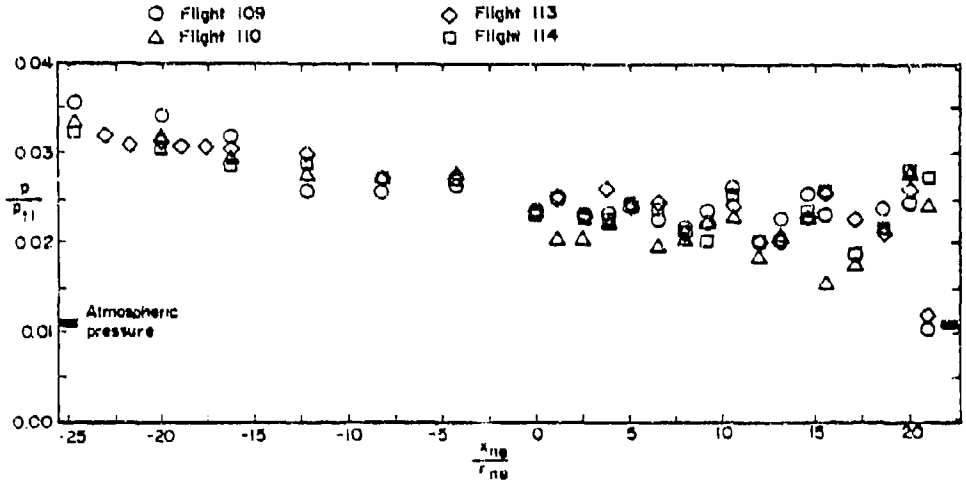

(b) As a function of nozzle exit location for all flights

Figure 30. - The pressure history for PS1 (x_g = +21.985 r_{ne}) in the Arrow flight-test program.

were qualitatively similar to the histories obtained during other programs while the rocket exhausted into a constant-area tube[18,19,38]. For the present tests, the peak pressure was greatest for the initial rise (i.e., the shock-induced pressure rise associated with the impingement of the exhaust flow on the launcher wall). For comparison with the data, the theoretical value of the static wall-pressure downstream of the impingement shock is included in Fig. 30a. The numerical code generates the solution for an underexpanded supersonic flow exhausting from a stationary nozzle into a constant-area tube. The base pressure was assumed to be equal to the atmospheric value. The theoretical value for the static pressure downstream of the impingement shock-wave was $0.0317\ p_{t_1}$. The theoretical value was within 15% of the initial peak value for the measured pressure.

As the exit plane of the rocket nozzle passed the change in cross section (at approximately 0.167 seconds), the pressure recorded by PS1 increased. However, the increase was relatively small, especially when compared with the corresponding pressure increase measured during the Rip-Zap program when the rocket passed the constriction of that launch tube[38], as will be discussed in the next section. The relatively low values for the static pressures from the Arrow launching are not, of themselves, definitive. However, as the discussion of the additional data will substantiate, the flow downstream of the impingement shock remained supersonic, even when the rocket exhausted into the forward tube. That is, the constrictive area ratio of the Arrow launch tube was such that the exhaust flow was not choked when it encountered the constriction.

To compare the data from different flights, the pressure measurements for PS1 are presented in Fig. 30b as a function of the nozzle exit location instead of time. The curve fits of the observed position histories were used to determine the time which corresponded to a particular location of the nozzle exit-plane. The nondimensionalized pressure data are presented as a function of the nozzle position relative to the departure edge (x_{ne}/r_{ne}). This position parameter was positive when the exit plane of the rocket was in the small-diameter, aft tube and negative for the large-diameter, forward tube. The periodic variations of the pressure which occurred during the interval when the nozzle exit-plane was located between the orifice and the departure edge were due to reflections of the impingement shock-wave in the fully supersonic flow. With the rocket exhausting into the large-diameter, forward tube, the static pressure increased slightly. The increase is attributed to the fact that the supersonic flow in the forward tube decelerated at the constriction. The magnitude and the apparently periodic variations of the pressure for $x_{ne} < 0$ suggest that even, after the deceleration process through the constriction had taken place, the flow was supersonic.

The static pressure measurements for PS5 are presented in Fig. 31. As long as the nozzle exit-plane is located in the aft tube, i.e., as long as the exhaust gases flow directly into the aft tube, the static pressure recorded by PS5 is essentially constant and equal to the atmospheric value. When the rocket exhaust impinged on the constriction, there was a slight increase in the pressure recorded by PS5 (which

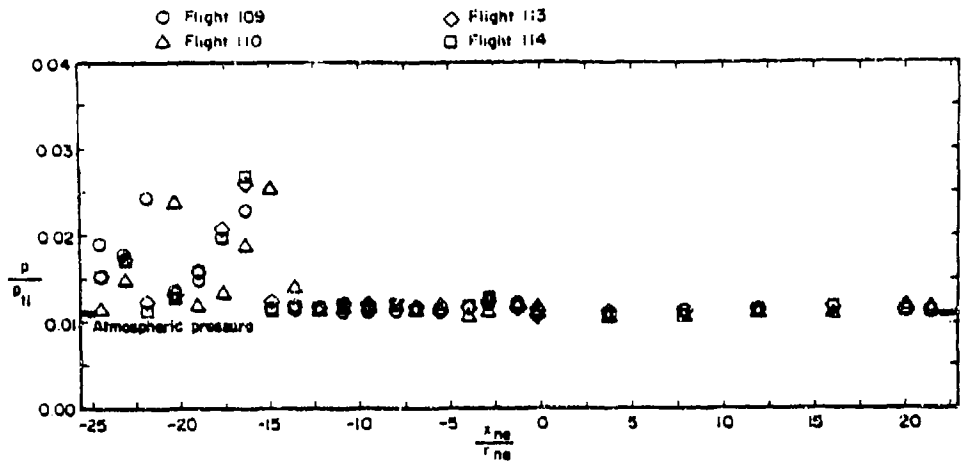

Figure 31. - The pressure history for the PS5 (x_g = -14.799 r_{ne}) in the Arrow flight-test program.

was upstream of the nozzle exit-plane in the annular region). The impingement-produced pressure rise on the constrictive surface of the launcher produced a favorable pressure gradient from the internal end of the forward tube (i.e., at the change in cross section) to the upstream end of the forward tube which is open to the atmosphere. This pressure drop produced a reverse, or blow-by, flow which, in turn, caused the pressure in the annular region (at PS4 and at PS5)[41] to rise slightly then decrease. The slight pressure variation recorded by PS5 was most clearly evident in the data of flight 114. However, the magnitude of the pressure variation measured during this pulse was much less than that measured during the Rip-Zap program. Thus, the splashback mass flow-rate apparently was relatively small for the Arrow test program. The fact that a measurable pressure variation due to the blow-by flow was not recorded[41] by PS6 (see Fig. 28a for the location of this gage) indicates that the splashback was so weak that it may have been dissipated in the annular region prior to reaching the forward end of the launcher.

As the exit plane of the rocket passed the station of PS5, the pressure rose suddenly. Again, there was good agreement between the pressure measured downstream of the impingement shock-wave and the theoretical value. The experimental value was within 9% of the theoretical value. As the rocket continued to accelerate away from the gage, the static pressure decreased then increased suddenly due to the reflected shock wave. The periodic character and the relatively low magnitude of the static pressures indicated that the downstream flow remained supersonic. These data were in marked contrast to the Rip-Zap data[38] where the flow choked and the pressure in the subsonic flow downstream of the impingement shock was approximately constant at 13 atmospheres.

A Review of the Pressure Histories for the Arrow Configuration - The pressure measurements presented in Figs. 30 and 31 provide several insights into the exhaust flow-field in the constrictive, Arrow launch tube.

(1) When the exit plane of the rocket nozzle was in the small-diameter aft tube, the flow was fully supersonic. There was not significant reverse, or blow-by, flow.

(2) When the exit plane of the rocket nozzle passed the constriction, the increase in the pressures measured at the orifices in the aft tube (downstream) was measurable but was much less than the corresponding increase measured during the Rip-Zap program[38]. The impingement produced a pressure rise at the constriction producing a favorable pressure gradient from the internal end of the forward tube to the upstream end of the forward tube (which exhausted to the atmosphere). This pressure gradient produced the reverse, or blow-by, flow which, in turn, caused the pressure in the annular region to rise slightly then decrease. The "splash-back" mass flow-rate apparently was very small (one might say "negligible") for the Arrow test program.

(3) When the exit plane of the rocket nozzle had moved well into the forward tube, the static pressure indicates that reflecting, weak shock waves were present both in the forward and in the aft tube. The constrictive area ratio is such that the flow was not choked at the constriction. Instead, the exhaust flow apparently remained fully supersonic downstream of the nozzle. There was not evidence of significant blow-by flow.

Static-Wall Pressure Distributions - If the static-pressure measured by the various gages when the nozzle exit-plane was at a specific location are presented as a function of the axial coordinate of the gage, one obtains the static-wall-pressure distribution for that nozzle-exit location. The nondimensionalized pressure measurements obtained for $x_{ne} = -16.419\ r_{ne}$ have been used to generate the pressure distribution of Fig. 32. Although there are too few gages to construct a meaningful flow model, the pressures can be interpreted in terms of the model that is based on the total knowledge of the flow. As the exhaust flow impinged on the tube wall, a weak oblique shock wave was generated. The theoretical value of the static pressure downstream of the impingement shock was $0.0235\ p_{t1}$, which compares reasonably well with the data. The streamwise variation in the static pressure measurements for those gages in the forward tube is attributed to the reflected shock waves. As the exhaust flow entered the aft tube, the pressure increased. Recall that, if the stream tube area decreases, a subsonic flow accelerates (i.e., the pressure decreases), whereas a supersonic flow decelerates (i.e., the pressure increases). Based on the data of Fig. 32, the flow in the forward tube is evidently supersonic.

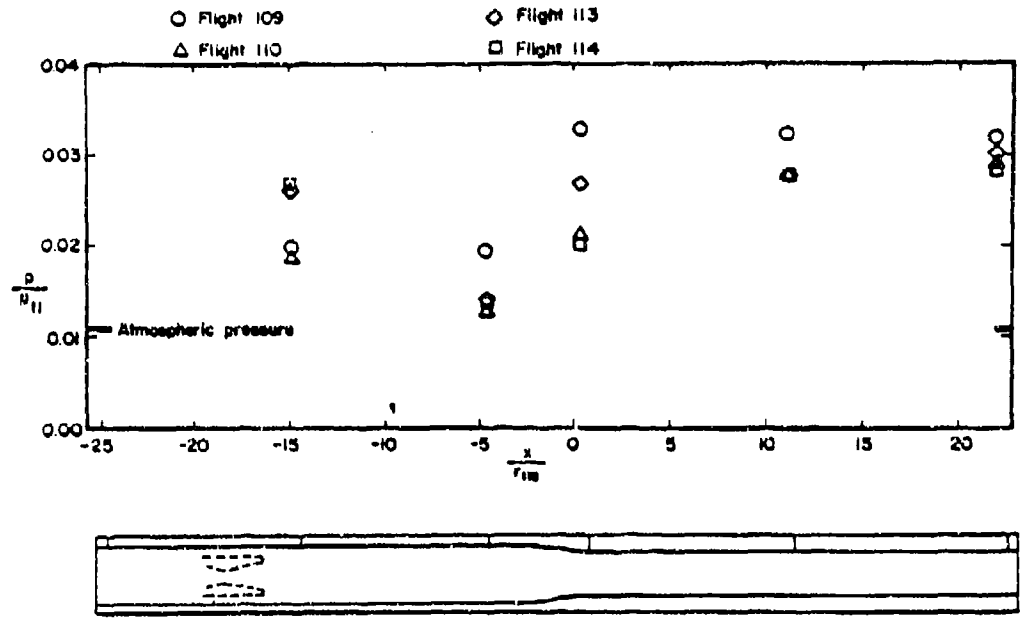

Figure 32. - The static wall-pressure distribution for the Arrow flight-test program for $x_{ne} = -16.419\ r_{ne}$.

Pressure Measurements from the Rip-Zap Program

Launch-tube flow-field measurements were made during twelve flight tests in which Rip-Zap configurations were launched from a nontipoff launcher. For the first eight flights, the launch tube was sparsely instrumented[4]. For the last four flights[51], the launch tube was instrumented as shown in Fig. 28. The data and their analysis, which were presented in Refs. 3, 38, and 42, will be reviewed here. It has been noted often in this paper that the large reduction in launch-tube cross-section for these tests caused the exhaust flow to be choked and a significant fraction of the exhaust gas to be turned upstream into the annular gap. The massive blow-by flow that results is graphically illustrated in Fig. 33. Note that even when the aft forty inches of the rocket are still in the tube, i.e., $x_{ne} = -10.1\ r_{ne}$, exhaust gases driven forward by the blow-by process can be seen surrounding the exposed rocket at the forward end of the launch tube.

The static-wall pressure measurements for PS1 are presented as a function of time for Flight 10 in Fig. 34a and as a function of the nondimensionalized nozzle-exit position, x_{ne}/r_{ne}, for Flights 9, 10, and 11 in Fig. 34b. The character of the launcher flow-field which existed when the rocket exhausted into the small-diameter section, or aft tube, can be best seen in Fig. 34a. The pressure recorded by PS1 periodically rose suddenly (due to a shock impinging on the wall), then decreased gradually. The period became shorter as the rocket accelerated away from the gage. Thus, these data are qualitatively similar to the fully supersonic flows for statically fired rockets as reported by Batson[18] and for dynamically fired rockets as reported by Batson and

(a) $x_{ne} = -10.1\ r_{ne}$
(40 inches in the tube)

(b) $x_{ne} = -13.6\ r_{ne}$
(30 inches in the tube)

(c) $x_{ne} = -17.2\ r_{ne}$
(20 inches in the tube)

(d) $x_{ne} = -20.7\ r_{ne}$
(10 inches in the tube)

(e) $x_{ne} = -24.2\ r_{ne}$
(exit plane coincides with departure plane of forward tube)

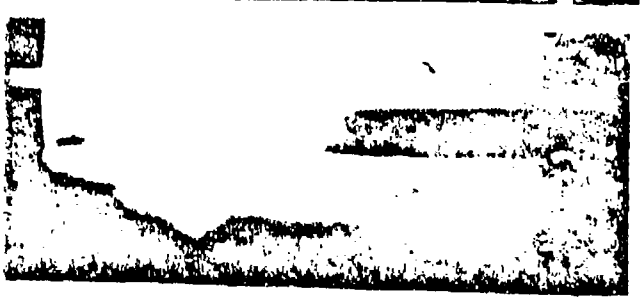

Figure 33. - Photographs of the launch sequence for Rip-Zap Flight No. 2.

Bertin[19]. The similarity between the pressure distribution for a statically fired rocket and that for a dynamically fired rocket results because the velocity of the exhaust gas is more than 20 times the velocity of the rocket as it leaves the launcher. Thus, the exhaust flow for the dynamic rocket launching can be assumed to be quasi-steady.

As the exit plane of the rocket nozzle entered the large-diameter forward tube (at approximately 85 msec for Flight 10), the static pressure increased suddenly. Although the increase is evident in Fig. 34a, the character of the pressure data is better illustrated by the parameter x_{ne}/r_{ne} used in Fig. 34b. The nozzle-exit position is a unique function of time, such that, as time increases (in Fig. 34a), the nozzle-exit parameter x_{ne}/r_{ne} decreases from large positive values through zero and then to large negative values. Since the pressure parameter is the ratio of the experimentally determined static pressure to the assumed stagnation pressure, the flight-to-flight variations in the ratio p/p_{t1} may be due in part to differences between the actual stagnation pressure and the assumed value. When the rocket was 5 radii, or more, into the large-diameter forward tube (i.e., $x_{ne} < 5.0\ r_{ne}$), the static pressure at PS1 (which was located far into the aft tube), was approximately constant. The magnitude of this constant pressure was the same whether the exhaust flow encountered the modified rectangular step (Flights 9 and 10) or the 15° ramp (Flight 11) before entering the aft tube. Thus, the variation in the geometry of the constriction did not significantly affect the downstream static pressure. Once the rocket had left the launcher, the static pressures recorded by PS1 decreased rapidly. The forward end of the launcher, for which $x_{ne} = -24.2\ r_{ne}$, is indicated by the atmospheric-pressure symbol.

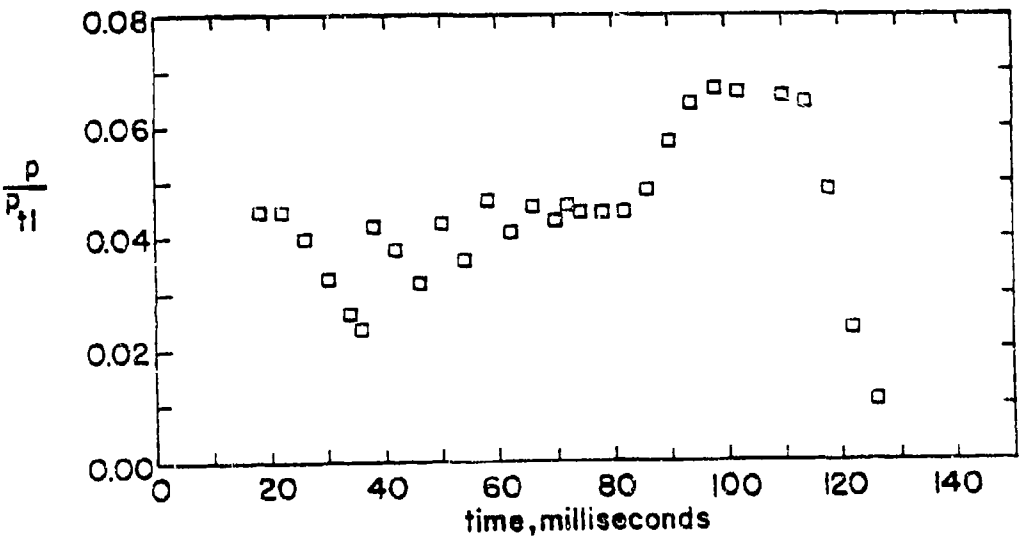

(a) As a function of time for Flight 10 (the constriction is the modified rectangular-step)

Figure 34. - The pressure history for PS1 ($x_g = +26.802\ r_{ne}$) in the Rip-Zap flight-test program.

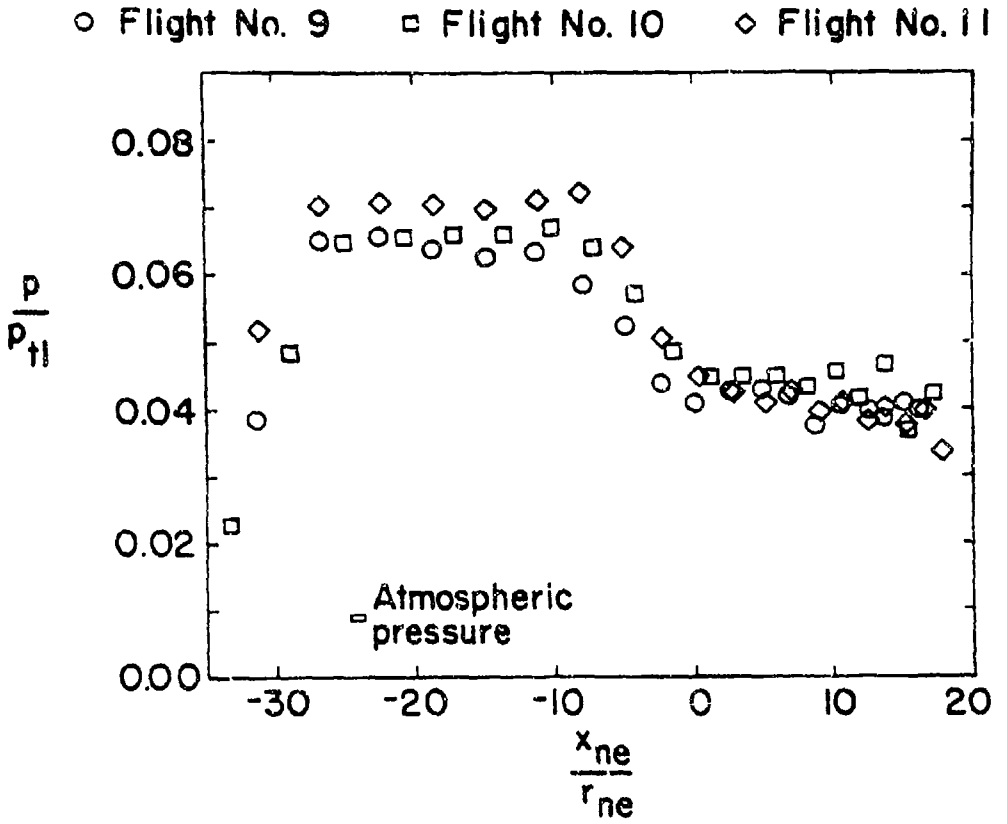

(b) As a function of nozzle exit-location for Flights 9, 10, and 11.

Figure 34. - Concluded.

When the rocket exhausted into the large-diamter forward tube, the pressure measurements in the vicinity of the constriction were more than 10 times the atmospheric pressure. Thus, there is a large pressure drop from the internal end of the forward tube (at the change in cross section) to the upstream end of the forward tube which exhausted to the atmosphere. As a result, there was a reverse, or blow-by , flow in the annular region between the rocket and the wall of the forward tube. Using photographs similar to those presented in Fig. 33, the velocity of gas in the annular region was calculated to be approximately 500 fps.

The existence of a blow-by flow was also evident in the static wall-pressure histories recorded by gages PS15, PS16, PS17, and PS18, all of which were located in the forward tube at $x_g = -6.649\ r_{ne}$. With the exit plane of the nozzle near the constriction (i.e., $x_{ne} = 0$), these gages provide measurements of the static pressure in the annular region between the rocket and the tube wall. The pressure histories for these gages are presented in Fig. 35. The measurements for Flight 11 represent the flow in the launcher with the 15° ramp. Pressure

measurements for gages PS15 and PS16 do not appear while the nozzle exit was in the region: - 10 r_{ne} > x_{ne} > - 25 r_{ne}. The gages for PS15 and PS16 saturated at approximately 100 psi and did not provide meaningful data while the rocket was in this region.

As the exit plane of the rocket nozzle passed the constriction and entered the forward tube (0 r_{ne} > x_{ne} > - 2.5 r_{ne}), the pressure recorded by these gages rose. Note that since the orifices are located at x_g = - 6.649 r_{ne} (i.e., in the annular gap between the missile and the launch-tube wall upstream of the nozzle exit-plane),

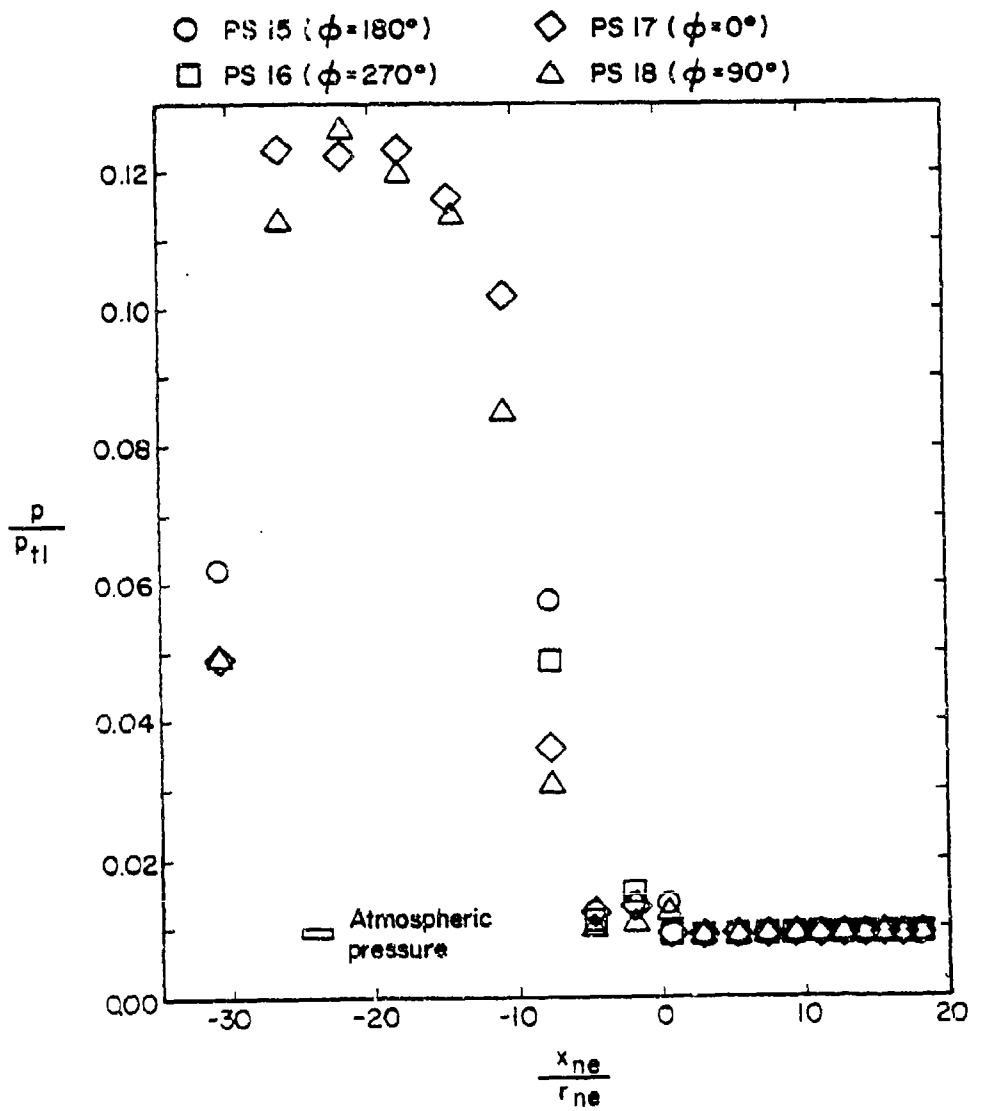

Figure 35. - Static pressure histories for the 4 orifices located at x_g = - 6.649 r_{ne} for Flight 11.

the increased pressure indicates the occurrence of significant blow-by flow. The pressure increase was greater[45] for the launcher with the modified rectangular step, i.e., Flights 9 and 10. When the exit plane of the cold-gas nozzle was within 2.5 r_{ne} of the step, the blow-by flow from the cold-gas tests[52] was greater for a rectangular-step configuration than for a 15° ramp. As the rocket moved further from the step ($-2.5\ r_{ne} > x_{ne} > -6.0\ r_{ne}$), the pressure recorded by these four gages decreased. Based on the previous discussion, the observed pressure decrease indicated that the blow-by flow rate decreased. Thus, as the rocket nozzle was moving away from the step, but had not yet reached the gage, the magnitude of the reverse flow increased and then diminished. The varying strength of the blow-by flow with the rocket nozzle in this region might be described as a "puff". For the cold-gas tests, the maximum blow-by flow rate for the rectangular-step occurred when $x_{ne} = -0.75\ r_{ne}$. The blow-by flow rate decreased as the nozzle moved farther from the step. For the 15° ramp configuration, the blow-by flow rate for the cold-gas tests had not begun to decrease with distance, but data were available only for $0 r_{ne} > x \geq -2.55\ r_{ne}$.

When the rocket passed the plane of these gages such that the exhaust flow impinged directly on them, the pressure rose dramatically. The pressure downstream of the impingement shock was approximately $0.12\ p_{t1}$, which is approximately 13 atm. Recall that, when the rocket exhausted into the small-diameter aft tube, the pressure downstream of the impingement shock was approximately $0.04\ p_{t1}$. Numerical solutions of the underexpanded exhaust (from a stationary rocket) impinging on the tube wall show that the pressure downstream of an oblique impingement shock would be less for the larger-diameter tube. The static-wall pressure immediately downstream of the impingement shock-wave was calculated to be $0.0529\ p_{t1}$ for the forward tube ($r_t = 1.54\ r_{ne}$) and $0.0667\ p_{t1}$ for the aft tube ($r_t = 1.19\ r_{ne}$). The numerical calculations assume that the rocket exhaust expands from the theoretical value of the exit-plane pressure to the base pressure, which is roughly atmospheric for these flows. Thus, in the theoretical solution the flow which impinges on the wall is turned approximately 30-35° by a weak, oblique shock wave. The fact that the experimentally recorded pressures were so much greater when the rocket exhausted into the larger-diameter forward tube suggests that the flow contained a strong, normal shock wave and was, therefore, not fully supersonic. This conclusion is supported by the cold-gas data of Ref. 37. Furthermore, this strong shock wave moves with the nozzle exit-plane.

A Review of the Pressure Histories for the Rip-Zap Configuration. - These pressure histories provide several insights into the mechanisms which govern the flow field which results when a rocket exhausts into the nontipoff launch-tube with a relatively large change in cross section.

(1) When the exit plane of the rocket nozzle was in the small-diameter, aft tube, the flow was fully supersonic. There was not significant reverse, or blow-by, flow.

(2) When the exit plane of the rocket nozzle passed the constriction, the pressures measured at the orifices downstream of the nozzle

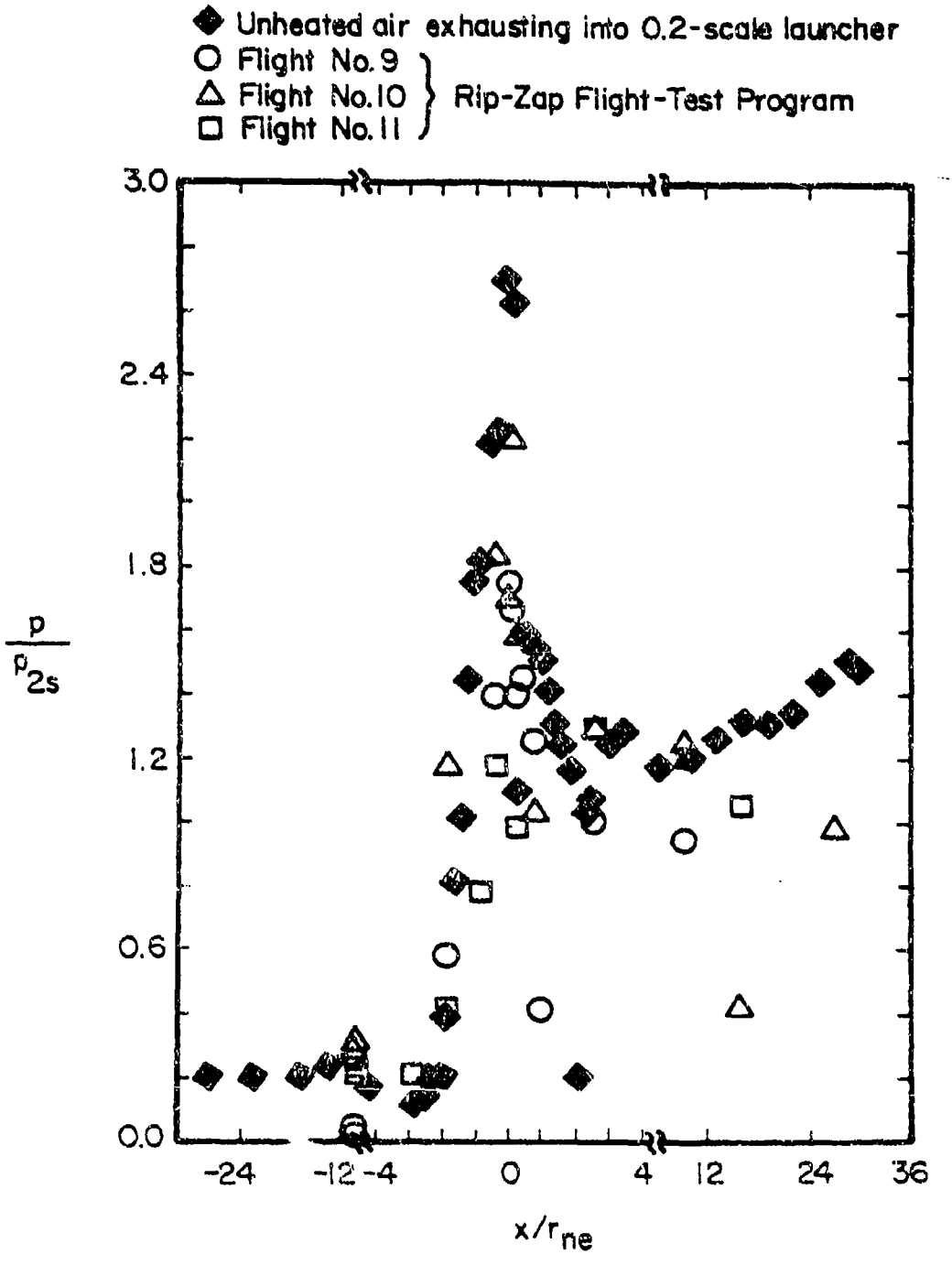

Figure 36. - A comparison of the Rip-Zap flight-test data with the cold-gas-simulation data when the nozzle exit-plane was just upstream of the constriction. $x_{ne} \approx -2.4\, r_{ne}$.

increased significantly. The pressures measured at the orifices upstream of the nozzle increased then decreased, indicating the occurrence of a blow-by flow, i.e., a splashback, of varying strength. The differences between the two constrictive geometries did not significantly affect the pressure measurements.

(3) When the exit plane of the rocket nozzle moved away from the constriction, the pressure for a particular orifice downstream of the nozzle rose reaching a relatively high, "constant" value. With the rocket in the large-diameter, forward tube, the static-wall pressure downstream of the impingement shock was much higher than when the rocket was in the small-diameter, aft tube. The upstream static-pressure data (from orifices located in the annular region) indicated the occurrence of the reverse flow.

Static-Wall Pressure Distributions - The cold-gas simulations not only provided a realistic flow model that could be used to interpret the flight-test data, but the cold-gas pressure measurements correlated reasonably well with the flight measurements. The static wall-pressure distributions for $x_{ne} = -2.4\ r_{ne}$ are presented in Fig. 36. Since the stagnation pressure for the Rip-Zap configuration was approximately 9.66×10^6 N/m^2 (1400 psia), only the cold-gas pressures for the highest reservoir pressure, i.e., 6.61×10^6 N/m^2 (958 psia), are presented. In order to minimize the effect of γ on the data, the experimentally-determined static-wall pressures have been divided by p_{2s}, the theoretical value of the static pressure just downstream of a weak, oblique shock wave for the exhaust flow impinging on the forward-tube wall. The data from the dynamic rocket launchings were in good agreement with the data from the cold-gas tests in which the nozzle was stationary. As noted earlier, the assumption that the exhaust flow was quasi-steady has been verified previously. However, the correlation between the hot-gas data and the cold-gas data was surprisingly close in view of the differences between the environments.

The data obtained during the cold-gas test program clearly indicate that, when the exit plane of the nozzle was well into the forward tube, the exhaust flow was choked by the constriction, and the impingement shock-wave was strong, i.e., normal to the axis of the launcher. Therefore, for the pressure distributions obtained with the nozzle exit-plane well into the forward tube, the experimentally-determined static-wall pressures have been divided by p_{t2}, the theoretical value of the stagnation pressure behind a normal shock wave. As discussed previously, the pressures measured during the cold-gas tests were in good agreement with the theoretical values. This can be seen in Fig. 37, where the static-wall pressure is approximately p_{t2} at the base of the forward-facing step and is approximately $0.5\ p_{t2}$ (the value for sonic flow) near the exit plane of the aft tube. The flight-test measurements at the base of the constrictive step and near the exit plane of the aft tube did not agree as well with the theoretical values. The differences may be the result of the difficulty in obtaining flight-test measurements of the rapidly varying static-wall pressure in the launcher and of possible differences between the actual value of γ for the flow in the

launcher and that used in the theoretical solution. The differences between the theoretical and the flight-test values for the pressures downstream of the normal shock wave are similar to those observed downstream of the weak shock-wave system which occurred when the nozzle exhausted directly into the aft tube. Nevertheless, the pressure distributions from the rocket launchings were repeatable and are considered to be in reasonable agreement with the flow model developed from the cold-gas tests.

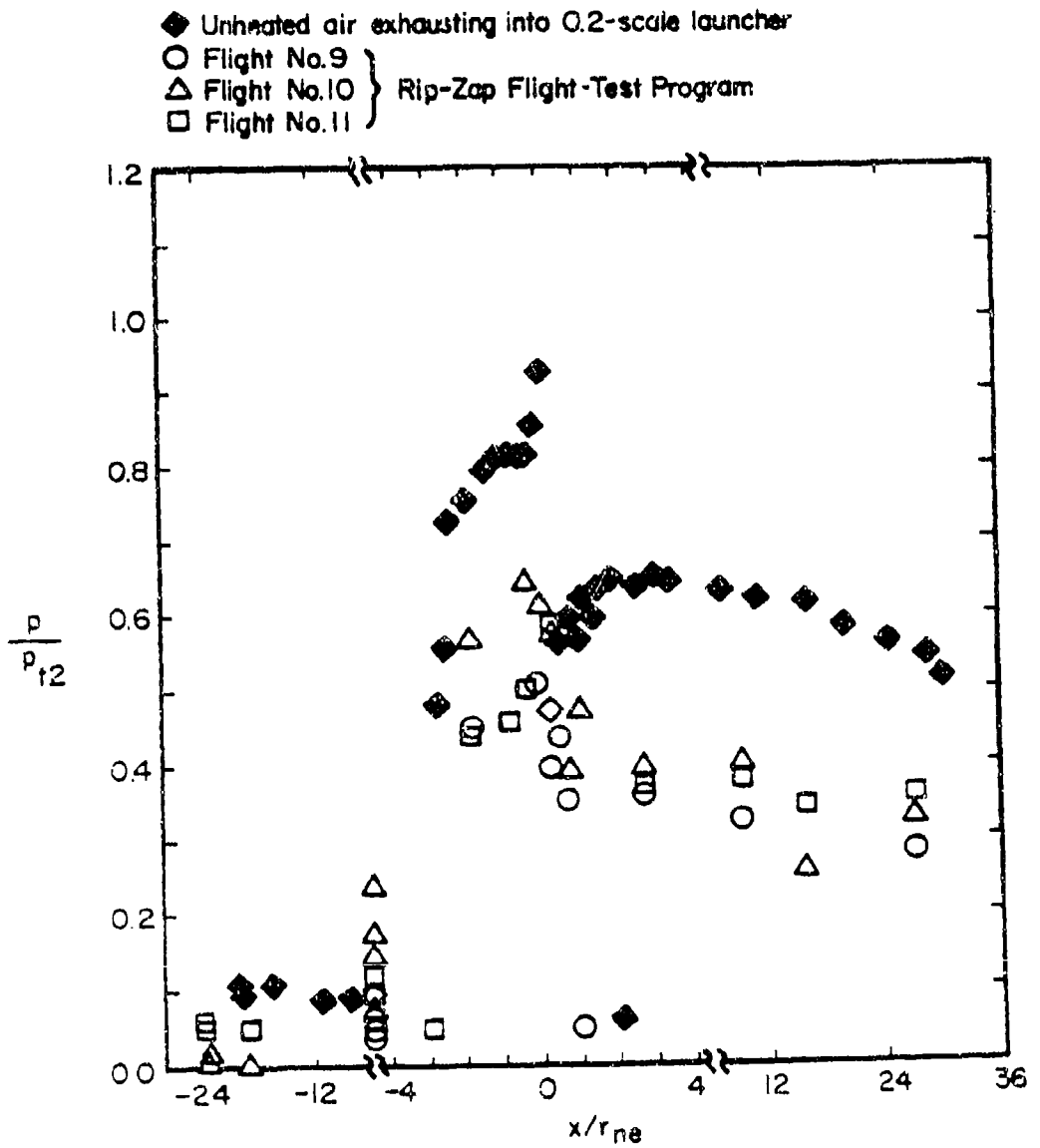

(a) $x_{ne} \approx -6.5\ r_{ne}$

Figure 37. - A comparison of the Rip-Zap flight-test data with the cold-gas-simulation data for choked flows.

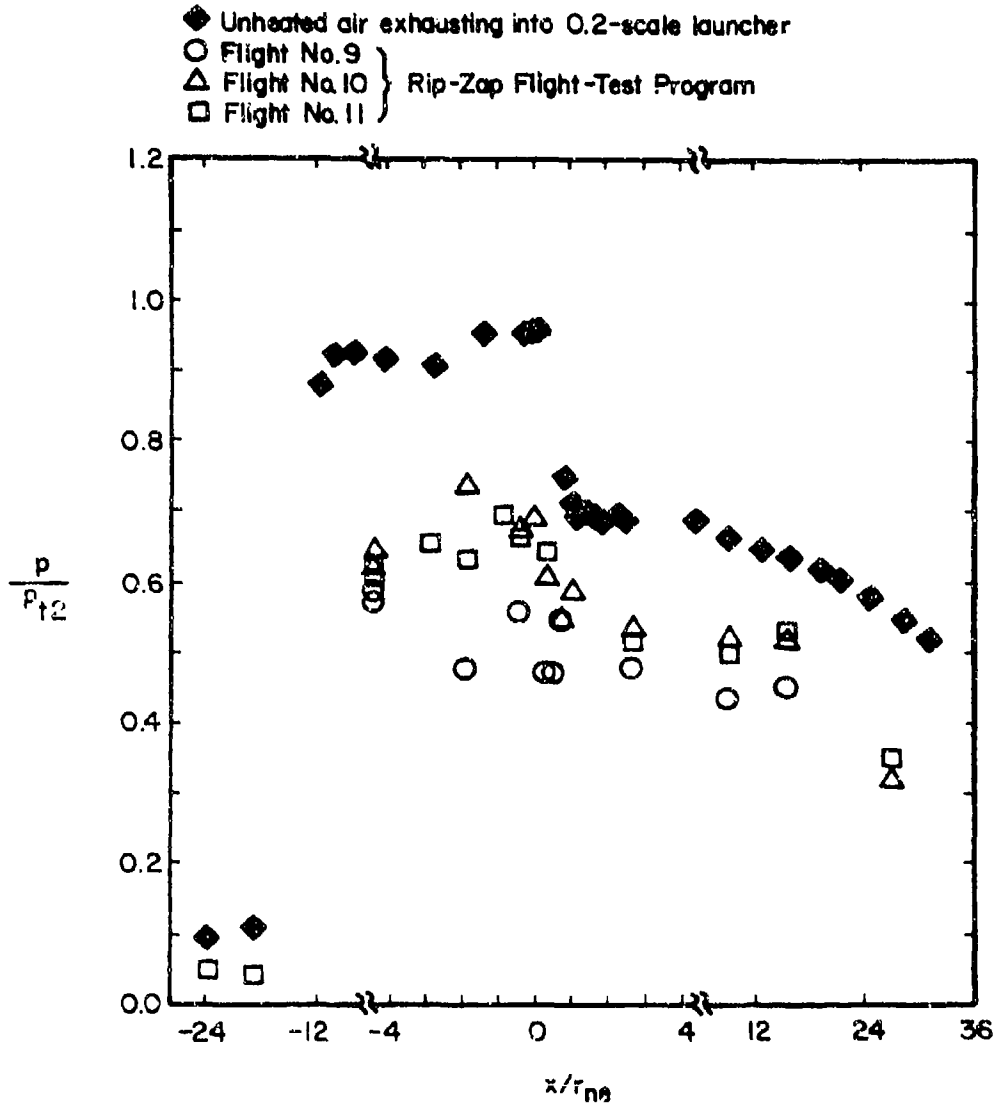

(b) $x_{ne} \approx -19.0\ r_{ne}$

Figure 37. - Concluded.

REFERENCES

1. D. W. Barnette, J. J. Bertin, and J. L. Batson, "Free-Flight Rocket's Initial Trajectory as Affected by Massive Blow-by", Journal of Spacecraft and Rockets, Vol. 15, No. 6, Nov.-Dec. 1978, pp. 334-340.

2. R. R. Morris, J. J. Bertin, and J. L. Batson, "Flow Field for an Underexpanded, Supersonic Nozzle Exhausting Into an Expansive Launch Tube", Proceedings of the 13th Annual Meeting of the Society of Engineering Science, Nov. 1976, Hampton, Va., reprinted in CP-2001, Vol. 4, NASA.

3. J. J. Bertin and J. L. Batson, "Comparison of Cold-Gas Simulations and Rocket-Launch Data for Constrictive Launchers", Journal of Spacecraft and Rockets, Vol. 13, No. 11, Nov. 1976, pp. 684-691.

4. -----, "Feasibility Flight Testing of Rocket Impelled Projectile (RIP)", Report Number 7-52100/3R-5, 1 May 1973, LTV Aerospace Corporation, Michigan Division.

5. H. H. Korst, R. A. White, S.-E. Nyberg, and J. Agrell, "The Simulation and Modeling of Jet Plumes in Wind Tunnel Facilities", Journal of Spacecraft and Rockets, Vol. 18, No. 5, Sept.-Oct. 1981, pp. 427-434.

6. S.-E. Nyberg, J. Agrell, and T. Hevreng, "Investigation of Modeling Concepts for Plume-Afterbody Flow Interactions", Second Annual Technical Report, Grant Number DA-ERO-78-G-028, Feb. 1980, The Aeronautical Research Institute of Sweden (FFA).

7. M. Pindzola, "Jet Simulation in Ground Test Facilities", AGARDograph 79, Nov. 1963, North Atlantic Treaty Organization.

8. H. H. Korst and R. A. Deep, "Modeling of Plume Induced Interference Problems in Missile Aerodynamics", AIAA Paper No. 79-0362, Presented at the 17th Aerospace Sciences Meeting, New Orleans, Jan. 1979.

9. J. J. Bertin, S. J. Sutter, Jr., D. P. Dannemiller, and D. L. Booker, "A Comparison of Theoretical and Experimental Flow Fields for an Underexpanded Rocket Exhaust", AIAA Paper No. 79-0340, Presented at the 17th Aerospace Sciences Meeting, New Orleans, Jan. 1979.

10. J. J. Bertin, E. S. Idar, and D. L. Booker, "Secondary Flows for a Tube-Launched Rocket Configuration", AIAA Paper No. 80-0372, Presented at the 18th Aerospace Sciences Meeting, Pasadena, California, Jan. 1980.

11. _____, "Equations, Tables, and Charts for Compressible Flow", Report 1135, 1953, NACA.

12. N. H. Johannesen and R. F. Meyer, "Axially-Symmetrical Supersonic Flow Near the Centre of an Expansion", The Aeronautical Quarterly,

Vol. 2, Aug. 1950, pp. 127-142.

13. H. H. Korst, "Analytical Concepts for the Modeling of Propulsive Jet Plume Interference Effects," UILU ENG 77-4010, Sept. 1977, The University of Illinois Experiment Station.

14. L. L. Galigher, S. F. Yaros, and R. C. Bauer, "Evaluation of Boattail Geometry and Exhaust Plume Temperature Effects on Nozzle Afterbody Drag at Transonic Mach Numbers", AEDC-TR-76-102, Oct. 1976, Arnold Engineering Development Center.

15. E. S. Love, C. E. Grigsby, L. P. Lee, and M. J. Woodling, "Experimental and Theoretical Studies of Axisymmetric Free Jets", Technical Report R-6, 1959, NASA.

16. S. A. Bouslog, E. J. Zihlman, Jr., and J. J. Bertin, "Unsteady Wall-Pressure Measurements for Underexpanded Nozzles Exhausting into Launch Tubes", TR-RL-CR-82-1, Jan. 1982, U. S. Army Missile Command.

17. S. A. Bouslog and J. J. Bertin, "Flows in the Annular Region When an Underexpanded Nozzle is Exhausted into a Stepped Launch Tube", TR-RL-CR-80-4, March 1980, U. S. Army Missile Command.

18. J. L. Batson, "A Study of the Flow Field Produced by an Axisymmetric Underexpanded Jet Exhausting into a Cylindrical Tube", Ph.D. Dissertation, Dec.1972, The University of Texas at Austin.

19. J. L. Batson and J. J. Bertin, "Experimental Study of Flow Field Produced When an Underexpanded Rocket Exhausts into Cylindrical Tube", AIAA Paper No. 73-1227, Presented at the AIAA/SAE 9th Propulsion Conference, Las Vegas, Nev., Nov. 1973.

20. H. H. Korst, "A Theory for Base Pressures in Transonic and Supersonic Flow", Journal of Applied Mechanics, Vol. 23, 1956, pp. 593-600.

21. P. Carriere, M. Sirieix, and J. Delery, "Methodes de Calcul des Ecoulements Turbulents Decolles en Supersonique", Progress in the Aerospace Sciences, Pergamon Press, Vol. 16, No. 4, 1975, pp. 385-429.

22. P. M. Gerhart and H. H. Korst, "On the Free Shear Layer Downstream of a Backstep in Supersonic Flow", Journal of Fluids Engineering, ASME, Vol. 95, Series 1, No. 3, 1973, pp. 361-366.

23. J. R. Kliegel and J. N. Levine, "Transonic Flow in Small Throat Radius of Curvature Nozzles", AIAA Journal, Vol. 7, No. 7, July 1969, pp. 1375-1378.

24. H. H. Korst and J. J. Bertin, "The Analysis of Secondary Flows for Tube-Launched Rocket Configurations", Journal of Spacecraft and Rockets, Jan.-Feb. 1983, Vol. 20, No. 1, pp. 35-42.

25. H. H. Korst and W. L. Chow, "Non-Isoenergetic Turbulent (Pr_t = 1) Jet Mixing Between Two Compressible Streams at Constant Pressure", CR-419, Apr. 1966, NASA.

26. H. H. Korst and W. L. Chow, "On the Correlation of Analytical and Experimental Free Shear Layer Similarity Profiles by Spread Rate Parameters", Journal of Basic Engineering, Trans. ASME, Series D, Vol. 93, 1971, pp. 377-382.

27. D. R. Bartz, "Turbulent Boundary Layers in Cooled, Convergent-Divergent Nozzles", ASME Transactions, Vol. 75, pp. 1235-1245, 1955.

28. H. H. Korst, "Effect of Turbulent Boundary Layer in Cooled C-D Nozzles on Plume Modeling", Final Report for Task Order 76-207, University of Illinois at Urbana-Champaign, Feb. 1976.

29. T. L. Butler, "Simulation of Jet Plume Interference in Gases of Dissimilar Specific Heat Ratio", M.S. Thesis, Department of Mechanical and Industrial Engineering, University of Illinois at Urbana-Champaign, 1976.

30. R. H. Page and V. Sernas, "Apparent Reverse Transition in an Expansion Fan", AIAA Journal, Vol. 8, No. 1, Jan. 1970, pp. 189-190.

31. J. Fabri and R. Siestrunck, "Supersonic Air Ejectors", Advances in Applied Mechanics. Vol. V, Academic Press, Inc., 1958, New York, pp. 1-34.

32. R. C. German, R. C. Bauer, and J. H. Panesci, "Methods for Determining the Performance of Ejector-Diffuser Systems", Journal of Spacecraft and Rockets, Vol. 3, No. 2, Feb. 1966, pp. 193-200.

33. H. H. Korst, W. L. Chow, and G. W. Zumwalt, "Research on Transonic and Supersonic Flow of a Real Fluid at Abrupt Increases in Cross-Section (With Special Consideration of Base Drag Problems) -- Final Report", Report No. ME-TN-392-5, Dec. 1959, The University of Illinois.

34. E. S. Idar, III, J. J. Bertin, and S. A. Bouslog, "The Effect of Geometry on Static Wall-Pressure Distributions and Secondary Flow for Tube-Launched Rocket Configurations", Aerospace Engineering Report 79005, Nov. 1979, The University of Texas at Austin.

35. J. J. Bertin, E. S. Idar, III, and D. L. Booker, "Secondary Flows in a Rocket Launcher Tube", Journal of Spacecraft and Rockets, Vol. 18, No. 2, Mar.-Apr. 1981, pp. 119-126.

36. W. H. Appich, Jr., and D. E. Tipping, "Free-Rocket Trajectory Errors from Plume-Induced Loading During Tube Launch", Journal of Spacecraft and Rockets, Vol. 14, No. 10, Oct. 1977, pp. 614-620.

37. J. J. Bertin, R. R. Morris, G. M. Garms, M. R. Motal, and H. T. Faria, "Experimental Study of an Underexpanded, Supersonic Nozzle Exhausting into a Constrictive Launch Tube", Aerospace Engineering Report 75001, June 1975, The University of Texas at Austin.

38. J. J. Bertin and R. A. Reiman, "The Analysis of the Launch-Tube Flow-Field for Rip-Zap Firings", Aerospace Engineering Report 74005, Oct. 1974, The University of Texas at Austin.

39. A. H. Shapiro, The Dynamics and Thermodynamics of Compressible Fluid Flow, Ronald Press, New York, 1953.

40. J. J. Bertin, G. M. Garms, and E. S. Idar, III, "Effect of the Constrictive Area Ratio on the Rocket Exhaust Flow-Field in the Launcher", Aerospace Engineering Report 76001, Feb. 1976, The University of Texas at Austin.

41. J. J. Bertin and S. R. Galanski, "The Analysis of Launch Tube Flow-Field for Arrow Firings", Aerospace Engineering Report 75004, May 1975, The University of Texas at Austin.

42. J. J. Bertin and J. L. Batson, "Experimentally Determined Rocket-Exhaust Flow Field in a Constrictive Tube Launcher", Journal of Spacecraft and Rockets, Dec. 1975, Vol. 12, No. 12, pp. 711-717.

43. W. L. Jones, H. G. Price, Jr., and C. F. Lorenzo, "Experimental Study of Zero-Flow Ejectors Using Gaseous Nitrogen", TN D-203, March 1960, NASA.

44. H. H. Korst, T. L. Butler, and M. B. Briski, "Simulation of Jet Plume Interference Effects During Launch Phase of Missiles", Journal of Spacecraft and Rockets, Vol. 18, No. 1, Jan.-Feb. 1981, pp. 24-30.

45. C. F. Colebrook, "Turbulence in Pipes with Particular Reference to the Transition Region Between the Smooth and Rough Pipe Laws", Journal of the Institute of Civil Engineering, Vol. 11, 1938-1939, pp. 133-156.

46. R. G. Deissler and M. F. Taylor, "Analysis of Fully Developed Turbulent Heat Transfer and Flow in an Annulus with Various Eccentricities", TN 3451, 1955, NACA.

47. J. J. Bertin, D. W. Cribbs, D. W. Barnette, and D. L. Booker, "Onset of Massive Blow-by, A Comparison of Cold-Gas Simulations and Flight Tests", AIAA Paper No. 78-16, Presented at the AIAA 16th Aerospace Sciences Meeting, Huntsville, Ala., Jan. 1978.

48. J. L. Batson and J. J. Bertin, "Rocket Exhaust Flow in Tube Launchers", Journal of Spacecraft and Rockets, Vol. 11, No. 11, Nov. 1974, pp. 739-740.

49. H. H. Korst and R. A. White, "Internal and External Ballistics of Missiles with Special Consideration of Jet-Plume Interference Effects During Launch and Free Flight Phases", UILU ENG 80-4007, Dec. 1980, The University of Illinois at Urbana-Champaign.

50. T. L. Butler, "Simulation of Jet Plume Interference in Gases of Dissimilar Specific Heat Ratio", M. S. Thesis, Department of Mechanical and Industrial Engineering, June 1978, The University of Illinois at Urbana-Champaign.

51. -----, "Non-Tipoff Tube Launcher Flight Test Program", Report Number 7-52100, 3R-61, 21 Dec. 1973, LTV Aerospace Corporation, Michigan Division.

52. J. J. Bertin, M. K. Horn, and T. L. Webber, "Experimental Study of Flow Field Produced When an Underexpanded Jet Exhausts into a Constrictive Stepped Launch Tube", Aerospace Engineering Report 74002, Jan. 1974, The University of Texas at Austin.

APPENDIX M

RESEARCH CONTRACT RELATED PUBLICATIONS

APPENDIX M

APPENDIX M

RESEARCH CONTRACT RELATED PUBLICATIONS

Much of the research conducted under the sponsorship of this contract has produced significant results which have been reported in the literature. The following is a list of those publications:

THESES

Chan, P. C. T., "The Study of the Effect of Gravity on Nozzle Flows by Hodograph Transformation," Ph.D. Thesis, Department of Mechanical and Industrial Engineering, University of Illinois at Urbana-Champaign, 1981.

Hampton, L. P., "The Effects of Sudden Expansions and Compressions on Turbulent Boundary Layer Momentum Thickness in Supersonic Flow," M.S. Thesis, Department of Mechanical and Industrial Engineering, University of Illinois at Urbana-Champaign, 1983.

Han, T., "Applications of Hodograph Transformation to Hydrodynamic Problems Influenced by Gravitation," Ph.D. Thesis, Department of Mechanical and Industrial Engineering, University of Illinois at Urbana-Champaign, 1979.

Marongiu, M. J., "Non-steady Plume-wall Interactions Due to Fluidic Entrainment and Critical Outflow," M.S. Thesis, Department of Mechanical and Industrial Engineering, University of Illinois at Urbana-Champaign, 1982.

Nakayama, A., "Three Dimensional Flow Within Conduits of Arbitrary Geometrical Configurations," Ph.D. Thesis, Department of Mechanical and Industrial Engineering, University of Illinois at Urbana-Champaign, 1981.

Rhie, C. M., "A Numerical Study of the Flow Past an Isolated Airfoil with Separation," Ph.D. Thesis, Department of Mechanical and Industrial Engineering, University of Illinois at Urbana-Champaign, 1981.

Wu, C. W., "Gas Dynamics of an Axisymmetric Nozzle as a Vector-Thrust Device," Ph.D. Thesis, Department of Mechanical and Industrial Engineering, University of Illinois at Urbana-Champaign, 1983.

JOURNAL ARTICLES

Chow, W. L. and Han, T., "Invisci[illegible]olution for the Problem of Free Overfall," Journal of Applied Mechanics, Vol. 46, No. 1, March 1979, pp. 1-5.

JOURNAL ARTICLES (cont.)

Chow, W. L. and Chan, P., "The Effect of Gravity on Curved Channel Potential Flow," Journal of Fluid Engineering, Vol. 103, No. 4, December 1981, pp. 639-643.

Dutton, J. C. and Addy, A. L., "Transonic Flow in the Throat Region of Axisymmetric Nozzles," AIAA Journal, Vol. 19, No. 6, June 1981, pp. 801-804.

Dutton, J. C. and Addy, A. L., "Transonic Flow in the Throat Region of Annular Supersonic Nozzles," AIAA Journal, Vol. 20, No. 9, September 1982, pp. 1236-1243.

Han, T. and Chow, W. L., "The Study of Sluice Gate and Sharp Crested Weir through Hodograph Transformations," Journal of Applied Mechanics, Vol. 48, No. 2, June 1981, pp. 229-238.

Korst, H. H. and Bertin, J. J., "The Analysis of Secondary Flows for Tube-Launched Rocket Configurations," AIAA Paper No. 81-1222, presented at the 14th Fluid and Plasma Dynamics Conference, Palo Alto, California, June 23-25, 1981.

Nakayama, A., Chow, W. L., and Sharma, D., "Calculation of Fully Developed Turbulent Flows in Ducts of Arbitrary Cross-section," paper to be published by the Journal of Fluid Mechanics.

SYMPOSIUM PAPERS, CONFERENCE PROCEEDINGS, AND REPORTS

Addy, A. L., Amatucci, V. A., Kuntz, D. W., Petrie, H. L., and Samimy, M., "Base Flow and Related Model Experiments," Proceedings of the Symposium on Rocket/Plume Fluid Dynamic Interactions, Vol. III, Huntsville, Alabama, April 1983.

Bertin, J. J. and Korst, H. H., "Launch-Tube Flow-Field Technology Based on Cold-Gas Simulations, Flight-Test Measurements and Theoretical Models," Proceedings of the Symposium on Rocket/Plume Fluid Dynamic Interactions, Vol. II, Huntsville, Alabama, April 1983.

Chow, W. L., "Base Pressure of a Transonic Flow Past a Projectile," Proceedings of the Symposium on Rocket/Plume Fluid Dynamic Interactions, Vol. I, Huntsville, Alabama, April 1983.

Dutton, J. C. and Addy, A. L., "A Theoretical and Experimental Investigation of Transonic Flow in the Throat Region of Annular Axisymmetric, Supersonic Nozzles," Report No. UILU-ENG-80-4001, Department of Mechanical and Industrial Engineering, University of Illinois at Urbana-Champaign, Urbana, Illinois, January 1980.

SYMPOSIUM PAPERS, CONFERENCE PROCEEDINGS, AND REPORTS (cont.)

Hampton, L. P. and White, R. A., "The Effect of Sudden Expansions and Compressions on Turbulent Boundary Layer Momentum Thickness in Supersonic Flow," Report No. UILU-ENG-83-4004, Department of Mechanical and Industrial Engineering, University of Illinois at Urbana-Champaign, Urbana, Illinois, May 1983.

Korst, H. H., "Analysis and Modeling of Plume Effects on Missile Aerodynamics -- An Overview," Proceedings of the Symposium on Rocket/Plume Fluid Dynamic Interactions, Vol. II, Huntsville, Alabama, April 1983.

Korst, H. H., "Axisymmetric Wakes in Supersonic Unpowered Missile Flight," Proceedings of the Symposium on Rocket/Plume Fluid Dynamic Interactions, Vol. I, Huntsville, Alabama, April 1983.

Nakayama, A., Chow, W. L., and Sharma, D., "Calculation of the Secondary Flow of the Second Kind Through a Fully Elliptic Procedure," Proceedings of the 1981 Conference on Complex Turbulent Flows, Vol. III, Stanford University, California, pp. 1312-1317 (also Vol. II, pp. 919-928).

Rhie, C. M. and Chow, W. L., "A Numerical Study of the Turbulent Flow Past an Isolated Airfoil with Trailing Edge Separation," Paper presented at the Third AIAA/ASME Joint Conference on Thermal Physics, Fluid, Plasma, and Heat Transfer, St. Louis, Missouri, July 1982.

Rhie, C. M., Chow, W. L., and Sharma, D., "A Numerical Study for the Two-Dimensional Stalled Airfoil," Proceedings of the 1981 Conference on Complex Turbulent Flows, Vol. III, Stanford University, California, pp. 1318-1325, (also Vol. II, pp. 880-884).

White, R. A., "Advanced Research/Analysis of Plume Induced Interference Flow," Proceedings of the Symposium on Rocket/Plume Fluid Dynamic Interactions, Vol. II, Huntsville, Alabama, April 1983.

APPENDIX N

PARTICIPATING PERSONNEL

APPENDIX N

APPENDIX N

PARTICIPATING PERSONNEL

This appendix lists the faculty, graduate students, and support staff who participated on a part-time basis during the performance of this research grant.

FACULTY

A. L. Addy
Principal Investigator, Research Program Coordinator
Professor and Associate Head of Mechanical Engineering

W. L. Chow
Principal Investigator
Professor of Mechanical Engineering

H. H. Korst
Principal Investigator
Professor of Mechanical Engineering

R. A. White
Principal Investigator
Professor of Mechanical Engineering

GRADUATE STUDENTS

V. A. Amatucci
M.S. 1981
Ph.D. Candidate

P. C. T. Chan
Ph.D. 1981
Research Scientist
Jaycor Company (San Diego, California)

S. E. Doerr
B.S. 1981
M.S. Candidate

M. E. Erickson
M.S. 1982

L. P. Hampton
M.S. 1983

GRADUATE STUDENTS (cont.)

D. W. Kuntz
M.S. 1981
Ph.D. Candidate

M. J. Marongiu
M.S. 1982

M. J. Morris
M.S. 1980
Ph.D. Candidate

A. Nakayama
Ph.D. 1981
Assistant Professor of Mechanical Engineering
Shizuoka University (Hamamatsu, Japan)

H. L. Petrie
M.S. 1980
Ph.D. Candidate

C. M. Rhie
Ph.D. 1981
Senior Engineer
Detroit Diesel-Allison Division
General Motors Corporation (Indianapolis, Indiana)

M. Samimy
M.S. 1981
Ph.D. Candidate

C. W. Wu
Ph.D. 1983
Assistant Professor of Mechanical Engineering
State University of California at Los Angeles

SUPPORT STAFF

Karen K. Bryan
Secretary-Stenographic

SHOP SERVICES

Allen F. Stephens
Research Machine Shop Supervisor

Kathy L. Armer
Laboratory Mechanic

SHOP SERVICES (cont.)

Gregory L. Cler
Laboratory Mechanic

Donald R. Deschene
Electronics Technician II

Lawrence W. Hirschler
Instrument Maker

Joseph L. Link
Electronics Engineering Assistant

William D. Morfey
Instrument Maker

William E. Schaede
Senior Laboratory Mechanic

Leroy W. Westendorf
Instrument Maker

PUBLICATIONS OFFICE

Amanda L. Horner
Word Processing Operator III

June W. Kempka
Chief Clerk

Suzanne F. Palmer
Illustrator

APPENDIX O

WALL STATIC PRESSURE DATA
FOR REATTACHMENT ON AN
AXISYMMETRIC SUDDEN ENLARGEMENT CONFIGURATION

APPENDIX O

A study was conducted in order to examine the static pressure characteristics of an axisymmetric jet reattaching onto a cylinder wall. The research effort was conducted by graduate research assistant Martin J. Morris and Appendix O contains some of the significant results presented in graphical form. Sonic and supersonic underexpanded jets were exhausted from a nozzle into a sudden enlargement and the wall static pressure distributions were measured. The research effort produced experimental data concerning the recompression/r attachment process for a large range of variables. Further information on these experiments and/or more extensive data results can be obtained from Professor A. L. Addy or graduate research assistant M. J. Morris.

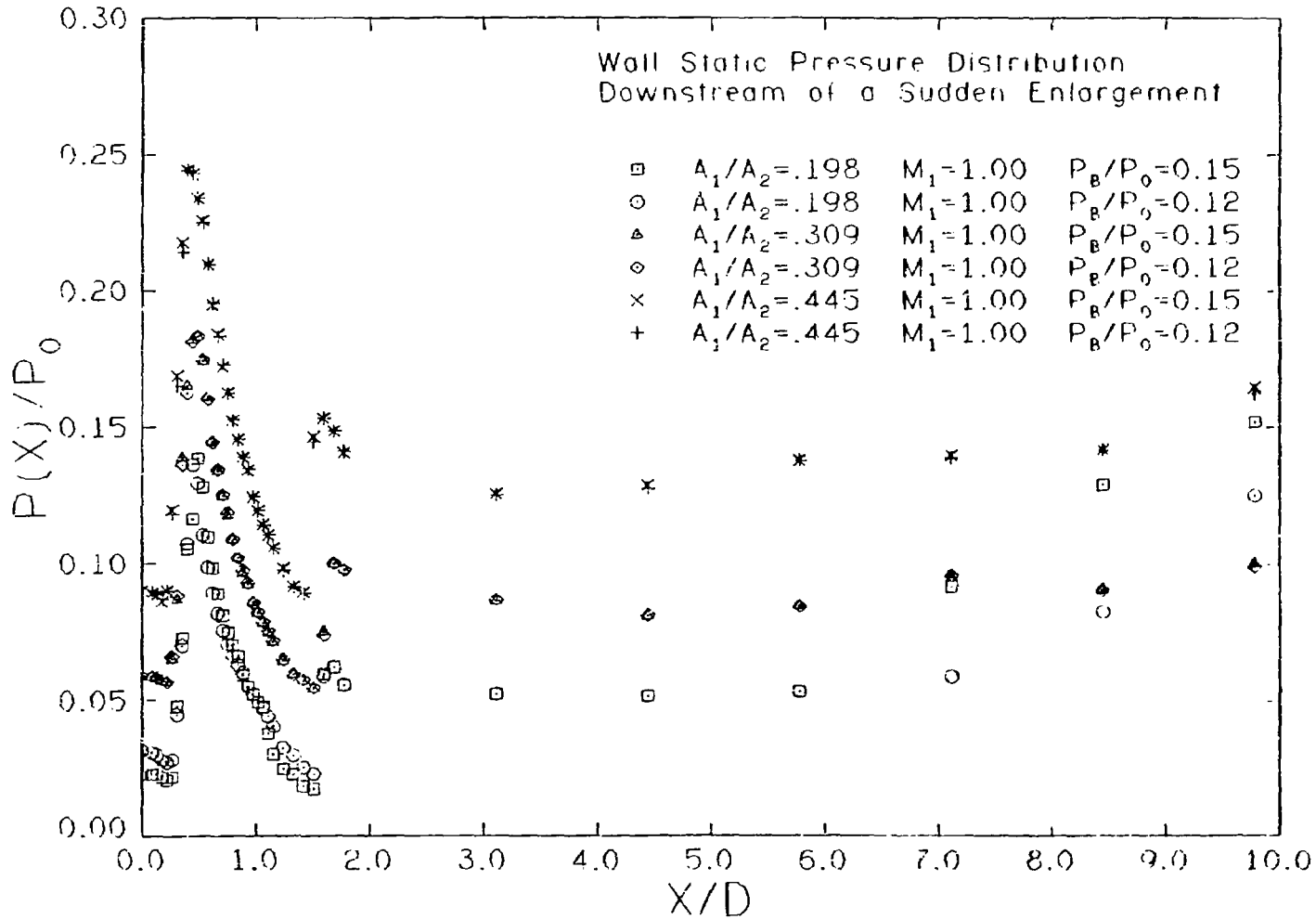

Figure 1 Wall static pressure distribution downstream of a sudden enlargement for a sonic incoming jet, $M_1 = 1$.

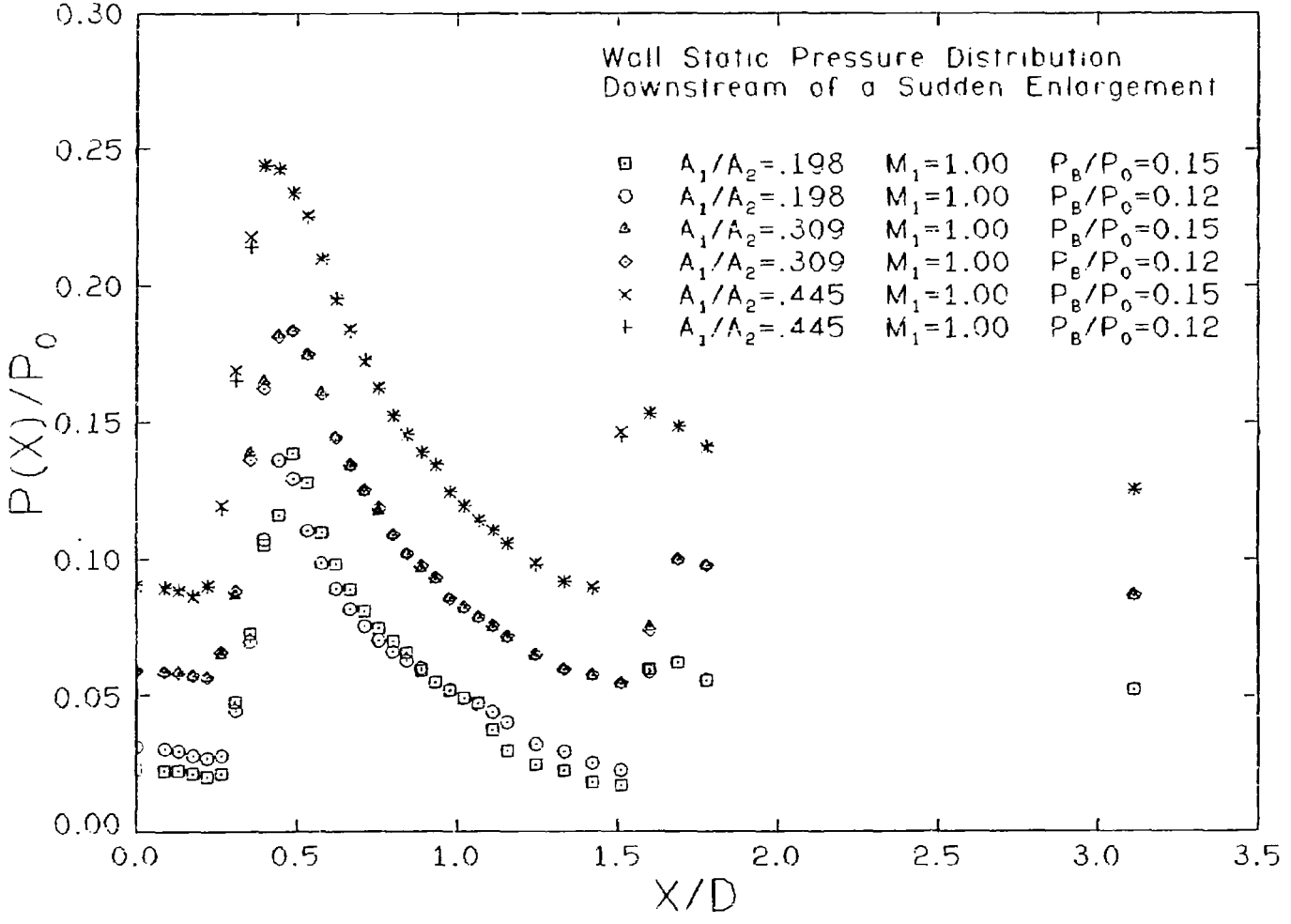

Figure 2 Wall static pressure distribution downstream of a sudden enlargement for a sonic incoming jet, $M_1 = 1$ (expanded axial scale).

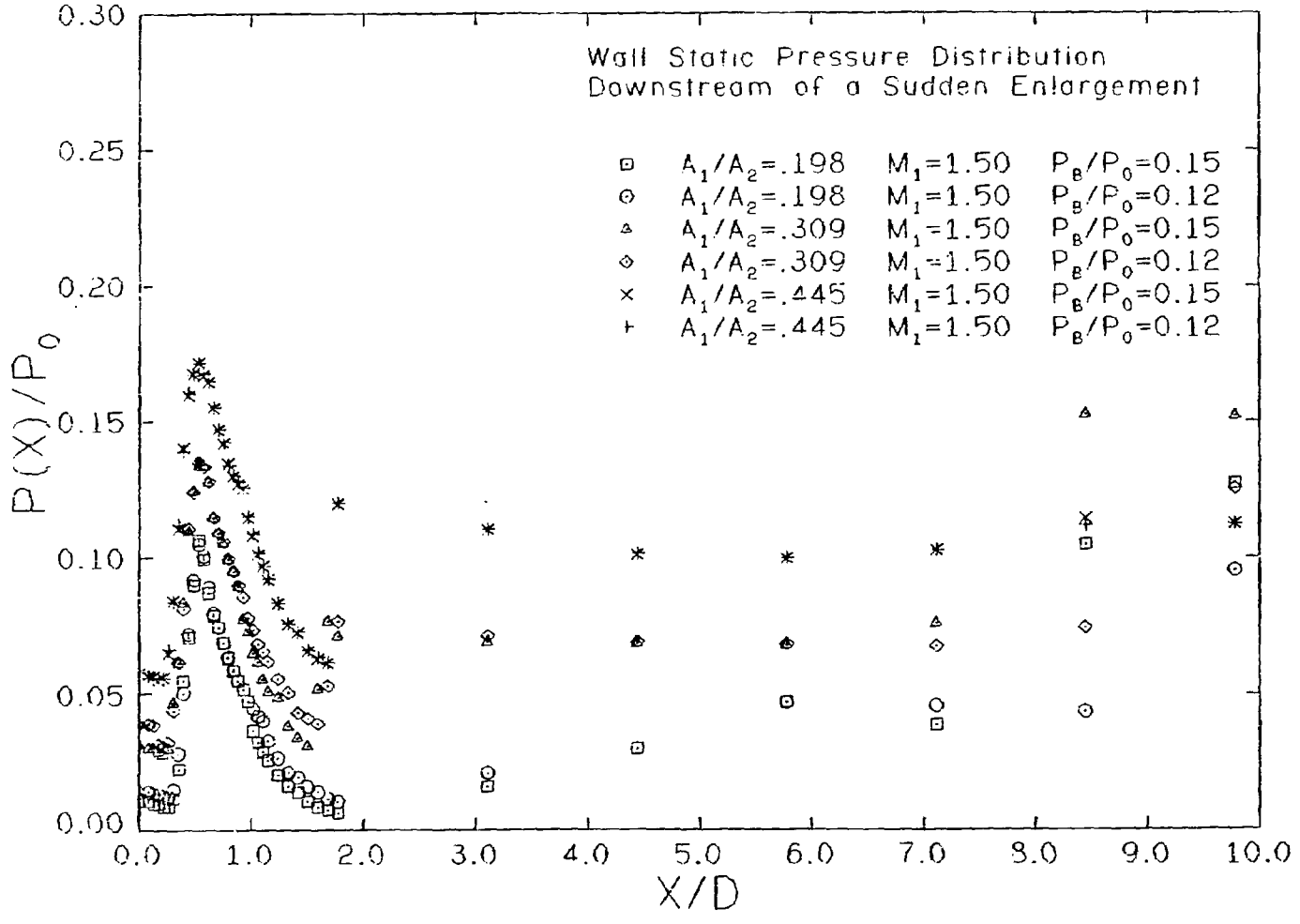

Figure 3 Wall static pressure distribution downstream of a sudden enlargement for an entrance jet Mach number of 1.50.

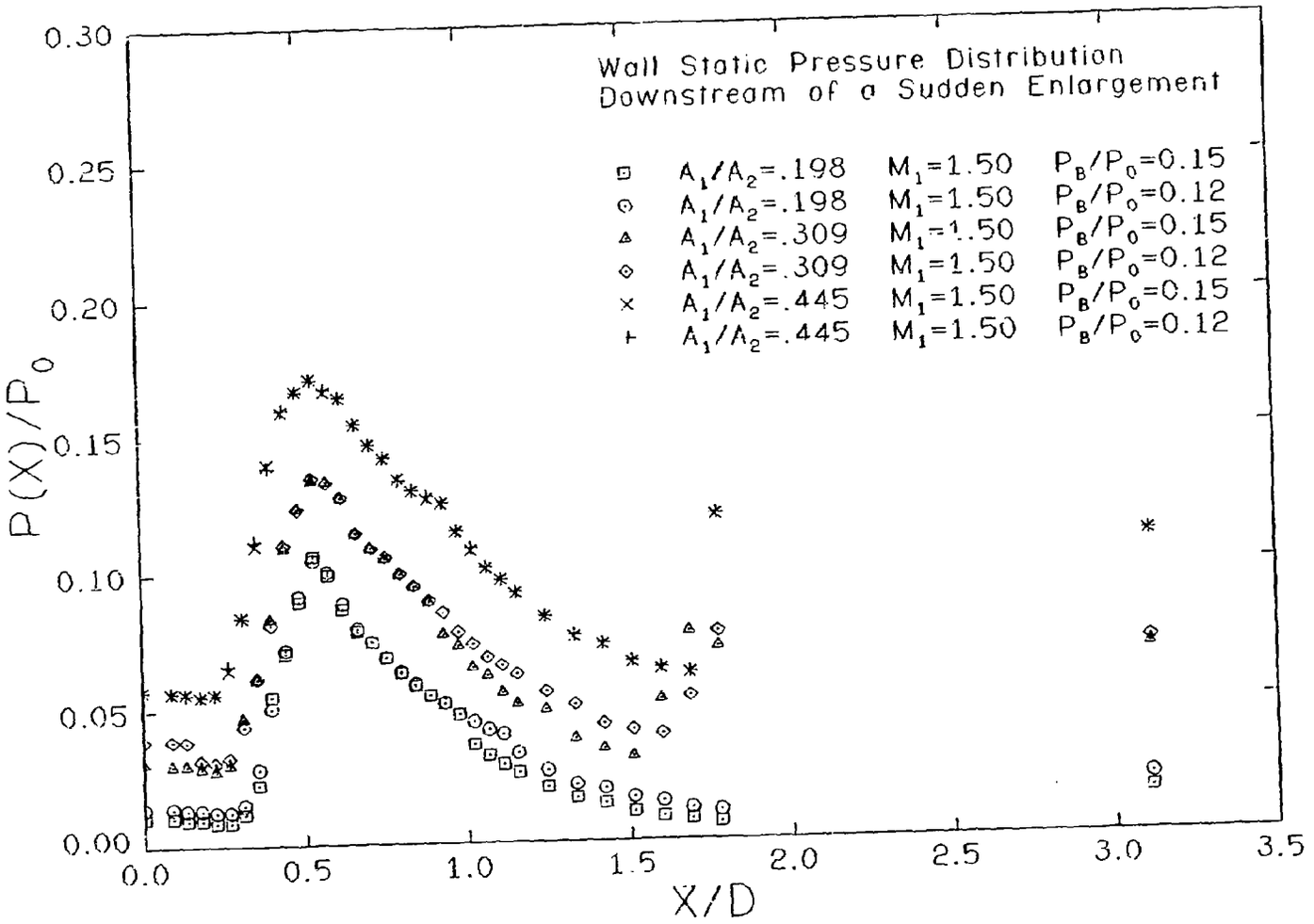

Figure 4 Wall static pressure distribution downstream of a sudden enlargement for an entrance jet Mach number of 1.50 (expanded axial scale).

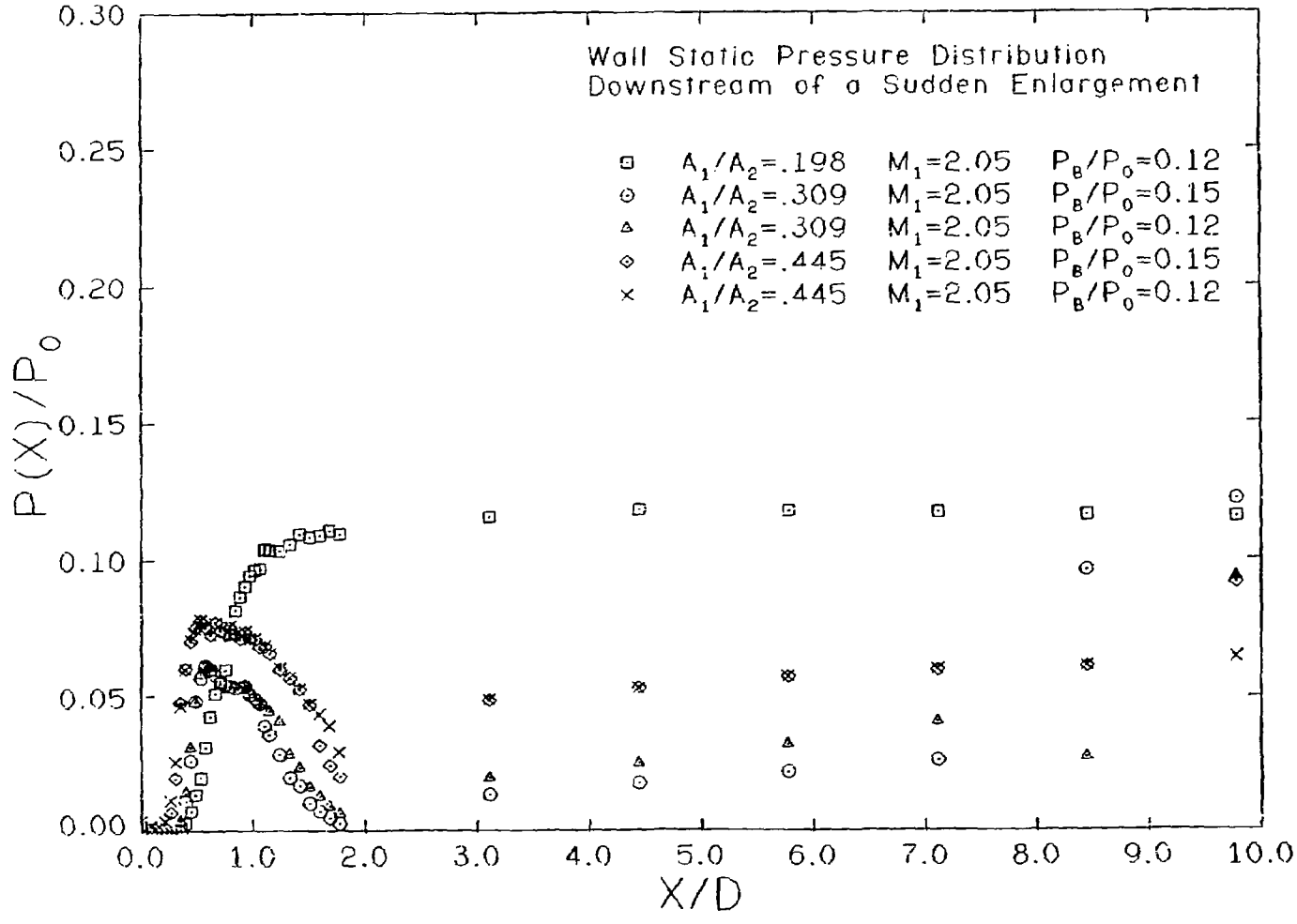

Figure 5 Wall static pressure distribution downstream of a sudden enlargement for an entrance jet Mach number of 2.05.

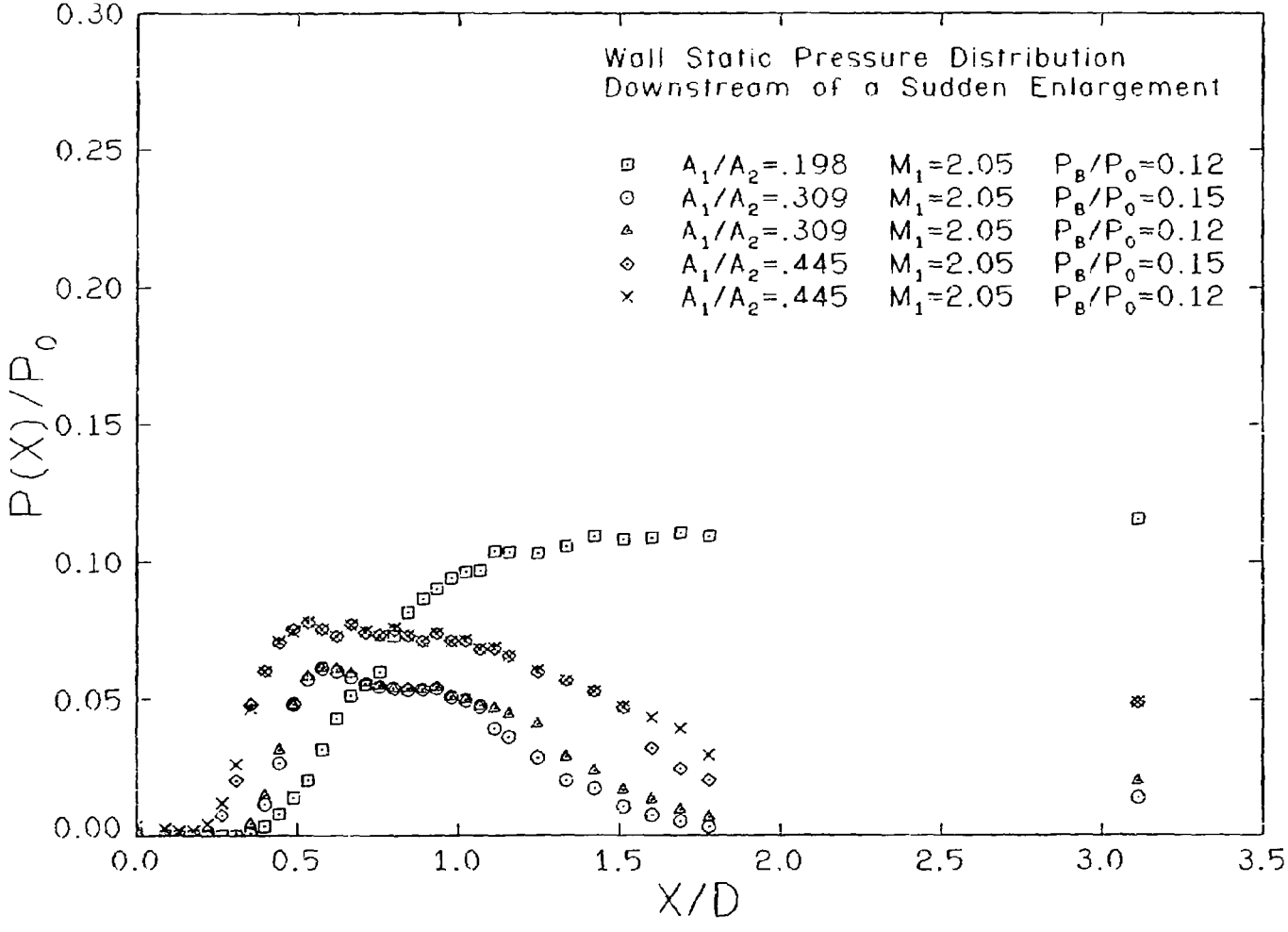

Figure 6 Wall static pressure distribution downstream of a sudden enlargement for an entrance jet Mach number of 2.05 (expanded axial scale).